VISIBLE LIGHT POSITIONING SYSTEMS: FUNDAMENTAL LIMITS, ALGORITHMS AND RESOURCE ALLOCATION APPROACHES

A DISSERTATION SUBMITTED TO

THE GRADUATE SCHOOL OF ENGINEERING AND SCIENCE

OF BILKENT UNIVERSITY

IN PARTIAL FULFILLMENT OF THE REQUIREMENTS FOR

THE DEGREE OF

DOCTOR OF PHILOSOPHY

IN

ELECTRICAL AND ELECTRONICS ENGINEERING

By

Musa Furkan Keskin

August 2018

Visible Light Positioning Systems: Fundamental Limits, Algorithms and Resource Allocation Approaches
By Musa Furkan Keskin
August 2018

We certify that we have read this dissertation and that in our opinion it is fully adequate, in scope and in quality, as a dissertation for the degree of Doctor of Philosophy.

Sinan Gezici(Advisor)

Orhan Arıkan

İbrahim Körpeoğlu

Berkan Dülek

Emre Özkan

Approved for the Graduate School of Engineering and Science:

Ezhan Karaşan
Director of the Graduate School

ABSTRACT

VISIBLE LIGHT POSITIONING SYSTEMS: FUNDAMENTAL LIMITS, ALGORITHMS AND RESOURCE ALLOCATION APPROACHES

Musa Furkan Keskin
Ph.D. in Electrical and Electronics Engineering
Advisor: Sinan Gezici
August 2018

Visible light communication (VLC) is an emerging paradigm that enables multiple functionalities to be accomplished concurrently, including illumination, high-speed data communications, and localization. Based on the VLC technology, visible light positioning (VLP) systems aim to estimate locations of VLC receivers by utilizing light-emitting diode (LED) transmitters at known locations. VLP presents a viable alternative to radio frequency (RF)-based positioning systems by providing inexpensive and accurate localization services. In this dissertation, we consider the problem of localization in visible light systems and investigate distance and position estimation approaches in synchronous and asynchronous scenarios, focusing on both theoretical performance characterization and algorithm development aspects. In addition, we design optimal resource allocation strategies for LED transmitters in VLP systems for improved localization performance. Moreover, we propose a cooperative localization framework for VLP systems, motivated by vehicular VLC networks involving vehicle-to-vehicle (V2V) and vehicle-to-infrastructure (V2I) communications.

First, theoretical limits and estimators are studied for distance estimation in synchronous and asynchronous VLP systems. Specifically, the Cramér-Rao lower bounds (CRLBs) and maximum likelihood estimators (MLEs) are investigated based on time-of-arrival (TOA) and/or received signal strength (RSS) parameters. Hybrid TOA/RSS based distance estimation is proposed for VLP systems, and its CRLB is compared analytically against the CRLBs of TOA based and RSS based distance estimation. In addition, to investigate effects of sampling, asymptotic performance results are obtained under sampling rate limitations as the noise variance converges to zero. A modified hybrid TOA/RSS based distance estimator is proposed to provide performance improvements in the presence of sampling rate limitations. Moreover, the Ziv-Zakai bound (ZZB) is derived for synchronous VLP systems. The proposed ZZB extracts ranging information from

the prior information, the time delay parameter, and the channel attenuation factor based on the Lambertian pattern. In addition to the ZZB, the Bayesian Cramér-Rao bound (BCRB) and the weighted CRB (WCRB) are calculated for synchronous VLP systems. Furthermore, a closed-form expression is obtained for the expectation of the conditional CRB (ECRB). Numerical examples are presented to compare the bounds against each other and against the maximum a-posteriori probability (MAP) estimator. It is observed that the ZZB can provide a reasonable lower limit on the performance of MAP estimators. On the other hand, the WCRB and the ECRB converge to the ZZB in regions of low and high source optical powers, respectively; however, they are not tight in other regions.

Second, direct and two-step positioning approaches are investigated for both synchronous and asynchronous VLP systems. In particular, the CRLB and the direct positioning based ML estimator are derived for three-dimensional localization of a VLC receiver in a synchronous scenario by utilizing information from both time delay parameters and channel attenuation factors. Then, a two-step position estimator is designed for synchronous VLP systems by exploiting the asymptotic properties of TOA and RSS estimates. The proposed two-step estimator is shown to be asymptotically optimal, i.e., converges to the direct estimator at high signal-to-noise ratios (SNRs). In addition, the CRLB and the direct and two-step estimators are obtained for positioning in asynchronous VLP systems. It is proved that the two-step position estimation is optimal in asynchronous VLP systems for practical pulse shapes. Various numerical examples are provided to illustrate the improved performance of the proposed estimators with respect to the current state-of-the-art and to investigate their robustness against model uncertainties in VLP systems.

Third, the problem of optimal power allocation among LED transmitters in a VLP system is considered for the purpose of improving localization performance of VLC receivers. Specifically, the aim is to minimize the CRLB on the localization error of a VLC receiver by optimizing LED transmission powers in the presence of practical constraints such as individual and total power limitations and illuminance constraints. The formulated optimization problem is shown to be convex and thus can efficiently be solved via standard tools. We also investigate the case of imperfect knowledge of localization parameters and develop robust power allocation algorithms by taking into account both overall system uncertainty and individual parameter uncertainties related to the location and orientation of the

VLC receiver. In addition, we address the total power minimization problem under predefined accuracy requirements to obtain the most energy-efficient power allocation vector for a given CRLB level. Numerical results illustrate the improvements in localization performance achieved by employing the proposed optimal and robust power allocation strategies over the conventional uniform and non-robust approaches.

In the final part of the dissertation, we propose to employ cooperative localization for visible light networks by designing a VLP system configuration that involves multiple LED transmitters with known locations and VLC units equipped with both LEDs and photodetectors (PDs) for the purpose of cooperation. In the proposed cooperative scenario, we derive the CRLB and the MLE for the localization of VLC units. To tackle the nonconvex structure of the MLE, we adopt a set-theoretic approach by formulating the problem of cooperative localization as a quasiconvex feasibility problem, where the aim is to find a point inside the intersection of convex constraint sets constructed as the sublevel sets of quasiconvex functions resulting from the Lambertian formula. Then, we devise two feasibility-seeking algorithms based on iterative gradient projections to solve the feasibility problem. Both algorithms are amenable to distributed implementation, thereby avoiding high-complexity centralized approaches. Capitalizing on the concept of quasi-Fejér convergent sequences, we carry out a formal convergence analysis to prove that the proposed algorithms converge to a solution of the feasibility problem in the consistent case. Numerical examples illustrate the improvements in localization performance achieved via cooperation among VLC units and evidence the convergence of the proposed algorithms to true VLC unit locations in both the consistent and inconsistent cases.

Keywords: Estimation, visible light communications, Cramér-Rao lower bound, Ziv-Zakai bound, Lambertian pattern, direct positioning, two-step positioning, power allocation, convex optimization, cooperative localization, quasiconvex feasibility, gradient projections.

ÖZET

GÖRÜNÜR IŞIK KONUMLANDIRMA SİSTEMLERİ: TEMEL SINIRLAR, ALGORİTMALAR VE KAYNAK TAHSİSİ YAKLAŞIMLARI

Musa Furkan Keskin
Elektrik ve Elektronik Mühendisliği, Doktora
Tez Danışmanı: Sinan Gezici
Ağustos 2018

Görünür ışık haberleşmesi (GIH); aydınlatma, yüksek hızlı veri haberleşmesi ve konumlama gibi birçok işlevselliğin eşzamanlı olarak gerçekleştirilmesini sağlayan yeni bir paradigmadır. GIH teknolojisine dayanan görünür ışık konumlandırma (GIK) sistemleri, konumları bilinen ışık yayan diyot (LED) vericileri kullanarak GIH alıcılarının konumlarını kestirmeyi amaçlamaktadır. GIK, ucuz ve isabetli konumlama hizmeti sağlayarak, radyo frekans (RF) tabanlı konumlandırma sistemlerine geçerli bir alternatif sunmaktadır. Bu tezde, görünür ışık sistemlerinde konumlama problemi ele alınmakta ve teorik performans belirleme ve algoritma geliştirme yönlerine odaklanarak, senkron ve asenkron senaryolarda mesafe ve konum kestirimi yaklaşımları araştırılmaktadır. Ek olarak, konumlama performansının iyileştirilmesi amacıyla GIK sistemlerindeki LED vericileri için optimal kaynak tahsisi stratejileri tasarlanmaktadır. Ayrıca, araçtan araca ve araçtan altyapıya haberleşmeleri içeren araç GIH ağlarından hareketle GIK sistemleri için işbirlikçi bir konumlama sistemi önerilmektedir.

İlk olarak, senkron ve asenkron GIK sistemlerinde mesafe kestirimi için teorik sınırlar ve kestiriciler çalışılmaktadır. Daha açık bir deyişle, varış zamanı (VZ) ve/veya alınan sinyal gücü (ASG) parametrelerine dayanarak Cramér-Rao sınırı (CRS) ve maksimum olabilirlik kestiricisi (MOK) araştırılmaktadır. GIK sistemleri için karma VZ/ASG tabanlı mesafe kestirimi önerilmekte ve CRS'si VZ tabanlı ve ASG tabanlı mesafe kestiriminin CRS'leriyle analitik olarak karşılaştırılmaktadır. Ek olarak, örneklemenin etkilerini araştırmak için, gürültü varyansı sıfıra yaklaşırken örnekleme oranı kısıtları altında asimptotik performans sonuçları elde edilmektedir. Örnekleme oranı kısıtları varlığında performans iyileştirmeleri sağlamak amacıyla değiştirilmiş karma VZ/ASG tabanlı mesafe kestiricisi önerilmektedir. Ayrıca, senkron GIK sistemleri için Ziv-Zakai sınırı (ZZS) türetilmektedir. Önerilen ZZS, mesafe bilgisini önsel bilgi,

zaman gecikmesi parametresi ve Lambert örüntüsüne dayanan kanal zayıflama faktöründen çıkarmaktadır. ZZS'ye ek olarak, senkron GIK sistemlerinde Bayes CRS (BCRS) ve ağırlıklı CRS (ACRS) hesaplanmaktadır. Bunun yanında, ortalama koşullu CRS (OCRS) için kapalı formda bir ifade elde edilmektedir. Teorik sınırları birbirleriyle ve maksimum sonsal olasılık (MSO) kestiricisi ile karşılaştırmak amacıyla sayısal sonuçlar sunulmaktadır. ZZS'nin MSO kestiricilerinin performansı için mantıklı bir alt sınır sağladığı gözlenmektedir. Öte yandan, ACRS ve OCRS, sırasıyla, düşük ve yüksek optik güç bölgelerinde ZZB'ye yakınsamaktadır; ancak, diğer bölgelerde sıkı değillerdir.

İkinci olarak, hem senkron hem asenkron GIK sistemleri için doğrudan ve iki adımlı konumlandırma yaklaşımları araştırılmaktadır. Özellikle, zaman gecikmesi parametreleri ve kanal zayıflama faktörlerinden gelen bilgi kullanılarak senkron bir senaryoda GIH alıcısının üç boyutlu konumlandırılması için CRS ve doğrudan konumlandırma tabanlı MO kestiricisi türetilmektedir. Daha sonra, VZ ve ASG kestirimlerinin asimptotik özelliklerinden faydalanılarak iki adımlı bir konum kestirici tasarlanmaktadır. Önerilen iki adımlı kestiricinin asimptotik olarak optimal olduğu; yani, yüksek sinyal gürültü oranı (SGO) altında doğrudan kestiriciye yakınsadığı gösterilmektedir. Ek olarak, asenkron GIK sistemlerinde konumlandırma için CRS ve doğrudan ve iki adımlı kestiriciler elde edilmektedir. Pratik sinyal şekilleri için asenkron GIK sistemlerinde iki adımlı konum kestiriminin optimal olduğu ispatlanmaktadır. Önerilen kestiricilerin mevcut yöntemlere kıyasla iyileşen performanslarını örneklemek ve GIK sistemlerindeki model belirsizliklerine karşı gürbüzlüğünü araştırmak üzere çeşitli sayısal örnekler sağlanmaktadır.

Üçüncüsü, GIH alıcılarının konumlama performanslarını iyileştirmek amacıyla bir GIK sisteminde LED vericileri arasında optimal güç tahsisi problemi ele alınmaktadır. Daha açık bir deyişle, bireysel ve toplam güç ve aydınlatma gibi pratik kısıtlar altında LED iletim güçlerini optimize ederek GIH alıcısının konumlama hatası üzerindeki CRS'nin küçültülmesi amaçlanmaktadır. Formüle edilen optimizasyon probleminin dışbükey olduğu ispatlanarak standart araçlarla verimli bir şekilde çözülebileceği gösterilmektedir. Ayrıca, konumlama parametrelerinin hatalı olarak bilindiği durum araştırılmakta ve toplam sistem belirsizliği ve GIH alıcısının konum ve yönüne dair bireysel parametre belirsizlikleri dikkate alınarak gürbüz güç tahsisi algoritmaları geliştirilmektedir. Ek olarak, verilen bir CRS seviyesi için en enerji verimli güç tahsisi vektörünü elde etmek amacıyla, önceden tanımlanmış doğruluk gereksinimleri altında toplam güç azaltma problemi ele

alınmaktadır. Sayısal sonuçlar, önerilen optimal ve gürbüz güç tahsisi stratejilerinin geleneksel eşit ve gürbüz olmayan yaklaşımlara kıyasla konumlama performansında gösterdiği iyileştirmeleri örneklemektedir.

Tezin son kısmında, konumları bilinen birçok LED vericisi ve işbirliği amacıyla hem LED'ler hem fotosezicilerle donatılmış GIH birimlerini içeren bir GIK sistem konfigürasyonu tasarlanarak, görünür ışık ağları için işbirlikçi konumlamanın kullanılması önerilmektedir. Önerilen işbirlikçi senaryoda, GIH birimlerinin konumlandırılması için CRS ve MOK türetilmektedir. MOK'un dışbükey olmayan yapısının üstesinden gelmek amacıyla, işbirlikçi konumlandırma problemi dışbükey benzeri fizibilite problemi olarak formüle edilerek küme-teorik bir yaklaşım benimsenmektedir. Bu problemde amaç, Lambert formülünden kaynaklanan dışbükey benzeri fonksiyonların alt seviye kümeleri olarak düzenlenen dışbükey kısıt kümelerinin kesişiminde bir nokta bulmaktır. Daha sonra, fizibilite problemini çözmek amacıyla, yinelemeli eğim izdüşümlerine dayanan iki algoritma tasarlanmaktadır. Her iki algoritma da, dağıtık olarak gerçekleştirilmeye uygundur; bu durum, yüksek karmaşıklı merkezi yaklaşımlardan kaçınabilmeyi sağlamaktadır. Quasi-Fejér yakınsak serilerden faydalanılarak, düzgün bir yakınsama analizi yapılmakta ve önerilen algoritmaların tutarlı durumda fizibilite probleminin bir çözümüne yakınsadıkları ispatlanmaktadır. Sayısal örnekler, GIH birimleri arasında işbirliği sayesinde elde edilen konumlandırma performansı iyileştirmelerini göstermekte ve önerilen algoritmaların hem tutarlı hem tutarsız durumlarda GIH birimlerinin doğru konumlarına yakınsadığını kanıtlamaktadır.

Anahtar sözcükler: Kestirim, görünür ışık haberleşmesi, Cramér-Rao sınırı, Ziv-Zakai sınırı, Lambert örüntüsü, doğrudan konumlandırma, iki adımlı konumlandırma, güç tahsisi, dışbükey optimizasyon, işbirlikçi konumlandırma, dışbükey benzeri fizibilite, eğim izdüşümleri.

Acknowledgement

I would like to express my gratitude to my supervisor Prof. Sinan Gezici for his invaluable guidance throughout the development of this thesis. It was a genuine pleasure and honor for me to work with him. Also, I would like to thank Prof. Orhan Arıkan for his support and advices. In addition, I am very thankful to Assoc. Prof. Selim Aksoy for accepting to be in my thesis monitoring committee. I also extend my special thanks to Prof. İbrahim Körpeoğlu, Assoc. Prof. Berkan Dülek and Asst. Prof. Emre Özkan for agreeing to serve on my dissertation examination committee.

I acknowledge the financial support of the Scientific and Technological Research Council of Turkey (TÜBİTAK) through 2211 Scholarship Program of BİDEB during my PhD studies.

I am sincerely grateful to all my friends and colleagues in Bilkent EEE Department for motivating and enjoyable discussions.

I wish to thank my family, my mother Mümine, my father Ahmet and my sister Kübra for their encouragement and support.

Finally, I would like to express my deepest gratitude to my wife Dudu for her love, support and patience throughout my studies. This thesis would not have been possible without her encouragement.

Contents

List of Figures

List of Tables

Chapter 1

Introduction

With the advent of low-cost and energy-efficient light emitting diode (LED) technologies, LED based visible light communication (VLC) systems have gathered a significant amount of research interest in the last decade [1–3]. Utilizing the vast unlicensed visible light spectrum, VLC has the potential to surmount the issue of spectrum scarcity encountered in radio frequency (RF) based wireless systems [4]. In indoor scenarios, VLC systems can employ the available lighting infrastructure to provide various capabilities simultaneously, such as illumination, high-speed data transmission, and localization [2, 5]. Apart from their basic function of illuminating indoor spaces, LEDs can be modulated at high frequencies to accomplish high data rate transmission [3, 6, 7]. On the other hand, the process of localization via visible light signals can be realized by visible light positioning (VLP) systems, where VLC receivers equipped with photo detectors can perform position estimation by exploiting signals emitted by LED transmitters at known locations [5, 7–10]. Since line-of-sight (LOS) links generally exist between LED transmitters and VLC receivers, and multipath effects are not very significant as compared to RF based solutions [11, 12], VLP systems can facilitate precise location estimation in indoor environments [9, 13–15]. Among various applications of VLP systems, robot navigation, asset tracking and location-aware services can be considered as the most prominent ones [3, 5].

The main purpose of this dissertation is to investigate distance and position estimation techniques in VLP systems by providing theoretical performance limits, developing efficient algorithms and proposing resource allocation approaches for accuracy improvement. In the first part of the dissertation containing Chapter 2 and Chapter 3, we derive various performance bounds on distance and position estimation in both synchronous and asynchronous VLP scenarios, design statistical estimators, and carry out a comprehensive accuracy analysis of VLP systems through theoretical and numerical results [16–18]. The second part (Chapter 4) of the dissertation focuses on power allocation strategies for LED transmitters in VLP systems with the aim of minimizing the localization error of VLC receivers [19]. In the final part (Chapter 5), we extend our analysis to consider the effects of cooperation among VLC receivers and devise iterative, distributed algorithms for cooperative localization in VLP systems [20]. In the following sections, we provide a literature review and summarize our main contributions.

1.1 Distance and Position Estimation in Visible Light Systems

1.1.1 Distance Estimation in Visible Light Systems

In VLP systems, various types of parameters such as received signal strength (RSS), time-of-arrival (TOA), time-difference-of-arrival (TDOA), and angle-of-arrival (AOA) can be employed for position estimation. In RSS based systems, the position of a VLC receiver is estimated based on RSS measurements between the VLC receiver and a number of LED transmitters [9, 13–15, 21, 22]. Unlike in RF based systems, the RSS parameter can provide very accurate position related information in VLP systems since the channel attenuation factor does not fluctuate significantly in LOS visible light channels. In [13], a complete VLP system based on RSS measurements and trilateration is implemented and the achieved sub-meter accuracy is compared against other positioning systems. In [21], Kalman and particle filtering are employed for RSS based position tracking

in VLP systems. The study in [15] utilizes a single LED transmitter and multiple optical receivers for position estimation, where the position of the receiver unit is determined based on RSS measurements at multiple receivers. In [14], an RSS based VLP system is designed and a multiaccess protocol is implemented. The proposed system can guarantee decimeter level accuracy in almost all scenarios in the presence and absence of direct sunlight exposure. A carrier allocation VLC system is proposed in [9] for RSS based positioning and experiments are performed to illustrate its centimeter level average positioning accuracy. The studies in [23] and [24] consider the use of the time delay parameter for positioning. In particular, [23] investigates the theoretical limits on TOA estimation for visible light systems. In [24], TDOAs are calculated at a VLC receiver based on signals from three LEDs and two-dimensional position estimation is performed based on TDOAs. As another alternative, the AOA parameter can be utilized for localization in VLP systems [25–27]. For example, the study in [27] considers a multi-element VLC system and exploits the narrow field of view of LEDs to extract position related information from connectivity conditions. Based on a least-squares estimator and Kalman filtering, average positioning accuracy on the order of 0.2 meter is reported.

Although there exist many studies on VLP systems, theoretical limits on estimation accuracy have been considered very rarely [23, 28]. Theoretical limits for estimation present useful performance bounds on mean-squared errors (MSEs) of estimators and provide important guidelines for system design. In [23], the Cramér-Rao lower bound (CRLB) is presented for distance (or, TOA) estimation in a synchronous VLC system. The effects of various system parameters, such as source optical power, center frequency, and the area of the photo detector, are investigated. Simulation results indicate centimeter level accuracy limits for typical system parameters. The study in [28] derives the CRLB for distance estimation based on the RSS parameter, and investigates the dependence of the CRLB expression on system parameters such as LED configuration, transmitter height, and the signal bandwidth. Again, CRLBs on the order of centimeters are observed for typical system parameters.

In the first part of Chapter 2, a generic signal model, which covers TOA

based [23] and RSS based [28] distance estimation as special cases, is considered, and theoretical limits and estimators are derived. In particular, the CRLBs and maximum likelihood estimators (MLEs) are investigated for both synchronous and asynchronous scenarios and in the presence and absence of a relation between distance and channel attenuation factor. In this way, in addition to TOA based and RSS based distance estimation, hybrid TOA/RSS based distance estimation is introduced for VLP systems, and theoretical links and comparisons are provided between the current study and those in the literature [23,28]. Also, via the CRLB expressions, the accuracy limits for TOA based, RSS based, and hybrid TOA/RSS based distance estimation are compared analytically. Furthermore, asymptotic results are obtained for the MLEs under sampling rate limitations, and a modified hybrid estimator is proposed to perform accurate distance estimation in practical scenarios.

Apart from the CRLB expressions, in Chapter 2, we also derive the Ziv-Zakai bound (ZZB) for distance estimation in synchronous VLP systems (that can utilize both TOA and RSS parameters) in the presence of prior information on the distance parameter. Therefore, unlike the theoretical limits in [16, 23, 28, 29], the aim in the second part of Chapter 2 is to provide theoretical limits for a synchronous VLP system by considering the effects of *prior information*, as well. Although the CRLB can provide tight limits on MSEs of unbiased estimators in high signal-to-noise ratio (SNR) conditions, it can be quite loose for low SNRs [30]. In addition, the CRLB derivations do not consider any prior statistical information about the range (or, position) parameter, which can in fact be available in indoor environments; e.g., based on physical dimensions and known system parameters such as the field of view of the photo detector. To address these issues, the ZZB can be used as a benchmark for ranging in VLP systems. The ZZB can provide tight limits on MSEs of estimators in all SNR conditions, and it also utilizes the available prior information [30, 31]. The study in [32] derives the ZZB on range estimation in an asynchronous VLP system based on RSS measurements and provides comparisons with the maximum a-posteriori probability (MAP) and the minimum mean-squared error (MMSE) estimators.

In the second part of Chapter 2, the ZZB on ranging is derived for a synchronous VLP system by utilizing the prior information and the ranging information from both the time delay (TOA) parameter and the channel attenuation factor (RSS) via the Lambertian pattern. Based on the ZZB, effects of various system parameters, such as the Lambertian order, the area of the photo detector, and the source optical power, are analyzed in terms of ranging accuracy, and design guidelines are provided for practical VLP systems. In addition, the expectation of the CRB (ECRB) is calculated and a closed-form expression is obtained for uniform prior information. The ECRB expression both illustrates the effects of prior information and provides a low-complexity alternative to the ZZB in high SNR conditions. Moreover, the Bayesian CRB (BCRB) and the weighted CRB (WCRB) are derived in order to present theoretical limits that effectively utilize the prior information, and they are compared against the ZZB.

1.1.2 Direct and Two-Step Position Estimation in Visible Light Systems

Commonly, the problem of wireless localization is investigated by employing two classes of approaches, which are *two-step positioning* and *direct positioning*. Widely applied in RF and VLP based localization systems, two-step positioning algorithms extract position related parameters, such as RSS, TOA, TDOA, and AOA in the first step, and perform position estimation based on those parameters in the second step [33]. There exist a multitude of applications of indoor VLP systems that employ two-step positioning, such as those using RSS [14, 34–36], AOA [27], hybrid RSS/AOA [26, 29, 37], TOA [16, 23], and TDOA [24]. However, the two-step method can be construed as a suboptimal solution to the localization problem since it does not exploit all the collected data related to the unknown location. On the other hand, direct positioning algorithms use the entire received signal in a one-step process in order to determine the unknown position, as opposed to two-step positioning [38–40]. Hence, all the available information regarding the unknown position can be effectively utilized in the direct position estimation approach, which can lead to the optimal solution to the localization

problem. A theoretical justification for the superiority of direct positioning over conventional two-step positioning is provided in [41, 42]. In [38], the direct position determination (DPD) technique is proposed for localization of narrowband RF emitters, where the multiple signal classification (MUSIC) algorithm is employed to formulate the cost function in the case of unknown signals. It is shown that the DPD approach outperforms the conventional AOA based two-step localization technique. The study in [43] investigates the localization of a stationary narrowband RF source using signals from multiple moving receivers in a single-step approach and demonstrates that the DPD method is superior to the two-step differential Doppler (DD) method at low SNRs. In addition, direct localization techniques are shown to enhance the performance of RF positioning in TOA [44], TDOA [45] and hybrid TOA/AOA [46] based systems. Direct positioning algorithms are also employed for target localization in radar systems [47, 48].

Although the DPD approach has been employed in numerous applications in RF localization systems, only a limited amount of research has been carried out on the utilization of DPD techniques in indoor VLP systems. In [49], RSS based VLP system with non-directional LEDs and a detector array consisting of multiple directional photo diodes (PDs) is proposed, where time-averaged RSS values at each PD are considered as the final observation for two-dimensional position estimation. In [50], which extends the study in [49], a correlation receiver is employed to obtain a single RSS estimate for each PD without optimizing for the correlator peak. However, from the direct positioning perspective, the proposed methods in [49] and [50] utilize only the time-averaged or correlation samples of the received signal, not the entire signal for localization. Furthermore, an asynchronous VLP system is designed in [51], where a Bayesian signal model is constructed to estimate the unknown position based on the entire received signal from multiple LEDs in the presence of obstruction of signals from several LEDs.

To provide performance benchmarks for positioning algorithms, theoretical bounds on distance ('range') and position estimation in VLP systems have been considered in several studies in the literature [16, 17, 23, 28, 29, 49, 52]. The work in [28] derives the CRLB for distance estimation based on RSS information, whereas [23] presents the CRLB for distance estimation in synchronous visible

light systems based on TOA measurements. The CRLB on hybrid TOA/RSS based ranging is investigated in [16]. In [17], the ZZB is derived for synchronous VLP systems in the presence of prior information about distance and it is compared against the ECRB, BCRB, and WCRB, all of which utilize prior information. Besides distance estimation, theoretical accuracy limits have also been derived for localization in visible light systems. In [29], the CRLB is derived for RSS based three-dimensional localization for an indoor VLP scenario with arbitrary LED transmitter and VLC receiver configurations. In [49] and [50], two-dimensional RSS-based localization is addressed with the assumption of a known receiver height, and an analytical CRLB expression is derived accordingly.

In Chapter 3, we study direct and two-step positioning approaches in both synchronous and asynchronous VLP systems. Considering a generic three-dimensional localization scenario, we first derive the CRLB and the direct positioning based ML estimator for a synchronous VLP system by taking into account both the time delays and the channel attenuation factors. Then, we design an asymptotically optimal two-step estimator that exploits the asymptotic unbiasedness and efficiency properties of the first-step TOA and RSS estimates. Moreover, we provide the CRLB and the direct and two-step ML estimators in an asynchronous VLP system, and demonstrate the optimality of two-step estimation (i.e., its equivalence to direct estimation) in asynchronous scenarios for practical waveforms.

1.2 Resource Allocation in Visible Light Systems

In order to provide satisfactory performance for mobile or stationary devices, it is essential to investigate performance optimization in visible light systems with respect to various criteria, such as MSE minimization (e.g., [53–56]) and transmission rate maximization (e.g., [57–65]). In the literature, transmit precoding

and DC offset[1] designs are extensively explored to improve the MSE performance of multiple-input multiple-output (MIMO) VLC systems [53–56]. In addition to transceiver and offset designs in VLC systems, an increasingly popular research strand focuses on power allocation for LED transmitters to enhance system performance [57–64, 66, 67]. Due to practical concerns related to energy efficiency and LED lifespan, transmission powers of LEDs in visible light systems are valuable resources that can have profound effects on both transmission rates of VLC systems and localization accuracy of VLP systems. In [57], the total instantaneous data rate of LED arrays is considered as the performance metric for a MIMO VLC system and the optimal strategy for LED power allocation is derived under sum optical power and non-negativity constraints. The studies in [58] and [60] perform power optimization for LEDs to maximize the sum transmission rate of all subcarriers in a VLC system employing optical orthogonal frequency-division multiplexing (OFDM). With the aim of achieving proportional fairness among users in a multi-user VLC network, the total logarithmic throughput is optimized in [61] and [64] to identify the optimal LED power control strategy. Although total and individual power constraints are extensively utilized in power allocation optimization in VLC systems, several studies incorporate color and luminance constraints into the power optimization framework, as well, in compliance with the illumination functionality of VLC systems [59, 62]. In general, power allocation algorithms in both VLC and VLP systems should take into account a variety of design requirements imposed by the multi-faceted nature of visible light applications.

The concept of power allocation has also been widely considered for RF based wireless localization networks [68–77], where the transmit powers of anchor nodes (the locations of which are known) can be optimized to improve the localization accuracy of target nodes (with unknown locations). The prevailing approach in such investigations is to adopt a mathematically tractable and tight bound on the localization error as the performance metric and to formulate the optimization problem under average and peak anchor power constraints. In [68]

[1]Optical intensity modulation in VLC systems requires that the amplitude of the electrical drive current of the LED must be non-negative [57].

and [69], anchor power allocation algorithms are designed to minimize the total power consumption subject to predefined accuracy requirements for localization of target nodes. For cooperative localization networks, distributed power allocation strategies are developed in [70], where the transmit powers of both anchors and targets are optimally allocated to minimize the squared position error bound (SPEB). Moreover, [73] explores the problem of optimal power allocation for OFDM subcarriers in the presence of both perfect and imperfect knowledge of network parameters. As commonly observed in RF wireless localization systems, optimal power allocation provides non-negligible performance benefits over the traditional uniform strategy for a wide range of localization scenarios.

In Chapter 4, motivated by the promising performance improvements achieved via power allocation in both RF localization networks and VLC systems, we propose the problem of optimal power allocation for LED transmitters in a VLP system, where the objective is to minimize the localization error of the VLC receiver subject to practical constraints related to power and illumination. To quantify the localization accuracy, the CRLB metric is adopted in the problem statement. Leveraging tools from convex optimization and semidefinite programming (SDP), we formulate and solve various optimization problems in both the absence and presence of parameter uncertainties. The power allocation problem for VLP systems has the following key differences from the one in RF based localization systems: *(i)* Due to the limited linear region of operation, the LEDs are subject to both the minimum and peak power constraints [55,59,78,79]. *(ii)* Since VLP systems serve the dual purpose of illumination and localization, the problem formulation should include lighting constraints that guarantee an acceptable level of illumination in indoor spaces [79–82]. *(iii)* In contrast to RF systems in which multipath components can severely affect the quality of localization, the received signal power in VLP systems can accurately be characterized by the Lambertian formula [12].

1.3 Cooperative Localization in Visible Light Systems

Based on the availability of internode measurements, wireless localization networks can broadly be classified into two groups: *cooperative* and *noncooperative*. In the conventional noncooperative approach, position estimation is performed by utilizing only the measurements between anchor nodes (which have known locations) and agent nodes (the locations of which are to be estimated) [83,84]. On the other hand, cooperative systems also incorporate the measurements among agent nodes into the localization process to achieve improved performance [84]. Benefits of cooperation among agent nodes are more pronounced specifically for sparse networks where agents cannot obtain measurements from a sufficient number of anchors for reliable positioning [85]. There exists an extensive body of research regarding the investigation of cooperation techniques and the development of efficient algorithms for cooperative localization in RF-based networks (see [83–85] and references therein). In terms of implementation of algorithms, centralized approaches attempt to solve the localization problem via the optimization of a global cost function at a central unit to which all measurements are delivered. Among various centralized methods, ML and nonlinear least squares (NLS) estimators are the most widely used ones, both leading to nonconvex and difficult-to-solve optimization problems, which are usually approximated through convex relaxation approaches such as SDP [86–88], second-order cone programming (SOCP) [89,90], and convex underestimators [91]. In distributed algorithms, computations related to position estimation are executed locally at individual nodes, thereby reinforcing scalability and robustness to data congestion [84]. Set-theoretic estimation [92–95], factor graphs [84], and multidimensional scaling (MDS) [96] constitute common tools employed for cooperative distributed localization in the literature.

Despite the ubiquitous use of cooperation techniques in RF-based wireless localization networks, no studies in the literature have considered the use of cooperation in VLP networks. In Chapter 5, we extend the cooperative paradigm

to visible light domain. More specifically, we set forth a cooperative localization framework for VLP networks whereby LED transmitters with fixed, known locations[2] function as anchors and VLC units with unknown locations are equipped with LEDs and PDs for the purpose of communications with both fixed LEDs and other VLC units. Utilization of the proposed framework is motivated by the following potential real-life applications:

- **Vehicular VLC for Intelligent Transportation:** Deployment of low-cost and energy-efficient LEDs in headlamps, taillights, and turn signals of modern vehicles makes vehicle-to-vehicle (V2V) communications via VLC a feasible approach for vehicular networks [97–99]. As VLC receivers, PDs can be placed in different sides of vehicles (e.g., near headlights, taillights or side mirrors [99, Fig. 1]) to enable inter-vehicle cooperation [97]. As illustrated in Fig. 1.1, by exploiting vehicle-to-infrastructure (V2I) communications between traffic infrastructures (e.g., traffic/street lights) and vehicles, together with V2V VLC links, a VLC-based cooperative vehicular localization system can be implemented to provide precise location information for cooperative ITS applications, especially in harsh scenarios where the global positioning system (GPS) signals are severely degraded (e.g., urban areas or tunnels) [99, 100].

- **Indoor VLC with Infrared Uplink Capability:** Since infrared LEDs and PDs are already available in some VLC systems for efficient uplink transmission [2, 4, 101–103], they can also be utilized for device-to-device communications to achieve cooperation among VLC units (see Fig. 1.2 for an illustration of an indoor cooperative VLP system). An additional benefit of using infrared wavelengths for cooperation is that it helps mitigate eye safety risks incurred by communications among VLC units [104].

The proposed network facilitates the definition of arbitrary connectivity sets between the LEDs on the ceiling and the VLC units, and also among the VLC

[2]In indoor scenarios, LEDs on ceiling have fixed locations and can be used as anchors for localization of VLC units. For the case of vehicular visible light networks, anchor LEDs correspond to the roadside infrastructure lightings, such as traffic lights and streetlamps [97].

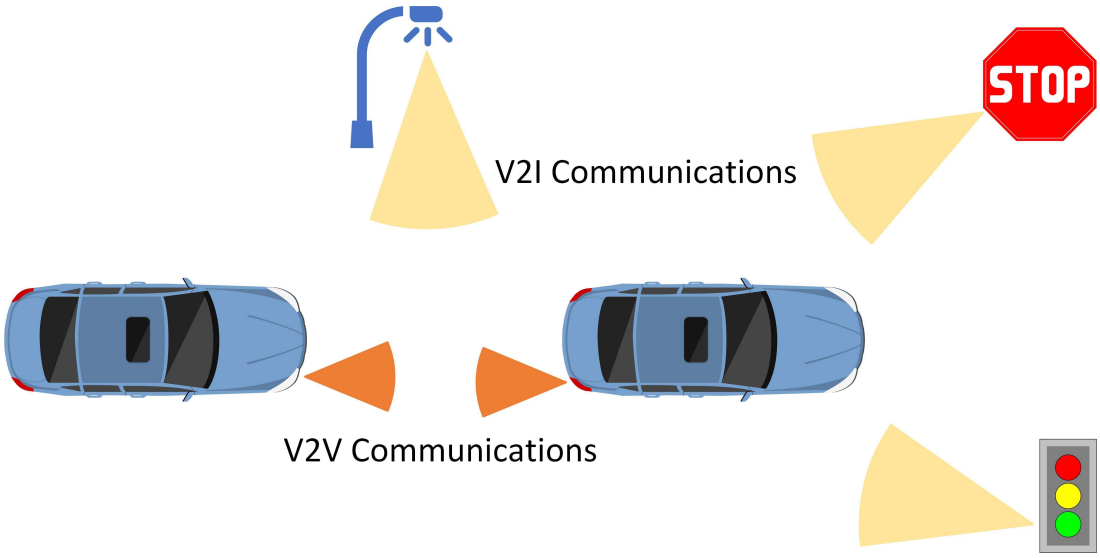

Figure 1.1: Vehicular VLC for cooperative intelligent transportation systems.

units, which can provide significant performance enhancements over the traditional noncooperative approach employed in the VLP literature. Based on the noncooperative (i.e., between LEDs on the ceiling and VLC units) and cooperative (i.e., among VLC units) RSS measurements, we first derive the CRLB and the MLE for the localization of VLC units. Since the MLE poses a challenging nonconvex optimization problem, we follow a set-theoretic estimation approach and formulate the problem of cooperative localization as a quasiconvex *feasibility* problem (QFP) [105], where feasible constraint sets correspond to sublevel sets of certain type of quasiconvex functions. The quasiconvexity arising in the problem formulation stems from the Lambertian formula, which characterizes the attenuation level of visible light channels. Next, we design two feasibility-seeking algorithms, having cyclic and simultaneous characteristics, which employ iterative gradient projections onto the specified constraint sets. From the viewpoint of implementation, the proposed algorithms can be implemented in a distributed architecture that relies on computations at individual VLC units and a broadcasting mechanism to update position estimates. Moreover, we provide a formal convergence proof for the projection-based algorithms based on quasi-Féjer convergence, which enjoys decent properties to support theoretical analysis [106].

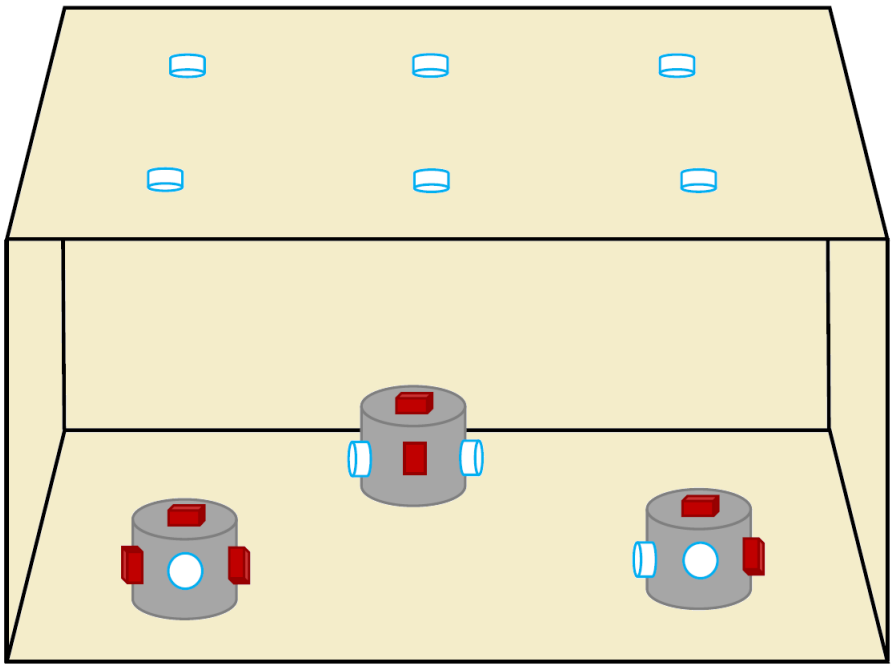

Figure 1.2: Illustration of an indoor cooperative VLP system with three VLC units (e.g., robots). The white cylinders on the ceiling and at the VLC units represent the LEDs, and the red rectangular prisms denote the PDs.

The applications of convex feasibility problems (CFPs) encompass a wide variety of disciplines, such as wireless localization [92–95, 107], compressed sensing [108], image recovery [109], image denoising [110] and intensity-modulated radiation therapy [111]. In contrary to optimization problems where the aim is to minimize the objective function while satisfying the constraints, feasibility problems seek to find a point that satisfies the constraints in the absence of an objective function [108]. Hence, the goal of a CFP is to identify a point inside the intersection of a collection of closed convex sets in a Euclidean (or, in general, Hilbert) space. In feasibility problems, a commonly pursued approach is to perform projections onto the individual constraint sets in a sequential manner, rather than projecting onto their intersection due to analytical intractability [112]. The work in [92] formulates the problem of acoustic source localization as a CFP and employs the well-known projections onto convex sets (POCS) technique for convergence to true source locations. Following a similar methodology, the noncooperative wireless positioning problem with noisy range measurements is modeled

as a CFP in [93], where POCS and outer-approximation (OA) methods are utilized to derive distributed algorithms that perform well under non-line-of-sight (NLOS) conditions. In [107], a cooperative localization approach based on projections onto nonconvex boundary sets is proposed for sensor networks, and it is shown that the proposed strategy can achieve better localization performance than the centralized SDP and the distributed MDS although it may get trapped into local minima due to nonconvexity. Similarly, the work in [94] designs a POCS-based distributed positioning algorithm for cooperative networks with a convergence guarantee regardless of the consistency of the formulated CFP, i.e., whether the intersection is nonempty or not.

Although CFPs have attracted a great deal of interest in the literature, QFPs have been investigated only rarely. QFPs represent generalized versions of CFPs in that the constraint sets are constructed from the lower level sets of quasiconvex functions in QFPs whereas such functions are convex in CFPs [105]. The study in [105] explores the convergence properties of subgradient projections based iterative algorithms utilized for the solution of QFPs. It is demonstrated that the iterations converge to a solution of the QFP if the quasiconvex functions satisfy Hölder conditions and the QFP is consistent, i.e., the intersection is nonempty. In Chapter 5, we show that the Lambertian model based (originally non-quasiconvex) functions can be approximated by appropriate quasiconvex lower bounds, which convexifies the (originally nonconvex) sublevel constraint sets, thus transforming the formulated feasibility problem into a QFP.

The previous work on VLP networks has addressed the problem of position estimation based mainly on the ML estimator [16,29,50], the least squares estimator [27,29], triangulation [14,113], and trilateration [24] methods. In Chapter 5, however, we consider the problem of localization in VLP networks as a feasibility problem and introduce efficient iterative algorithms with convergence guarantees in the consistent case. In addition, the theoretical bounds derived for position estimation are significantly different from those in [29,50] via the incorporation of terms related to cooperation, which allows for the evaluation of the effects of cooperation on the localization performance in any three dimensional cooperative VLP scenario. Furthermore, unlike the previous research on localization

in RF-based wireless networks via CFP modeling [92–94, 107], where a common approach is to employ POCS-based iterative algorithms, we formulate the localization problem as a QFP for VLP systems, which necessitates the development of more sophisticated algorithms (e.g., gradient projections) and different techniques for studying the convergence properties of those algorithms (e.g., quasiconvexity and quasi-Fejér convergence).

1.4 Organization of the Dissertation

This dissertation is organized as follows. In Chapter 2, comparative theoretical analysis of distance estimation in VLP systems is carried out by providing performance benchmarks and statistical estimators. In Chapter 3, direct and two-step position estimation methods are studied for VLP systems. Then, Chapter 4 considers the performance metrics derived in Chapter 3 for designing optimal resource allocation strategies for LED transmitters in VLP systems. In Chapter 5, cooperative localization scenarios are investigated for VLP systems. Finally, Chapter 6 presents concluding remarks for this dissertation and provides a discussion of future research directions.

Chapter 2

Distance Estimation in Visible Light Positioning Systems: Theoretical Limits and Statistical Estimators

In this chapter, theoretical limits and statistical estimators are studied for distance estimation in synchronous and asynchronous VLP systems [16, 17]. The main contributions of this chapter can be summarized as follows:

- The hybrid RSS/TOA based distance estimation is proposed for VLP systems for the first time. In addition, the CRLB and the MLE corresponding to the hybrid RSS/TOA based distance estimation are derived, which have not been available in the literature.[1]
- Analytical expressions are derived for the ratios between the CRLBs for the TOA based, RSS based, and hybrid TOA/RSS based distance estimation.

[1]The hybrid RSS/TOA based estimation and the corresponding CRLB and MLE expressions in RF positioning systems [114–117] are different from those in this study due to the distinct characteristics of the visible light channel.

In particular, it is shown that the CRLB for the hybrid TOA/RSS based estimation converges to that of the TOA based distance estimation for $\beta \gg c/x$, and to that of the RSS based distance estimation for $\beta \ll c/x$, where β is the effective bandwidth of the transmitted signal, x is the distance between the LED transmitter and the VLC receiver, and c is the speed of light.

- Effects of sampling rate limitations on the TOA based, RSS based, and hybrid TOA/RSS based MLEs are characterized via asymptotic MSE expressions as the noise variance converges to zero.

- To provide performance improvements in the presence of sampling rate limitations, a modified hybrid TOA/RSS based estimator is proposed based on the hybrid TOA/RSS based MLE.

- The ZZB on ranging is derived for a synchronous VLC system by utilizing prior information together with the ranging information extracted from the time delay parameter and the channel attenuation factor. (The provided ZZB expression is different from those for synchronous RF systems [30, 118, 119] due to the facts that (i) synchronous VLP systems utilize both time delay and received signal power information whereas synchronous RF systems use time delay information only, and (ii) the Lambertian formula is available for VLP systems to specify the received signal power, which is not valid for RF systems.)

- A closed-form ECRB expression is derived for ranging in synchronous VLC systems, which converges to the ZZB in the high SNR regime.

- The BCRB and the WCRB expressions are provided for a synchronous VLC system, which have not been available in the literature.

- Performance of the MAP estimator is compared against the theoretical limits. It is demonstrated that the theoretical limits on the performance of the MAP estimators can be characterized by the ZZB, which provides important guidelines for designers of practical VLP systems. In addition, the ECRB and the WCRB are observed to converge to the ZZB in the high and low SNR regimes, respectively.

In addition, slightly more general CRLB expressions than those in [23] and [28] are presented for the TOA based and RSS based distance estimation, and the conditions under which the CRLB expressions in [23] and [28] arise are specified. Furthermore, comparisons among different approaches are provided in terms of theoretical estimation accuracy and robustness to sampling rate limitations. Numerical examples are provided to investigate the theoretical results.

This chapter is organized as follows: The system model is introduced and the parameters are defined in Section 2.1. The CRLBs and the MLEs are derived for synchronous and asynchronous scenarios in Section 2.2, and comparisons are presented among the CRLBs in various cases. In Section 2.3, the asymptotic MSEs are derived for the MLEs when the noise variance goes to zero, and the modified hybrid TOA/RSS based distance estimator is proposed. The ZZB for synchronous VLP systems is derived in Section 2.4, and a closed-form ECRB expression is provided in Section 2.5. The BCRB and the WCRB expressions are obtained in Section 2.6. Numerical examples are presented in Section 2.7, followed by discussions on position estimation in Section 2.8. Finally, the concluding remarks are presented in Section 2.9.

2.1 System Model

In an indoor VLP system, LED transmitters are commonly located on the ceiling of a room, and a VLC receiver is located on an object on the floor. Based on the signals received from the LED transmitters (which have known positions), the VLC receiver can estimate its distance (range) to each LED transmitter and determine its position based on distance estimates. The aim in this study is to investigate the fundamental limits on distance estimation.

Consider an LED transmitter at location $\boldsymbol{l}_t \in \mathbb{R}^3$ and a VLC receiver at location $\boldsymbol{l}_r \in \mathbb{R}^3$ in an LOS scenario. The distance between the LED transmitter and the VLC receiver is represented by x, which is given by $x = \|\boldsymbol{l}_r - \boldsymbol{l}_t\|_2$. The received

signal at the VLC receiver is expressed as [23]

$$r(t) = \alpha R_p \, s(t - \tau) + n(t) \tag{2.1}$$

for $t \in [T_1, T_2]$, where T_1 and T_2 specify the observation interval, α is the attenuation factor of the optical channel ($\alpha > 0$), R_p is the responsivity of the photo detector, $s(t)$ is the transmitted signal which is nonzero over an interval of $[0, T_s]$, τ is the TOA, and $n(t)$ is zero-mean additive white Gaussian noise with a spectral density level of σ^2. It is assumed that R_p and $s(t)$ are known by the VLC receiver. Also, the TOA parameter is modeled as

$$\tau = \frac{x}{c} + \Delta \tag{2.2}$$

where x is the distance between the LED transmitter and the VLC receiver, c is the speed of light, and Δ denotes the time offset between the clocks of the LED transmitter and the VLC receiver. For a synchronous system, $\Delta = 0$, whereas for an asynchronous system, Δ is modeled as a deterministic unknown parameter. It is assumed that coarse acquisition is performed so that the signal component in (2.1) resides completely in the observation interval $[T_1, T_2]$.

The channel attenuation factor α in (2.1) is modeled as

$$\alpha = \frac{m+1}{2\pi} \cos^m(\phi) \cos(\theta) \frac{S}{x^2} \tag{2.3}$$

where m is the Lambertian order, S is the area of the photo detector at the VLC receiver, ϕ is the irradiation angle, and θ is the incidence angle [13, 23]. For compactness of analytical expressions, it is assumed, similarly to [15, 23, 28], that the LED transmitter is pointing downwards (which is commonly the case) and the photo detector at the VLC receiver is pointing upwards such that $\phi = \theta$ and $\cos(\phi) = \cos(\theta) = h/x$, where h denotes the height of the LED transmitter relative to the VLC receiver.[2] In addition, as in [15, 21, 23, 28], it is assumed that the height of the VLC receiver is known; that is, possible positions of the VLC receiver are confined to a two-dimensional plane. This assumption holds in

[2]It is straightforward to extend the theoretical bounds in this study to the cases with arbitrary transmitter and receiver orientations. However, it is not performed as the expressions become lengthy and inconvenient.

various practical scenarios; e.g., when the VLC receiver is attached to a cart or a robot that is tracked via a VLP system as VLC receivers have fixed and known heights in such applications (e.g., Fig. 3 in [5]). Under these assumptions, (2.3) becomes

$$\alpha = \frac{m+1}{2\pi}\left(\frac{h}{x}\right)^{m+1}\frac{S}{x^2} \triangleq \gamma\, x^{-m-3} \tag{2.4}$$

where

$$\gamma \triangleq (m+1)h^{m+1}S/(2\pi) \tag{2.5}$$

is a known constant.[3]

2.2 CRLBs and ML Estimators

In order to calculate the CRLB, the log-likelihood function corresponding to the received signal model in (2.1) is specified as follows [120], [121]:

$$\Lambda(\boldsymbol{\varphi}) = k - \frac{1}{2\sigma^2}\int_{T_1}^{T_2}\left(r(t) - \alpha R_p\, s(t-\tau)\right)^2 dt \tag{2.6}$$

where $\boldsymbol{\varphi}$ denotes the set of unknown parameters including x and other nuisance parameters, if any, depending on the considered scenario (as discussed below), and k represents a normalizing constant that is a function of σ and does not depend on the unknown parameter(s). The CRLB is obtained based on the inverse of the Fisher information matrix (FIM) for $\boldsymbol{\varphi}$, which can be calculated from the log-likelihood function in (2.6) as [122]

$$\mathbf{J}(\boldsymbol{\varphi}) = \mathbb{E}\left\{\left(\nabla_{\boldsymbol{\varphi}}\Lambda(\boldsymbol{\varphi})\right)\left(\nabla_{\boldsymbol{\varphi}}\Lambda(\boldsymbol{\varphi})\right)^T\right\} \tag{2.7}$$

where $\nabla_{\boldsymbol{\varphi}}$ represents the gradient operator with respect to $\boldsymbol{\varphi}$. From the FIM in (2.7), the CRLB on the covariance matrix of any unbiased estimator $\hat{\boldsymbol{\varphi}}$ of $\boldsymbol{\varphi}$ can be calculated as follows:

$$\mathbb{E}\big\{(\hat{\boldsymbol{\varphi}} - \boldsymbol{\varphi})(\hat{\boldsymbol{\varphi}} - \boldsymbol{\varphi})^T\big\} \succeq \mathbf{J}(\boldsymbol{\varphi})^{-1} \tag{2.8}$$

[3]The assumption of a known height is required for unambiguous estimation of distance based on an RSS measurement (cf. (2.4)).

where $\boldsymbol{A} \succeq \boldsymbol{B}$ means that $\boldsymbol{A} - \boldsymbol{B}$ is positive semidefinite [122].

In the following, the CRLBs and MLEs are derived for different cases.

2.2.1 Case 1: Synchronous System

Firstly, the following assumptions are considered: (i) the LED transmitter and the VLC receiver are synchronized (i.e., $\Delta = 0$ in (2.2)) and (ii) the relation of channel attenuation factor α to distance x is unknown; i.e., a relation as in (2.4) is not available. The latter is a common assumption in RF based distance estimation systems (e.g., [123]) since the channel coefficient fluctuates significantly due to multipath effects (fading). However, in visible light systems, the channel attenuation factor can accurately be related to distance, especially in LOS scenarios, and this relation can be used to improve the accuracy of distance estimation, as will be discussed later in this section. The main aims behind studying distance estimation in the absence of the relation between α and x are to provide a benchmark for analyzing the effects of this relation, and to investigate the previous results in the literature [23].

In the presence of synchronization and in the absence of a relation between the channel attenuation factor and distance, the ML estimator [122] can be obtained from (2.6) as follows:

$$\begin{aligned} \hat{x}_{\mathrm{ML,TOA}} &= \arg\max_{\boldsymbol{\varphi}} \frac{-1}{2\sigma^2} \int_{T_1}^{T_2} \left(r(t) - \alpha R_p\, s(t-\tau)\right)^2 dt \\ &= \arg\max_{x} \int_{T_1}^{T_2} r(t) s\left(t - \frac{x}{c}\right) dt \end{aligned} \tag{2.9}$$

where the final expression is obtained due to the facts that $\alpha > 0$ and the TOA parameter in (2.2) becomes $\tau = x/c$ for a synchronous system.

For the CRLB derivation in this scenario, it is first assumed that the channel attenuation factor α is known by the VLC receiver. Then, the unknown parameter vector in (2.6) becomes $\boldsymbol{\varphi} = x$, and the Fisher information in (2.7) can be

obtained, from (2.6), as

$$\mathrm{J}(x) = \mathbb{E}\left\{\left(\frac{d\Lambda(x)}{dx}\right)^2\right\} = \left(\frac{R_p\alpha}{\sigma c}\right)^2 E_1 \tag{2.10}$$

where

$$E_1 \triangleq \int_0^{T_s} \left(s'(t)\right)^2 dt \tag{2.11}$$

with $s'(t)$ denoting the derivative of $s(t)$ [122, 124]. Based on (2.8) and (2.10), the CRLB is computed as follows:

$$\mathbb{E}\{(\hat{x}-x)^2\} \geq \frac{1}{E_1}\left(\frac{\sigma c}{R_p\alpha}\right)^2 \triangleq \mathrm{CRLB}_{\mathrm{TOA}}\,. \tag{2.12}$$

To provide an alternative expression for the CRLB in (2.12), E_1 in (2.11) is expressed, via Parseval's relation, as follows [122]:

$$\begin{aligned} E_1 &= \int_{-\infty}^{\infty} |j2\pi f S(f)|^2\, df = 4\pi^2 \int_{-\infty}^{\infty} f^2\, |S(f)|^2\, df \\ &= 4\pi^2\beta^2 \int_{-\infty}^{\infty} |S(f)|^2\, df = 4\pi^2 E_2 \beta^2 \end{aligned} \tag{2.13}$$

where $S(f)$ denotes the Fourier transform of $s(t)$,

$$E_2 \triangleq \int_{-\infty}^{\infty} |S(f)|^2\, df = \int_0^{T_s} \left(s(t)\right)^2 dt \tag{2.14}$$

and β is the effective bandwidth of $s(t)$ defined as

$$\beta^2 = \frac{1}{E_2}\int_{-\infty}^{\infty} f^2\, |S(f)|^2\, df\ . \tag{2.15}$$

From (2.13), (2.12) can be stated as

$$\mathbb{E}\{(\hat{x}-x)^2\} \geq \frac{\sigma^2 c^2}{4\pi^2 R_p^2\, \alpha^2 E_2 \beta^2} \triangleq \mathrm{CRLB}_{\mathrm{TOA}}\,. \tag{2.16}$$

It is noted that the CRLB in (2.16) is equivalent to that in eqn. (5) of [23] for $\sigma^2 = N_0/2$. Hence, the CRLB expression presented in [23] corresponds to a synchronous system in which the channel attenuation factor α is known by the VLC receiver but the relation of α to distance x is unknown. Since only the time delay information is employed to estimate the distance, this scenario is referred to as *TOA based distance estimation*.

When the channel attenuation factor, α, is unknown, the CRLB can be expressed for this scenario as in the following lemma.

Lemma 1 [117]. *When the channel attenuation factor α in (2.1) is unknown, the CRLB for TOA based distance estimation is given by*

$$\mathbb{E}\{(\hat{x}-x)^2\} \geq \frac{E_2}{E_1E_2-E_3^2}\left(\frac{\sigma c}{R_p\alpha}\right)^2 \tag{2.17}$$

where E_1 is as in (2.11), E_2 is given by (2.14), and

$$E_3 \triangleq \int_0^{T_s} s'(t)s(t)dt = 0.5\left(s^2(T_s)-s^2(0)\right). \tag{2.18}$$

Proof: Although the proof can be obtained as a special case of the derivation in [117], it is provided below for completeness.

When α is unknown, the vector of unknown parameters becomes $\boldsymbol{\varphi}=(x,\alpha)$ and the log-likelihood function in (2.6) can be expressed as $\Lambda(x,\alpha)$. Then, the FIM in (2.7) is given by

$$\mathbf{J}(x,\alpha) = \begin{bmatrix} \mathbb{E}\left\{\left(\frac{\partial\Lambda(x,\alpha)}{\partial x}\right)^2\right\} & \mathbb{E}\left\{\frac{\partial\Lambda(x,\alpha)}{\partial x}\frac{\partial\Lambda(x,\alpha)}{\partial\alpha}\right\} \\ \mathbb{E}\left\{\frac{\partial\Lambda(x,\alpha)}{\partial\alpha}\frac{\partial\Lambda(x,\alpha)}{\partial x}\right\} & \mathbb{E}\left\{\left(\frac{\partial\Lambda(x,\alpha)}{\partial\alpha}\right)^2\right\} \end{bmatrix} \tag{2.19}$$

which can be calculated, after some manipulation, as

$$\mathbf{J}(x,\alpha) = \left(\frac{R_p}{\sigma}\right)^2 \begin{bmatrix} \alpha^2E_1/c^2 & -\alpha E_3/c \\ -\alpha E_3/c & E_2 \end{bmatrix} \tag{2.20}$$

where E_1, E_2, and E_3 are given by (2.11), (2.14), and (2.18), respectively. Then, the CRLB on the MSE of any unbiased estimator $\hat{x}$ of x is given by the first element of the inverse of the FIM [122]; that is,

$$\mathbb{E}\{(\hat{x}-x)^2\} \geq \left[\mathbf{J}(x,\alpha)^{-1}\right]_{1,1} \tag{2.21}$$

which can be obtained as in (2.17) based on (2.20). ■

As expected, the CRLB in (2.17) is larger than or equal to the CRLB in (2.12) due to the presence of an additional unknown parameter. It is also observed

that the CRLBs become equal when E_3 in (2.18) is equal to zero. Therefore, for $E_3 = 0$, the CRLB in [23] also corresponds to a synchronous system in which the channel attenuation factor α is unknown and the relation of α to distance x is unavailable.

Secondly, the following assumptions are considered: (i) the LED transmitter and the VLC receiver are synchronized (i.e., $\Delta = 0$ in (2.2)) and (ii) the relation between channel attenuation factor α and distance x is known, which is as stated in (2.4). The second assumption is practical for VLP systems since the channel attenuation factor can be specified accurately as a function of distance in LOS visible light channels.

In this scenario, the ML estimator can be obtained from (2.2) with $\Delta = 0$, (2.4), and (2.6) as follows:[4]

$$\hat{x}_{\mathrm{ML,hyb}} = \arg\max_{x}\; x^{-m-3} \int_{T_1}^{T_2} r(t) s\left(t - \frac{x}{c}\right) dt - 0.5\gamma R_p\, x^{-2m-6} E_2\,. \tag{2.22}$$

Compared to the MLE in (2.9), the MLE in (2.22) also exploits the relation of the channel attenuation factor with the distance, as noted from the x^{-m-3} and x^{-2m-6} terms.

Based on (2.2) with $\Delta = 0$ and the relation in (2.4), the unknown parameter vector in (2.6) becomes $\boldsymbol{\varphi} = x$. Then, from (2.4)-(2.7), the Fisher information can be calculated as

$$\mathrm{J}(x) = \left(\frac{R_p \gamma}{\sigma x^{m+4}}\right)^2 h_1(x) \tag{2.23}$$

with

$$h_1(x) \triangleq (m+3)^2 E_2 + 2(m+3)\frac{x}{c} E_3 + \frac{x^2}{c^2} E_1 \tag{2.24}$$

where E_1, E_2, and E_3 are given by (2.11), (2.14), and (2.18), respectively. From (2.8) and (2.23), the CRLB is computed as follows:

$$\mathbb{E}\big\{(\hat{x} - x)^2\big\} \geq \frac{1}{h_1(x)} \left(\frac{\sigma x^{m+4}}{R_p \gamma}\right)^2 \triangleq \mathrm{CRLB}_{\mathrm{hyb}}\,. \tag{2.25}$$

[4]The meaning of subscript hyb (hybrid) will be clear towards the end of this section.

The comparison between the CRLBs in (2.12) and (2.25) is provided in the following proposition:

Proposition 1. *The CRLB in* (2.25) *is smaller than that in* (2.12) *if and only if*

$$(m+3)E_2 + \frac{2x}{c}E_3 > 0 \ . \tag{2.26}$$

Proof: First, the CRLB in (2.25) is expressed based on (2.4) as

$$\mathbb{E}\big\{(\hat{x}-x)^2\big\} \geq \frac{x^2}{c^2 h_1(x)} \left(\frac{\sigma c}{R_p \alpha}\right)^2 \tag{2.27}$$

Then, the ratio of the CRLB in (2.12) to the CRLB in (2.27) is given by

$$\frac{c^2 h_1(x)}{E_1 x^2} = \frac{c^2(m+3)^2 E_2 + 2(m+3)xcE_3 + x^2 E_1}{E_1 x^2} \tag{2.28}$$

$$= 1 + \frac{c^2(m+3)^2 E_2 + 2(m+3)xcE_3}{E_1 x^2} \tag{2.29}$$

where the relation in (2.24) is employed. Since E_1, E_2, m, c, and x are positive by definition, the second term in (2.29) is positive if and only if the condition in (2.26) holds. ■

The condition in Proposition 1 commonly holds in practice since x/c is very small (on the order of 10^{-8} for indoor scenarios) and/or E_3 is zero for many practical pulses [23]. Hence, the utilization of the relation in (2.4) is useful for improving the accuracy of distance estimation. From a practical point of view, this implies that instead of estimating (learning) the value of α first and then using that estimate in the TOA based distance estimation, a more efficient approach is to estimate the distance directly based on the model in (2.1) and (2.4) since the information in α related to distance x is effectively utilized in that scenario. In other words, in the presence of the relation between the channel attenuation factor and the distance, information in both the channel attenuation factor and the time delay parameter are utilized for distance estimation. Hence, this scenario corresponds to *hybrid TOA/RSS based distance estimation* as the channel attenuation factor is related to RSS.

Remark 1. To illustrate the improvements that can be achieved by utilizing the relation between α and x, the relation in (2.29) can be considered for $E_3 = 0$, which becomes $1 + c^2(m+3)^2 E_2/(E_1 x^2)$. From (2.13), this expression can be stated as $1 + c^2(m+3)^2/(4\pi^2\beta^2 x^2)$. Hence, for typical system parameters, the CRLB for the TOA based distance estimation is significantly larger than the CRLB for the hybrid TOA/RSS based distance estimation for $\beta \ll c/x$, and they become comparable for high effective bandwidths (on the order of 100 MHz or higher). As an example, for $x = 10\,\text{m.}$, $m = 1$, and $\beta = 1\,\text{MHz}$, $1 + c^2(m+3)^2/(4\pi^2\beta^2 x^2) = 365.76$, which means that the lower limit on the root MSEs (RMSEs) of unbiased estimators is 19.125 times smaller for the hybrid TOA/RSS based distance estimation than that for the TOA based distance estimation. On the other hand, when $\beta = 100\,\text{MHz}$, $1+c^2(m+3)^2/(4\pi^2\beta^2 x^2) = 1.0365$ is obtained, leading to comparable CRLBs.

2.2.2 Case 2: Asynchronous System

In this case, it is assumed the channel attenuation factor α and distance x are related as in (2.4). However, the LED transmitter and the VLC receiver are not synchronized; that is, Δ in (2.2) is unknown. Hence, the delay parameter τ in (2.1) and (2.2) is modeled as an unknown parameter, and the vector of unknown parameters in (2.6) is specified by $\boldsymbol{\varphi} = (x, \tau)$. Then, the ML estimator can be expressed based on (2.6) as follows:

$$\hat{x}_{\text{ML,RSS}} = \underset{(x,\tau)}{\arg\max}\; x^{-m-3} \int_{T_1}^{T_2} r(t)s(t-\tau)dt - 0.5\gamma R_p\, x^{-2m-6} E_2 \tag{2.30}$$

which can be re-stated as

$$\hat{x}_{\text{ML,RSS}} = \underset{x}{\arg\max}\; x^{-m-3}\tilde{C}_{rs} - 0.5\gamma R_p\, x^{-2m-6} E_2 \tag{2.31}$$

where

$$\tilde{C}_{rs} \triangleq \max_{\tau} \int_{T_1}^{T_2} r(t)s(t-\tau)dt\ . \tag{2.32}$$

The solution of (2.31) can be obtained as

$$\hat{x}_{\text{ML,RSS}} = \left(\frac{\gamma R_p E_2}{\tilde{C}_{rs}}\right)^{\frac{1}{m+3}} \tag{2.33}$$

under the assumption that $\tilde{C}_{rs}$ is positive. It is noted that in the ML estimator in (2.30), the value of τ is estimated as the one that maximizes the correlation between the transmitted and received signals, as shown in (2.32). Then, that estimate is employed in the ML estimator, leading to the expression in (2.31).

Since the TOA parameter τ cannot be related to distance in this case due to asynchronism (see (2.2)), the distance estimation relies on the RSS information via (2.4) in this case, which is therefore referred to as *RSS based distance estimation*.

The CRLB for the RSS based distance estimation is given by the following lemma.

Lemma 2. *For the signal model in* (2.1)*, where the delay parameter is unknown and the channel attenuation factor is given by* (2.4)*, the CRLB for distance estimation is expressed as*

$$\mathbb{E}\big\{(\hat{x}-x)^2\big\} \geq \frac{E_1}{E_1E_2-E_3^2}\left(\frac{\sigma x}{\alpha R_p(m+3)}\right)^2 \triangleq \mathrm{CRLB}_{\mathrm{RSS}} \tag{2.34}$$

where E_1, E_2, and E_3 are given by (2.11)*,* (2.14)*, and* (2.18)*, respectively.*

Proof: For the model in (2.1), when the TOA parameter τ is modeled as unknown and the channel attenuation factor α is given by (2.4), the vector of unknown parameters becomes $\boldsymbol{\varphi}=(x,\tau)$ and the log-likelihood function in (2.6) can be denoted by $\Lambda(x,\tau)$. Then, the FIM in (2.7) becomes

$$\mathbf{J}(x,\tau)=\begin{bmatrix} \mathbb{E}\left\{\left(\frac{\partial\Lambda(x,\tau)}{\partial x}\right)^2\right\} & \mathbb{E}\left\{\frac{\partial\Lambda(x,\tau)}{\partial x}\frac{\partial\Lambda(x,\tau)}{\partial \tau}\right\} \\ \mathbb{E}\left\{\frac{\partial\Lambda(x,\tau)}{\partial \tau}\frac{\partial\Lambda(x,\tau)}{\partial x}\right\} & \mathbb{E}\left\{\left(\frac{\partial\Lambda(x,\tau)}{\partial \tau}\right)^2\right\} \end{bmatrix}. \tag{2.35}$$

The elements of $\mathbf{J}(x,\tau)$ in (2.35) are obtained, after some manipulation, as

$$\mathbf{J}(x,\tau)=\left(\frac{\gamma R_p}{\sigma}\right)^2 x^{-2m-7}\begin{bmatrix} (m+3)^2E_2/x & (m+3)E_3 \\ (m+3)E_3 & xE_1 \end{bmatrix} \tag{2.36}$$

where E_1, E_2, and E_3 are given by (2.11), (2.14), and (2.18), respectively. Then, the CRLB on the MSE of any unbiased estimator $\hat{x}$ of x is given by the first

element of the inverse of the FIM as stated in (2.21), which can be obtained as in (2.34) based on (2.4) and (2.36). ■

It is noted that the CRLB expression in Lemma 2 covers that in [28] as a special case for $E_3 = 0$ (please see eqn. (15) in [28]).

In the following proposition, the CRLB in Lemma 2 is compared to those corresponding to the TOA based and hybrid TOA/RSS based distance estimation.

Proposition 2. *For $E_3 = 0$, the ratios of the CRLB in* (2.34) *to that in* (2.25) *and to that in* (2.12) *are expressed as*

$$\frac{\mathrm{CRLB}_{\mathrm{RSS}}}{\mathrm{CRLB}_{\mathrm{hyb}}} = 1 + \frac{4\pi^2\beta^2 x^2}{c^2(m+3)^2} = 1 + \frac{\mathrm{CRLB}_{\mathrm{RSS}}}{\mathrm{CRLB}_{\mathrm{TOA}}}\,. \tag{2.37}$$

Proof: For $E_3 = 0$, the CRLB in (2.25) (equivalently, (2.27)) becomes

$$\mathbb{E}\big\{(\hat{x} - x)^2\big\} \geq \frac{1}{(m+3)^2 E_2 + E_1(x/c)^2} \left(\frac{\sigma x}{R_p \alpha}\right)^2. \tag{2.38}$$

Then, the ratio of the CRLB in (2.34) for $E_3 = 0$ to the CRLB in (2.38) is obtained as $1 + E_1 x^2/(E_2 c^2 (m+3)^2)$, which becomes equal to the central expression in (2.37) based on (2.13). In addition, the ratio of the CRLB in (2.34) for $E_3 = 0$ to the CRLB in (2.12) is given by $E_1 x^2/(E_2 c^2 (m+3)^2)$, which is equal to $4\pi^2\beta^2 x^2/(c^2(m+3)^2)$ due to (2.13), leading to the second equality in (2.37). ■

Based on Proposition 2, the following conclusions are made:

- The CRLB for the RSS based distance estimation is very close to the CRLB for the hybrid TOA/RSS based distance estimation for practical indoor positioning systems when $\beta \ll c/x$. Since x is less than 10 meters in typical indoor scenarios, an effective bandwidth lower than about 1 MHz results in approximately equal CRLBs (cf. Remark 1). In such a case, the distance related information gathered from the time delay parameter becomes negligible compared to the information gathered from the channel attenuation factor (equivalently, RSS).

- For $\beta \ll c/x$, the CRLB for the RSS based distance estimation is significantly lower than the CRLB for the TOA based distance estimation; that is, the RSS based distance estimation is much more accurate than the TOA based distance estimation.

- The TOA based distance estimation is more accurate than the RSS based distance estimation when $\beta > (m+3)c/(2\pi x)$. As an example, for $m = 1$ and $x = 5\,\text{m}$, the effective bandwidth should satisfy $\beta > 38.2\,\text{MHz}$ for the TOA based distance estimation to be more accurate.

- When β is on the order of $(m+3)c/(2\pi x)$, the hybrid TOA/RSS based distance estimation can provide non-negligible improvements over both the TOA based and the RSS based distance estimation. When $\beta \gg c/x$, the CRLBs for the TOA based and hybrid TOA/RSS based distance estimation get very close.

Remark 2. Proposition 2 provides comparisons among different approaches based on the CRLBs (i.e., the distance estimation accuracy). On the other hand, with respect to implementation complexity, the RSS based distance estimation has an important practical advantage over the other approaches as it does not require synchronization between the clocks of the LED transmitter and the VLC receiver. Therefore, if the RSS based distance estimation can provide the required level of accuracy for an application, it can be the preferred approach. However, in some scenarios (e.g., for $\beta \gg c/x$), a synchronized system design may be required for achieving the desired accuracy level for distance estimation.

Remark 3. Based on the CRLB expressions obtained in this section, the effects of various parameters on the ranging accuracy can be analyzed. For example, the shape of the transmitted signal $s(t)$ can have different effects in the synchronous and asynchronous cases. For synchronous systems, the CRLB depends on the pulse shape via the E_1 parameter (equivalently, the effective bandwidth parameter β in (2.13)). In particular, for signals with larger E_1 (equivalently, larger β), the TOA based CRLB in (2.16) and the hybrid TOA/RSS based CRLB in

(2.24) and (2.25) get smaller; i.e., the accuracy improves.[5] On the other hand, for asynchronous systems, the RSS based CRLB in (2.34) does not depend on the pulse shape parameter, E_1, when $E_3 = 0$, which is commonly the case. As another important parameter, the height, h, can affect the accuracy of ranging systems. For instance, if the height parameter is increased while the irradiation angle ϕ and the incidence angle θ are unchanged, the distance between the LED transmitter and the VLC receiver increases. Then, it can be observed from (2.3) that the channel attenuation factor α reduces (i.e., the received power decreases) since the distance gets larger and the other parameters are fixed. Hence, based on (2.16), (2.25), and (2.34), all the CRLBs increase; that is, the accuracy degrades. On the other hand, if the height parameter is increased from h to $\tilde{h}$ while the horizontal distance D between the LED transmitter and the VLC receiver is kept the same, the accuracy can increase, decrease, or stay the same depending on the parameters h, $\tilde{h}$, D, and m, which can be analyzed based on (2.4), (2.16), (2.25), and (2.34).

2.3 Effects of Sampling and Modified Hybrid Estimator

It is noted from the MLEs in (2.9), (2.22), and (2.30) that the correlator outputs (i.e., the $\int_{T_1}^{T_2} r(t)s(t-x/c)dt$ and $\int_{T_1}^{T_2} r(t)s(t-\tau)dt$ terms) should be evaluated for all possible distance (delay) values to obtain the ML distance estimates. However, in practical systems, it is costly and power consuming to obtain samples of correlator outputs (equivalently, matched filter outputs) at very high rates [33]. Therefore, it is important to investigate the effects of sampling rate limitations on the MSE performance of the MLEs. In this section, asymptotical analyses are performed (as the noise variance goes to zero) in order to quantify the effects of sampling.

[5]For the hybrid TOA/RSS based scenario, if the information from the TOA parameter is negligible compared to that from the RSS parameter (i.e., if $\beta \ll c/x$), then the hybrid TOA/RSS based CRLB does not change significantly with the pulse shape (E_1 or β).

Suppose that the correlator outputs are sampled at integer multiples of T_{smp} seconds, where T_{smp} denotes the sampling period. Also, the normalized autocorrelation function of signal $s(t)$ is defined as

$$\rho(\upsilon) \triangleq \frac{1}{E_2} \int_{-\infty}^{\infty} s(t)s(t-\upsilon)dt\,. \tag{2.39}$$

In the following lemma, the asymptotic performance of the TOA based and the RSS based ML distance estimation is specified in the presence of sampling rate limitations.

Lemma 3. *Suppose that* $\rho(\upsilon) > \rho(\varsigma)$, $\forall \upsilon \in [-0.5T_{\text{smp}}, 0.5T_{\text{smp}}]$ *and* $\forall \varsigma \notin [-0.5T_{\text{smp}}, 0.5T_{\text{smp}}]$. *Then, in the absence of noise (that is, for* $\sigma = 0$*) and for a sampling period of* T_{smp}*, the MSE of the TOA based MLE in* (2.9) *is given by*

$$\text{MSE}_{\text{TOA}} = \left(x - c\,T_{\text{smp}}\,\text{round}\left(\frac{x}{cT_{\text{smp}}}\right)\right)^2 \tag{2.40}$$

and the MSE of the RSS based MLE in (2.33) *is expressed as*

$$\text{MSE}_{\text{RSS}} = x^2 \left(1 - \left(\rho\left(\tau - T_{\text{smp}}\,\text{round}\left(\frac{\tau}{T_{\text{smp}}}\right)\right)\right)^{\frac{-1}{m+3}}\right)^2 \tag{2.41}$$

where x *is the distance between the LED transmitter and the VLC receiver,* $\tau = x/c + \Delta$ *as stated in* (2.2), $\rho(\cdot)$ *is as defined in* (2.39), *and* $\text{round}(y)$ *represents the closest integer to* y.

Proof: The expression in (2.40) simply follows from (2.9) based on (2.1) without noise. In particular, for a sampling period of T_{smp} and for $\sigma = 0$, (2.9) becomes

$$\hat{x}_{\text{ML,TOA}} = \underset{icT_{\text{smp}}}{\arg\max}\ \alpha R_p E_2 \rho\left(\frac{x - icT_{\text{smp}}}{c}\right) \tag{2.42}$$

where i is an integer, x denotes the true distance, and $\rho(\cdot)$ is as in (2.39). Under the assumption in the lemma, the autocorrelation term in (2.42) is maximized for $i = \text{round}(x/(cT_{\text{smp}}))$. Hence, the ML estimate becomes $\hat{x}_{\text{ML,TOA}} = cT_{\text{smp}}\text{round}(x/(cT_{\text{smp}}))$ and the (mean) squared error is obtained as in (2.40).

For the RSS based ML estimator in (2.33), $\tilde{C}_{rs}$ in (2.32) can be calculated, for a sampling period of T_{smp} and for $\sigma = 0$, as

$$\tilde{C}_{rs} = \max_{iT_{\text{smp}}}\ \alpha R_p E_2 \rho\big(\tau - iT_{\text{smp}}\big) = \alpha R_p E_2 \rho\big(\tau - T_{\text{smp}}\text{round}(\tau/T_{\text{smp}})\big) \tag{2.43}$$

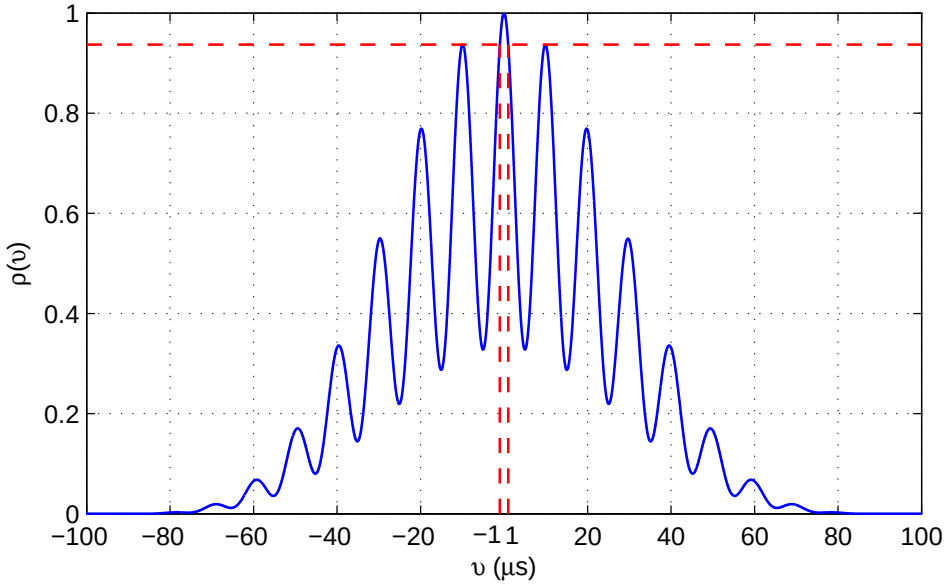

Figure 2.1: Normalized autocorrelation function in (2.39) for $s(t)$ in (2.86) with $T_s = 0.1\,\text{ms}$, $f_c = 100\,\text{kHz}$, and $A = 0.1$.

where $\tau = x/c + \Delta$ denotes the time delay as stated in (2.2), and the assumption in the lemma is employed to obtain the final expression. Then, the RSS based ML estimator in (2.33) becomes

$$\hat{x}_{\text{ML,RSS}} = \left(\frac{\gamma R_p E_2}{\alpha R_p E_2 \rho\big(\tau - T_{\text{smp}}\text{round}(\tau/T_{\text{smp}})\big)} \right)^{\frac{1}{m+3}} \tag{2.44}$$

which can be expressed via (2.4) as

$$\hat{x}_{\text{ML,RSS}} = \frac{x}{\big(\rho(\tau - T_{\text{smp}}\text{round}(\tau/T_{\text{smp}}))\big)^{\frac{1}{m+3}}} \cdot \tag{2.45}$$

From (2.45), the (mean) squared error can be obtained as in (2.41). ■

The assumption in Lemma 3 commonly holds in practice for a sufficiently small T_{smp}. For example, $\rho(v)$ in (2.39) corresponding to $s(t)$ in (2.86) is presented in Fig. 2.1 for $T_s = 0.1\,\text{ms}$, $f_c = 100\,\text{kHz}$, and $A = 0.1$. It is observed that the assumption in Lemma 3 holds for $T_{\text{smp}} < 1\,\mu\text{s}$; that is, when the sampling rate is higher than 1 MHz. It should be noted that high sampling rates are already required for accurate distance estimation; hence, the assumption is Lemma 3 is realistic for most practical applications.

From Lemma 3, it is deduced that the TOA based MLE is directly affected from the mismatches between the sampling time instant and the true delay of the incoming signal whereas the effects on the RSS based MLE is through the sensitivity of the normalized autocorrelation function, $\rho(\upsilon)$, to timing mismatches. For example, if $\rho(\upsilon)$ does not change significantly for $\upsilon \in [-0.5T_{\text{smp}}, 0.5T_{\text{smp}}]$, then effects of the sampling rate can become negligible for the RSS based MLE. Also, it is noted from (2.40) and (2.41) that, depending on the value of distance x and the time delay, the maximum squared error due to sampling is equal to $(0.5cT_{\text{smp}})^2$ for the TOA based MLE and it is given by $x^2(1-(\rho(0.5T_{\text{smp}}))^{-1/(m+3)})^2$ for the RSS based MLE.

For the asymptotic performance of the hybrid TOA/RSS based MLE, the following lemma is presented.

Lemma 4. *Define the following function*

$$g_x(u) \triangleq (ux)^{-m-3}\rho\left(\frac{x-u}{c}\right) - 0.5u^{-2m-6} \tag{2.46}$$

where x denotes the distance between the LED transmitter and the VLC receiver and ρ is as in (2.39)*. Assume that $g_x(u) > g_x(v)$, $\forall u \in [x, x+cT_{\text{smp}}]$ and $\forall v > x+cT_{\text{smp}}$, and that $g_x(u) > g_x(v)$, $\forall u \in [x-cT_{\text{smp}}, x]$ and $\forall v < x-cT_{\text{smp}}$. In addition, define i_1 and i_2 as*

$$i_1 \triangleq \left\lfloor \frac{x}{cT_{\text{smp}}} \right\rfloor \ , \quad i_2 \triangleq \left\lceil \frac{x}{cT_{\text{smp}}} \right\rceil \tag{2.47}$$

where $\lfloor y \rfloor$ denotes the largest integer smaller than or equal to y and $\lceil y \rceil$ represents the smallest integer larger than or equal to y. Then, the MSE of the hybrid TOA/RSS based MLE in (2.22) *is expressed as*

$$\text{MSE}_{\text{hyb}} = \left(x - \hat{i}cT_{\text{smp}}\right)^2 \tag{2.48}$$

where

$$\hat{i} = \underset{i \in \{i_1, i_2\}}{\arg\max}\ g_x(icT_{\text{smp}}) \ . \tag{2.49}$$

Proof: In the absence of noise, $r(t)$ in (2.1) becomes $r(t) = \alpha R_p s(t - x/c)$ for a synchronized system, where x is the distance between the LED transmitter and

the VLC receiver. Replacing the dummy variable x in (2.22) with u, and then inserting $r(t) = \alpha R_p s(t - x/c)$, the objective function for the hybrid TOA/RSS based MLE in (2.22) can be expressed as

$$u^{-m-3}\alpha R_p E_2 \rho\left(\frac{x-u}{c}\right) - 0.5\gamma R_p u^{-2m-6} E_2 \tag{2.50}$$

where ρ is given by (2.39). Based on (2.4), (2.50) can be expressed as

$$\gamma R_p E_2 \left(u^{-m-3}x^{-m-3}\rho\left(\frac{x-u}{c}\right) - 0.5u^{-2m-6}\right) \triangleq \gamma R_p E_2 g_x(u) \tag{2.51}$$

where the equality follows from (2.46). For a sampling period of T_{smp}, the hybrid TOA/RSS based ML estimator in (2.22) can be stated based on (2.51) as

$$\hat{x}_{\text{ML,hyb}} = \underset{icT_{\text{smp}}}{\arg\max}\ \gamma R_p E_2 g_x(icT_{\text{smp}}) \ . \tag{2.52}$$

Under the assumptions in the lemma about $g_x(\cdot)$, the MLE in (2.52) becomes equal to either $i_1 cT_{\text{smp}}$ or $i_2 cT_{\text{smp}}$, where i_1 and i_2 are as in (2.47). If $g_x(i_1 cT_{\text{smp}}) > g_x(i_2 cT_{\text{smp}})$, then $\hat{x}_{\text{ML,hyb}} = i_1 cT_{\text{smp}}$; otherwise, $\hat{x}_{\text{ML,hyb}} = i_2 cT_{\text{smp}}$. Hence, the (mean) squared error can expressed as in (2.48) and (2.49). ■

It can be shown that $g_x(u)$ in (2.46) achieves the maximum value at $u = x$. Hence, the assumption in Lemma 4 is valid for practical scenarios for a sufficiently small T_{smp} and as long as the normalized autocorrelation function, $\rho((x-u)/c)$, does not change rapidly compared to u^{-m-3}. In Fig. 2.2, $g_x(u)$ is presented for $s(t)$ in (2.86), where $x = 5\,\text{m}$, $T_s = 0.1\,\text{ms}$, $f_c = 100\,\text{kHz}$, and $A = 0.1$. It is observed that the assumption in Lemma 4 holds for all values of T_{smp} in this case.

Lemma 4 indicates that, similar to the TOA based MLE, the hybrid TOA/RSS based MLE is directly affected from the mismatches between the sampling time instant and the true delay of the incoming signal, and it is subject to a maximum squared error of $(0.5cT_{\text{smp}})^2$ due to sampling.

For high distance estimation accuracy, the maximum absolute error of $0.5cT_{\text{smp}}$ can be quite undesirable. For example, for a sampling period of $T_{\text{smp}} = 1\,\text{ns}$, the absolute error induced by sampling can be as high as 15 cm. Hence, the accuracy limits promised by the CRLBs may not be achievable. To alleviate this problem,

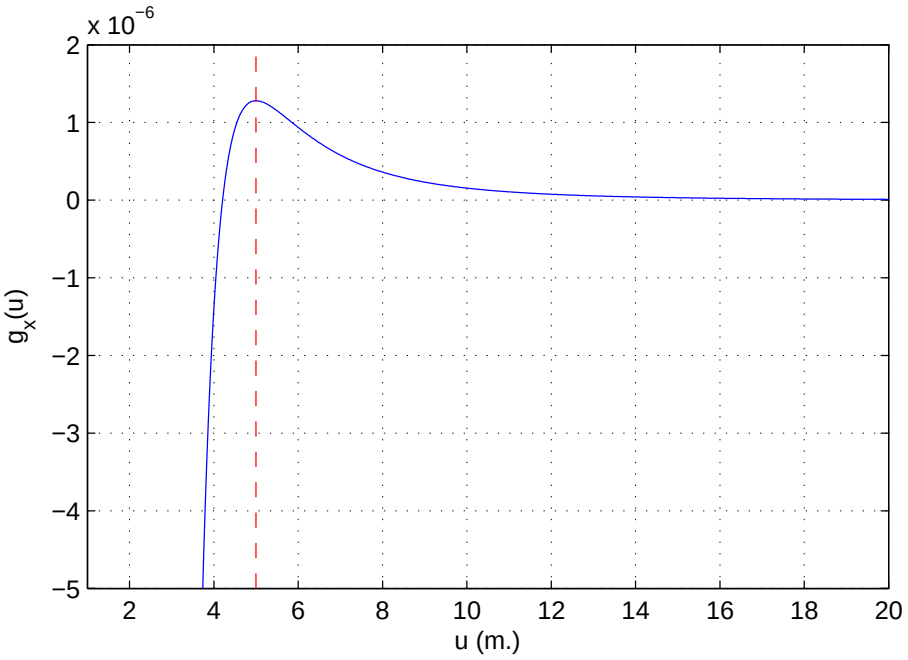

Figure 2.2: Function $g_x(u)$ in (2.46) for $s(t)$ in (2.86), where $x = 5\,\text{m}$, $T_s = 0.1\,\text{ms}$, $f_c = 100\,\text{kHz}$, and $A = 0.1$.

a modified version of the hybrid TOA/RSS based ML estimator is proposed in this section. The *modified hybrid TOA/RSS based estimator* is implemented in two steps:

(i) Obtain the hybrid TOA/RSS based ML estimate $\hat{x}_{\text{ML,hyb}}$ from (2.22).

(ii) Calculate the final distance estimate as

$$\hat{x}_{\text{modi-hyb}} = \left(\frac{\gamma R_p E_2}{\int_{T_1}^{T_2} r(t) s(t - \hat{x}_{\text{ML,hyb}}/c) dt} \right)^{\frac{1}{m+3}}. \tag{2.53}$$

The main intuition behind the modified hybrid TOA/RSS based estimator is as follows: When the estimate $\hat{x}_{\text{ML,hyb}}$ in (2.22) is obtained in the presence of sampling errors, the correlator term $\int_{T_1}^{T_2} r(t) s(t - x/c) dt$ in (2.22) can be evaluated for $x = \hat{x}_{\text{ML,hyb}}$ and then the distance estimate can be obtained with higher resolution by calculating the maximizer of $x^{-m-3} \int_{T_1}^{T_2} r(t) s(t - \hat{x}_{\text{ML,hyb}}/c) dt - 0.5\gamma R_p\, x^{-2m-6} E_2$ as in (2.53) (similar to (2.33)).

Under the conditions in Lemma 4, the MSE of the modified hybrid TOA/RSS

based estimator in (2.53) can be expressed in the absence of noise and for a sampling period of T_{smp} as[6]

$$\text{MSE}_{\text{mod}} = x^2 \left(1 - \left(\rho\big(\tau - \hat{i}T_{\text{smp}}\big)\right)^{\frac{-1}{m+3}}\right)^2 \tag{2.54}$$

where $\hat{i}$ is as in (2.49). It is noted from (2.54) that, similar to the RSS based MLE, the modified hybrid TOA/RSS based estimator is affected from the sampling induced errors through the normalized autocorrelation function, and it is subject to a maximum squared error of $x^2(1 - (\rho(0.5T_{\text{smp}}))^{-1/(m+3)})^2$ due to sampling. Hence, when the normalized autocorrelation function is not very sensitive to timing mismatches, the modified hybrid TOA/RSS based estimator can have robustness against the effects of sampling.

2.4 Ziv-Zakai Bound (ZZB)

The ZZB provides a lower limit on MSEs of estimators based on a relation in terms of the probability of error in a binary hypothesis-testing problem. It is expressed as [31]

$$\xi \geq \frac{1}{2}\int_0^\infty \int_{-\infty}^\infty (w(\vartheta) + w(\vartheta+\delta))\text{P}_{\min}(\vartheta, \vartheta+\delta)d\vartheta\,\delta\,d\delta \tag{2.55}$$

where $\xi = \mathbb{E}\{|\hat{x} - x|^2\}$ is the MSE of an estimator $\hat{x}$, $w(\cdot)$ represents the prior probability density function (PDF) of parameter x, and $\text{P}_{\min}(\vartheta, \vartheta+\delta)$ denotes the probability of error corresponding to the optimal decision rule for the following hypothesis-testing problem:

$$\begin{aligned} \mathcal{H}_0 &: p(r(t)|x = \vartheta) \\ \mathcal{H}_1 &: p(r(t)|x = \vartheta + \delta) \end{aligned} \tag{2.56}$$

In practical indoor scenarios, lower and upper limits on the range parameter x are available based on physical dimensions of the environment and the field of view of the photo detector. Hence, it is reasonable to assume that the prior PDF

[6]The derivation is not presented as it is similar to that in Lemma 3.

of x is zero outside the interval $[D_1, D_2]$, where D_1 and D_2 denote the minimum and maximum possible distances, respectively. (For the signal model in (2.1), the observation interval $[T_1, T_2]$ can be related to D_1 and D_2 as $T_1 = D_1/c$ and $T_2 = D_2/c + T_s$.) In this case, the ZZB in (2.55) is expressed as

$$\xi \geq \frac{1}{2} \int_0^{D_2-D_1} \int_{D_1}^{D_2-\delta} (w(\vartheta) + w(\vartheta+\delta)) \mathrm{P}_{\min}(\vartheta, \vartheta+\delta) d\vartheta \, \delta \, d\delta. \tag{2.57}$$

For example, if the prior PDF of x corresponds to uniform distribution over $[D_1, D_2]$ (that is, $w(x) = 1/(D_2 - D_1)$ if $x \in [D_1, D_2]$ and $w(x) = 0$ otherwise), the ZZB in (2.57) reduces to

$$\xi \geq \frac{1}{D_2 - D_1} \int_0^{D_2-D_1} \int_{D_1}^{D_2-\delta} \mathrm{P}_{\min}(\vartheta, \vartheta+\delta) d\vartheta \, \delta \, d\delta \, . \tag{2.58}$$

To obtain an explicit expression for the ZZB, $\mathrm{P}_{\min}(\vartheta, \vartheta+\delta)$ in (2.57) should be specified. Based on the PDF $w(x)$ of x, the prior probabilities of hypotheses $\mathcal{H}_0$ and $\mathcal{H}_1$ in (2.56) are equal to $w(\vartheta)/(w(\vartheta) + w(\vartheta+\delta))$ and $w(\vartheta+\delta)/(w(\vartheta) + w(\vartheta+\delta))$, respectively. Then, the optimal decision rule for the problem in (2.56) is the MAP rule [122], which is expressed as

$$\frac{w(\vartheta+\delta)}{w(\vartheta) + w(\vartheta+\delta)} p(r(t)|x = \vartheta+\delta) \underset{\mathcal{H}_1}{\overset{\mathcal{H}_0}{\gtrless}} \frac{w(\vartheta)}{w(\vartheta) + w(\vartheta+\delta)} p(r(t)|x = \vartheta) \, . \tag{2.59}$$

After taking the natural logarithm of both sides, (2.59) becomes

$$-\log p(r(t)|x = \vartheta) + \log p(r(t)|x = \vartheta+\delta) \underset{\mathcal{H}_1}{\overset{\mathcal{H}_0}{\lessgtr}} \log \left(\frac{w(\vartheta)}{w(\vartheta+\delta)} \right). \tag{2.60}$$

From (2.1), (2.2), and (2.4), the log-likelihood function is expressed as [120]

$$\log p(r(t)|x) = k - \frac{1}{2\sigma^2} \int_{T_1}^{T_2} \left(r(t) - \frac{R_p \gamma}{x^{m+3}} s\left(t - \frac{x}{c} \right) \right)^2 dt \tag{2.61}$$

where k is a constant that does not depend on x. From (2.61), the decision rule in (2.60) can be stated as

$$\begin{aligned} &\int_{T_1}^{T_2} \left(r(t) - \gamma \, \vartheta^{-m-3} R_p \, s\left(t - \frac{\vartheta}{c} \right) \right)^2 dt \\ &- \int_{T_1}^{T_2} \left(r(t) - \gamma \, (\vartheta+\delta)^{-m-3} R_p \, s\left(t - \frac{\vartheta+\delta}{c} \right) \right)^2 dt \underset{\mathcal{H}_1}{\overset{\mathcal{H}_0}{\lessgtr}} 2\sigma^2 \log \left(\frac{w(\vartheta)}{w(\vartheta+\delta)} \right) \end{aligned}$$

which reduces, via some rearrangement, to

$$\frac{C_{rs}(\vartheta+\delta)}{(\vartheta+\delta)^{m+3}} - \frac{C_{rs}(\vartheta)}{\vartheta^{m+3}} \underset{\mathcal{H}_1}{\overset{\mathcal{H}_0}{\lessgtr}} \frac{R_p\gamma E_2}{2}\left(\frac{1}{(\vartheta+\delta)^{2m+6}} - \frac{1}{\vartheta^{2m+6}}\right) + \frac{\sigma^2}{R_p\gamma}\log\left(\frac{w(\vartheta)}{w(\vartheta+\delta)}\right) \tag{2.62}$$

where

$$C_{rs}(x) \triangleq \int_{T_1}^{T_2} r(t)s\left(t-\frac{x}{c}\right)dt \tag{2.63}$$

and E_2 is given by (2.14).

The probability of error for the decision rule in (2.62) is calculated as

$$\mathrm{P}_{\min}(\vartheta,\vartheta+\delta) = \frac{w(\vartheta)}{w(\vartheta)+w(\vartheta+\delta)}\mathrm{P}\big(\hat{\mathcal{H}}_1|\mathcal{H}_0\big) + \frac{w(\vartheta+\delta)}{w(\vartheta)+w(\vartheta+\delta)}\mathrm{P}\big(\hat{\mathcal{H}}_0|\mathcal{H}_1\big) \tag{2.64}$$

where $\mathrm{P}\big(\hat{\mathcal{H}}_i|\mathcal{H}_j\big)$ denotes the probability of deciding for hypothesis $\mathcal{H}_i$ when $\mathcal{H}_j$ is true. Under $\mathcal{H}_0$, it can be shown from (2.1), (2.4), (2.56), and (2.63) that $C_{rs}(\vartheta)$ and $C_{rs}(\vartheta+\delta)$ are jointly Gaussian distributed as

$$\begin{bmatrix} C_{rs}(\vartheta) \\ C_{rs}(\vartheta+\delta) \end{bmatrix} \sim \mathcal{N}\left(\begin{bmatrix} \frac{\gamma R_p E_2}{\vartheta^{m+3}} \\ \frac{\gamma R_p E_2 \rho(\frac{\delta}{c})}{\vartheta^{m+3}} \end{bmatrix}, \begin{bmatrix} \sigma^2 E_2 & \sigma^2 E_2 \rho\big(\frac{\delta}{c}\big) \\ \sigma^2 E_2 \rho\big(\frac{\delta}{c}\big) & \sigma^2 E_2 \end{bmatrix}\right) \tag{2.65}$$

where $\mathcal{N}(\boldsymbol{\mu},\boldsymbol{\Sigma})$ represents Gaussian distribution with mean $\boldsymbol{\mu}$ and covariance matrix $\boldsymbol{\Sigma}$, and $\rho(\cdot)$ is given by (2.39).

From (2.62) and (2.65), $\mathrm{P}\big(\hat{\mathcal{H}}_1|\mathcal{H}_0\big)$ can be calculated as

$$\mathrm{P}\big(\hat{\mathcal{H}}_1|\mathcal{H}_0\big) = Q\left(\frac{0.5R_p\gamma\, E_2\, g(\vartheta,\vartheta+\delta) + \frac{\sigma^2}{\gamma R_p}\log\left(w(\vartheta)/w(\vartheta+\delta)\right)}{\sqrt{\sigma^2 E_2\, g(\vartheta,\vartheta+\delta)}}\right) \tag{2.66}$$

where $Q(y) = \frac{1}{\sqrt{2\pi}}\int_y^\infty \mathrm{e}^{-t^2/2}dt$ denotes the Q-function, and

$$g(\vartheta,\vartheta+\delta) \triangleq \frac{1}{(\vartheta+\delta)^{2m+6}} + \frac{1}{\vartheta^{2m+6}} - \frac{2\rho(\delta/c)}{(\vartheta(\vartheta+\delta))^{m+3}}\,. \tag{2.67}$$

Also, via similar derivations, $\mathrm{P}\big(\hat{\mathcal{H}}_0|\mathcal{H}_1\big)$ can be obtained as follows:

$$\mathrm{P}\big(\hat{\mathcal{H}}_0|\mathcal{H}_1\big) = Q\left(\frac{0.5R_p\gamma\, E_2\, g(\vartheta,\vartheta+\delta) - \frac{\sigma^2}{\gamma R_p}\log\left(w(\vartheta)/w(\vartheta+\delta)\right)}{\sqrt{\sigma^2 E_2\, g(\vartheta,\vartheta+\delta)}}\right). \tag{2.68}$$

Then, the probability of error for the decision rule in (2.62) can be evaluated via (2.64), (2.66), and (2.68), which can be expressed in a compact form as follows:

$$\mathrm{P}_{\min}(\vartheta, \vartheta+\delta) = \frac{\sum_{i=0}^{1} w(\vartheta+i\delta)\mathrm{P}\big(\hat{\mathcal{H}}_{1-i}|\mathcal{H}_i\big)}{w(\vartheta)+w(\vartheta+\delta)}\,. \tag{2.69}$$

Based on the obtained minimum probability of error expression in (2.69), the ZZB in (2.57) can be calculated.

As a special case, when the prior PDF of x is uniform over $[D_1, D_2]$, the logarithm terms in (2.66) and (2.68) become zero, and $\mathrm{P}_{\min}(\vartheta, \vartheta+\delta)$ in (2.69) can be simplified as follows:

$$\mathrm{P}_{\min}(\vartheta, \vartheta+\delta) = 0.5\,\mathrm{P}\big(\hat{\mathcal{H}}_1|\mathcal{H}_0\big) + 0.5\,\mathrm{P}\big(\hat{\mathcal{H}}_0|\mathcal{H}_1\big) = Q\left(\frac{R_p\gamma\sqrt{E_2}\sqrt{g(\vartheta, \vartheta+\delta)}}{2\sigma}\right). \tag{2.70}$$

For the uniform prior case, the ZZB can be calculated based on (2.58) and (2.70).

Since the integral limits in (2.57) and (2.58) are finite, the ZZB can accurately be evaluated via numerical approaches. From (2.57), (2.66), (2.68), and (2.69), it is observed that the ZZB reduces as E_2 increases; that is, improved ranging accuracy is achieved with higher transmitted signal energy, as expected. It is also noted that the ZZB expression in (2.57) and (2.69) is different from both the ZZB expression in asynchronous VLP systems [32] since the range related information from both the time delay parameter and the channel attenuation factor is employed in the synchronous case.

Remark 4. It is important to emphasize that the ZZB expression in (2.57) and (2.69) has important distinctions compared to the ZZB expressions for synchronous RF based ranging systems (e.g., [30]) due to the facts that (i) the synchronous VLP system utilizes both time delay and received signal power (channel attenuation factor) information whereas synchronous RF systems use time delay information only (since the received power parameter carries negligible information compared to the time delay parameter in most practical RF localization systems), and (ii) the Lambertian equation in (2.4) is available for VLP systems to relate the channel attenuation factor (the received signal power) to distance

x in LOS visible light channels, which is not valid for RF systems. Overall, the Lambertian formula is utilized, together with the time delay information and the prior information, for the purpose of range estimation in this study.

2.5 ECRB Derivations

In this section, the Cramér-Rao bound (CRB) expressions for range estimation in VLP systems are investigated to provide comparisons against the ZZB.

For a given value of the unknown parameter, the *conditional CRB* presents a lower limit on the MSEs of unbiased estimators, which is expressed as [31]

$$\mathbb{E}\{|\hat{x}-x|^2\} \geq \left(\mathbb{E}\left\{ \left(\frac{\partial \log p(r(t)|x)}{\partial x} \right)^2 \right\} \right)^{-1} \triangleq (\mathrm{J_F}(x))^{-1} = \mathrm{CRB}(x) \tag{2.71}$$

where $\hat{x}$ is an unbiased estimate of x and the expectation operators are conditioned on x. For the estimation of the range parameter x, the conditional CRB in the synchronous case can be obtained from (2.71) as [16]

$$\mathrm{CRB}(x) = (\mathrm{J_F}(x))^{-1} = \frac{(\sigma x^{m+4}/(\gamma\, R_p))^2}{(m+3)^2 E_2 + \tilde{E}_s (x/c)^2} \tag{2.72}$$

where $\tilde{E}_s \triangleq \int_0^{T_s} (s'(t))^2 dt$, with $s'(t)$ denoting the first-order derivative of $s(t)$.[7] The conditional CRB expression in (2.72) is a function of the unknown parameter x, and no prior information is considered in the derivation of this bound.

The expectation of the conditional CRB (ECRB) is obtained by calculating the average of the conditional CRB over the prior distribution of the unknown parameter [31], which results in the following expression for the considered scenario:

$$\mathrm{ECRB} = \mathbb{E}\left\{\mathrm{CRB}(x)\right\} = \int_{D_1}^{D_2} w(x)\mathrm{CRB}(x)\, dx \tag{2.73}$$

[7]For the expression in (2.72), it is assumed that $s(0) = s(T_s)$, which is commonly the case [16].

where CRB(x) denotes the conditional CRB in (2.72), and $w(x)$ is the prior PDF of x, which is zero outside $[D_1, D_2]$. For the uniform prior PDF, the ECRB is specified as in the following lemma:

Lemma 5. *Suppose that the prior PDF of x is specified by a uniform distribution over $[D_1, D_2]$. Then, the ECRB in the synchronous case is given by*

$$\text{ECRB} = \frac{(\sigma/(\gamma\, R_p))^2}{(D_2 - D_1)\tilde{E}_s/c^2} \int_{D_1}^{D_2} \frac{x^{2m+8}}{x^2 + a}\, dx \tag{2.74}$$

with $a \triangleq (m+3)^2 c^2 E_2/\tilde{E}_s$, which can be stated as in the following expression when $2m$ is an integer:

$$\begin{aligned}\text{ECRB} = \frac{(\sigma/(\gamma\, R_p))^2}{(D_2 - D_1)\tilde{E}_s/c^2} \Bigg(& (-a)^{\lfloor m+3 \rfloor + 1} H_m(D_1, D_2, a) \\ & + \sum_{i=0}^{\lfloor m+3 \rfloor} \frac{(-a)^i \big(D_2^{2(m+3-i)+1} - D_1^{2(m+3-i)+1}\big)}{2(m+3-i)+1} \Bigg)\end{aligned} \tag{2.75}$$

where

$$H_m(D_1, D_2, a) \triangleq \begin{cases} \left(\tan^{-1}(D_2/\sqrt{a}) - \tan^{-1}(D_1/\sqrt{a})\right)/\sqrt{a}\,, & \text{if } m \in \mathbb{Z}^+ \\ 0.5\left(\ln(D_2^2 + a) - \ln(D_1^2 + a)\right), & \text{if } 2m \in \mathbb{Z}^+ \;\&\; m \notin \mathbb{Z}^+ \end{cases} \tag{2.76}$$

Proof: The generic expression in (2.74) directly follows from (2.72) and (2.73). To derive the specific expressions in (2.75) and (2.76), consider the division of x^{2m+8} by $x^2 + a$, which results in the following relation:

$$x^{2m+8} = (x^2 + a) \sum_{i=0}^{j} (-a)^i x^{2(m+3-i)} - (-1)^j a^{j+1} x^{2(m+3-j)} \tag{2.77}$$

where $j \leq m+3$ is an integer. Then, the integral in (2.74) becomes

$$\int_{D_1}^{D_2} \frac{x^{2m+8}}{x^2 + a}\, dx = \int_{D_1}^{D_2} \sum_{i=0}^{j} (-a)^i x^{2(m+3-i)}\, dx - (-1)^j a^{j+1} \int_{D_1}^{D_2} \frac{x^{2(m+3-j)}}{x^2 + a}\, dx\,. \tag{2.78}$$

If m is a positive integer, $j = m+3$ can be employed to obtain the result specified by (2.75) and the first part of (2.76). (Note that the last integral term in (2.78)

becomes $\int_{D_1}^{D_2}(x^2+a)^{-1}dx$ in this case, which leads to the $\tan^{-1}$ terms in (2.76).) Similarly, if m is not an integer but $2m$ is a positive integer, then $j = \lfloor m+3 \rfloor$ can be used to derive the expression specified by (2.75) and the second part of (2.76). (Note that the last integral term in (2.78) becomes $\int_{D_1}^{D_2} x\,(x^2+a)^{-1}dx$ in this case, which results in the logarithm terms in (2.76).) ■

The ECRB may not provide a lower bound on the performance of MAP estimators since the conditional CRBs, which are the basis for the ECRB as described above, do not take the prior information into account [31]. However, at high SNRs, the ECRB can converge to the ZZB, which is expected since the prior information becomes negligible compared to the information gathered from the measurements in high SNR conditions. Overall, the ECRB provides useful benchmarks for comparisons against the ZZB and helps quantify the range related information gathered from prior information, as investigated in Section 2.7. In addition, the ECRB expressions provide a low-complexity approach (compared to the ZZB expressions) for calculating the theoretical limits on range estimation in high SNR scenarios.

2.6 Bayesian CRB (BCRB) and Weighted CRB (WCRB)

In order to incorporate the prior information into the lower bound effectively, the *Bayesian CRB (BCRB)* can be considered [31]. The BCRB is expressed as

$$\xi \geq \left(\mathbb{E}\left\{ \left(\frac{\partial \log p(r(t)|x)}{\partial x} \right)^2 \right\} + \mathbb{E}\left\{ \left(\frac{\partial \log w(x)}{\partial x} \right)^2 \right\} \right)^{-1} \tag{2.79}$$

where $\xi = \mathbb{E}\{|\hat{x}-x|^2\}$ denotes the MSE of an estimator $\hat{x}$ [31]. In (2.79), the first expectation operator is with respect to both $r(t)$ and x while the second expectation is over parameter x only. From (2.71) and (2.72), the first term in

(2.79) can be calculated as follows:

$$\mathbb{E}\left\{\left(\frac{\partial \log p(r(t)|x)}{\partial x}\right)^2\right\} = \mathbb{E}\left\{\mathrm{J_F}(x)\right\} = \int_{D_1}^{D_2} w(x)\frac{(m+3)^2 E_2 + \tilde{E}_s(x/c)^2}{(\sigma x^{m+4}/(\gamma\, R_p))^2}\, dx\,. \tag{2.80}$$

For a given prior PDF, the BCRB can be obtained based on (2.79) and (2.80). One of the limitations of the BCRB is due to the existence and absolute integrability requirement for the partial derivative of the joint PDF of the observation and the parameter [31]. Therefore, it may not be applicable in some scenarios. For example, when the range parameter is uniformly distributed over $[D_1, D_2]$, the BCRB does not exist.

The *weighted CRB (WCRB)* provides an alternative to the BCRB and handles the existence problem. It is defined as [31]

$$\xi \geq \frac{\left(\mathbb{E}\{q(x)\}\right)^2}{\mathbb{E}\{q^2(x)\mathrm{J_F}(x)\} + \mathbb{E}\left\{q^2(x)\left(\frac{d\log(w(x)q(x))}{dx}\right)^2\right\}} \tag{2.81}$$

where ξ is the MSE of any estimator, $\mathrm{J_F}(x)$ is as in (2.71), $q(x)$ is a weighting function, and the expectations are with respect to x. As in [31], the following weighting function can be employed:

$$q(x) = \left(\frac{x - D_1}{D_2 - D_1}\right)^{\nu}\left(1 - \frac{x - D_1}{D_2 - D_1}\right)^{\nu} \tag{2.82}$$

for $x \in [D_1, D_2]$ and $q(x) = 0$ otherwise, where ν is a parameter used to enhance the bound. Namely, the value of ν that maximizes the bound in (2.81) is employed to obtain the tightest bound. For the uniform prior PDF, $\mathbb{E}\{q(x)\}$ in (2.81) is calculated from (2.82) as follows:

$$\mathbb{E}\{q(x)\} = \frac{1}{D_2 - D_1}\int_{D_1}^{D_2} q(x)dx = \beta(\nu+1, \nu+1) \tag{2.83}$$

where $\beta(a,b) \triangleq \int_0^1 x^{a-1}(1-x)^{b-1}dx$ denotes the beta function. In addition, the second term in the denominator of (2.81) can be expressed for the uniform prior PDF as [32]

$$\mathbb{E}\left\{q^2(x)\left(\frac{d\log(w(x)q(x))}{dx}\right)^2\right\} = \frac{\nu\,\beta(2\nu+1, 2\nu-1)}{(D_2 - D_1)^2}\,. \tag{2.84}$$

Also, the first term in the denominator of (2.81) can be calculated based on (2.72) and (2.82) as

$$\mathbb{E}\left\{q^2(x)\mathrm{J_F}(x)\right\} = \frac{\gamma^2 R_p^2/\sigma^2}{(D_2-D_1)^{4\nu+1}} \times \left((m+3)^2 E_2 \int_{D_1}^{D_2} \frac{(x-D_1)^{2\nu}(D_2-x)^{2\nu}}{x^{2\nu+8}}\,dx + \frac{\tilde{E}_2}{c^2}\int_{D_1}^{D_2} \frac{(x-D_1)^{2\nu}(D_2-x)^{2\nu}}{x^{2m+6}}\,dx\right). \tag{2.85}$$

Then, the WCRB in (2.81) can be evaluated via (2.83)–(2.85). In order to obtain the tightest bound, the value of ν that yields the maximum lower bound is obtained.

Remark 5. The theoretical limits obtained in this study do not consider the effects of multipath (see (2.1)). In the presence of multipath propagation, higher MSEs would be observed in general; hence, the lower bounds for the LOS scenario provided in this chapter present lower limits for the multipath scenario, as well. The tightness of the bounds depends on the severity of multipath effects.

2.7 Numerical Results

In this section, numerical examples are presented to investigate the theoretical limits and the statistical estimators for different approaches.

2.7.1 Results for CRLBs and ML Estimators

A system model similar to that in [23] is considered. Namely, the Lambertian order is taken as $m = 1$, h in (2.4) is set to 2.5 meters, and the responsivity of the photo detector is given by $R_p = 0.4\,\mathrm{mA/mW}$. In addition, the area S of the photo detector at the VLC receiver is equal to $1\,\mathrm{cm}^2$, and the spectral density level of the noise is set to $\sigma^2 = 1.336 \times 10^{-22}\,\mathrm{W/Hz}$ based on the employed parameters

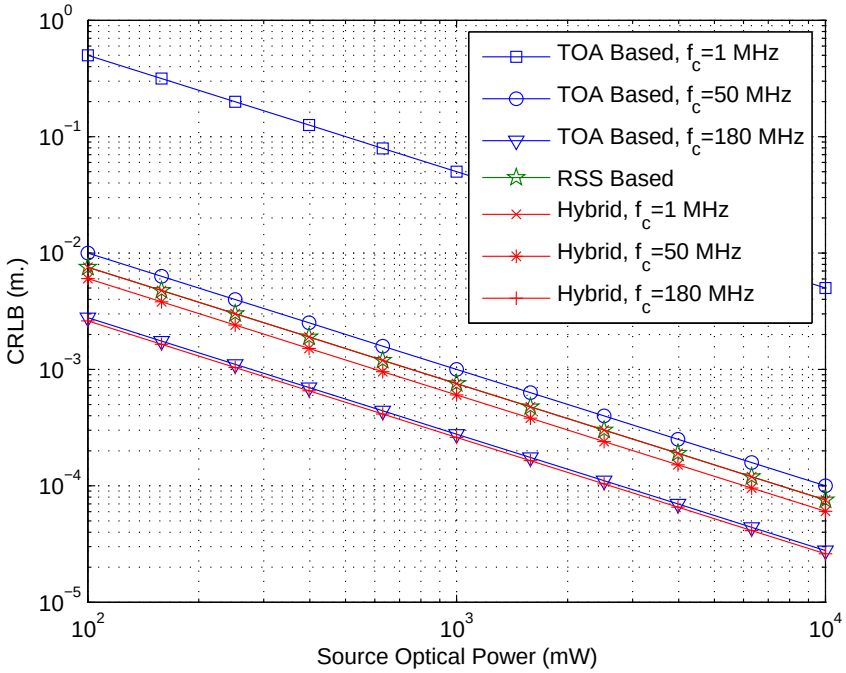

Figure 2.3: CRLB versus source optical power for TOA based, hybrid TOA/RSS based, and RSS based approaches, where $x = 5\,\text{m}.$ and $T_s = 0.01\,\text{s}.$

in [23].[8] Signal $s(t)$ in (2.1) is modeled as follows [23]:

$$s(t) = A\left(1 - \cos\left(\frac{2\pi t}{T_s}\right)\right)(1 + \cos(2\pi f_c t)) \tag{2.86}$$

for $t \in [0, T_s]$, where f_c is the center frequency, and A corresponds to the average emitted optical power (i.e., source optical power). For $f_c \gg 1/T_s$, it can be shown that the electrical energy of $s(t)$ defined in (2.14) and the effective bandwidth of $s(t)$ specified by (2.15) can be approximated as $E_2 = 9A^2T_s/4$ and $\beta = f_c/\sqrt{3}$, respectively [23]. In addition, parameter E_3 in (2.18) is obtained as $E_3 = 0$ for the signal in (2.86).

First, the CRLBs are calculated for $T_s = 0.01\,\text{s}.$ when the distance between the LED transmitter and the VLC receiver is given by $x = 5\,\text{m}.$ In Fig. 2.3,

[8]From (18) in [23], $\sigma^2 = qR_p p_n S\Delta\lambda$, where q denotes the charge on an electron, $p_n = 5.8\times10^{-6}\,\text{W/cm}^2\text{.nm}$ is the background spectral irradiance, and $\Delta\lambda = 360\,\text{nm}$ is the bandwidth of the optical filter in front of the photodiode. (It should be noted that the results in the previous sections are valid for a generic zero-mean Gaussian noise component, which can consist of any types of noise such as shot noise and thermal noise.)

the CRLBs are plotted versus the source optical power A for the TOA based, hybrid TOA/RSS based, and RSS based approaches considering different center frequencies. As expected, the hybrid TOA/RSS approach achieves the minimum CRLB in all cases since it utilizes information from both the time delay and channel attenuation factor. It is also noted that the performance of the RSS based distance estimation does not depend on the center frequency. This is due to the fact that RSS information is related to the energy of the signal but does not change with the other signal characteristics, which can be observed from (2.34) in Lemma 2 for $E_3 = 0$; that is, $\mathrm{CRLB}_{\mathrm{RSS}} = \sigma^2 x^2/(E_2 \alpha^2 R_p^2 (m+3)^2)$. Another observation from Fig. 2.3 is that the TOA based distance estimation has significantly higher CRLBs than the other approaches for relatively low center frequencies, for which the RSS based and hybrid TOA/RSS based approaches achieve almost the same accuracy (as the distance related information obtained from the TOA parameter becomes negligible). On the other hand, the TOA based distance estimation achieves lower CRLBs than the RSS based approach for high center frequencies; e.g., $f_c = 180\,\mathrm{MHz}$ [6, 125]. In that case, the information obtained from the TOA parameter becomes more significant than that extracted from the RSS parameter (channel attenuation factor), and the TOA based and hybrid TOA/RSS based approaches have almost the same performance. All these observations are in accordance with the relation in Proposition 2.

In order to provide further insights, the theoretical limits are plotted versus f_c in Fig. 2.4 for the TOA based, hybrid TOA/RSS based, and RSS based approaches, where $x = 5\,\mathrm{m}.$ and $A = 0.1$. It is observed that the accuracy of the TOA based distance estimation improves with f_c since E_1 in (2.13) increases with f_c. Also, there exists a critical frequency, which is equal to 66.16 MHz in this scenario, after (before) which the TOA based distance estimation achieves a lower (higher) CRLB than the RSS based approach. It is also noted that the hybrid TOA/RSS based approach provides nonnegligible improvements over both the TOA based and RSS based approaches around that critical frequency.

Next, the CRLBs are plotted versus the signal duration T_s in Fig. 2.5 for the TOA based, hybrid TOA/RSS based, and RSS based approaches, where $x = 5\,\mathrm{m}.$ and $A = 0.1$. As the signal energy increases with T_s (note that $E_2 = 9A^2 T_s/4$), the

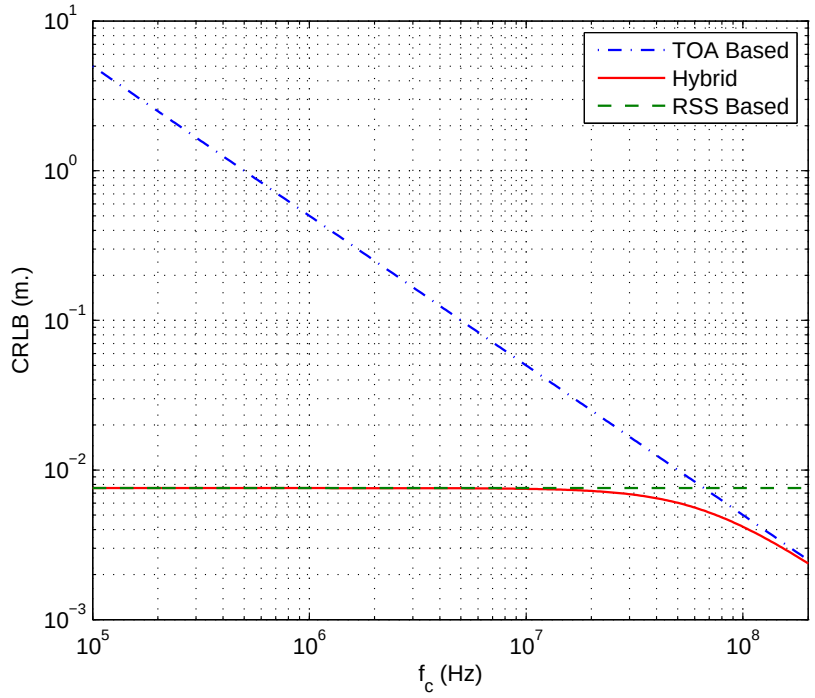

Figure 2.4: CRLB versus f_c for TOA based, hybrid TOA/RSS based, and RSS based approaches, where $x = 5\,\text{m.}$ and $A = 0.1$.

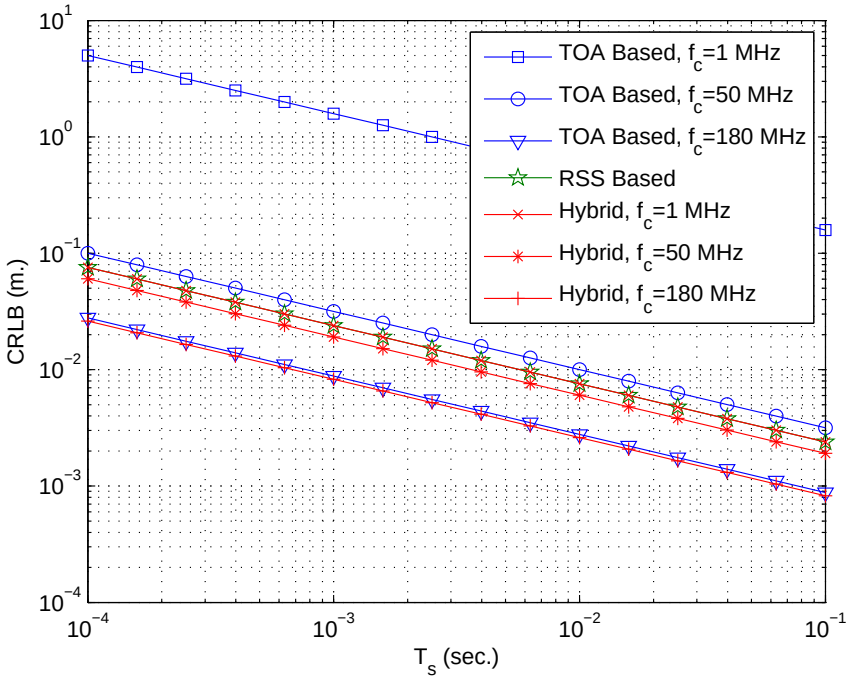

Figure 2.5: CRLB versus T_s for TOA based, hybrid TOA/RSS based, and RSS based approaches, where $x = 5\,\text{m.}$ and $A = 0.1$.

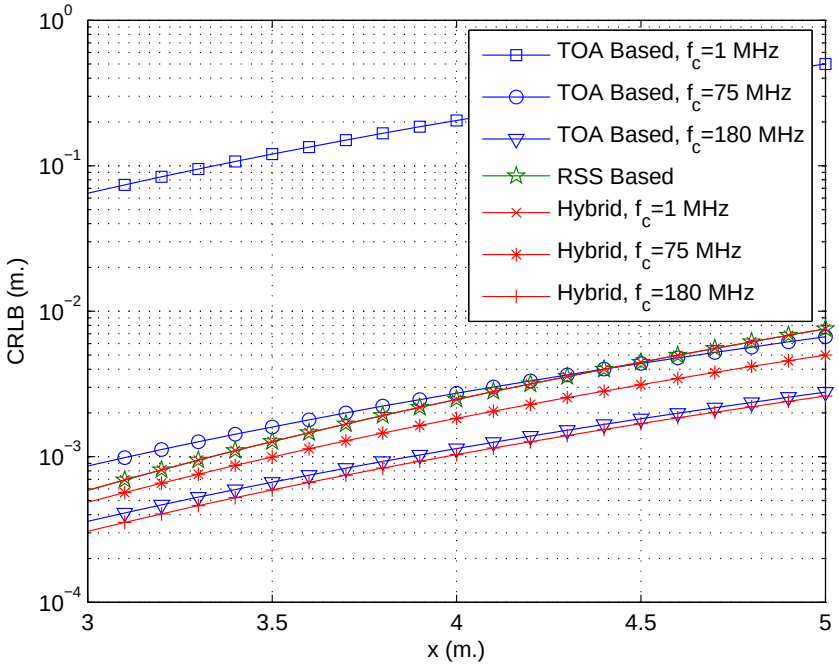

Figure 2.6: CRLB versus distance x for TOA based, hybrid TOA/RSS based, and RSS based approaches, where $T_s = 0.01\,\text{s}.$ and $A = 0.1$.

performance of distance estimation improves with T_s, as expected. As in Fig. 2.3, it is observed that the TOA based distance estimation achieves lower (higher) CRLBs than RSS based distance estimation for higher (lower) center frequencies. It is also noted that for the RSS based distance estimation to achieve a CRLB of 1 cm, the signal duration should be around 6 ms. On the other hand, shorter signal durations can be employed by the TOA based and hybrid TOA/RSS based approaches for high center frequencies (e.g., $T_s \approx 0.6-0.7\,\text{ms}.$ for $f_c = 180\,\text{MHz}.$).

In Fig. 2.6, the CRLBs are plotted versus the distance x between the LED transmitter and the VLC receiver for $f_c = 1\,\text{MHz}$, $f_c = 75\,\text{MHz}$, and $f_c = 180\,\text{MHz}$, where $T_s = 0.01\,\text{s}.$ and $A = 0.1$. It is intuitive that the estimation accuracy degrades (i.e., the CRLBs increase) as the distance gets larger. This intuitive observation is also verified by the expressions in (2.12), (2.25), and (2.34) via the relations in (2.4) and (2.24). Also, it is noted from Fig. 2.6 that in some cases (e.g., for $f_c = 75\,\text{MHz}$) the RSS based distance estimation can have lower

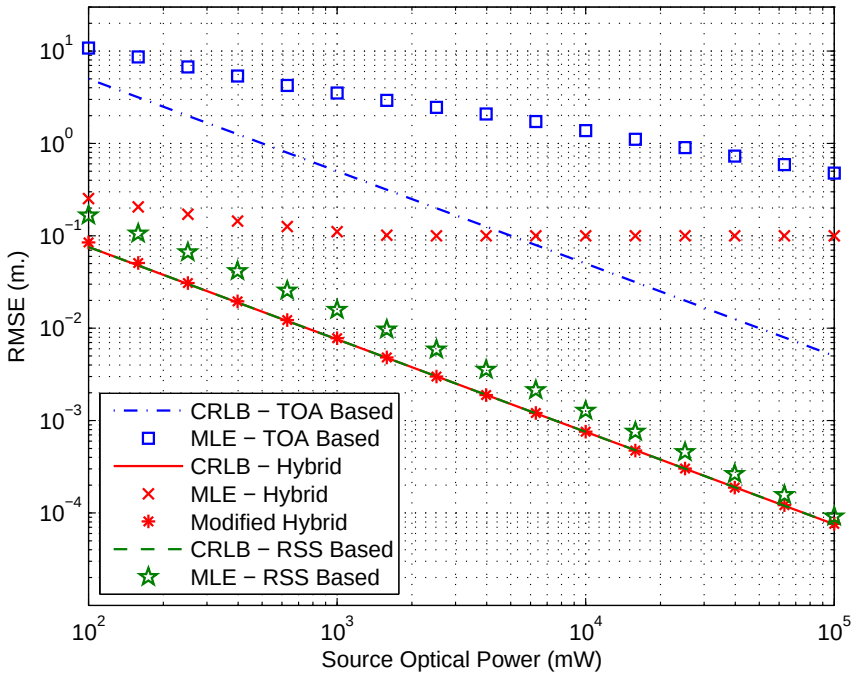

Figure 2.7: RMSEs of the MLEs and the CRLBs for different approaches, where $x = 5\,\text{m.}$, $T_s = 0.1\,\text{ms.}$ $f_c = 1\,\text{MHz}$, and $T_{\text{smp}} = 1\,\text{ns.}$

CRLBs than the TOA based approach up to a certain distance and then it results in higher CRLBs after that distance. This is due to fact that the CRLB (in meters) increases with x^{m+4} for the RSS based approach whereas it increases with x^{m+3} for the TOA based approach, as can be deduced from (2.4), (2.12), and (2.34).

It should be emphasized that although the comparisons in Figs. 2.3-2.6 are based on the CRLBs (i.e., the distance estimation accuracy), implementation complexity should also be considered for practical applications. As stated in Remark 2, the RSS based distance estimation has an important practical advantage over the other approaches since it does not require synchronization between the clocks of the LED transmitter and the VLC receiver. Hence, if the RSS based distance estimation can provide the required level of accuracy for an application, it can be the preferred approach. Otherwise, a synchronized system design may be required for achieving the desired accuracy level for distance estimation.

Finally, the MLEs in Sections 2.2 and 2.3 are implemented and compared for a scenario with $x = 5\,\text{m.}$, $T_s = 0.1\,\text{ms}$, $f_c = 1\,\text{MHz}$, $\Delta = 0$ (see (2.2)), and $T_{\text{smp}} = 1\,\text{ns}$. In Fig. 2.7, the RMSEs of the TOA based MLE in (2.9), the hybrid TOA/RSS based MLE in (2.22), the RSS based MLE in (2.33), and the modified hybrid TOA/RSS based estimator in (2.53) are illustrated along with the CRLBs.[9] As expected from the analysis in Section 2.3, the TOA based MLE and the hybrid TOA/RSS based MLE are directly affected by the sampling rate limitation and their RMSEs converge towards 0.1 m. in accordance with (2.40) and (2.48). On the other hand, the asymptotic RMSEs of the RSS based MLE and the modified hybrid TOA/RSS based estimator are calculated from (2.41) and (2.54) as $9.14 \times 10^{-7}\,\text{m.}$, which is outside the practical accuracy range. Hence, the sampling rate limitation does not have any significant effects on these estimators in this scenario. It is also noted that the modified hybrid TOA/RSS based estimator converges to the CRLB faster than the RSS based MLE, and achieves the best performance for all power levels of interest. In addition, the hybrid TOA/RSS based MLE has lower CRLBs than the TOA based MLE since it utilizes both the time delay and RSS information. In Fig. 2.8, the RMSEs of the MLEs are plotted versus T_{smp} in the absence of noise to investigate the effects of the sampling period, where $x = 5\,\text{m.}$, $T_s = 0.1\,\text{ms}$, $f_c = 1\,\text{MHz}$, and $\Delta = 0$. In the figure, the sampling period T_{smp} is incremented with a step size of $10^{-12}\,\text{s}$. It is observed that the RMSEs of the MLEs fluctuate as T_{smp} changes, which is due to the fact that the RMSE converges towards zero as the distance, x, gets close to an integer multiple of cT_{smp} (where c is the speed of light). This observation can also be verified based on (2.40), (2.41), (2.48), and (2.54). In addition, Fig. 2.8 indicates that the local averages of the RMSEs reduce in general as the sampling rate increases (i.e., as T_{smp} decreases). Furthermore, the asymptotic RMSEs of the modified hybrid TOA/RSS based MLE and the RSS based MLE are observed to be outside the practical accuracy limits whereas those of the TOA based MLE and the hybrid TOA/RSS based MLE are in the range of practical accuracy limits. Hence, the sampling rate limitation can be crucial for the TOA based

[9] The search space for possible distance values is set to $[0, 100]\,\text{m.}$ for all the estimators. Therefore, the MLEs in Fig. 2.7 can also be considered as MAP estimators [122] for a uniform prior distribution of x over $[0, 100]\,\text{m.}$

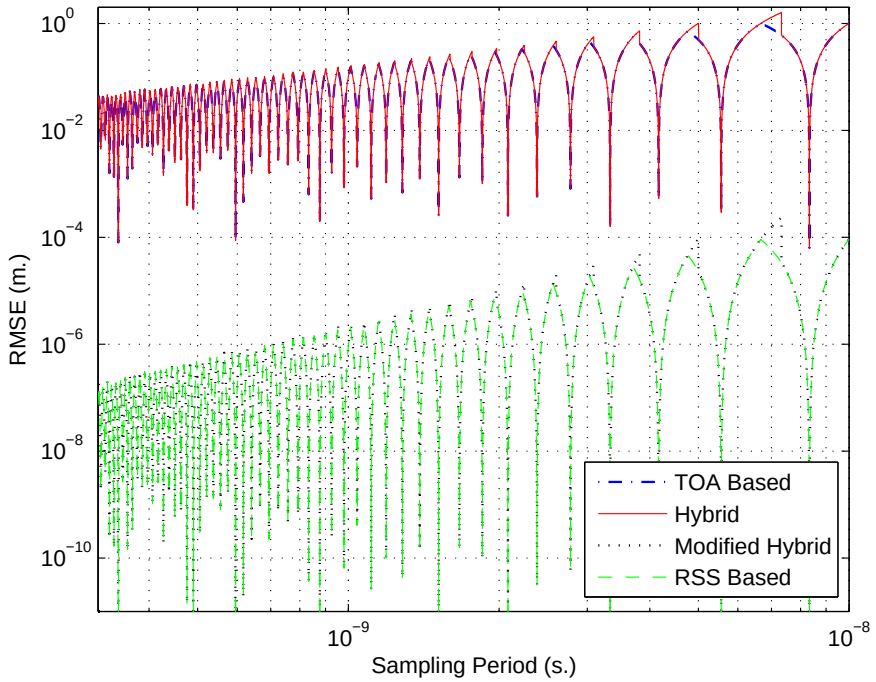

Figure 2.8: RMSEs of the MLEs for different approaches in the absence of noise, where $x = 5\,\text{m.}$, $T_s = 0.1\,\text{ms.}$, and $f_c = 1\,\text{MHz}$.

MLE and the hybrid TOA/RSS based MLE.

2.7.2 Results for ZZB, ECRB, WCRB, and MAP Estimators

To illustrate the results for ZZB, ECRB, WCRB, and MAP estimators, we consider a new scenario where h in (2.4) is set to 5 m. and the prior PDF of the distance, x, is taken to be uniform over the interval $[D_1, D_2]$, where $D_1 = 5\,\text{m.}$ and $D_2 = 10\,\text{m.}$ (cf. (2.57) and (2.58)).

In the first example, $T_s = 0.1\,\text{ms.}$, $f_c = 1\,\text{MHz}$, and the area S of the photo detector at the VLC receiver is set to $1\,\text{cm}^2$. In Fig. 2.9, the ZZBs in Section 2.4 are plotted versus the source optical power A in (2.86) for various values of the Lambertian order m. It is observed that the ranging accuracy degrades as m increases for practical values of the source optical power. Although the exact

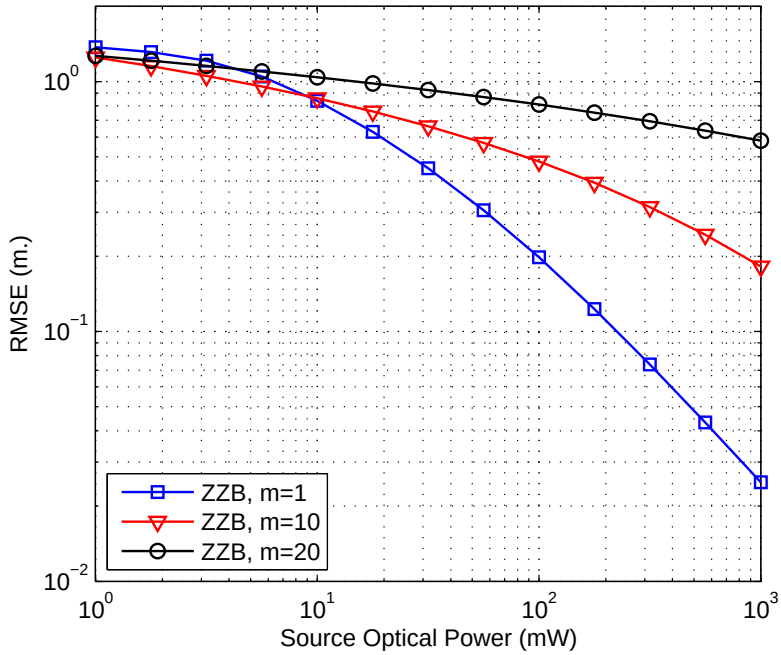

Figure 2.9: ZZB versus source optical power for various values of the Lambertian order, where $S = 1\,\mathrm{cm}^2$.

relation between the ZZB and m can be deduced from (2.5), (2.58), and (2.70), an intuitive explanation can also be provided as follows: Parameter m determines the directionality of the LED transmitter, and a large value of m corresponds to a fast power decay as the irradiation angle increases from zero (see (2.3)). Hence, lower SNRs are expected at higher distances for larger values of m, which can lead to higher ZZBs, as observed in Fig. 2.9.

In Fig. 2.10, the ZZBs in Section 2.4 are presented versus the source optical power for various values of S, the area of the photo detector at the VLC receiver, where $T_s = 0.1\,\mathrm{ms.}$, $f_c = 1\,\mathrm{MHz}$, and $m = 10$ are employed. From the figure, it is observed that the ZZB increases (i.e., the estimation accuracy degrades) as S decreases. This observation can be explained based on the ZZB expression in (2.58) and (2.70) as follows: From (2.5), γ is proportional to S, and from eqn. (18) in [23], σ is proportional to $\sqrt{S}$. Hence, the γ/σ term in (2.70) changes in proportion to $\sqrt{S}$, which leads to lower ZZBs as S increases due to the monotone decreasing nature of the Q-function. In other words, as the area of the photo

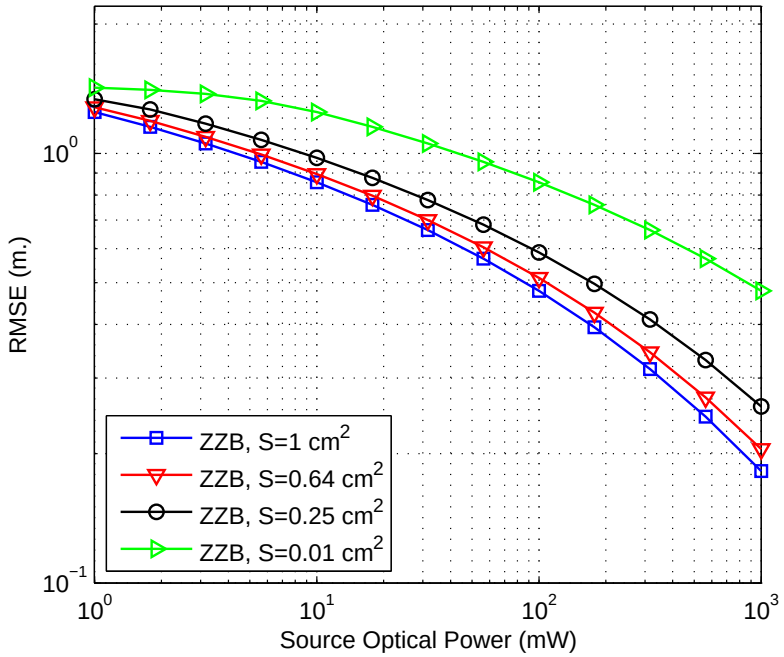

Figure 2.10: ZZB versus source optical power for various values of the area of the photo detector, where $m = 10$.

detector increases, higher SNRs are obtained at the VLC receiver and lower ZZBs are achieved.

Next, the ZZB in Section 2.4, the ECRB in Section 2.5, and the WCRB in Section 2.6 are investigated in Fig. 2.11, together with the performance of the MAP estimator, where $T_s = 0.1\,\text{ms.}$, $f_c = 1\,\text{MHz}$, $S = 1\,\text{cm}^2$, and $m = 1$. The MAP estimator can be obtained based on the ML estimator in [16, eqn. (18)] by confining the search space for the distance parameter x to the interval $[D_1, D_2]$ (since the prior distribution of x is uniform over $[D_1, D_2]$) with $D_1 = 5\,\text{m.}$ and $D_2 = 10\,\text{m.}$ Fig. 2.11 shows that the ECRB converges to the ZZB at high source optical powers; i.e., at high SNRs, since the prior information becomes less important as the SNR increases. However, for lower optical powers, the ECRB gets significantly higher than the ZZB since the ECRB calculations do not effectively utilize the prior information, which becomes significant in the low SNR regime.[10] On the

[10]In the ECRB calculations in (2.73), the prior information is used to calculate the average of the conditional CRBs; however, each conditional CRB expression is obtained without utilizing

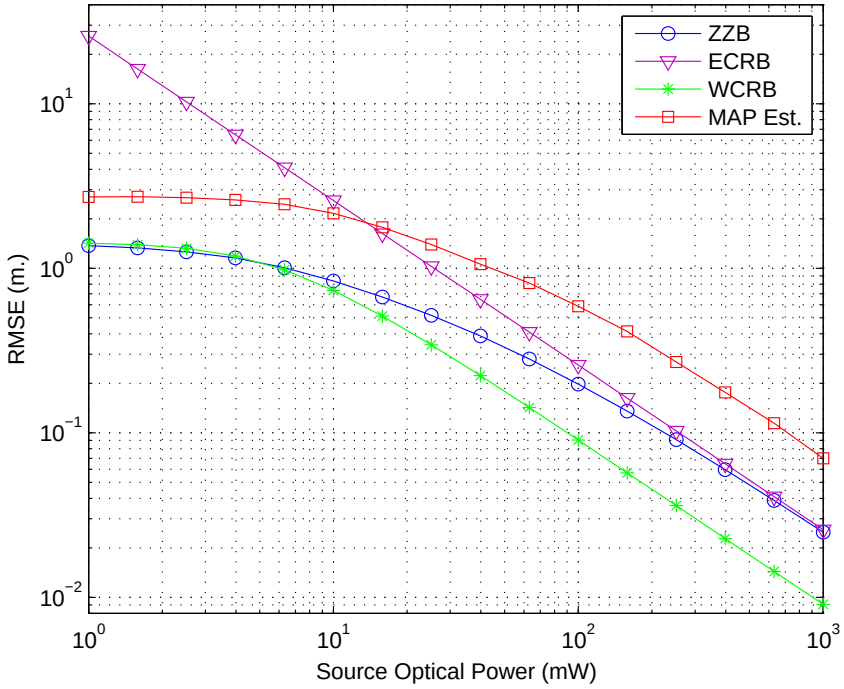

Figure 2.11: RMSE versus source optical power for the MAP estimator, the ZZB, the ECRB, and the WCRB, where $T_s = 0.1\,\text{ms.}$, $f_c = 1\,\text{MHz}$, $S = 1\,\text{cm}^2$, and $m = 1$.

other hand, the WCRB is close to the ZZB at low SNRs but it becomes looser as the SNR increases. The main reason for this behavior is that the WCRB (and the BCRB) may not provide a tight bound at high SNRs when the conditional Fisher information depends on the unknown parameter [31, p. 7], which is the case for the considered VLP system (that is, the conditional Fisher information in (2.72) depends on the unknown parameter x, the distance between the LED transmitter and the VLC receiver). In addition, it is observed from Fig. 2.11 that the ZZB provides a reasonably tight bound for the performance of the MAP estimator in all SNR regions. Furthermore, since the MAP estimator utilizes the prior information, its performance cannot be lower bounded by the ECRB in the low SNR regime, which does not effectively utilize the prior information. Therefore, the ECRB expression can provide useful lower bounds only in the high SNR regime, where the prior information is not crucial in the estimation process compared to the information obtained from the received signal.

In the final example, the same parameters as in the previous scenario are employed except that a larger value of f_c is used, namely, $f_c = 50\,\text{MHz}$. The results presented in Fig. 2.12 illustrate that the RMSEs are reduced (i.e., the ranging performance is improved) in the medium and high SNR regimes compared to the previous scenario, which can be explained as follows: In a synchronous VLP system, in addition to the prior information, information from both the time delay parameter and the channel attenuation factor can be utilized for range estimation. Since the information gathered from the time delay parameter increases with f_c [16], improved estimation performance can be observed at sufficiently high SNRs, where the prior information becomes less significant than the information gathered from the time delay parameter and the channel attenuation factor. However, in the low SNR regime, the prior information becomes the most significant source of information, which leads to similar performance for the MAP estimators in Fig. 2.11 and Fig. 2.12. In addition, it is noted from Fig. 2.12 that the MAP estimator cannot get very close to the theoretical limits at high SNRs, which is due to the finite sampling rate (namely, $10^{-11}\,\text{s.}$) employed in the simulations. In

the prior information. Hence, the ECRBs do not effectively utilize the prior information.

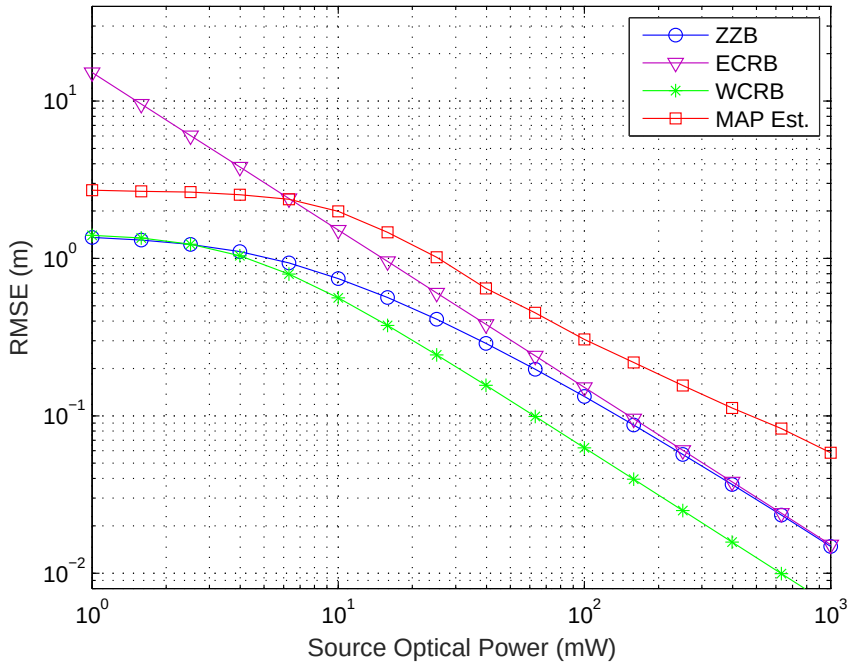

Figure 2.12: RMSE versus source optical power for the MAP estimator, the ZZB, the ECRB, and the WCRB, where $T_s = 0.1\,\text{ms.}$, $f_c = 50\,\text{MHz}$, $S = 1\,\text{cm}^2$, and $m = 1$.

particular, the finite resolution of the search for the distance parameter can introduce additional errors in the high SNR regime where the theoretical accuracy limits are quite low (see [16, eqn. (18)]). Please refer to Section IV in [16] for a detailed discussion.

2.8 Relation to Position Estimation

Wireless position estimation is commonly performed in two steps, where position related parameters such as distances or angles are estimated in the first step and the position is estimated based on those estimated parameters in the second step [33]. Therefore, distance estimation investigated in this study can be considered as the first step in a wireless localization system. As the accuracy of distance estimation improves, position estimation also gets more accurate in general. To present a formal relation between position estimation and distance estimation accuracy, let $\boldsymbol{l}_r = [l_{r,1}\ l_{r,2}\ l_{r,3}]$ denote the location of the VLC receiver, and $\boldsymbol{l}_{t_1}, \ldots, \boldsymbol{l}_{t_N}$, with $\boldsymbol{l}_{t_i} = [l_{t_i,1}\ l_{t_i,2}\ l_{t_i,3}]$, represent the known locations of the LED transmitters, which are utilized for the localization of the VLC receiver. For sufficiently high SNRs (which is commonly the case in LOS visible light channels), the ML estimate for the distance between the VLC receiver and the ith LED transmitter can be stated as

$$\hat{x}_i = x_i + \varsigma_i \tag{2.87}$$

for $i = 1, \ldots, N$, where the noise components $\varsigma_1, \ldots, \varsigma_N$ are independent, $x_i = \|\boldsymbol{l}_r - \boldsymbol{l}_{t_i}\|_2$, and ς_i is modeled as a zero-mean Gaussian random variable with a variance that is equal to CRLB_i, i.e., the CRLB for estimating x_i based on the received signal coming from the ith LED transmitter [122, 126]. In other words, at high SNRs, the ML estimate for the distance is modeled by a Gaussian random variable with a mean that is equal to the true distance and a variance that is equal to the CRLB [122, 126]. It is noted that the results in Section 2.2 specify CRLB_i for various estimation approaches (TOA based, RSS based, and TOA/RSS based).

The CRLB for estimating the position $\boldsymbol{l}_r$ of the VLC receiver based on

$\hat{x}_1, \ldots, \hat{x}_N$ can be expressed as [122]

$$\mathrm{E}\{\|\hat{\boldsymbol{l}}_r - \boldsymbol{l}_r\|^2\} \geq \mathrm{trace}\left\{\mathbf{J}(\boldsymbol{l}_r)^{-1}\right\} \tag{2.88}$$

where $\mathbf{J}(\boldsymbol{l}_r)$ denotes the FIM related to $\boldsymbol{l}_r$ (cf. (2.7)). Since the height of the VLC receiver is assumed to be known (cf. Section 2.1), the aim is to estimate the first two elements of $\boldsymbol{l}_r$; that is, $l_{r,1}$ and $l_{r,2}$. Hence, based on (2.7), the FIM can be specified for the model in (2.87) as follows:

$$[\mathbf{J}(\boldsymbol{l}_r)]_{11} = \sum_{i=1}^{N} \frac{(l_{t_i,1} - l_{r,1})^2}{\mathrm{CRLB}_i\, x_i^2},\ [\mathbf{J}(\boldsymbol{l}_r)]_{22} = \sum_{i=1}^{N} \frac{(l_{t_i,2} - l_{r,2})^2}{\mathrm{CRLB}_i\, x_i^2},$$
$$[\mathbf{J}(\boldsymbol{l}_r)]_{12} = [\mathbf{J}(\boldsymbol{l}_r)]_{21} = \sum_{i=1}^{N} \frac{(l_{t_i,1} - l_{r,1})(l_{t_i,2} - l_{r,2})}{\mathrm{CRLB}_i\, x_i^2}\,.$$

Then, the CRLB in (2.88) is calculated as

$$\mathrm{E}\{\|\hat{\boldsymbol{l}}_r - \boldsymbol{l}_r\|^2\} \geq \left(\sum_{i=1}^{N} \frac{1}{\mathrm{CRLB}_i}\right)\left(\sum_{i=1}^{N} \frac{(l_{t_i,1} - l_{r,1})^2}{\mathrm{CRLB}_i\, x_i^2}\right.$$
$$\left.\times \sum_{i=1}^{N} \frac{(l_{t_i,2} - l_{r,2})^2}{\mathrm{CRLB}_i\, x_i^2} - \left(\sum_{i=1}^{N} \frac{(l_{t_i,1} - l_{r,1})(l_{t_i,2} - l_{r,2})}{\mathrm{CRLB}_i\, x_i^2}\right)^2\right)^{-1} \tag{2.89}$$

From (2.89), the CRLB for position estimation can be specified based on the CRLBs for estimating the distances between the VLC receiver and a number of LED transmitters. Therefore, the results related to distance estimation in Section 2.2 provide guidelines for position estimation, as well.

It is important to note that, in the presence of multiple LED transmitters, the VLC receiver can observe and process the signals from the LED transmitters individually by employing multiple access techniques such as time division multiplexing and frequency division multiplexing [9, 22, 127].

2.9 Concluding Remarks and Extensions

In this chapter, theoretical limits and estimators have been obtained for both synchronous and asynchronous VLP systems and in the presence and absence of

a relation between distance and channel attenuation factor. In particular, the CRLBs and MLEs have been derived for the TOA based, RSS based, and hybrid TOA/RSS based distance estimation. Comparisons among the CRLBs have been provided, and it has been shown that the CRLB for the hybrid TOA/RSS based estimation converges to that of the TOA based distance estimation for $\beta \gg c/x$, and to that of the RSS based distance estimation for $\beta \ll c/x$. Also, asymptotic results have been obtained for the MLEs under sampling rate limitations, and a modified hybrid TOA/RSS based distance estimator has been proposed to perform accurate distance estimation in practical scenarios. It has been shown that the RSS based and the modified hybrid TOA/RSS based distance estimators can provide robustness against sampling rate limitations, and the modified hybrid TOA/RSS based distance estimator achieves the lowest MSEs among all the estimators in practical scenarios.

In addition, the ZZB has been derived for range estimation in synchronous VLP systems. The proposed ZZB exploits ranging information from the prior information, the time delay parameter, and the channel attenuation factor. Moreover, a closed-form ECRB expression has been obtained, and the BCRB and the WCRB derivations have been presented for synchronous VLP systems. Via the numerical examples, the bounds have been compared against each other and against the MAP estimator. The ZZB has been shown to provide a reasonable lower bound for the MAP estimator. Hence, it can provide important guidelines for design of practical VLP systems. For example, based on the ZZB expression, effects of various system parameters, such as the Lambertian order, the area of the photo detector, and the source optical power, on ranging accuracy can be analyzed. On the other hand, the ECRB and the WCRB (BCRB) can provide useful bounds in the high and low SNR regimes, respectively.

As future work, theoretical limits on distance estimation will be considered in the presence of uncertainty about the height of the VLC receiver. In addition, measurements from multiple LED transmitters will be employed to perform hybrid TOA/RSS based estimation in three dimensional VLP systems (as outlined below). Another important direction would be to perform an experimental study for evaluating the performance of the MLEs and the tightness of the CRLBs in

real-world conditions. Moreover, theoretical limits for synchronous VLP systems can be considered for three-dimensional scenarios (i.e., when the height of the VLC receiver is unknown). In that case, the extended ZZB for vector parameter estimation [128] should be employed.

In the presence of multiple LED transmitters, the VLC receiver can process the received signals from the LED transmitters for determining its three dimensional position. If $r_i(t)$ denotes the received signal from the ith LED transmitter, where $i = 1, \ldots, N$, the CRLB expressions and the ML estimators should be derived based on the conditional distribution of $r_1(t), \ldots, r_N(t)$ given the unknown parameters, which include the location of the VLC receiver and other nuisance parameters, if any. As a practical approach, the VLC receiver can perform two-step position estimation, which has lower implementation complexity and can achieve similar performance to the one-step (joint) optimal processing at high SNRs [33]. In this common approach, position related parameters such as TOA and/or RSS are estimated in the first step and the position of the VLC receiver is estimated based on those position related parameters in the second step. The detailed theoretical analyses and the derivations of the ML estimators and the two step estimators in the presence of multiple LED transmitters are considered as future work.

For the theoretical limits in Sections 2.4–2.6, the generic expressions have been presented first, and then the particular expressions have been obtained for the special case of uniform prior distribution for the distance parameter x. As another special case with practical importance, the scenario in which the VLC receiver is uniformly distributed on the floor (ground) can be considered. In that case, a two dimensional uniform distribution can be employed over the area where the VLC receiver can communicate with the LED transmitter. Let $\mathcal{A}_v$ denote this area. Based on the minimum and the maximum possible distances, which are denoted by D_1 and D_2, respectively (see Section 2.4) and the fact that the LED transmitter and the VLC receiver are pointing in vertical directions, area $\mathcal{A}_v$ can be represented by a circle with a radius of $\sqrt{D_2^2 - D_1^2}$, the center of which is located at the projection of the LED transmitter to the floor (please see

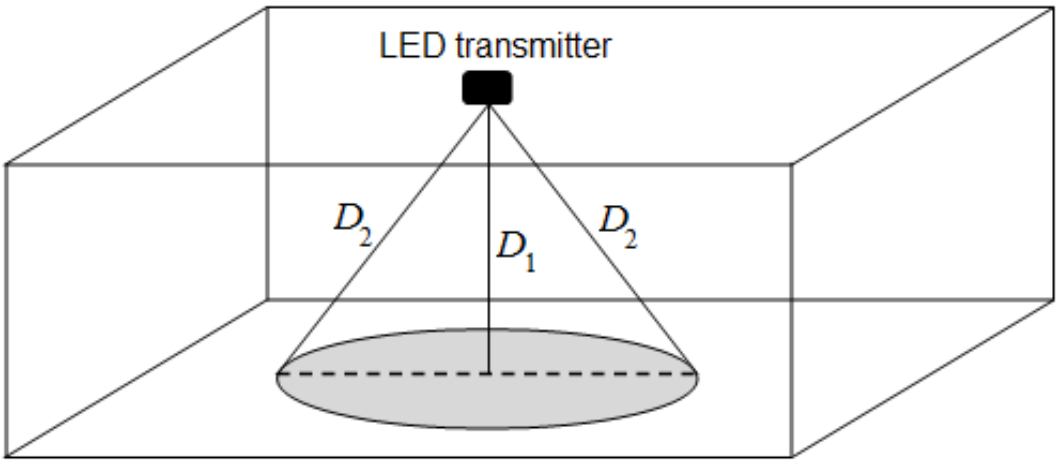

Figure 2.13: The scenario in which the VLC receiver is located in the gray circular area according to a uniform distribution.

Fig. 2.13 for an illustration).[11] The use of such a circular area can be justified by the field of view of the VLC receiver, which imposes an upper limit on the incidence angle θ (see (2.3)) for communication between the LED transmitter and the VLC receiver [32]. When the position of the VLC receiver is uniformly distributed over the circular area $\mathcal{A}_v$, it can be shown, via some manipulation of random variables, that the distance x between the LED transmitter and the VLC receiver is characterized by the following prior PDF:

$$w(x) = \begin{cases} 2x/(D_2^2 - D_1^2)\,, & \text{if } D_1 \leq x \leq D_2 \\ 0\,, & \text{otherwise} \end{cases}. \tag{2.90}$$

The ZZB bound can easily be evaluated for the prior PDF in (2.90) by inserting it into (2.57), (2.64), (2.66), and (2.68). Similarly, the ECRB expressions can be specified based on (2.73) and (2.90), which leads to similar expressions to those in (2.74)–(2.76). (In fact, the use of the prior PDF in (2.90) instead of the uniform PDF mainly increases the degree of x in the numerator of the integral in (2.74); hence, the derivations stay almost the same.) In a similar fashion, the BCRB and the WCRB in Section 2.6 can also be evaluated for (2.57). Hence, specific expressions for the bounds can be obtained for the prior PDF in (2.90), as well.

[11] In this case, D_1 corresponds to the height of the LED transmitter relative to the VLC receiver, which is also denoted by h (see (2.4)).

In practical systems, due to synchronization errors and finite resolution of time delay estimates, the relation in (2.2) may not hold exactly. In order to derive the ZZB in the presence of such effects, (2.2) can be updated as $\tau = x/c + \varepsilon$, where ε has a PDF denoted by $p_\varepsilon(\cdot)$. Then, from (2.1), the likelihood function can be obtained as (cf. (2.61))

$$p(r(t)|x) = e^k \int p_\varepsilon(\epsilon) e^{-\frac{1}{2\sigma^2}\int_{T_1}^{T_2}\left(r(t)-\frac{R_p\gamma}{x^{m+3}}s(t-\frac{x}{c}-\epsilon)\right)^2 dt} d\epsilon. \tag{2.91}$$

Based on (2.91), the decision rule in (2.60) can be expressed, after some manipulation, as follows:

$$\begin{aligned} &\log\left(\int p_\varepsilon(\epsilon) e^{\frac{R_p\gamma\tilde{C}_{rs}(\vartheta+\delta,\epsilon)}{\sigma^2(\vartheta+\delta)^{m+3}}} d\epsilon\right) - \log\left(\int p_\varepsilon(\epsilon) e^{\frac{R_p\gamma\tilde{C}_{rs}(\vartheta,\epsilon)}{\sigma^2\vartheta^{m+3}}} d\epsilon\right) \\ &\underset{\mathcal{H}_1}{\overset{\mathcal{H}_0}{\lessgtr}} \frac{R_p^2\gamma^2 E_2}{2\sigma^2}\left(\frac{1}{(\vartheta+\delta)^{2m+6}} - \frac{1}{\vartheta^{2m+6}}\right) + \log\left(\frac{w(\vartheta)}{w(\vartheta+\delta)}\right) \end{aligned} \tag{2.92}$$

where $\tilde{C}_{rs}(x,\epsilon) \triangleq \int_{T_1}^{T_2} r(t)s(t-x/c-\epsilon)dt$. Since it is difficult to specify the PDF of the decision statistics in (2.92), a closed-form expression for $\mathrm{P}_{\min}$ in (2.69) may not be obtained. However, a Monte-Carlo approach can be adopted to evaluate $\mathrm{P}_{\min}$ based on the decision rule in (2.92). Then, the ZZB can be calculated numerically via (2.57).

Chapter 3

Direct and Two-Step Positioning in Visible Light Systems

In this chapter, we investigate the fundamental limits of three-dimensional localization of a VLC receiver in synchronous and asynchronous VLP systems, design ML estimators by employing direct and two-step positioning techniques, and characterize the asymptotic performance of the proposed estimators via theoretical derivations [18]. The main contributions of this chapter can be summarized as follows:

- *Theoretical Bounds for Synchronous Scenarios:* For the first time in the literature, a general CRLB expression is derived for three-dimensional localization of a VLC receiver in synchronous VLP systems by utilizing information from both time delay parameters (i.e., TOA) and channel attenuation factors (i.e., RSS) (Proposition 1).

- *Algorithms/Estimators for Synchronous Scenarios:* The direct and two-step ML position estimators are proposed for synchronous VLP systems by taking into account both TOA and RSS information. The direct positioning approach, which exploits the whole observation signal, is considered for the

first time for synchronous VLP systems. In addition, the two-step estimator is designed by exploiting the asymptotic properties of TOA and RSS estimates in the high SNR regime (Lemma 1). Moreover, it is shown that the proposed two-step estimator is *asymptotically optimal*, i.e., converges to the direct estimator at high SNRs (Proposition 2 and Remark 1).

- *Theoretical Bounds for Asynchronous Scenarios:* The CRLB for three-dimensional RSS-based localization is derived for asynchronous VLP systems (Proposition 3). The derived CRLB expression constitutes a generalization of that in [29] to cases in which transmitted pulses can have arbitrary shapes and LED transmission powers can have any values.

- *Algorithms/Estimators for Asynchronous Scenarios:* The ML estimators are designed for direct and two-step positioning in asynchronous VLP scenarios. It is proved that the two-step estimator is equivalent to the direct estimator for practical pulse shapes (Proposition 4). Hence, the two-step position estimation is shown to be optimal in the ML sense under practical conditions in asynchronous VLP systems.

The key differences between this work and the previous results on VLP systems can be listed as follows:

- *Theoretical Bounds:*
  - Different from the previous work on synchronous VLP systems (e.g., [16, 17, 23, 129]), which analyzes only distance estimation, this study investigates three-dimensional position estimation and puts forward a fundamental limit on the accuracy of localization in synchronous scenarios, which is valid for arbitrary transmitter/receiver positions and orientations.
  - Although there exist previous studies that focus on the CRLB derivation for localization in asynchronous VLP systems (e.g., [29, 49, 50]), theoretical bounds on localization in synchronous VLP systems are provided for the first time.

  - The analytical derivations are based *directly* on the received signal itself, not on measured/extracted quantities (as in, e.g., [29, 49, 50]), which leads to generalized expressions that can address scenarios with any type of transmitted signals.

- *Positioning Algorithms:*

  - Position estimators are proposed for generic three-dimensional VLP configurations. However, most of the existing work on positioning algorithms in VLP systems relies on the assumption of a known receiver height and/or perpendicular LED and VLC orientations (e.g., [9, 13, 14, 34, 36]), which can make those algorithms impractical in certain applications.

  - For asynchronous scenarios, different from the three-dimensional ML position estimator in [29], which is effectively a two-step estimator through the use of measured RSS values, we derive both the direct and the two-step estimators, and identify conditions under which these two positioning paradigms become equivalent.

  - As opposed to the previous VLP studies, we employ the optimal way of obtaining the RSS observations from the received signals via an ML approach (Section 3.2.3 and Section 3.3.2).

  - Regarding synchronous scenarios, there exist no previous studies in the literature that propose a positioning algorithm for synchronous VLP systems.

The rest of this chapter is organized as follows: Section 3.1 presents the VLP system model. The CRLBs and the ML estimators are derived for synchronous and asynchronous systems in Section 3.2 and Section 3.3, respectively. Numerical results are presented in Section 3.4, and concluding remarks are provided in Section 3.5.

3.1 System Model

3.1.1 Received Signal Model

Consider a VLP system in which a number of LED transmitters are employed to estimate the position of a VLC receiver. An LOS scenario is assumed between each LED transmitter and the VLC receiver, which is commonly the case for visible light systems [5, 23]. Then, the received signal at the VLC receiver due to the signal emitted by the ith LED transmitter is formulated as [23]

$$r_i(t) = \alpha_i R_p \, s_i(t - \tau_i) + \eta_i(t) \tag{3.1}$$

for $i \in \{1, \ldots, N_{\mathrm{L}}\}$ and $t \in [T_{1,i}, T_{2,i}]$, where N_{L} denotes the number of LED transmitters, $T_{1,i}$ and $T_{2,i}$ determine the observation interval for the signal coming from the ith LED transmitter, α_i is the attenuation factor of the optical channel between the ith LED transmitter and the VLC receiver ($\alpha_i > 0$), R_p is the responsivity of the photo detector, $s_i(t)$ is the transmitted signal from the ith LED transmitter, which is nonzero over an interval of $[0, T_{s,i}]$, τ_i is the TOA of the signal emitted by the ith LED transmitter, and $\eta_i(t)$ is zero-mean additive white Gaussian noise with spectral density level σ^2. It is assumed that a certain type of multiple access protocol, such as frequency-division or time-division multiple access [130], is employed in order to facilitate separate processing of signals from each LED transmitter at the VLC receiver [4]. Therefore, the noise processes corresponding to the received signals from different LED transmitters are modeled to be independent. It is also assumed that R_p and $s_i(t)$, $i \in \{1, \ldots, N_{\mathrm{L}}\}$, are known by the VLC receiver.

The TOA parameter in (3.1) is modeled as

$$\tau_i = \frac{\|\boldsymbol{l}_{\mathrm{r}} - \boldsymbol{l}_{\mathrm{t}}^i\|}{c} + \Delta_i \tag{3.2}$$

where c is the speed of light, Δ_i denotes the time offset between the clocks of the ith LED transmitter and the VLC receiver, $\boldsymbol{l}_{\mathrm{r}} = [l_{\mathrm{r},1} \; l_{\mathrm{r},2} \; l_{\mathrm{r},3}]^T$ and $\boldsymbol{l}_{\mathrm{t}}^i = \left[l_{\mathrm{t},1}^i \; l_{\mathrm{t},2}^i \; l_{\mathrm{t},3}^i\right]^T$ are three-dimensional column vectors that denote the locations of

the VLC receiver and the ith LED transmitter, respectively, and $\|\boldsymbol{l}_{\rm r}-\boldsymbol{l}_{\rm t}^i\|$ denotes the distance between the ith LED transmitter and the VLC receiver. For a synchronous scenario, $\Delta_i = 0$ for $i = 1, \ldots, N_{\rm L}$, whereas for an asynchronous scenario, Δ_i's are modeled as deterministic unknown parameters. It is assumed that the signal component in (3.1) is contained completely in the observation interval $[T_{1,i}, T_{2,i}]$; that is, $\tau_i \in [T_{1,i}, T_{2,i} - T_{s,i}]$. In (3.1), the channel attenuation factor α_i is modeled as

$$\alpha_i = -\frac{(m_i+1)S}{2\pi}\frac{\left[(\boldsymbol{l}_{\rm r}-\boldsymbol{l}_{\rm t}^i)^T\boldsymbol{n}_{\rm t}^i\right]^{m_i}(\boldsymbol{l}_{\rm r}-\boldsymbol{l}_{\rm t}^i)^T\boldsymbol{n}_{\rm r}}{\|\boldsymbol{l}_{\rm r}-\boldsymbol{l}_{\rm t}^i\|^{m_i+3}} \tag{3.3}$$

where m_i is the Lambertian order for the ith LED transmitter, S is the area of the photo detector at the VLC receiver, and $\boldsymbol{n}_{\rm r} = [n_{{\rm r},1}\ n_{{\rm r},2}\ n_{{\rm r},3}]^T$ and $\boldsymbol{n}_{\rm t}^i = \left[n_{{\rm t},1}^i\ n_{{\rm t},2}^i\ n_{{\rm t},3}^i\right]^T$ denote the orientation vectors ('normals') of the VLC receiver and the ith LED transmitter, respectively [23, 29].[1] It is assumed that the VLC receiver knows S, $\boldsymbol{n}_{\rm r}$, m_i, $\boldsymbol{l}_{\rm t}^i$, and $\boldsymbol{n}_{\rm t}^i$ for $i = 1, \ldots, N_{\rm L}$. For example, the orientation of the VLC receiver, $\boldsymbol{n}_{\rm r}$, can be determined by a gyroscope and the parameters of the LED transmitters (m_i, $\boldsymbol{l}_{\rm t}^i$ and $\boldsymbol{n}_{\rm t}^i$) can be sent to the receiver via visible light communications.

3.1.2 Log-Likelihood Function and CRLB

Considering the received signal model in (3.1), the log-likelihood function for the received signal vector $\boldsymbol{r}(t) \triangleq [r_1(t) \ldots r_{N_{\rm L}}(t)]^T$ is obtained as follows [120, 121]:

$$\Lambda(\boldsymbol{\varphi}) = k - \frac{1}{2\sigma^2}\sum_{i=1}^{N_{\rm L}}\int_{T_{1,i}}^{T_{2,i}}\left(r_i(t) - \alpha_i R_p\, s_i(t-\tau_i)\right)^2 dt \tag{3.4}$$

where $\boldsymbol{\varphi}$ represents the set of unknown parameters and k is a normalizing constant that does not depend on the unknown parameters. While the set of unknown parameters consists only of the coordinates of the VLC receiver in the synchronous case, it also contains the delay parameters in the asynchronous case, as investigated in Sections 3.2 and 3.3.

[1] For example, if the VLC receiver is pointing up directly, then $\boldsymbol{n}_{\rm r} = [0\ 0\ 1]^T$.

The CRLB on the covariance matrix of any unbiased estimator $\hat{\boldsymbol{\varphi}}$ of $\boldsymbol{\varphi}$ can be expressed as [122]

$$\mathbb{E}\big\{(\hat{\boldsymbol{\varphi}}-\boldsymbol{\varphi})(\hat{\boldsymbol{\varphi}}-\boldsymbol{\varphi})^T\big\} \succeq \mathbf{J}(\boldsymbol{\varphi})^{-1} \tag{3.5}$$

where $\boldsymbol{A} \succeq \boldsymbol{B}$ means that $\boldsymbol{A}-\boldsymbol{B}$ is positive semidefinite and $\mathbf{J}(\boldsymbol{\varphi})$ is the Fisher information matrix (FIM) for $\boldsymbol{\varphi}$, which can be calculated as follows:

$$\mathbf{J}(\boldsymbol{\varphi}) = \mathbb{E}\left\{\left(\nabla_{\boldsymbol{\varphi}}\Lambda(\boldsymbol{\varphi})\right)\left(\nabla_{\boldsymbol{\varphi}}\Lambda(\boldsymbol{\varphi})\right)^T\right\} \tag{3.6}$$

with $\nabla_{\boldsymbol{\varphi}}$ representing the gradient operator with respect to $\boldsymbol{\varphi}$ and $\Lambda(\boldsymbol{\varphi})$ being the log-likelihood function as defined in (3.4).

3.2 Positioning in Synchronous Systems

In the synchronous scenario, the VLC receiver is synchronized with the LED transmitters; that is, $\Delta_i = 0$ in (3.2) for $i = 1, \ldots, N_{\mathrm{L}}$. In this section, the CRLB is derived for synchronous VLP systems, the direct position estimation is proposed, and the two-step position estimation is developed by considering both time delay and channel attenuation information.

3.2.1 CRLB

In the synchronous case, α_i and τ_i are functions of $\boldsymbol{l}_{\mathrm{r}}$ only (since $\Delta_i = 0$ in (3.2)); hence, the set of unknown parameters in (3.4) is defined as

$$\boldsymbol{\varphi} = [l_{\mathrm{r},1}\ l_{\mathrm{r},2}\ l_{\mathrm{r},3}]^T = \boldsymbol{l}_{\mathrm{r}}\,. \tag{3.7}$$

Then, the CRLB for estimating $\boldsymbol{l}_{\mathrm{r}}$ based on $r_1(t), \ldots, r_{N_{\mathrm{L}}}(t)$ in (3.1) is specified by the following proposition.

Proposition 1. *For synchronous VLP systems, the CRLB on the mean-squared error (MSE) of any unbiased estimator $\hat{\boldsymbol{l}}_{\mathrm{r}}$ for the location of the VLC*

receiver is given by

$$\mathbb{E}\big\{\|\hat{\boldsymbol{l}}_{\mathrm{r}}-\boldsymbol{l}_{\mathrm{r}}\|^2\big\}\geq \mathrm{trace}\big\{\mathbf{J}_{\mathrm{syn}}^{-1}\big\} \tag{3.8}$$

where

$$\begin{aligned}[\mathbf{J}_{\mathrm{syn}}]_{k_1,k_2}=&\frac{R_p^2}{\sigma^2}\sum_{i=1}^{N_{\mathrm{L}}}\Bigg(E_2^i\frac{\partial\alpha_i}{\partial l_{\mathrm{r},k_1}}\frac{\partial\alpha_i}{\partial l_{\mathrm{r},k_2}}+E_1^i\alpha_i^2\frac{\partial\tau_i}{\partial l_{\mathrm{r},k_1}}\frac{\partial\tau_i}{\partial l_{\mathrm{r},k_2}}\\&-E_3^i\alpha_i\bigg(\frac{\partial\alpha_i}{\partial l_{\mathrm{r},k_1}}\frac{\partial\tau_i}{\partial l_{\mathrm{r},k_2}}+\frac{\partial\tau_i}{\partial l_{\mathrm{r},k_1}}\frac{\partial\alpha_i}{\partial l_{\mathrm{r},k_2}}\bigg)\Bigg)\end{aligned} \tag{3.9}$$

for $k_1,k_2\in\{1,2,3\}$ *with*

$$E_1^i\triangleq\int_0^{T_{s,i}}\big(s_i'(t)\big)^2dt \tag{3.10}$$

$$E_2^i\triangleq\int_0^{T_{s,i}}\big(s_i(t)\big)^2dt \tag{3.11}$$

$$E_3^i\triangleq\int_0^{T_{s,i}}s_i(t)s_i'(t)dt \tag{3.12}$$

$$\frac{\partial\tau_i}{\partial l_{\mathrm{r},k}}=\frac{l_{\mathrm{r},k}-l_{\mathrm{t},k}^i}{c\|\boldsymbol{l}_{\mathrm{r}}-\boldsymbol{l}_{\mathrm{t}}^i\|} \tag{3.13}$$

$$\begin{aligned}\frac{\partial\alpha_i}{\partial l_{\mathrm{r},k}}=&-\frac{(m_i+1)S}{2\pi}\Bigg(\frac{\big((\boldsymbol{l}_{\mathrm{r}}-\boldsymbol{l}_{\mathrm{t}}^i)^T\boldsymbol{n}_{\mathrm{t}}^i\big)^{m_i-1}}{\|\boldsymbol{l}_{\mathrm{r}}-\boldsymbol{l}_{\mathrm{t}}^i\|^{m_i+3}}\\&\times\big(m_i\,n_{\mathrm{t},k}^i(\boldsymbol{l}_{\mathrm{r}}-\boldsymbol{l}_{\mathrm{t}}^i)^T\boldsymbol{n}_{\mathrm{r}}+n_{\mathrm{r},k}(\boldsymbol{l}_{\mathrm{r}}-\boldsymbol{l}_{\mathrm{t}}^i)^T\boldsymbol{n}_{\mathrm{t}}^i\big)\\&-\frac{(m_i+3)(l_{\mathrm{r},k}-l_{\mathrm{t},k}^i)}{\|\boldsymbol{l}_{\mathrm{r}}-\boldsymbol{l}_{\mathrm{t}}^i\|^{m_i+5}}\big((\boldsymbol{l}_{\mathrm{r}}-\boldsymbol{l}_{\mathrm{t}}^i)^T\boldsymbol{n}_{\mathrm{t}}^i\big)^{m_i}(\boldsymbol{l}_{\mathrm{r}}-\boldsymbol{l}_{\mathrm{t}}^i)^T\boldsymbol{n}_{\mathrm{r}}\Bigg).\end{aligned} \tag{3.14}$$

Proof: Consider the likelihood function in (3.4), where τ_i and α_i are related to $\boldsymbol{l}_{\mathrm{r}}$ as in (3.2) (with $\Delta_i=0$) and (3.3), respectively. Since the set of unknown parameters in the synchronous case is equal to $\boldsymbol{l}_{\mathrm{r}}$ as stated in (3.7), the elements of the FIM in (3.6) can be expressed as

$$[\mathbf{J}(\boldsymbol{\varphi})]_{k_1,k_2}=\mathbb{E}\left\{\frac{\partial\Lambda(\boldsymbol{\varphi})}{\partial l_{\mathrm{r},k_1}}\frac{\partial\Lambda(\boldsymbol{\varphi})}{\partial l_{\mathrm{r},k_2}}\right\} \tag{3.15}$$

for $k_1,k_2\in\{1,2,3\}$. From (3.4), the expression in (3.15) can be calculated as follows:

$$[\mathbf{J}(\boldsymbol{\varphi})]_{k_1,k_2}=\frac{R_p^2}{\sigma^2}\sum_{i=1}^{N_{\mathrm{L}}}\Bigg(E_2^i\frac{\partial\alpha_i}{\partial l_{\mathrm{r},k_1}}\frac{\partial\alpha_i}{\partial l_{\mathrm{r},k_2}}+\alpha_i\frac{\partial\alpha_i}{\partial l_{\mathrm{r},k_1}}\int_{T_{1,i}}^{T_{2,i}}s_i(t-\tau_i)\frac{\partial s_i(t-\tau_i)}{\partial l_{\mathrm{r},k_2}}dt$$

$$+ \alpha_i \frac{\partial \alpha_i}{\partial l_{\mathrm{r},k_2}} \int_{T_{1,i}}^{T_{2,i}} s_i(t-\tau_i) \frac{\partial s_i(t-\tau_i)}{\partial l_{\mathrm{r},k_1}} dt + \alpha_i^2 \int_{T_{1,i}}^{T_{2,i}} \frac{\partial s_i(t-\tau_i)}{\partial l_{\mathrm{r},k_1}} \frac{\partial s_i(t-\tau_i)}{\partial l_{\mathrm{r},k_2}} dt \Bigg) \tag{3.16}$$

where $E_2^i \triangleq \int_{T_{1,i}}^{T_{2,i}} s_i^2(t-\tau_i)dt$, which is equal to the expression in (3.11) as $s_i(t-\tau_i)$ is assumed to be contained completely in the observation interval $[T_{1,i}, T_{2,i}]$. Since $\partial s_i(t-\tau_i)/\partial l_{\mathrm{r},k} = -(\partial \tau_i/\partial l_{\mathrm{r},k}) s_i'(t-\tau_i)$, the expression in (3.16) can be shown to be equal to that in (3.9) based on the definitions in (3.10) and (3.12); hence, $\mathbf{J}(\boldsymbol{\varphi}) = \mathbf{J}_{\mathrm{syn}}$. In addition, the partial derivatives in (3.13) and (3.14) can be obtained from (3.2) (with $\Delta_i = 0$) and (3.3), respectively. Finally, the CRLB on the MSE of any unbiased estimator $\hat{\boldsymbol{l}}_{\mathrm{r}}$ for the location of the VLC receiver, $\boldsymbol{l}_{\mathrm{r}}$, can be expressed based on the inequality in (3.5) as

$$\mathrm{E}\big\{\|\hat{\boldsymbol{l}}_{\mathrm{r}} - \boldsymbol{l}_{\mathrm{r}}\|^2\big\} \geq \mathrm{trace}\big\{\mathbf{J}(\boldsymbol{\varphi})^{-1}\big\}. \tag{3.17}$$

Since $\mathbf{J}(\boldsymbol{\varphi})$ in (3.16) is equal to $\mathbf{J}_{\mathrm{syn}}$ in (3.9), as discussed above, the expression in (3.8) follows from (3.17). ■

The CRLB expression specified by (3.8)–(3.14) illustrates the effects of the transmitted signals via the E_1^i, E_2^i, and E_3^i parameters and the impact of the geometry (configuration) via the $\partial \tau_i/\partial l_{\mathrm{r},k}$ and $\partial \alpha_i/\partial l_{\mathrm{r},k}$ terms. Hence, the theoretical limit on the localization accuracy can be evaluated for any given system based on the provided expression. It is noted that the CRLB expression in Proposition 1 has not been available in the literature, and provides a theoretical limit for synchronous VLP systems by utilizing information from both channel attenuation factors (RSS) and time delay parameters (TOA). Compared to the CRLB in Proposition 1, those in [16, 23, 28] are for distance estimation only, and those in [29, 49, 50] focus on RSS based localization. As noted from Proposition 1 and its proof, the main technical difference and difficulty in obtaining the proposed CRLB expression is related to the simultaneous use of the TOA and RSS parameters, which requires the calculation of the partial derivatives of both $\{\alpha_i\}_{i=1}^{N_{\mathrm{L}}}$ and $\{\tau_i\}_{i=1}^{N_{\mathrm{L}}}$.

The CRLB expression in Proposition 1 is generic since the LED transmitters and the VLC receiver can have any locations and orientations and the transmitted

signals can be in generic forms. Special cases can easily be obtained from (3.8)–(3.14). For example, if the transmitted signals satisfy $s_i(T_{s,i}) = s_i(0)$ for $i = 1, \ldots, N_{\mathrm{L}}$, then E_3^i in (3.12) becomes zero[2] and $[\mathbf{J}_{\mathrm{syn}}]_{k_1,k_2}$ in (3.9) reduces to

$$[\mathbf{J}_{\mathrm{syn}}]_{k_1,k_2} = \frac{R_p^2}{\sigma^2} \sum_{i=1}^{N_{\mathrm{L}}} \left(E_2^i \frac{\partial \alpha_i}{\partial l_{\mathrm{r},k_1}} \frac{\partial \alpha_i}{\partial l_{\mathrm{r},k_2}} + E_1^i \alpha_i^2 \frac{\partial \tau_i}{\partial l_{\mathrm{r},k_1}} \frac{\partial \tau_i}{\partial l_{\mathrm{r},k_2}} \right) \tag{3.18}$$

From (3.18), the contribution of the channel attenuation factors and time delays can be observed individually. Namely, the first and the second elements in (3.18) are related to the location information obtained from the channel attenuation factors and the time delay parameters, respectively. Hence, it is noted that both RSS and TOA parameters are utilized for localization in the synchronous scenario.

3.2.2 Direct Positioning

Direct positioning refers to the estimation of the unknown location directly from the received signals without any intermediate steps for estimating location related parameters such as TOA or RSS [38–40, 42–45, 47, 48] (cf. Section 3.2.3). Direct positioning has not been considered before for synchronous VLP systems, which carry significant differences from RF based positioning systems.

In direct positioning, the aim is to estimate the location of the VLC receiver, $\boldsymbol{l}_{\mathrm{r}}$, based on the received signals in (3.1). From (3.4) and (3.7), the ML estimator for $\boldsymbol{l}_{\mathrm{r}}$ can be obtained as follows [122]:

$$\hat{\boldsymbol{l}}_{\mathrm{r}}^{\mathrm{DP,syn}} = \arg\max_{\boldsymbol{l}_{\mathrm{r}}} \; -\sum_{i=1}^{N_{\mathrm{L}}} \int_{T_{1,i}}^{T_{2,i}} \left(r_i(t) - \alpha_i R_p \, s_i(t - \tau_i) \right)^2 dt$$

which can be simplified, after some manipulation, into

$$\hat{\boldsymbol{l}}_{\mathrm{r}}^{\mathrm{DP,syn}} = \arg\max_{\boldsymbol{l}_{\mathrm{r}}} \; \sum_{i=1}^{N_{\mathrm{L}}} \alpha_i \int_{T_{1,i}}^{T_{2,i}} r_i(t) s_i(t - \tau_i) dt - \frac{R_p}{2} \sum_{i=1}^{N_{\mathrm{L}}} \alpha_i^2 E_2^i \tag{3.19}$$

where E_2^i is as defined in (3.11). It should be noted that τ_i and α_i in (3.19) are functions of $\boldsymbol{l}_{\mathrm{r}}$ as specified in (3.2) (with $\Delta_i = 0$) and (3.3), respectively. Hence,

[2]Since $E_3^i = \int_0^{T_{s,i}} s_i(t) s_i'(t) dt = (s_i(T_{s,i})^2 - s_i(0)^2)/2$, $E_3^i = 0$ if $s_i(T_{s,i}) = s_i(0)$, which is satisfied for most practical pulse shapes (cf. (3.61) and [23, Eq. 3]).

the direct ML position estimator in (3.19) searches over all possible values of the unknown position $\boldsymbol{l}_{\mathrm{r}}$ based on the relations of $\boldsymbol{l}_{\mathrm{r}}$ with the channel attenuation factors and the time delays.

The main advantage of the direct positioning approach in (3.19) is related to its performance (optimality in the ML sense), as investigated in Section 3.4. On the other hand, it can lead to high complexity in certain applications due to increased storage and communication requirements. For example, if the location estimation should be performed at a central unit, then it becomes cumbersome to transmit all the received signals to the center.

3.2.3 Two-Step Positioning

A common method for positioning in wireless networks is to apply a two-step estimation process where estimation of location related parameters such as RSS, TOA, TDOA, and/or AOA is performed in the first step and the unknown location is estimated based on those parameters in the second step [33].

Although two-step positioning has commonly been considered for VLP systems (e.g., [9, 14, 24, 26, 27, 29, 34, 37]), there exist no studies on the design of two-step estimators for synchronous VLP systems in which both RSS and TOA information can be utilized. In the proposed two-step estimator for synchronous VLP systems, the ML estimates of the TOA and RSS parameters are obtained for each of the N_{L} LED transmitters in the first step, and the location of the VLC receiver is estimated based on those location related parameters, i.e., TOA and RSS estimates, in the second step.

In the first step, the ML estimates of the TOA and RSS parameters[3] are obtained for each LED transmitter. For the ith LED transmitter, the received signal $r_i(t)$ is expressed as in (3.1) and the corresponding log-likelihood function for $r_i(t)$ is given by $k_i - \frac{1}{2\sigma^2}\int_{T_{1,i}}^{T_{2,i}} \left(r_i(t) - \alpha_i R_p\, s_i(t-\tau_i)\right)^2 dt$, where k_i is a constant

[3]The channel attenuation factor α_i is referred to as the RSS parameter in this study since $\alpha_i \geq 0$ in visible light channels and it determines the received signal energy (power).

that does not depend on α_i and τ_i (cf. (3.4)). Then, the ML estimates of the TOA and RSS parameters corresponding to the ith LED transmitter are obtained as follows:

$$(\hat{\tau}_i, \hat{\alpha}_i) = \underset{(\tau_i, \alpha_i)}{\arg\max}\ 2\alpha_i \int_{T_{1,i}}^{T_{2,i}} r_i(t) s_i(t-\tau_i) dt - \alpha_i^2 R_p E_2^i \tag{3.20}$$

for $i = 1, \ldots, N_{\mathrm{L}}$. Since α_i is nonnegative, the solution for $\hat{\tau}_i$ is obtained by maximizing the integral expression in (3.20). Hence, the ML estimate $\hat{\tau}_i$ of the TOA parameter τ_i for the ith LED transmitter is calculated from

$$\hat{\tau}_i = \underset{\tau_i}{\arg\max} \int_{T_{1,i}}^{T_{2,i}} r_i(t) s_i(t-\tau_i) dt\,. \tag{3.21}$$

Then, $\hat{\alpha}_i$ can be expressed from (3.20) and (3.21) as

$$\hat{\alpha}_i = \underset{\alpha_i}{\arg\max}\ 2\alpha_i \tilde{C}_{rs}^i - \alpha_i^2 R_p E_2^i \tag{3.22}$$

where

$$\tilde{C}_{rs}^i \triangleq \int_{T_{1,i}}^{T_{2,i}} r_i(t) s_i(t-\hat{\tau}_i) dt\,. \tag{3.23}$$

The problem in (3.22) leads to the following closed-form expression for the ML estimate of the RSS parameter α_i corresponding to the ith LED transmitter:

$$\hat{\alpha}_i = \frac{\tilde{C}_{rs}^i}{R_p E_2^i}\,. \tag{3.24}$$

In the second step, the aim is to estimate the location of the VLC receiver, $\boldsymbol{l}_{\mathrm{r}}$, based on the TOA and RSS estimates in the first step; that is, $\{\hat{\alpha}_i, \hat{\tau}_i\}_{i=1}^{N_{\mathrm{L}}}$. To that aim, the following lemma is presented first in order to characterize the statistics of the estimates obtained in the first step.

Lemma 1. *Assume that $E_3^i = 0$ for $i = 1, \ldots, N_{\mathrm{L}}$. Then, at high SNRs (i.e., for $\alpha_i^2 R_p^2 E_2^i \gg \sigma^2$), the TOA estimate in* (3.21) *and the RSS estimate in* (3.24) *can approximately be modeled as*

$$\hat{\tau}_i = \tau_i + \nu_i \tag{3.25}$$

$$\hat{\alpha}_i = \alpha_i + \varsigma_i \tag{3.26}$$

for $i = 1, \ldots, N_{\mathrm{L}}$, where ν_i and ς_i are independent zero mean Gaussian random variables with variances $\sigma^2/(R_p^2 \alpha_i^2 E_1^i)$ and $\sigma^2/(R_p^2 E_2^i)$, respectively, and ν_i and ν_j (ς_i and ς_j) are independent for $i \neq j$.

Proof: Consider the estimation of τ_i and α_i based on the received signal from the ith LED transmitter, i.e., $r_i(t)$ in (3.1). The log-likelihood function for $r_i(t)$ is given by

$$\Lambda_i(\tau_i, \alpha_i) = k_i - \frac{1}{2\sigma^2} \int_{T_{1,i}}^{T_{2,i}} \left(r_i(t) - \alpha_i R_p \, s_i(t - \tau_i) \right)^2 dt \tag{3.27}$$

where k_i is a constant that does not depend on α_i and τ_i (cf. (3.4)). The FIM for (τ_i, α_i) can be expressed based on (3.6) as follows:

$$\mathbf{J}(\tau_i, \alpha_i) = \begin{bmatrix} \mathrm{E}\left\{ \left(\frac{\partial \Lambda_i(\tau_i, \alpha_i)}{\partial \tau_i} \right)^2 \right\} & \mathrm{E}\left\{ \frac{\partial \Lambda_i(\tau_i, \alpha_i)}{\partial \tau_i} \frac{\partial \Lambda_i(\tau_i, \alpha_i)}{\partial \alpha_i} \right\} \\ \mathrm{E}\left\{ \frac{\partial \Lambda_i(\tau_i, \alpha_i)}{\partial \alpha_i} \frac{\partial \Lambda_i(\tau_i, \alpha_i)}{\partial \tau_i} \right\} & \mathrm{E}\left\{ \left(\frac{\partial \Lambda_i(\tau_i, \alpha_i)}{\partial \alpha_i} \right)^2 \right\} \end{bmatrix} \tag{3.28}$$

the elements of which can be computed from (3.27) as

$$[\mathbf{J}(\tau_i, \alpha_i)]_{11} = \frac{\alpha_i^2 R_p^2 E_1^i}{\sigma^2} \tag{3.29}$$

$$[\mathbf{J}(\tau_i, \alpha_i)]_{22} = \frac{R_p^2 E_2^i}{\sigma^2} \tag{3.30}$$

$$[\mathbf{J}(\tau_i, \alpha_i)]_{12} = [\mathbf{J}(\tau_i, \alpha_i)]_{21} = \frac{-\alpha_i R_p^2 E_3^i}{\sigma^2} \tag{3.31}$$

where E_1^i, E_2^i, and E_3^i are as defined in (3.10), (3.11), and (3.12), respectively. Since $E_3^i = 0$ for $i = 1, \ldots, N_{\mathrm{L}}$ as stated in the lemma, the FIM in (3.28) can be expressed from (3.29)–(3.31) as

$$\mathbf{J}(\tau_i, \alpha_i) = \begin{bmatrix} \frac{R_p^2 \alpha_i^2 E_1^i}{\sigma^2} & 0 \\ 0 & \frac{R_p^2 E_2^i}{\sigma^2} \end{bmatrix}. \tag{3.32}$$

As studied in [124, 126], the ML estimates for τ_i and α_i can be approximated, at high SNRs, by a Gaussian random vector, where the mean of each component is equal to the true value of the parameter and the covariance matrix is given by the inverse of the FIM. Hence, at high SNRs, the joint probability distribution

of $\hat{\tau}_i$ in (3.21) and $\hat{\alpha}_i$ in (3.24) can approximately be expressed as

$$\begin{bmatrix} \hat{\tau}_i \\ \hat{\alpha}_i \end{bmatrix} \sim \mathcal{N}\left(\begin{bmatrix} \tau_i \\ \alpha_i \end{bmatrix}, \begin{bmatrix} \frac{\sigma^2}{R_p^2 \alpha_i^2 E_1^i} & 0 \\ 0 & \frac{\sigma^2}{R_p^2 E_2^i} \end{bmatrix} \right) \tag{3.33}$$

where $\mathcal{N}(\boldsymbol{\mu}, \boldsymbol{\Sigma})$ denotes Gaussian distribution with mean vector $\boldsymbol{\mu}$ and covariance matrix $\boldsymbol{\Sigma}$. Hence, $\hat{\tau}_i$ and $\hat{\alpha}_i$ are independent Gaussian random variables as specified by (3.25) and (3.26) in the lemma. In addition, since the noise $\eta_i(t)$ in the received signal, $r_i(t)$, is independent for different LED transmitters (see (3.1)), the noise components in the ML estimates $\hat{\tau}_i$ and $\hat{\alpha}_i$ are also independent for different transmitters. Hence, the noise components in (3.25) and (3.26) are independent as specified in the lemma. ■

Lemma 1 states the asymptotic unbiasedness and efficiency properties of the ML estimates $\hat{\tau}_i$ in (3.21) and $\hat{\alpha}_i$ in (3.24) [122], [126]. Based on Lemma 1, the following estimator can be obtained for the second step of the two-step estimator:

$$\hat{\boldsymbol{l}}_{\mathrm{r}}^{\mathrm{TS,syn}} = \arg\min_{\boldsymbol{l}_{\mathrm{r}}} \sum_{i=1}^{N_{\mathrm{L}}} \left(E_1^i \alpha_i^2 \left(\hat{\tau}_i - \tau_i\right)^2 + E_2^i \left(\hat{\alpha}_i - \alpha_i\right)^2 \right) - \frac{2\sigma^2}{R_p^2} \sum_{i=1}^{N_{\mathrm{L}}} \log \alpha_i \tag{3.34}$$

where τ_i and α_i are functions of $\boldsymbol{l}_{\mathrm{r}}$ as defined in (3.2) (with $\Delta_i = 0$) and (3.3), respectively, and log denotes the natural logarithm. The estimator in (3.34) corresponds to the ML estimator for $\boldsymbol{l}_{\mathrm{r}}$ based on the TOA and RSS estimates in the first step when they are Gaussian distributed as specified in Lemma 1 (please see Appendix 3.6.1 for the derivation). In other words, at high SNRs, $\hat{\boldsymbol{l}}_{\mathrm{r}}^{\mathrm{TS,syn}}$ in (3.34) is approximately the ML estimator for $\boldsymbol{l}_{\mathrm{r}}$ based on $\{\hat{\alpha}_i, \hat{\tau}_i\}_{i=1}^{N_{\mathrm{L}}}$. Since the last term in (3.34) is commonly smaller than the others at high SNRs, a simpler version of (3.34) can be proposed as follows:

$$\hat{\boldsymbol{l}}_{\mathrm{r}}^{\mathrm{TS,syn}} = \arg\min_{\boldsymbol{l}_{\mathrm{r}}} \sum_{i=1}^{N_{\mathrm{L}}} \left(E_1^i \hat{\alpha}_i{}^2 \left(\hat{\tau}_i - \tau_i\right)^2 + E_2^i \left(\hat{\alpha}_i - \alpha_i\right)^2 \right) \tag{3.35}$$

where the estimate $\hat{\alpha}_i$ is replaced with α_i in the first term, as well, considering high SNRs. The simplified estimator in (3.35) corresponds to an NLS estimator.

In summary, the proposed two-step positioning approach first calculates the TOA and RSS estimates via (3.21) and (3.24) for each LED transmitter, and

then uses those estimates for determining the position of the VLC receiver via (3.35). In Section 3.4, comparisons between the two-step and direct positioning approaches are provided via simulations. In order to present a theoretical comparison under the conditions in Lemma 1, the following proposition specifies the CRLB for estimating the VLC receiver location, $\boldsymbol{l}_{\rm r}$, based on the TOA and RSS estimates $\{\hat{\alpha}_i, \hat{\tau}_i\}_{i=1}^{N_{\rm L}}$ obtained in the first step.

Proposition 2. *Suppose that the conditions in Lemma 1 hold. Then, the CRLB on the MSE of any unbiased estimator $\hat{\boldsymbol{l}}_{\rm r}$ for the location of the VLC receiver, $\boldsymbol{l}_{\rm r}$, based on the TOA and RSS estimates $\{\hat{\alpha}_i, \hat{\tau}_i\}_{i=1}^{N_{\rm L}}$ obtained from* (3.21) *and* (3.24)*, is stated as*

$$\mathbb{E}\big\{\|\hat{\boldsymbol{l}}_{\rm r} - \boldsymbol{l}_{\rm r}\|^2\big\} \geq \mathrm{trace}\big\{\mathbf{J}_{\rm TS,syn}^{-1}\big\} \tag{3.36}$$

where $\mathbf{J}_{\rm TS,syn}$ is a 3×3 matrix with the following elements:

$$[\mathbf{J}_{\rm TS,syn}]_{k_1,k_2} = \frac{R_p^2}{\sigma^2} \sum_{i=1}^{N_{\rm L}} \left(E_2^i \frac{\partial \alpha_i}{\partial l_{{\rm r},k_1}} \frac{\partial \alpha_i}{\partial l_{{\rm r},k_2}} + E_1^i \alpha_i^2 \frac{\partial \tau_i}{\partial l_{{\rm r},k_1}} \frac{\partial \tau_i}{\partial l_{{\rm r},k_2}} \right) \tag{3.37}$$

for $k_1, k_2 \in \{1,2,3\}$, with E_1^i, E_2^i, $\partial\tau_i/\partial l_{{\rm r},k}$ and $\partial\alpha_i/\partial l_{{\rm r},k}$ being as defined in (3.10), (3.11), (3.13) *and* (3.14)*, respectively.*

Proof: The derivative of the log-likelihood function in (3.65) with respect to the kth parameter of the unknown parameter vector $\boldsymbol{l}_{\rm r}$ is computed as

$$\begin{aligned} \frac{\partial \tilde{\Lambda}(\boldsymbol{l}_{\rm r})}{\partial l_{{\rm r},k}} = \sum_{i=1}^{N_{\rm L}} \Bigg(& \frac{1}{\alpha_i} \frac{\partial \alpha_i}{\partial l_{{\rm r},k}} + \frac{(\hat{\alpha}_i - \alpha_i) R_p^2 E_2^i}{\sigma^2} \frac{\partial \alpha_i}{\partial l_{{\rm r},k}} \\ & + \frac{(\hat{\tau}_i - \tau_i) \alpha_i^2 R_p^2 E_1^i}{\sigma^2} \frac{\partial \tau_i}{\partial l_{{\rm r},k}} - \frac{(\hat{\tau}_i - \tau_i)^2 \alpha_i R_p^2 E_1^i}{\sigma^2} \frac{\partial \alpha_i}{\partial l_{{\rm r},k}} \Bigg) \end{aligned} \tag{3.38}$$

for $k \in \{1,2,3\}$. Using the formula in (3.6) with the expression in (3.38), the (k_1,k_2)th entry of the FIM can be obtained after some manipulation as

$$[\mathbf{J}_{\rm TS,syn}]_{k_1,k_2} = \frac{R_p^2}{\sigma^2} \sum_{i=1}^{N_{\rm L}} \left(\left(1 + \frac{2\sigma^2}{\alpha_i^2 R_p^2 E_2^i} \right) E_2^i \frac{\partial \alpha_i}{\partial l_{{\rm r},k_1}} \frac{\partial \alpha_i}{\partial l_{{\rm r},k_2}} + E_1^i \alpha_i^2 \frac{\partial \tau_i}{\partial l_{{\rm r},k_1}} \frac{\partial \tau_i}{\partial l_{{\rm r},k_2}} \right) \tag{3.39}$$

for $k_1, k_2 \in \{1,2,3\}$. By invoking the assumption of high SNRs in Lemma 1 ($\alpha_i^2 R_p^2 E_2^i \gg \sigma^2$), the FIM for the unknown receiver location $\boldsymbol{l}_{\rm r}$ can be obtained as in (3.37). ■

The CRLB expression in Proposition 2 presents an important guideline for asymptotic comparison of the direct and two-step positioning approaches in synchronous VLP systems as detailed in the following remark.

Remark 1. It is observed that the expression in (3.18), which is obtained for direct positioning under the assumption of $E_3^i = 0$, is equal to that in (3.37), which is for two-step positioning under the assumptions of $E_3^i = 0$ and $\alpha_i^2 R_p^2 E_2^i \gg \sigma^2$. In other words, referring to the signal model in (3.1), the performance of direct positioning and two-step positioning algorithms converges to each other at high SNRs. Hence, it can be concluded that the benefits of direct positioning are more prominent in the low SNR regime, which is in compliance with the results obtained for RF systems [38, 43]. This conclusion is intuitive since the consistency between TOA and RSS estimates (measurements) gets higher as the SNR increases. In the low SNR regime, the TOA estimate in (3.21) may be far away from the true time delay, leading possibly to a mismatch between the corresponding RSS estimate in (3.24) and the position information inferred from that TOA information. In such cases, the direct positioning approach is capable of estimating the unknown location more accurately than the two-step approach by utilizing entire signals and thus producing consistent location estimates.

3.2.4 Complexity Analysis

In this part, computational complexity analyses are presented for the proposed direct and two-step estimators in Section 3.2.2 and Section 3.2.3.

Consider an indoor localization scenario where the VLC receiver moves inside a certain volume and tries to estimate its position. Then, complexity analyses can be performed by implementing the direct ML estimator in (3.19) and the two-step ML estimator in (3.35) over a finite search space corresponding to that volume for the location of the VLC receiver. Since the objective functions in (3.19) and (3.35) are nonconvex with respect to the VLC receiver location, $\boldsymbol{l}_{\mathrm{r}}$, the exhaustive search method is considered for identifying the global optimum. For complexity calculations, it is assumed that range (or, equivalently, time)

dimensions are sampled with a sampling interval on the order of Δd. To that aim, we consider a three-dimensional uniform grid $\mathcal{U}$ consisting of $\mathcal{O}(1/\Delta d^3)$ possible locations in the considered volume for the location of the VLC receiver. Based on $\mathcal{U}$, the complexity analyses for the direct and two-step positioning algorithms are provided as follows.

3.2.4.1 Direct Positioning

For the computation of the objective function in (3.19) at each search location $\boldsymbol{l}_\mathrm{r} \in \mathcal{U}$, it is necessary to compute α_i via (3.3), τ_i via (3.2), and the correlator output $\int_{T_{1,i}}^{T_{2,i}} r_i(t)s_i(t-\tau_i)dt$ using the computed τ_i value. First, the computation of α_i in (3.3) and τ_i in (3.2) has $\mathcal{O}(1)$ complexity since these operations take a constant time for a given value of $\boldsymbol{l}_\mathrm{r}$. Secondly, evaluating the integral $\int_{T_{1,i}}^{T_{2,i}} r_i(t)s_i(t-\tau_i)dt$ requires $\mathcal{O}(1/\Delta d)$ operations. Taking into account the whole search space $\mathcal{U}$ (which contains $\mathcal{O}(1/\Delta d^3)$ points) and all N_L LEDs, the overall complexity of the direct positioning method becomes

$$\mathcal{O}(N_\mathrm{L} \times 1/\Delta d^4) \ . \tag{3.40}$$

3.2.4.2 Two-Step Positioning

In the first step of the two-step estimator in (3.35), $\hat{\tau}_i$ in (3.21) and $\hat{\alpha}_i$ in (3.24) must be computed. Assuming that continuous signals are sampled with the number of samples on the order of $\mathcal{O}(1/\Delta d)$, as in direct positioning, the computation of the integral expression in (3.21) requires $\mathcal{O}(1/\Delta d)$ operations for a given τ_i. Since τ_i lies in the finite interval $[T_{1,i}, T_{2,i} - T_{s,i}]$, it can be assumed that there exists $\mathcal{O}(1/\Delta d)$ different values of τ_i. Hence, the overall complexity of (3.21) becomes $\mathcal{O}(1/\Delta d^2)$. On the other hand, the computation of $\hat{\alpha}_i$ via (3.24) has a computational complexity of $\mathcal{O}(1)$ once the results of (3.21) and (3.23) are obtained. In the second step, τ_i and α_i in (3.35) must be evaluated for each $\boldsymbol{l}_\mathrm{r} \in \mathcal{U}$,

whose size is on the order of $\mathcal{O}(1/\Delta d^3)$. Therefore, the computational complexity of the two-step positioning is given by

$$\underbrace{\mathcal{O}(N_{\mathrm{L}} \times 1/\Delta d^2)}_{\text{First Step}} + \underbrace{\mathcal{O}(N_{\mathrm{L}} \times 1/\Delta d^3)}_{\text{Second Step}} = \mathcal{O}(N_{\mathrm{L}} \times 1/\Delta d^3) \tag{3.41}$$

where the term corresponding to the second step calculations dominates as the sampling interval Δd approaches zero.

The proposed direct and two-step positioning approaches can be compared based on the expressions in (3.40) and (3.41) in terms of the computational complexity. For instance, if Δd is sufficiently small, i.e., range/time dimensions are sampled fast enough to achieve high resolution, then the direct position estimator has a higher complexity than its two-step counterpart. Moreover, it is observed, by comparing (3.40) and (3.41), that the task of integral evaluation is performed at each search location $\boldsymbol{l}_{\mathrm{r}} \in \mathcal{U}$ in direct positioning, whereas it only appears in the first-step calculations in two-step positioning. This alleviates the strain on the second-step calculations in the two-step approach, which makes it computationally less demanding than the direct approach. Hence, the main computational burden of direct positioning consists in evaluating the correlator output $\int_{T_{1,i}}^{T_{2,i}} r_i(t)s_i(t-\tau_i)dt$ at each search location $\boldsymbol{l}_{\mathrm{r}}$.

3.3 Positioning in Asynchronous Systems

In the asynchronous scenario, the VLC receiver is not synchronized with the LED transmitters; that is, Δ_i in (3.2) is a deterministic unknown parameter for each $i \in \{1, \ldots, N_{\mathrm{L}}\}$. In this section, the CRLB is derived for asynchronous VLP systems, and the direct position estimation and its relation to the two-step position estimation are investigated.

3.3.1 CRLB

In an asynchronous VLP system, the unknown parameters include the TOAs of the received signals coming from the LED transmitters in addition to the location of the VLC receiver. Hence, the vector of unknown parameters in (3.4) for the asynchronous case can be expressed as

$$\boldsymbol{\varphi} = [l_{\mathrm{r},1}\ l_{\mathrm{r},2}\ l_{\mathrm{r},3}\ \tau_1\ \ldots\ \tau_{N_{\mathrm{L}}}]^T . \tag{3.42}$$

Then, the CRLB for estimating $\boldsymbol{l}_{\mathrm{r}}$ based on $r_1(t), \ldots, r_{N_{\mathrm{L}}}(t)$ in (3.1) is stated in the following proposition.

Proposition 3. *For asynchronous VLP systems, the CRLB on the MSE of any unbiased estimator $\hat{\boldsymbol{l}}_{\mathrm{r}}$ for the location of the VLC receiver is given by*

$$\mathbb{E}\big\{\|\hat{\boldsymbol{l}}_{\mathrm{r}} - \boldsymbol{l}_{\mathrm{r}}\|^2\big\} \geq \mathrm{trace}\big\{\mathbf{J}_{\mathrm{asy}}^{-1}\big\} \tag{3.43}$$

where $\mathbf{J}_{\mathrm{asy}}$ denotes a 3×3 matrix with the following elements:

$$[\mathbf{J}_{\mathrm{asy}}]_{k_1,k_2} = \frac{R_p^2}{\sigma^2} \sum_{i=1}^{N_{\mathrm{L}}} \left(E_2^i - \frac{(E_3^i)^2}{E_1^i} \right) \frac{\partial \alpha_i}{\partial l_{\mathrm{r},k_1}} \frac{\partial \alpha_i}{\partial l_{\mathrm{r},k_2}} \tag{3.44}$$

for $k_1, k_2 \in \{1,2,3\}$, with E_1^i, E_2^i, E_3^i, and $\partial\alpha_i/\partial l_{\mathrm{r},k}$ being as defined in (3.10), (3.11), (3.12), *and* (3.14), *respectively.*

Proof: Consider the log-likelihood function in (3.4) for the unknown parameter vector in (3.42). Then, from (3.6), the FIM can be obtained after some manipulation as

$$\mathbf{J}(\boldsymbol{\varphi}) = \begin{bmatrix} \mathbf{J_A} & \mathbf{J_B} \\ \mathbf{J_B}^T & \mathbf{J_D} \end{bmatrix} \tag{3.45}$$

where $\mathbf{J_A}$ is a 3×3 matrix with elements

$$[\mathbf{J_A}]_{k_1,k_2} = \frac{R_p^2}{\sigma^2} \sum_{i=1}^{N_{\mathrm{L}}} E_2^i \frac{\partial \alpha_i}{\partial l_{\mathrm{r},k_1}} \frac{\partial \alpha_i}{\partial l_{\mathrm{r},k_2}} \tag{3.46}$$

for $k_1, k_2 \in \{1,2,3\}$, $\mathbf{J_B}$ is a $3 \times N_{\mathrm{L}}$ matrix with elements

$$[\mathbf{J_B}]_{k,i} = -\frac{R_p^2}{\sigma^2} E_3^i \alpha_i \frac{\partial \alpha_i}{\partial l_{\mathrm{r},k}} \tag{3.47}$$

for $k \in \{1,2,3\}$ and $i \in \{1,\ldots,N_{\rm L}\}$, and $\mathbf{J_D}$ is an $N_{\rm L} \times N_{\rm L}$ matrix with elements

$$[\mathbf{J_D}]_{i_1,i_2} = \begin{cases} \frac{R_p^2}{\sigma^2}\,\alpha_{i_1}^2 E_1^{i_1}\,, & \text{if } i_1 = i_2 \\ 0\,, & \text{if } i_1 \neq i_2 \end{cases} \tag{3.48}$$

for $i_1, i_2 \in \{1,\ldots,N_{\rm L}\}$. In (3.46)–(3.48), E_1^i, E_2^i, E_3^i, and $\partial\alpha_i/\partial l_{{\rm r},k}$ are as defined in (3.10), (3.11), (3.12), and (3.14), respectively.

The CRLB on the location $\boldsymbol{l}_{\rm r}$ of the VLC receiver can be expressed, based on (3.5), as

$$\mathbb{E}\big\{\|\hat{\boldsymbol{l}}_{\rm r} - \boldsymbol{l}_{\rm r}\|^2\big\} \geq \text{trace}\Big\{\big[\mathbf{J}^{-1}(\boldsymbol{\varphi})\big]_{3\times 3}\Big\} \tag{3.49}$$

where $\hat{\boldsymbol{l}}_{\rm r}$ is any unbiased estimator for $\boldsymbol{l}_{\rm r}$. From (3.45), $\big[\mathbf{J}^{-1}(\boldsymbol{\varphi})\big]_{3\times 3}$ can be stated as

$$\big[\mathbf{J}^{-1}(\boldsymbol{\varphi})\big]_{3\times 3} = \big(\mathbf{J_A} - \mathbf{J_B}\mathbf{J_D}^{-1}\mathbf{J_B}\big)^{-1}\,. \tag{3.50}$$

Based on (3.46)–(3.48), $\mathbf{J_A} - \mathbf{J_B}\mathbf{J_D}^{-1}\mathbf{J_B}$ can be calculated after some manipulation as

$$\big[\mathbf{J_A} - \mathbf{J_B}\mathbf{J_D}^{-1}\mathbf{J_B}\big]_{k_1,k_2} = \frac{R_p^2}{\sigma^2}\sum_{i=1}^{N_{\rm L}}\left(E_2^i - \frac{(E_3^i)^2}{E_1^i}\right)\frac{\partial\alpha_i}{\partial l_{{\rm r},k_1}}\frac{\partial\alpha_i}{\partial l_{{\rm r},k_2}}\,. \tag{3.51}$$

Hence, (3.49)–(3.51) lead to the expressions in (3.43) and (3.44) in the proposition. ■

It is noted from the CRLB expression in Proposition 3 that the position related information in the channel attenuation factors (RSS) is utilized in the asynchronous case for estimating the location of the VLC receiver (see (3.44)). On the other hand, information from both the channel attenuation factors (RSS) and the time delay (TOA) parameters is available in the synchronous case as can be noted from Proposition 1. In addition, the CRLB expression presented in Proposition 3 has been obtained for the first time in the literature; hence, provides a theoretical contribution to localization in asynchronous VLP systems. Since the expression in (3.44) is obtained based on the entire observation signals, $r_i(t)$'s in (3.1), it differs from the CRLB expression in [29], which is derived for asynchronous VLP

systems based on the RSS measurements without directly using the received signals (eqn. (32) in [29]). On the other hand, when $E_3^i = 0$ for $i = 1, \ldots, N_{\mathrm{L}}$, which is valid for many practical pulses, the FIM expression in (3.44) is equivalent to that in [29]. Hence, the CRLB provided by Proposition 3 also covers the more general case of $E_3^i \neq 0$ as compared to the CRLB in [29], which constitutes a special case of (3.44).[4]

Remark 2. From Proposition 1 and Proposition 3, it is observed that if $E_3^i = 0$ and $\alpha_i^2 E_1^i \ll E_2^i$ for $i = 1, \ldots, N_{\mathrm{L}}$, the CRLB expressions in the synchronous and asynchronous cases converge to each other. This corresponds to scenarios in which the position related information in the time delay (TOA) parameters is negligible compared to that in the channel attenuation factors (RSS parameters). Hence, synchronism does not provide any significant benefits in such scenarios. Since E_1^i/E_2^i can be expressed from Parseval's relation as $4\pi^2\beta_i^2$, where β_i is the effective bandwidth of $s_i(t)$,[5] it can be concluded that the synchronous and asynchronous cases lead to similar CRLBs when the transmitted signals have small effective bandwidths. This is an intuitive result because TOA information gets less accurate as the effective bandwidth decreases [33].

3.3.2 Direct and Two-Step Estimation

Direct position estimation involves the estimation of $\boldsymbol{l}_{\mathrm{r}}$, the location of the VLC receiver, directly from the received signals in (3.1). From (3.4), the ML estimator for direct positioning in the asynchronous case can be obtained as follows:

$$\hat{\boldsymbol{\varphi}}_{\mathrm{ML}} = \arg\max_{\boldsymbol{\varphi}} \sum_{i=1}^{N_{\mathrm{L}}} \left(\alpha_i \int_{T_{1,i}}^{T_{2,i}} r_i(t) s_i(t - \tau_i) dt - \frac{R_p}{2} \alpha_i^2 E_2^i \right) \tag{3.52}$$

[4]Indeed, it is proved in Proposition 4 in Section 3.3.2 that the direct positioning approach adopted for the derivation of (3.44) is equivalent to the two-step method for asynchronous VLP systems under the condition of $E_3^i = 0$. This result explains the equivalence of the two expressions in (3.44) and [29] for practical localization scenarios.

[5]The effective bandwidth is defined as $\beta_i = \sqrt{(1/E_2^i) \int f^2 |S_i(f)|^2 df}$, where $S_i(f)$ is the Fourier transform of $s_i(t)$.

where $\boldsymbol{\varphi}$ is defined by (3.42), α_i is related to $\boldsymbol{l}_{\mathrm{r}}$ as in (3.3), and E_2^i is given by (3.11). Since α_i's are nonnegative and the integral expressions depend only on τ_i's (3.52), the ML estimates for τ_i's can be calculated as in (3.21). Then, the ML estimate for $\boldsymbol{l}_{\mathrm{r}}$ is obtained from (3.52) as

$$\hat{\boldsymbol{l}}_{\mathrm{r}}^{\mathrm{DP,asy}} = \arg\max_{\boldsymbol{l}_{\mathrm{r}}} \sum_{i=1}^{N_{\mathrm{L}}} \left(\alpha_i \tilde{C}_{rs}^i - 0.5 R_p \alpha_i^2 E_2^i \right) \tag{3.53}$$

where $\tilde{C}_{rs}^i$ is as defined in (3.23).

For the two-step position estimation in the asynchronous case, the RSS parameters related to N_{L} LED transmitters are estimated in the first step and the location of the VLC receiver is estimated based on those RSS estimates in the second step. Due to the asynchronism between the LED transmitters and the VLC receiver, the TOA parameters cannot be related to the location of the VLC receiver (see (3.2)); hence, cannot be utilized for positioning in this case (cf. Section 3.2.3).

In the first step of the two-step estimator, the ML estimator for the RSS parameter, α_i, is calculated based on $r_i(t)$ for $i = 1, \ldots, N_{\mathrm{L}}$. Similar to that in the synchronous case (see Section 3.2.3), the ML estimate $\hat{\alpha}_i$ of α_i is expressed as

$$\hat{\alpha}_i = \frac{\tilde{C}_{rs}^i}{R_p E_2^i} \tag{3.54}$$

for $i = 1, \ldots, N_{\mathrm{L}}$, where $\tilde{C}_{rs}^i$ is as in (3.23) and E_2^i is given by (3.11).

The second step utilizes the RSS estimates in (3.54) for $i = 1, \ldots, N_{\mathrm{L}}$ for estimating the location of the VLC receiver based on the following NLS estimator:

$$\hat{\boldsymbol{l}}_{\mathrm{r}}^{\mathrm{TS,asy}} = \arg\min_{\boldsymbol{l}_{\mathrm{r}}} \sum_{i=1}^{N_{\mathrm{L}}} w_i (\hat{\alpha}_i - \alpha_i)^2 \tag{3.55}$$

where α_i is as defined in (3.3) and the following expression is proposed for the weighting coefficients:

$$w_i = \frac{E_1^i E_2^i - (E_3^i)^2}{E_1^i} \tag{3.56}$$

for $i = 1, \ldots, N_{\mathrm{L}}$, where E_1^i and E_3^i are as in (3.10) and (3.12), respectively. As illustrated in Appendix 3.6.2, the proposed weighting coefficient in (3.56) is inversely proportional to the CRLB for estimating α_i from $r_i(t)$. Hence, the RSS estimates with higher accuracy (i.e., lower CRLBs) are assigned higher weights in the NLS estimator in (3.55).

In the following proposition, it is shown that the direct position estimator in (3.53) is equivalent to the two-step estimator specified by (3.54)–(3.56) under certain conditions.

Proposition 4. *Consider an asynchronous VLP system with $E_3^i = 0$ for $i = 1, \ldots, N_{\mathrm{L}}$. Then, the direct position estimator in* (3.53) *is equivalent to the two-step position estimator in* (3.54)–(3.56).

Proof: When $E_3^i = 0$, the weighting coefficient in (3.56) reduces to

$$w_i = E_2^i \tag{3.57}$$

for $i = 1, \ldots, N_{\mathrm{L}}$. Inserting (3.54) and (3.57) into (3.55) yields the following:

$$\hat{\boldsymbol{l}}_{\mathrm{r}}^{\mathrm{TS,asy}} = \arg\min_{\boldsymbol{l}_{\mathrm{r}}} \sum_{i=1}^{N_{\mathrm{L}}} E_2^i \left(\frac{\tilde{C}_{rs}^i}{R_p E_2^i} - \alpha_i \right)^2 . \tag{3.58}$$

After some manipulation, the estimator in (3.58) can be expressed as

$$\hat{\boldsymbol{l}}_{\mathrm{r}}^{\mathrm{TS,asy}} = \arg\min_{\boldsymbol{l}_{\mathrm{r}}} \sum_{i=1}^{N_{\mathrm{L}}} \left(-2\alpha_i \tilde{C}_{rs}^i + \alpha_i^2 R_p E_2^i \right) \tag{3.59}$$

which is equivalent to the direct position estimator in (3.53). ■

Proposition 4 implies that the two-step position estimator is optimal in the ML sense for asynchronous VLP systems; that is, the direct positioning (based on ML estimation) is equivalent to the two-step positioning when $E_3^i = 0$ for $i = 1, \ldots, N_{\mathrm{L}}$. Since $s_i(0) = s_i(T_{s,i})$ for many practical pulses, $E_3^i = 0$ is encountered in practice (see (3.12)); hence, the two-step estimator can be employed in real systems as the optimal approach in the ML sense.

Remark 3. As proved in Proposition 4, if $E_3^i = 0$ for $i = 1, \ldots, N_{\mathrm{L}}$, the direct positioning approach is equivalent to the two-step approach for the asynchronous

scenario, whereas Remark 1 states that the two approaches are only *asymptotically* equivalent for the synchronous scenario. The intuition behind these results is that the measurement of RSS information is performed at the peak of the correlator output over the observation interval, irrespective of the true time delay of the received signal. Hence, direct positioning reduces to two-step positioning for the asynchronous case. On the other hand, when the TOA information corresponding to the location of the correlator peak is incorporated into the estimation process in the synchronous case, the direct positioning approach can identify a more accurate location that accounts for the observed signal, which is also implied in Remark 1.

3.3.3 Complexity Analysis

In this part, the complexity analysis is performed for the proposed ML position estimators in Section 3.3.2. Specifically, the computational complexity of the direct estimator in (3.53) is investigated as in Section 3.2.4.[6] First, $\tilde{C}_{rs}^{i}$ can be computed via (3.23) and (3.21) using $\mathcal{O}(1/\Delta d^2)$ operations. Then, for each $\boldsymbol{l}_{\mathrm{r}} \in \mathcal{U}$ and $i \in \{1, \ldots, N_{\mathrm{L}}\}$, the summand in (3.53) requires $\mathcal{O}(1)$ operations. Therefore, the overall complexity of the ML estimator in asynchronous VLP systems is obtained as

$$\mathcal{O}(N_{\mathrm{L}} \times 1/\Delta d^2) + \mathcal{O}(N_{\mathrm{L}} \times 1/\Delta d^3) = \mathcal{O}(N_{\mathrm{L}} \times 1/\Delta d^3) \ . \tag{3.60}$$

It follows from (3.40), (3.41) and (3.60) that the asynchronous estimator has the same order of complexity as that of the synchronous TS estimator and a lower complexity than the synchronous DP estimator.

[6] Since the direct and two-step estimators in asynchronous systems are equivalent for $E_3^i = 0$ via Proposition 4, the computational complexity analysis is carried out only for the direct estimator in (3.53). When $E_3^i \neq 0$, the estimators in (3.53) and (3.55) still have the same complexity as the computation of E_3^i requires constant time, i.e., of complexity $\mathcal{O}(1)$.

3.4 Numerical Results

In this section, numerical results are presented to corroborate the theoretical derivations in the previous sections. As in [23], the responsivity of the photo detector is taken as $R_p = 0.4\,\mathrm{mA/mW}$, and the spectral density level of the noise is set to $\sigma^2 = 1.336 \times 10^{-22}\,\mathrm{W/Hz}$. In addition, the Lambertian order is taken as $m = 1$ and the area S of the photo detector at the VLC receiver is equal to $1\,\mathrm{cm}^2$. The transmitted signal $s(t)$ in (3.1) is modeled as [23]

$$s(t) = A\left(1 - \cos\left(2\pi\, t/T_s\right)\right)\left(1 + \cos(2\pi f_c t)\right)\mathbb{I}_{t\in[0,T_s]} \tag{3.61}$$

where f_c denotes the center frequency, A corresponds to the average emitted optical power; that is, source optical power, and $\mathbb{I}_{t\in[0,T_s]}$ represents an indicator function, which is equal to 1 if $t \in [0, T_s]$ and zero otherwise.

We consider a room with a width, depth, and height of [8 8 5] m, respectively, where $N_{\mathrm{L}} = 4$ LED transmitters are attached to the ceiling at positions $\boldsymbol{l}_{\mathrm{t}}^1 = [2\ 2\ 5]^T$ m, $\boldsymbol{l}_{\mathrm{t}}^2 = [6\ 2\ 5]^T$ m, $\boldsymbol{l}_{\mathrm{t}}^3 = [2\ 6\ 5]^T$ m, and $\boldsymbol{l}_{\mathrm{t}}^4 = [6\ 6\ 5]^T$ m, as illustrated in Fig. 3.1. The orientation vectors of the LEDs are given by

$$\boldsymbol{n}_{\mathrm{t}}^i = [\sin\theta_i \cos\phi_i \ \ \sin\theta_i \sin\phi_i \ \ \cos\theta_i]^T \tag{3.62}$$

for $i = 1, \ldots, N_{\mathrm{L}}$, where θ_i and ϕ_i denote the polar and the azimuth angles, respectively [131].[7] In the configuration in Fig. 3.1, the polar and the azimuth angles are taken as $(\theta_1, \phi_1) = (150^\circ, 45^\circ)$, $(\theta_2, \phi_2) = (150^\circ, 135^\circ)$, $(\theta_3, \phi_3) = (150^\circ, -45^\circ)$ and $(\theta_4, \phi_4) = (150^\circ, -135^\circ)$. The VLC receiver is located at $\boldsymbol{l}_{\mathrm{r}} = [4\ 4\ 1]^T$ m and looks upwards, i.e., the orientation vector is given by $\boldsymbol{n}_{\mathrm{r}} = [0\ 0\ 1]^T$.

In the following subsections, the CRLBs and the performance of the direct position (DP) estimators and the two-step (TS) estimators are evaluated for both synchronous and asynchronous VLP systems. The CRLBs are computed based on Proposition 1 and Proposition 3, and the DP estimators are implemented via (3.19) and (3.53) for the synchronous and asynchronous cases, respectively. Also,

[7] For example, when $\theta_i = 180^\circ$ and $\phi_i = 0^\circ$, the LED orientation vector is directed downwards, i.e., $\boldsymbol{n}_{\mathrm{t}}^i = [0\ 0\ -1]$.

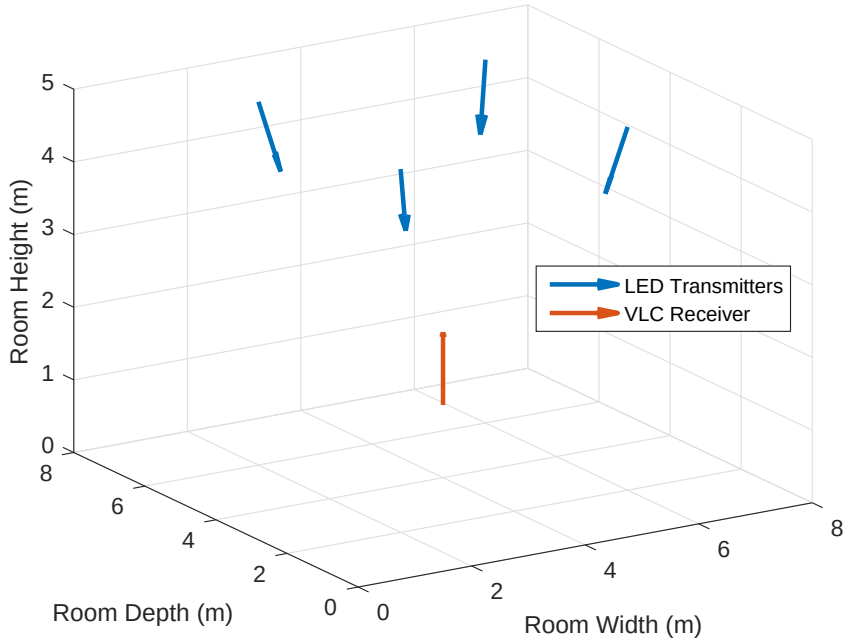

Figure 3.1: VLP system configuration in the simulations, where wall reflections are omitted by assuming an LOS scenario.

the two-step (TS) estimator in the synchronous scenario is obtained via (3.21), (3.24), and (3.35). Furthermore, the minimum mean absolute error (MMAE) estimator in [13] is implemented to compare the proposed estimators with the current state-of-the-art.[8,9]

3.4.1 Theoretical Accuracy Limits over the Room

In order to observe the localization performance throughout the entire room, the CRLBs for the synchronous and asynchronous VLP systems are computed

[8]Since the localization algorithm in [13] depends on the assumption of a perpendicular LED orientation, implementing it directly for the configuration of Fig. 3.1 would yield poor localization performance. To perform a fair evaluation of the algorithm in [13], we express the irradiation and the incidence angles in [13, Eq. 10] as a function of positions and orientations as in (3.3), which makes the algorithm applicable for Fig. 3.1.

[9]For the implementation of all the estimators in this work, the search interval in all the dimensions is taken to be $[-100\ 100]$ m.

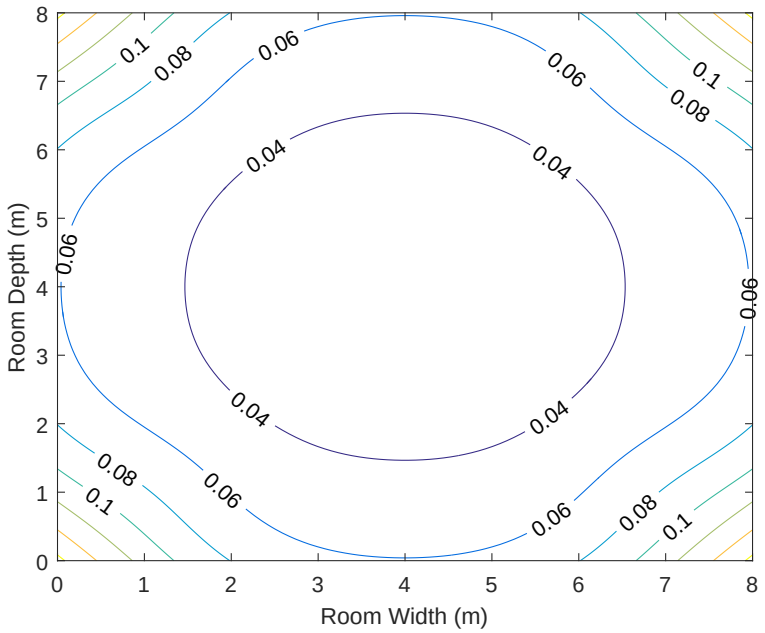

Figure 3.2: CRLB (in meters) for a synchronous VLP system as the VLC receiver moves inside the room, where $T_s = 0.1\,\text{ms}$, $f_c = 100\,\text{MHz}$, and $A = 100\,\text{mW}$.

as the VLC receiver moves inside the room and the resulting contour plots are shown in Fig. 3.2 and Fig. 3.3, respectively. The CRLBs are obtained for position estimation of a VLC receiver with a fixed height $l_{\text{r},3} = 1\,\text{m}$, which is moved along the $x-y$ plane over the room. As noted from Fig. 3.2 and Fig. 3.3, the localization performance decreases as the receiver moves away from the center of the room, which is an expected outcome since that movement leads to an increase in the distance, the incidence angle, and the irradiation angle between the VLC receiver and the LED transmitters, thereby reducing the signal strength, as implied by the Lambertian formula in (3.3). In addition, the level of increase in the CRLB from the center to the corners is much higher in the asynchronous case than that in the synchronous case as the TOA information can be effectively exploited to facilitate the localization process at the room corners, where the RSS information becomes less useful. Furthermore, the CRLBs are significantly lower in the synchronous case than those in the asynchronous case as the carrier frequency is quite high, which is in agreement with Remark 2.

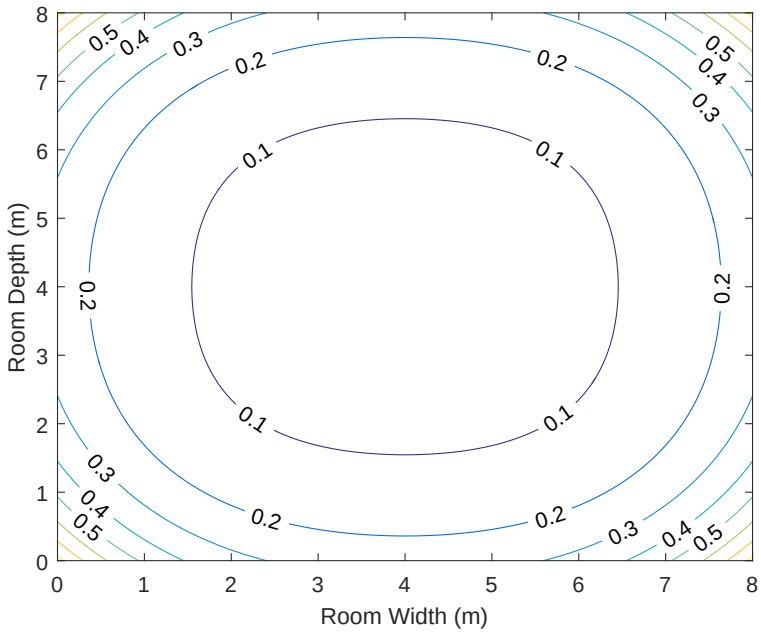

Figure 3.3: CRLB (in meters) for an asynchronous VLP system as the VLC receiver moves inside the room, where $T_s = 0.1\,\text{ms}$, $f_c = 100\,\text{MHz}$, and $A = 100\,\text{mW}$.

3.4.2 Performance of Direct and Two-Step Estimators with Respect to Optical Power

In this subsection, the root mean-squared errors (RMSEs) corresponding to the proposed DP and TS estimators, the MMAE estimator in [13], and the CRLBs are plotted with respect to the source optical power, A, for $f_c = 100\,\text{MHz}$ and $f_c = 10\,\text{MHz}$ in Fig. 3.4 and Fig. 3.5, respectively.[10] First, it is seen that the DP approach can provide significant performance improvements over the TS approach for synchronous scenarios, especially in the low-to-medium SNR region (about 4.5 m improvement for $A = 4.64$ W and $f_c = 100\,\text{MHz}$). Also, it can be inferred from the figures that the utilization of the time delay information in the synchronous DP estimator leads to considerable performance gains as compared to its asynchronous counterpart (0.26 m gain for $A = 215$ mW and $f_c = 100\,\text{MHz}$).

[10]The estimators can achieve lower RMSEs than the corresponding CRLBs at low SNRs since the theoretically infinite search space for the unknown parameter is confined to a finite region when implementing the estimators due to practical concerns, as described in Footnote 9.

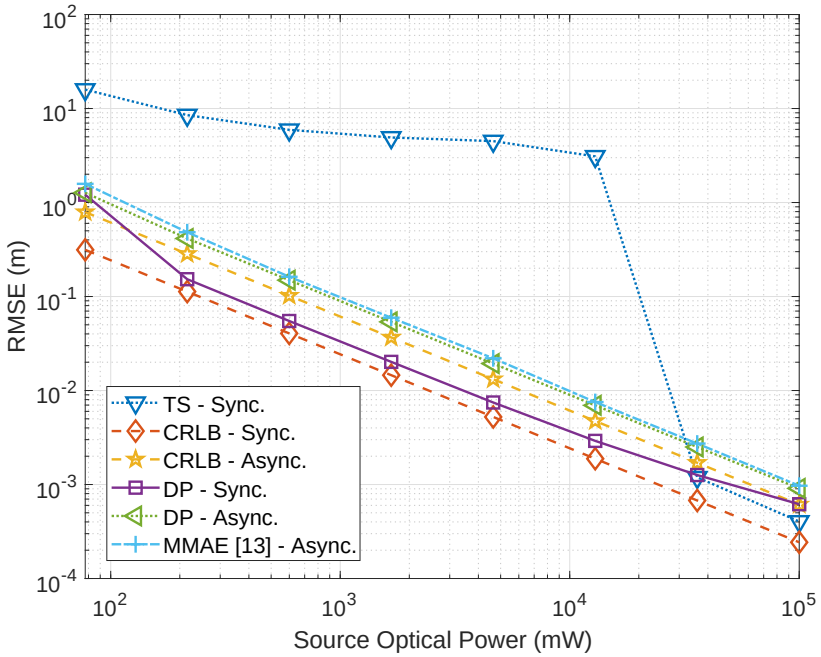

Figure 3.4: CRLBs and RMSEs of the estimators for synchronous and asynchronous VLP systems versus source optical power, where $T_s = 1\,\mu$s and $f_c = 100\,$MHz.

It is important to highlight that performance enhancement due to synchronism becomes larger as the center frequency increases, in compliance with Remark 2. Next, it is observed that the performance of the DP estimator in the synchronous case converges to that of the TS estimator at high SNR values (at high source optical powers) since the benefits of direct positioning get negligible as the SNR increases, which complies with Proposition 2 and Remark 1. Hence, the extra information acquired by utilizing the entire received signal for localization as opposed to using a set of intermediate measurements (i.e., TOA and RSS estimates) leads to higher performance gains in low-to-medium SNR regimes. Therefore, it is deduced that the two-step positioning approach in the synchronous VLP systems is best suited for high SNR scenarios, where direct and two-step positioning achieve similar localization performance with the latter method requiring reduced computational resources, as explored in Section 3.2.4. Moreover, the proposed DP approach outperforms the algorithm in [13] at all SNR levels and center frequencies.

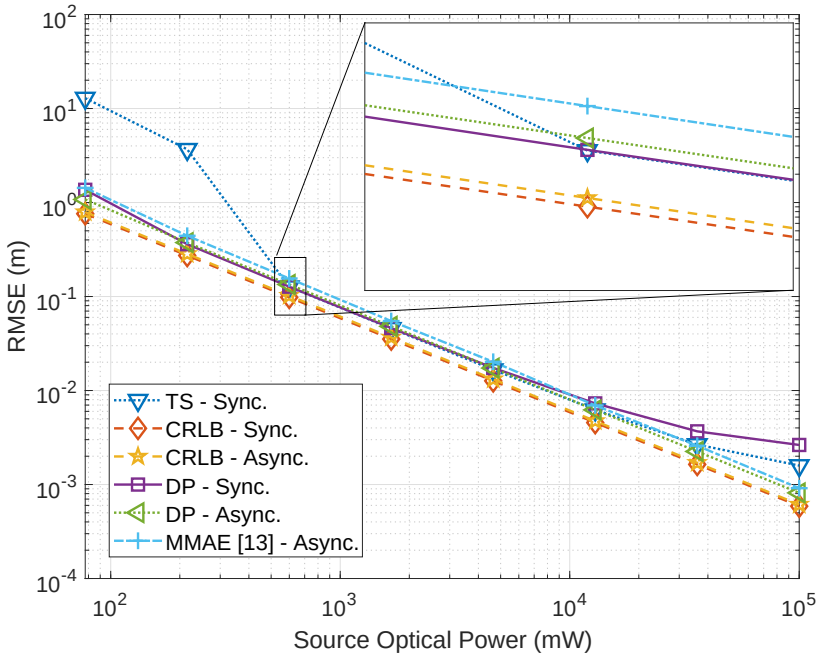

Figure 3.5: CRLBs and RMSEs of the estimators for synchronous and asynchronous VLP systems versus source optical power, where $T_s = 1\,\mu$s and $f_c = 10\,$MHz.

3.4.3 Performance of Direct and Two-Step Estimators with Respect to VLC Receiver Coordinates

In this subsection, theoretical bounds and estimator performances are investigated along a horizontal path inside the room. In Fig. 3.6 and Fig. 3.7, the CRLBs and the RMSEs of the DP and TS estimators and the algorithm in [13] are illustrated for $f_c = 100\,$MHz and $f_c = 10\,$MHz, respectively, as the VLC receiver moves on a straight line starting from $[4\ 0\ 1]\,$m and ending at $[4\ 8\ 1]\,$m inside the room. It is observed that the estimator performances tend to decrease as the receiver moves towards the edge of the room, as indicated by the Lambertian formula in (3.3). In addition, the TS estimator for $f_c = 10\,$MHz exhibits significantly higher performance than that for $f_c = 100\,$MHz. The reason for this behaviour is that the first-step TOA estimation errors are weighted by the inverse of the corresponding analytical CRLBs in (3.35), which do not provide tight bounds at low SNRs for the ML estimates of the TOA in the first step in

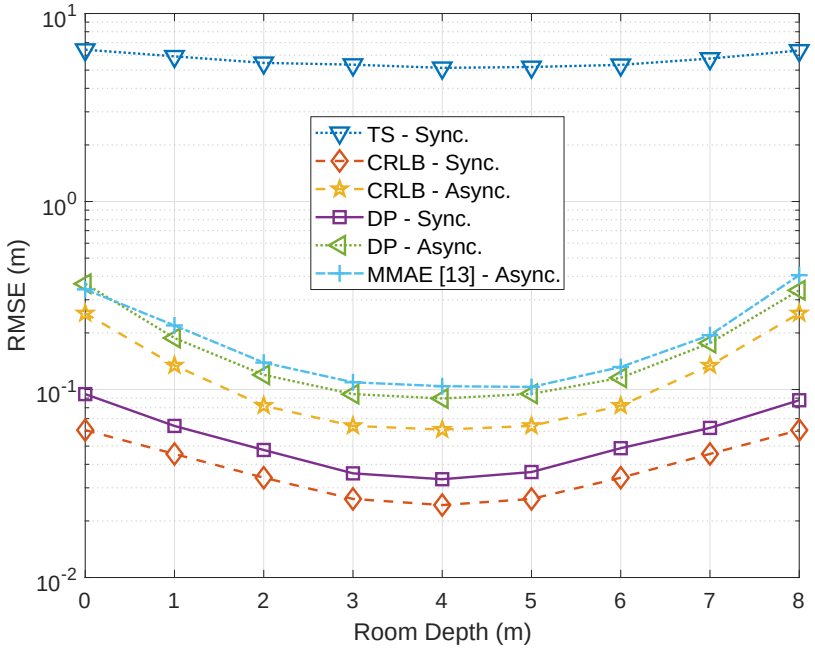

Figure 3.6: CRLBs and RMSEs of the estimators for synchronous and asynchronous VLP systems as the VLC receiver moves on a straight line in the room, where $T_s = 1\,\mu$s, $A = 1\,$W and $f_c = 100\,$MHz.

(3.21). Furthermore, the figures show that the proposed direct scheme in the asynchronous case attains higher performance than the localization algorithm in [13] at most of the locations in the room.

3.4.4 Performance of Direct and Two-Step Estimators in the Presence of Model Uncertainties

In this part, the performances of the proposed direct and two-step estimators are evaluated in the presence of uncertainties related to the attenuation model for visible light channels, i.e., the Lambertian model in (3.3). Since the knowledge of model-related parameters is imperfect in practical localization scenarios, it is important to assess the localization performance under various degrees of uncertainty, which is useful to reveal the robustness of the proposed algorithms against parameter/model mismatches.

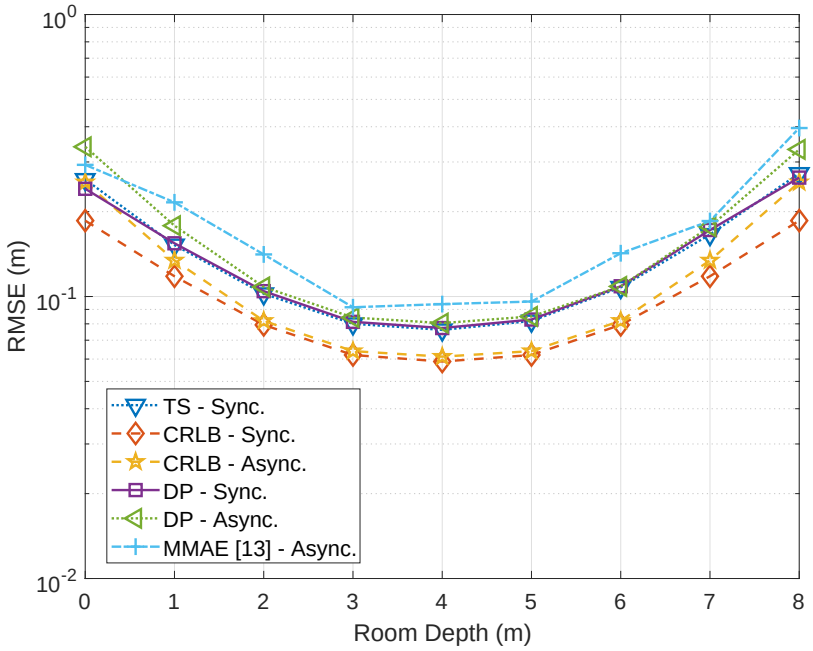

Figure 3.7: CRLBs and RMSEs of the estimators for synchronous and asynchronous VLP systems as the VLC receiver moves on a straight line in the room, where $T_s = 1\,\mu$s, $A = 1\,$W and $f_c = 10\,$MHz.

3.4.4.1 Performance with Respect to Uncertainty in Lambertian Order

First, we consider the case in which the Lambertian order m_i in (3.3) is known with a certain degree of uncertainty. To that aim, a measured (estimated) value $\hat{m}_i$, which does not perfectly match the true value m_i, is used in the proposed DP and TS estimators and in the localization algorithm in [13]. In the simulations, m_i is set to 1 and $\hat{m}_i$ is varied over the interval $[0.75\ 1.25]$ for $i \in \{1, \ldots, N_{\mathrm{L}}\}$. Fig. 3.8 and Fig. 3.9 show the localization performance of the considered approaches with respect to the measured value of the Lambertian order for $f_c = 100\,$MHz and $f_c = 10\,$MHz, respectively. It is observed from the figures that the localization performance deteriorates as the measured/estimated Lambertian order deviates from the true value, as expected. In addition, it is noted that the synchronous DP estimator is more robust to Lambertian order mismatches than the asynchronous algorithms. The reason is that the TOA information, which is independent of the

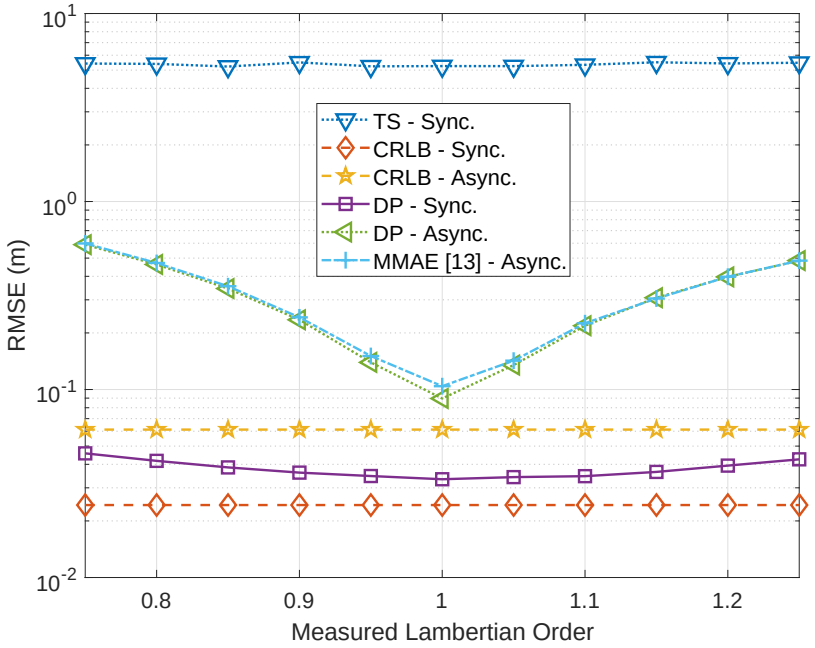

Figure 3.8: CRLBs and RMSEs of the estimators for synchronous and asynchronous VLP systems under imperfect knowledge of Lambertian order, where true Lambertian order is 1, $T_s = 1\,\mu$s, $A = 1\,$W, and $f_c = 100\,$MHz.

Lambertian order (see (3.2)), becomes the dominant factor affecting the localization performance as the uncertainty in the Lambertian order grows, hindering the effective use of the RSS information (see (3.3)). Hence, the robustness of the synchronous positioning against uncertainties in the Lambertian order is more evident at high center frequencies with an increase in the accuracy of TOA information [33], which can also be observed by comparing Fig. 3.8 and Fig. 3.9. Moreover, in the asynchronous case, the proposed algorithm performs slightly better than that in [13] for various degrees of uncertainty.

3.4.4.2 Performance with Respect to Uncertainty in Transmission Model

Next, we investigate the estimator performances in the presence of uncertainty in the overall transmission model in (3.3). As in [131], we assume a multiplicative uncertainty model that represents all the individual uncertainties embedded in

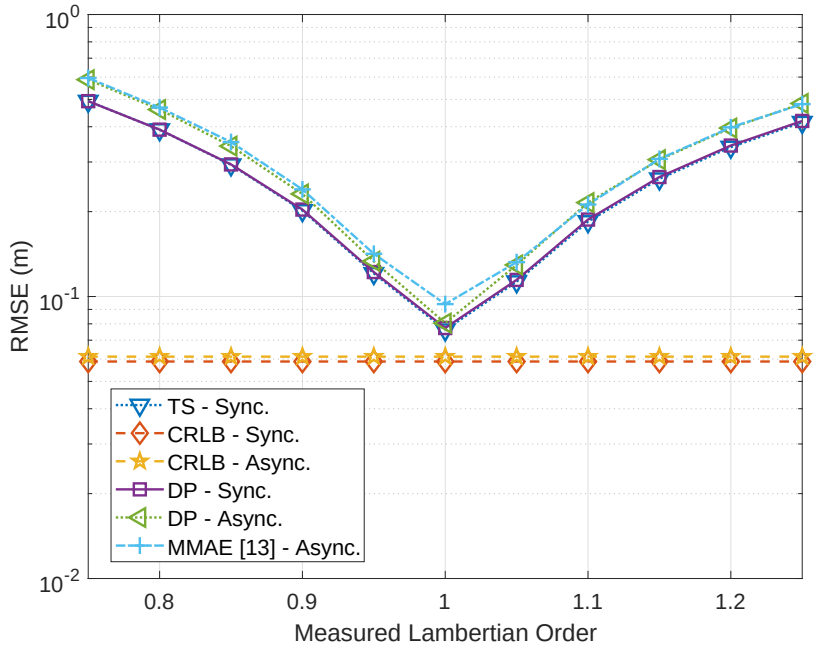

Figure 3.9: CRLBs and RMSEs of the estimators for synchronous and asynchronous VLP systems under imperfect knowledge of Lambertian order, where true Lambertian order is 1, $T_s = 1\,\mu$s, $A = 1\,$W, and $f_c = 10\,$MHz.

(3.3) (e.g., $\boldsymbol{l}_{\rm t}^i$, $\boldsymbol{n}_{\rm t}^i$, $\boldsymbol{n}_{\rm r}$, and m_i) in the form of a multiplication of the true transmission model. More specifically, the position estimation is performed by considering the following transmission model:

$$\alpha_i^{\rm meas} = (1+\varepsilon_i)\alpha_i,\ \ i = 1, \ldots, N_{\rm L} \tag{3.63}$$

where α_i is as defined in (3.3) and $\varepsilon_i \in \left[\varepsilon_i^{\rm min}, \varepsilon_i^{\rm max}\right]$ specifies the degree of mismatch between the true and the estimated transmission models. In Fig. 3.10 and Fig. 3.11, the RMSEs of the estimators are plotted against the degree of uncertainty, ε_i, for $f_c = 100\,$MHz and $f_c = 10\,$MHz, respectively, where $\varepsilon_i^{\rm min} = -0.25$ and $\varepsilon_i^{\rm max} = 0.25$ for $i = 1, \ldots, N_{\rm L}$. As observed from the figures, the localization performance curves with respect to the degree of uncertainty in the transmission model exhibit similar trends to those for the case of uncertainty in the Lambertian order.

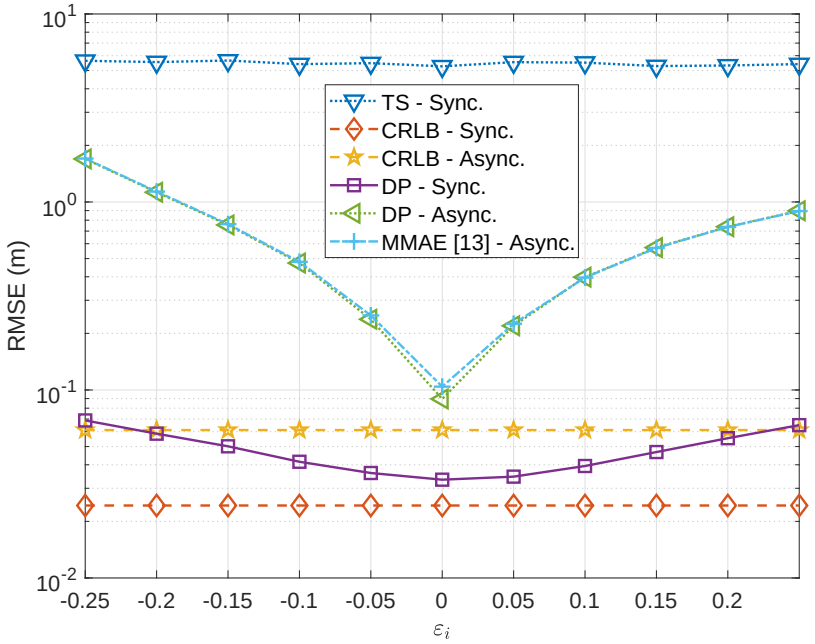

Figure 3.10: CRLBs and RMSEs of the estimators for synchronous and asynchronous VLP systems under mismatched transmission model, where $T_s = 1\,\mu$s, $A = 1\,$W, and $f_c = 100\,$MHz.

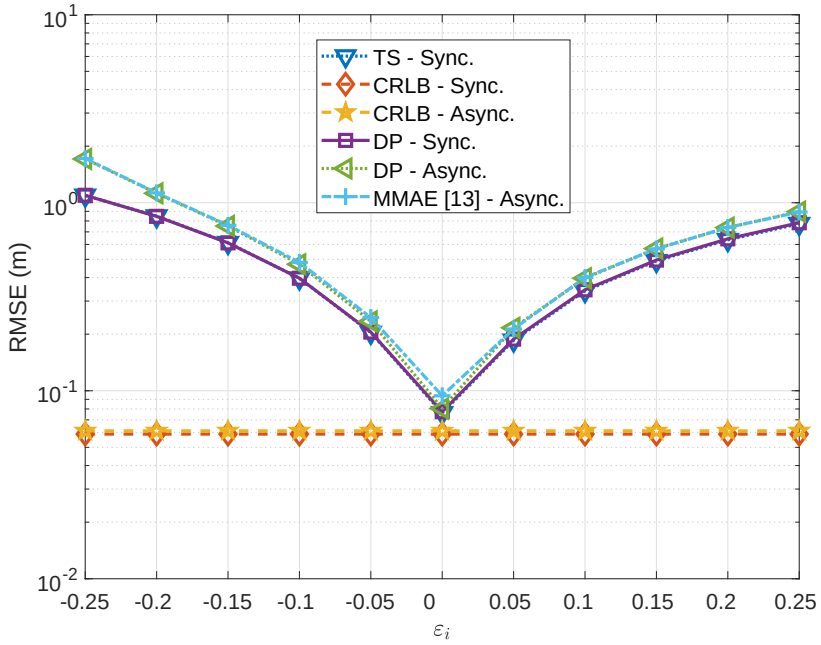

Figure 3.11: CRLBs and RMSEs of the estimators for synchronous and asynchronous VLP systems under mismatched transmission model, where $T_s = 1\,\mu$s, $A = 1\,$W, and $f_c = 10\,$MHz.

3.4.5 Special Case: Two-Dimensional Localization

In this part, we investigate the two-dimensional localization performance of the proposed estimators and perform comparisons with the trilateration method, which is one of the most commonly used methods in two-dimensional visible light localization. Specifically, we implement the linear least-squares (LLS) based trilateration algorithm in [9] via Eqs. (6), (7), (9), and (17) therein.[11] For the CRLB computations and algorithm implementations, we assume that the receiver height is known and perform two-dimensional position estimation accordingly. We carry out two experiments to assess the relative performance of the proposed estimators, the MMAE estimator in [13], and the LLS based trilateration algorithm in [9]. In the experiments, the polar and azimuth angles of the LEDs are set to be $(\theta_i, \phi_i) = (180^\circ, 0^\circ)$ for $i = 1, \ldots, N_{\mathrm{L}}$, i.e., the LEDs are facing downwards.

3.4.5.1 Performance with Respect to Optical Power

In Fig. 3.12, we present the RMSE performance of the proposed DP and TS algorithms, the algorithm in [13], and the LLS based trilateration algorithm in [9] with respect to the optical power for $f_c = 100\,\mathrm{MHz}$ and $\boldsymbol{l}_{\mathrm{r}} = [4\ 6\ 1]\,\mathrm{m}$. It is observed that, in the asynchronous case, the proposed direct estimator is able to outperform both the MMAE estimator in [13] and the trilateration algorithm in [9] at almost all SNR levels. For instance, for $A = 215\,\mathrm{mW}$, the improvements in localization performance achieved by the proposed DP method are about 10 cm and 40 cm as compared to the positioning methods in [13] and [9], respectively. In addition, we note that the synchronous DP estimator outperforms all the asynchronous estimators by using the time delay information. Moreover, the proposed synchronous TS estimator converges to the CRLB at high SNR regime, which results from its asymptotic optimality property, as shown in Proposition 2 and Remark 1. Therefore, similarly to Fig. 3.4 and Fig. 3.5 in Section 3.4.2, Fig. 3.12

[11] For the implementation in [9], the Lambertian modeling in (12) and (13) is used. The parameters in (17) are taken as $A = 1$, $h = 4\,\mathrm{m}$, and $CS = 6\sqrt{2}\,\mathrm{m}$ in accordance with the configuration in Fig. 3.1.

illustrates the trade-off between direct and two-step positioning in terms of localization performance and computational complexity at different SNR regimes.

3.4.5.2 Performance with Respect to VLC Receiver Coordinates

Fig. 3.13 depicts the two-dimensional localization performance as the VLC receiver moves along the horizontal line starting from $[4\ 0\ 1]\,\mathrm{m}$ and ending at $[4\ 8\ 1]\,\mathrm{m}$ for $f_c = 100\,\mathrm{MHz}$. It is observed that the proposed ML-based direct positioning technique can attain higher localization performance than the algorithms in [13] and [9] at all the locations along the line. Also, the performance of the algorithm in [9] gets worse as the receiver moves away from the center of the room towards the edges. This is because the trilateration-based method in [9] is a suboptimal three-step approach that first estimates the distances to the LEDs by using the RSS observations, then adjusts the estimated distances via normalization and finally employs the LLS method based on the normalized distances. As the symmetry is reduced at the room edges, the normalization method applied in [9] (see (6) and (7) therein), which assigns the same normalizing constant and factor to distance estimates from different LEDs, becomes less accurate. The proposed ML-based estimator, on the other hand, achieves RMSE levels close to the CRLB at all positions along the line and therefore leads to a substantial improvement in localization performance as compared to the method in [9] (about 63 cm improvement for $\boldsymbol{l}_{\mathrm{r}} = [4\ 8\ 1]\,\mathrm{m}$).

3.5 Concluding Remarks

In this chapter, direct and two-step positioning paradigms have been investigated for VLP systems. In particular, the CRLBs and the direct and two-step position estimators are derived in synchronous and asynchronous VLP systems. The proposed CRLB expressions exploit the entire observation signal at the VLC receiver and can be applied to any VLP system in which the LED transmitters

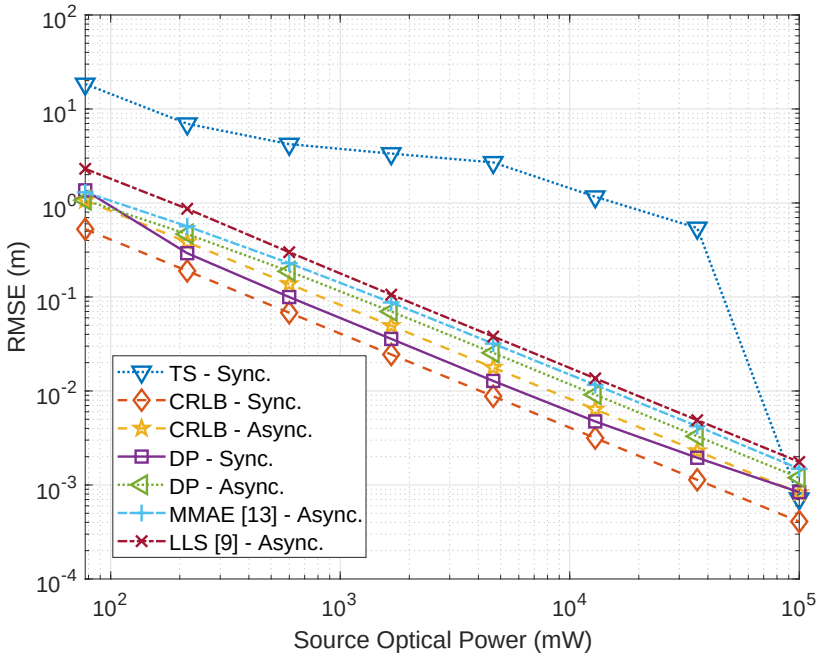

Figure 3.12: CRLBs and RMSEs of the estimators for two-dimensional localization in synchronous and asynchronous VLP systems with respect to source optical power, where $T_s = 1\,\mu$s and $f_c = 100\,$MHz.

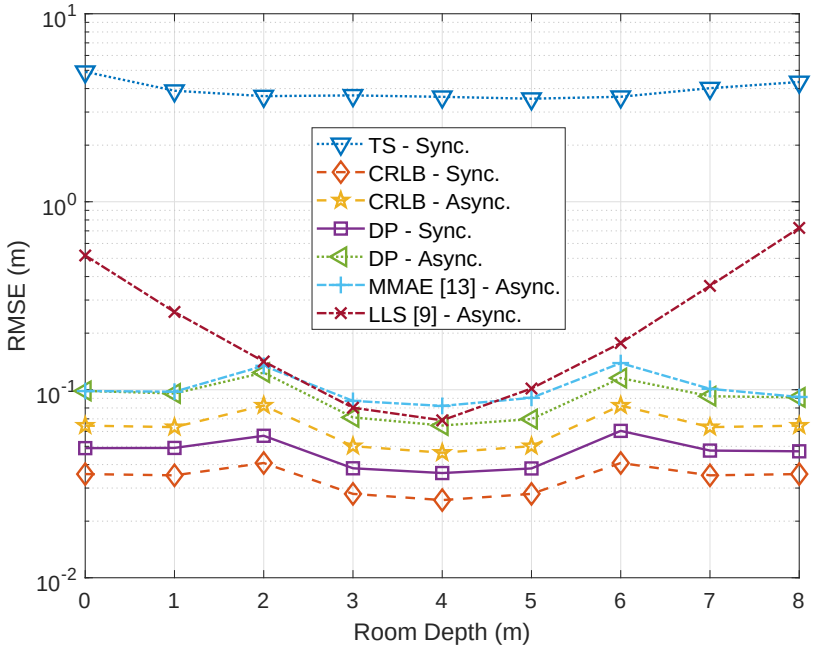

Figure 3.13: CRLBs and RMSEs of the estimators for two-dimensional localization in synchronous and asynchronous VLP systems with respect to room depth, where $T_s = 1\,\mu$s, $A = 1\,$W and $f_c = 100\,$MHz.

and the VLC receiver can have arbitrary orientations. The CRLB on the localization accuracy of synchronous VLP systems that utilize both TOA and RSS information has been derived for the first time in the literature. In addition, the CRLB presented for the asynchronous case generalizes an expression available in the literature to any type of transmitted pulses. Comparative analysis on the performance of synchronous and asynchronous systems has indicated that the advantage of synchronous positioning becomes more noticeable as the effective bandwidth of the transmitted pulse increases. Furthermore, in order to explore the relationship between direct and two-step positioning approaches, the conditions of (asymptotic) equivalence of these two approaches have been identified. It has been proved that the two-step estimator converges to the direct estimator at high SNRs for synchronous systems, whereas the two estimators are equivalent for asynchronous systems at all SNRs for practical pulse shapes. Therefore, the benefits of direct positioning on localization accuracy can be significant for synchronous systems at low-to-medium SNRs. Furthermore, the computational complexities of the proposed approaches have been presented to demonstrate the trade-off between implementation complexity and localization accuracy. Various numerical examples have been provided to illustrate the effects of direct positioning on the performance of VLP systems and to present a comparative evaluation of synchronous and asynchronous scenarios. As future work, the effects of synchronization errors can be analyzed for three-dimensional localization in VLP systems. In particular, in the presence of significant synchronization errors, it may not be useful to utilize TOA measurements in addition to RSS measurements for localization purposes. Therefore, quantifying the information that can be extracted from TOA measurements with synchronization errors is an important issue. As another direction for future work, VLP in the presence of model and parameter uncertainty can be considered with the aim of designing robust position estimators.

3.6 Appendices

3.6.1 Derivation of (3.34)

Based on Lemma 1, the joint distribution of $\hat{\tau}_i$ and $\hat{\alpha}_i$ can be specified as in (3.33), and $\hat{\tau}_i$ and $\hat{\tau}_j$ ($\hat{\alpha}_i$ and $\hat{\alpha}_j$) are conditionally independent for a given value of $\boldsymbol{l}_{\rm r}$ whenever $i \neq j$. Therefore, the joint probability density function of $\{\hat{\tau}_i, \hat{\alpha}_i\}_{i=1}^{N_{\rm L}}$ for a given value of $\boldsymbol{l}_{\rm r}$; that is, the likelihood function for $\boldsymbol{l}_{\rm r}$, is obtained as follows:

$$p(\hat{\boldsymbol{\tau}}, \hat{\boldsymbol{\alpha}} | \boldsymbol{l}_{\rm r}) = \prod_{i=1}^{N_{\rm L}} \frac{R_p \alpha_i \sqrt{E_1^i}}{\sqrt{2\pi}\,\sigma} \exp\left\{ -\frac{R_p^2 \alpha_i^2 E_1^i}{2\sigma^2} (\hat{\tau}_i - \tau_i)^2 \right\} \times \prod_{i=1}^{N_{\rm L}} \frac{R_p \sqrt{E_2^i}}{\sqrt{2\pi}\,\sigma} \exp\left\{ -\frac{R_p^2 E_2^i}{2\sigma^2} (\hat{\alpha}_i - \alpha_i)^2 \right\} \tag{3.64}$$

where $\hat{\boldsymbol{\tau}} = (\hat{\tau}_1, \ldots, \hat{\tau_{N_{\rm L}}})$ and $\hat{\boldsymbol{\alpha}} = (\hat{\alpha}_1, \ldots, \hat{\alpha_{N_{\rm L}}})$. From (3.64), the log-likelihood function can be expressed as

$$\tilde{\Lambda}(\boldsymbol{l}_{\rm r}) = \tilde{k} + \sum_{i=1}^{N_{\rm L}} \log \alpha_i - \frac{R_p^2}{2\sigma^2} \sum_{i=1}^{N_{\rm L}} \left(\alpha_i^2 E_1^i (\hat{\tau}_i - \tau_i)^2 + E_2^i (\hat{\alpha}_i - \alpha_i)^2 \right) \tag{3.65}$$

where $\tilde{k}$ is a constant that is independent of α_i's and τ_i's. Hence, the ML estimate for $\boldsymbol{l}_{\rm r}$ can be obtained from (3.65) as in (3.34). ■

3.6.2 Derivation of (3.56)

Consider the estimation of τ_i and α_i from $r_i(t)$ in (3.1). As derived in the proof of Lemma 1, the FIM can be expressed, from (3.28)–(3.31), as

$$\mathbf{J}(\tau_i, \alpha_i) = \begin{bmatrix} \frac{\alpha_i^2 R_p^2 E_1^i}{\sigma^2} & \frac{-\alpha_i R_p^2 E_3^i}{\sigma^2} \\ \frac{-\alpha_i R_p^2 E_3^i}{\sigma^2} & \frac{R_p^2 E_2^i}{\sigma^2} \end{bmatrix}. \tag{3.66}$$

Then, the CRLB on estimating α_i can be obtained as

$$\mathrm{E}\{(\hat{\alpha}_i - \alpha_i)^2\} \geq [\mathbf{J}^{-1}(\tau_i, \alpha_i)]_{2,2} = \frac{E_1^i\, \sigma^2 / R_p^2}{E_1^i E_2^i - (E_3^i)^2} \tag{3.67}$$

Hence, the weighting coefficient in (3.56) is inversely proportional to the CRLB for estimating α_i from $r_i(t)$. ■

Chapter 4

Optimal and Robust Power Allocation for Visible Light Positioning Systems under Illumination Constraints

In this chapter, optimal power allocation strategies are studied for LED transmitters in a VLP system under both perfect and imperfect knowledge of localization related parameters [19]. The main contributions of this chapter can be listed as follows:

- *Problem Formulation for LED Power Allocation:* For the first time in the literature, we investigate the problem of optimal power allocation among LED transmitters in a VLP system for maximizing the localization accuracy of a VLC receiver. Specifically, we employ the CRLB on the localization error as the performance measure and formulate the power allocation problem to minimize the CRLB in the presence of transmission power and illumination constraints.

- *Robustness Under Overall System Uncertainty*[1]*:* We consider the problem of robust power allocation under imperfect knowledge of system parameters and demonstrate that the resulting worst-case CRLB minimization problem can equivalently be transformed into a convex program, which further simplifies to an SDP via constraint relaxation.

- *Robustness Under Individual Parameter Uncertainties:* We present robust power allocation schemes in the presence of uncertainties in the location and orientation of the VLC receiver. To tackle the resulting intractable optimization problems, we propose an iterative entropic regularization approach where, at each iteration, a convex problem is solved and a three (two)-dimensional grid search is executed over the uncertainty region corresponding to the location (orientation) of the VLC receiver.

- *Sum Power Minimization Under Preset Accuracy Constraints:* We formulate the minimum power consumption problem under the constraint that the CRLB for localization of the VLC receiver does not exceed a certain threshold. We also extend the problem to the case of overall system uncertainty and prove that the resulting worst-case accuracy constrained optimization problem is shown to be reformulated as a convex one, leading to efficient solutions.

In addition, numerical results show that the proposed optimal power allocation approach for LED transmitters yields significant localization performance gains over the conventional uniform power assignment method. For the case of imperfect knowledge of localization related parameters, the proposed robust power allocation strategies are shown to outperform the uniform and non-robust (which disregards the uncertainty in parameter measurements) strategies.

This chapter is organized as follows: Section 4.1 introduces the system model and Section 4.2 presents a theoretical framework for LED power allocation. In Section 4.3 and Section 4.4, robust power allocation strategies are considered in

[1]Overall system uncertainty is defined as the uncertainty related to all the system parameters except for the transmit powers and mathematically formulated as a perturbation matrix.

the presence of overall system uncertainty and individual parameter uncertainties, respectively. Section 4.5 focuses on the minimum power consumption problem. Numerical results are provided in Section 4.6, followed by concluding remarks in Section 4.7.

4.1 System Model

We consider a VLP system with N_{L} LED transmitters and a VLC receiver, where the objective is to estimate the unknown location of the VLC receiver by utilizing signals emitted by the LED transmitters. As is commonly the case for visible light systems [5, 23], we assume an LOS scenario between each LED transmitter and the VLC receiver. Then, the received signal at the VLC receiver due to the ith LED transmitter is formulated as [23]

$$r_i(t) = \alpha_i R_p \, s_i(t - \tau_i) + \eta_i(t) \tag{4.1}$$

for $i \in \{1, \ldots, N_{\mathrm{L}}\}$ and $t \in [T_{1,i}, T_{2,i}]$, where $T_{1,i}$ and $T_{2,i}$ specify the observation interval for the signal coming from the ith LED transmitter, α_i is the optical channel attenuation factor between the ith LED transmitter and the VLC receiver ($\alpha_i > 0$), R_p is the responsivity of the photo detector at the VLC receiver, $s_i(t)$ is the transmitted signal of the ith LED transmitter, which is nonzero over an interval of $[0, T_{s,i}]$, τ_i is the TOA of the signal emitted by the ith LED transmitter, and $\eta_i(t)$ is zero-mean additive white Gaussian noise with a spectral density level of σ^2. To enable independent processing of signals coming from different LED transmitters, a certain type of multiple access protocol, such as frequency-division or time-division multiple access [130,132], can be employed [4]. Thus, the noise processes, $\eta_1(t), \ldots, \eta_{N_{\mathrm{L}}}(t)$, are modeled to be independent. In addition, we assume that the VLC receiver has the knowledge of R_p and $s_i(t)$, $i \in \{1, \ldots, N_{\mathrm{L}}\}$.

The TOA parameter in (4.1) can be expressed as

$$\tau_i = \|\boldsymbol{l}_{\mathrm{r}} - \boldsymbol{l}_{\mathrm{t}}^i\| / c + \Delta_i \tag{4.2}$$

where c is the speed of light, Δ_i denotes the time offset between the clocks of the ith LED transmitter and the VLC receiver, $\boldsymbol{l}_{\mathrm{r}} = [l_{\mathrm{r},1} \; l_{\mathrm{r},2} \; l_{\mathrm{r},3}]^T$ and

$\boldsymbol{l}_{\rm t}^i = \left[l_{\rm t,1}^i\ l_{\rm t,2}^i\ l_{\rm t,3}^i\right]^T$ denote the locations of the VLC receiver and the ith LED transmitter, respectively, and $\|\boldsymbol{l}_{\rm r} - \boldsymbol{l}_{\rm t}^i\|$ specifies the distance between the ith LED transmitter and the VLC receiver. For synchronous VLP systems, $\Delta_i = 0$ for $i = 1, \ldots, N_{\rm L}$ as all the LED transmitters and the VLC receiver are synchronized to a common time reference. On the other hand, for asynchronous systems, where there is no synchronization between the LED transmitters and the VLC receiver, Δ_i's are modeled as deterministic unknown parameters.

Using the Lambertian model [104], the channel attenuation factor α_i in (4.1) can be written as[2]

$$\alpha_i = -\frac{(m_i+1)S}{2\pi} \frac{\left[(\boldsymbol{l}_{\rm r} - \boldsymbol{l}_{\rm t}^i)^T \boldsymbol{n}_{\rm t}^i\right]^{m_i} (\boldsymbol{l}_{\rm r} - \boldsymbol{l}_{\rm t}^i)^T \boldsymbol{n}_{\rm r}}{\|\boldsymbol{l}_{\rm r} - \boldsymbol{l}_{\rm t}^i\|^{m_i+3}} \tag{4.3}$$

where m_i is the Lambertian order for the ith LED transmitter, S is the area of the photo detector at the VLC receiver, and $\boldsymbol{n}_{\rm r} = [n_{\rm r,1}\ n_{\rm r,2}\ n_{\rm r,3}]^T$ and $\boldsymbol{n}_{\rm t}^i = \left[n_{\rm t,1}^i\ n_{\rm t,2}^i\ n_{\rm t,3}^i\right]^T$ specify the orientation vectors of the VLC receiver and the ith LED transmitter, respectively [23, 29].[3]

It is assumed that the parameters S, $\boldsymbol{n}_{\rm r}$, m_i, $\boldsymbol{l}_{\rm t}^i$, and $\boldsymbol{n}_{\rm t}^i$ for $i = 1, \ldots, N_{\rm L}$ are known by the VLC receiver. For example, the orientation of the VLC receiver, $\boldsymbol{n}_{\rm r}$, can be measured through a gyroscope and the parameters of the LED transmitters (m_i, $\boldsymbol{l}_{\rm t}^i$ and $\boldsymbol{n}_{\rm t}^i$) can be transmitted to the receiver via visible light communications.[4]

Remark 1. In VLP systems, the types of signal metrics that can be utilized for position estimation depend on whether the considered system is synchronous or asynchronous. The TOA parameter in (4.2) can be used only for synchronous

[2]As the optical channel attenuation α_i is non-negative and governs the received signal level, it can be regarded as the RSS parameter in VLP systems [18].

[3]For example, $\boldsymbol{n}_{\rm r} = [0\ 0\ 1]^T$ means that the VLC receiver is pointing upwards.

[4]The communication interval between each LED transmitter and the VLC receiver can be divided into two non-overlapping time slots, in which the ranging signals $s_i(t)$ can be transmitted in the first one and the parameters of the transmitter can be sent in the second one. The VLC receiver can estimate its own location using the ranging signals and the related parameters transmitted by the LEDs via a consistent LOS link between each LED transmitter and the VLC receiver.

systems as Δ_i's are unknown in asynchronous scenarios. On the other hand, the RSS parameter in (4.3) conveys information related to the unknown location of the VLC receiver, $\boldsymbol{l}_{\mathrm{r}}$, in both synchronous and asynchronous VLP systems since it does not depend on the time offsets Δ_i's. Hence, in synchronous scenarios, both the TOA and RSS parameters can be employed for positioning, whereas in asynchronous scenarios, only the RSS parameter can be used for estimating $\boldsymbol{l}_{\mathrm{r}}$.

4.2 Optimal Power Allocation for LEDs

In this section, we establish a theoretical framework for the optimization of LED transmit powers with the aim of maximizing the localization performance of the VLC receiver. First, we describe the optimization variables and the optimization performance metric. Then, by incorporating several practical constraints related to indoor visible light scenarios, we present the formulation of the optimal power allocation problem.

4.2.1 Optimization Variables

The transmitted signal $s_i(t)$ from the ith LED transmitter can be expressed as

$$s_i(t) = \sqrt{P_i}\,\widetilde{s}_i(t) \tag{4.4}$$

for $i \in \{1, \ldots, N_{\mathrm{L}}\}$, where $\widetilde{s}_i(t)$ is a base signal such that $\int_0^{T_{s,i}} (\widetilde{s}_i(t))^2 dt/T_{s,i} = 1$, and P_i is a parameter that specifies the transmit power of the ith LED. Then, the *optical power* of $s_i(t)$ can be obtained as [23]

$$E_i^{\mathrm{opt}} = \int_0^{T_{s,i}} s_i(t) dt \big/ T_{s,i} = \sqrt{P_i}\,\widetilde{E}_i^{\mathrm{opt}} \tag{4.5}$$

where $T_{s,i}$ denotes the period of $s_i(t)$ and $\widetilde{E}_i^{\mathrm{opt}}$ is the optical power of $\widetilde{s}_i(t)$, defined as

$$\widetilde{E}_i^{\mathrm{opt}} \triangleq \int_0^{T_{s,i}} \widetilde{s}_i(t) dt \big/ T_{s,i}\ . \tag{4.6}$$

On the other hand, the *electrical power* consumed by the ith LED, E_i^{elec}, is proportional to P_i [104]; that is, $E_i^{\text{elec}} \propto \int_0^{T_{s,i}} (s_i(t))^2 dt / T_{s,i} = P_i$. In this study, we aim at optimizing the electrical powers of the transmitted signals by adjusting $\{P_i\}_{i=1}^{N_{\text{L}}}$ to maximize the localization performance.

4.2.2 Optimization Metric

The CRLB on the variance of any unbiased estimator $\hat{\boldsymbol{l}}_{\text{r}}$ for the location of the VLC receiver $\boldsymbol{l}_{\text{r}}$ can be expressed as

$$\mathbb{E}\big\{\|\hat{\boldsymbol{l}}_{\text{r}} - \boldsymbol{l}_{\text{r}}\|^2\big\} \geq \text{trace}\big\{\mathbf{J}^{-1}(\mathbf{p})\big\} \tag{4.7}$$

where the Fisher information matrix (FIM) is given by [18]

$$\mathbf{J}(\mathbf{p}) = (\mathbf{I}_3 \otimes \mathbf{p})^T \boldsymbol{\Gamma} \tag{4.8}$$

with

$$\mathbf{p} \triangleq [P_1 \ \ldots \ P_{N_{\text{L}}}]^T \in \mathbb{R}^{N_{\text{L}}} \tag{4.9}$$

$$\boldsymbol{\Gamma} \triangleq \begin{bmatrix} \boldsymbol{\gamma}_{1,1} & \boldsymbol{\gamma}_{1,2} & \boldsymbol{\gamma}_{1,3} \\ \boldsymbol{\gamma}_{2,1} & \boldsymbol{\gamma}_{2,2} & \boldsymbol{\gamma}_{2,3} \\ \boldsymbol{\gamma}_{3,1} & \boldsymbol{\gamma}_{3,2} & \boldsymbol{\gamma}_{3,3} \end{bmatrix} \in \mathbb{R}^{3N_{\text{L}} \times 3} \tag{4.10}$$

$$\boldsymbol{\gamma}_{k_1,k_2} \triangleq \begin{bmatrix} \gamma_{k_1,k_2}^{(1)} & \cdots & \gamma_{k_1,k_2}^{(N_{\text{L}})} \end{bmatrix}^T \in \mathbb{R}^{N_{\text{L}}} \tag{4.11}$$

for $k_1, k_2 \in \{1, 2, 3\}$. $\mathbf{I}_3$ and $\otimes$ in (4.8) represents, respectively, the 3×3 identity matrix and the Kronecker product, P_i in (4.9) is as defined in Section 4.2.1 and $\gamma_{k_1,k_2}^{(i)}$ in (4.11) is given by Appendix 4.8.1.

We employ the CRLB in (4.7) as the optimization performance metric for quantifying the localization accuracy of the VLC receiver.[5] The reason for this

[5]It should be emphasized that this performance metric constitutes a lower bound on the positioning error of unbiased estimators and therefore may not be the same as the actual positioning error. However, as will be shown in Section 4.6.2, the optimization based on the CRLB leads to a similar level of improvement on the RMSE performance of the ML estimators.

choice is that the ML estimator for the location of the VLC receiver can attain the CRLB for sufficiently high SNRs [122, 133]. In addition, the CRLB expression facilitates theoretical analyses and results in mathematically tractable formulations. Also, the usage of the CRLB as a performance measure renders the analysis independent of any specific location estimator, thereby providing a generic framework for power allocation in VLP systems.

4.2.3 VLP System Constraints

Certain constraints must be imposed on a VLP system while designing LED power optimization schemes in order to satisfy illumination, energy, and hardware related requirements. In particular, the following system constraints are taken into account in the power optimization problem:

4.2.3.1 Individual Power Constraints

Lower and upper bound constraints for LED powers must be incorporated to ensure that transmission powers of LEDs lie inside the linear region of operation so that the LED output power is proportional to the input drive current, which provides efficient electrical-to-optical conversion [55, 59, 78, 79, 134]. In addition, self-heating induced by a high drive current may shorten the LED lifetime [135]. Hence, the resulting constraint set is given by

$$\mathcal{P}_1 \triangleq \{\mathbf{p} \in \mathbb{R}^{N_{\mathrm{L}}} : \mathbf{p}_{\mathrm{lb}} \preceq \mathbf{p} \preceq \mathbf{p}_{\mathrm{ub}}\} \tag{4.12}$$

where $\mathbf{p}_{\mathrm{lb}} \in \mathbb{R}^{N_{\mathrm{L}}}$ and $\mathbf{p}_{\mathrm{ub}} \in \mathbb{R}^{N_{\mathrm{L}}}$ denote, respectively, the lower and upper bounds on $\mathbf{p}$ in (4.9).

4.2.3.2 Total Power Constraint

Due to power consumption restrictions of LEDs and human eye safety considerations, the total electrical power of LEDs in a VLP system must be limited [60, 79, 104, 136]. Therefore, we have the following constraint set regarding the total power limit:

$$\mathcal{P}_2 \triangleq \{\mathbf{p} \in \mathbb{R}^{N_\mathrm{L}} : \mathbf{1}^T\mathbf{p} \leq P_\mathrm{T}\} \tag{4.13}$$

where P_T determines the total electrical power constraint of LEDs.

4.2.3.3 Individual Illumination Constraints

Since VLP systems are utilized also for indoor lighting in addition to other benefits such as data transmission and localization, a certain level of brightness must be maintained over the room and/or at specified locations [79–82]. The illuminance ($\mathrm{lm/m^2}, \mathrm{lx}$) is used as a measure of brightness, which is defined as the luminous flux (lm) per unit area [137]. Combining [82, Eq. 3], [137, Eq. 16.3] and (4.5), the horizontal illuminance at location $\mathbf{x}$ generated by the ith LED can be calculated as

$$\mathcal{I}^i_{\mathrm{ind}}(\mathbf{x}, P_i) = \sqrt{P_i}\,\phi_i(\mathbf{x}) \tag{4.14}$$

where

$$\phi_i(\mathbf{x}) \triangleq \frac{(m_i+1)\kappa_i \widetilde{E}^{\mathrm{opt}}_i}{2\pi} \frac{\left[(\mathbf{x}-\boldsymbol{l}^i_\mathrm{t})^T\boldsymbol{n}^i_\mathrm{t}\right]^{m_i}(l^i_{\mathrm{t},3}-x_3)}{\|\mathbf{x}-\boldsymbol{l}^i_\mathrm{t}\|^{m_i+3}} \tag{4.15}$$

with $\widetilde{E}^{\mathrm{opt}}_i$ being as defined in (4.6) and κ_i denoting the luminous efficacy (lm/W) of the ith LED, defined as the optical power to luminous flux conversion efficiency [137]. Then, the total illuminance at $\mathbf{x}$ produced by all the LEDs can be obtained as follows [138]:

$$\mathcal{I}_{\mathrm{ind}}(\mathbf{x}, \mathbf{p}) = \sum_{i=1}^{N_\mathrm{L}} \mathcal{I}^i_{\mathrm{ind}}(\mathbf{x}, P_i) = \sum_{i=1}^{N_\mathrm{L}} \sqrt{P_i}\,\phi_i(\mathbf{x}) \tag{4.16}$$

Let L denote the number of locations at which the illuminance constraint is to be satisfied. Then, the corresponding constraint set can be defined as

$$\mathcal{P}_3 \triangleq \{\mathbf{p} \in \mathbb{R}^{N_{\mathrm{L}}} : \mathcal{I}_{\mathrm{ind}}(\mathbf{x}_\ell, \mathbf{p}) \geq \widetilde{\mathcal{I}}_\ell,\ \ell = 1, \ldots, L\} \tag{4.17}$$

where $\widetilde{\mathcal{I}}_\ell$ is the illuminance constraint defined for location $\mathbf{x}_\ell$.

4.2.3.4 Average Illumination Constraint

The expression in (4.16) quantifies the illuminance level at a specified location in the room. It may also be necessary to keep the average illuminance over the room above a certain threshold to comply with average brightness requirements. Then, the average illuminance is

$$\mathcal{I}_{\mathrm{avg}}(\mathbf{p}) = \sum_{i=1}^{N_{\mathrm{L}}} \sqrt{P_i}\, \frac{\int_{\mathcal{A}} \phi_i(\mathbf{x}) d\mathbf{x}}{|\mathcal{A}|} \tag{4.18}$$

where $\mathcal{A}$ denotes the region where the average illuminance constraint must be satisfied and $|\mathcal{A}|$ denotes the volume of $\mathcal{A}$. The constraint set associated with the average illuminance is given by

$$\mathcal{P}_4 \triangleq \{\mathbf{p} \in \mathbb{R}^{N_{\mathrm{L}}} : \mathcal{I}_{\mathrm{avg}}(\mathbf{p}) \geq \widetilde{\mathcal{I}}_{\mathrm{avg}}\} \tag{4.19}$$

where $\widetilde{\mathcal{I}}_{\mathrm{avg}}$ is the average illuminance constraint.

Remark 2. In addition to the lower bounds on the illumination levels in (4.17) and (4.19), we can also impose upper bound constraints to alleviate eye safety risks in human environments. However, since the total power constraint in (4.13) effectively limits the illumination level, an additional upper bound constraint in (4.17) and (4.19) is not required. To express this observation in a formal manner, let $\{\widetilde{\mathcal{I}}_\ell^{\mathrm{ub}}\}_{\ell=1}^{L}$ and $\widetilde{\mathcal{I}}_{\mathrm{avg}}^{\mathrm{ub}}$ denote the upper bounds on the individual and average illuminance levels in (4.17) and (4.19), respectively. Then, it follows from the Cauchy-Schwarz inequality that these upper bound constraints are satisfied if we choose the total power limit in (4.13) as

$$P_{\mathrm{T}} \leq \min\left\{ \min_{\ell \in \{1,\ldots,L\}} \frac{(\widetilde{\mathcal{I}}_\ell^{\mathrm{ub}})^2}{\|\boldsymbol{\phi}(\mathbf{x}_\ell)\|^2}, \frac{(\widetilde{\mathcal{I}}_{\mathrm{avg}}^{\mathrm{ub}})^2}{\|\boldsymbol{\varphi}\|^2} \right\}, \tag{4.20}$$

where $\boldsymbol{\phi}(\mathbf{x}) = [\phi_1(\mathbf{x}) \dots \phi_{N_\mathrm{L}}(\mathbf{x})]^T$ and $\boldsymbol{\varphi} = [\varphi_1 \dots \varphi_{N_\mathrm{L}}]^T$ with $\varphi_i \triangleq \frac{\int_{\mathcal{A}} \phi_i(\mathbf{x}) d\mathbf{x}}{|\mathcal{A}|}$ for $i \in \{1, \dots, N_\mathrm{L}\}$.

4.2.4 Problem Formulation

Considering the optimization metric in Section 4.2.2 and the system constraints in Section 4.2.3, the problem of optimal power allocation for LED transmitters can be formulated as follows:

$$\underset{\mathbf{p}}{\text{minimize}} \quad \mathrm{trace}\big\{\mathbf{J}^{-1}(\mathbf{p})\big\} \tag{4.21a}$$

$$\text{subject to} \quad \mathbf{p} \in \mathcal{P} \tag{4.21b}$$

where $\mathcal{P} \triangleq \bigcap_{i=1}^{4} \mathcal{P}_i$ and $\mathbf{J}(\mathbf{p})$ is given by (4.8). In the proposed power optimization framework in (4.21), we search for the optimal power vector that minimizes the CRLB for the localization of the VLC receiver subject to power and illumination constraints.[6] The following lemma establishes the convexity of (4.21).

Lemma 1. *The optimization problem in* (4.21) *is convex.*

Proof: First, the convexity of $f(\mathbf{p}) \triangleq \mathrm{trace}\big\{\mathbf{J}^{-1}(\mathbf{p})\big\}$ in $\mathbf{p}$ is shown as follows: Consider any $\mathbf{p}_1 \in \mathbb{R}^{N_\mathrm{L}}$, $\mathbf{p}_2 \in \mathbb{R}^{N_\mathrm{L}}$, and $\lambda \in [0, 1]$. Then,

$$f(\lambda\mathbf{p}_1 + (1-\lambda)\mathbf{p}_2) = \mathrm{trace}\Big\{\Big(\big[\mathbf{I}_3 \otimes (\lambda\mathbf{p}_1 + (1-\lambda)\mathbf{p}_2)\big]^T\boldsymbol{\Gamma}\Big)^{-1}\Big\} \tag{4.22}$$

$$= \mathrm{trace}\Big\{\Big(\lambda(\mathbf{I}_3 \otimes \mathbf{p}_1)^T\boldsymbol{\Gamma} + (1-\lambda)(\mathbf{I}_3 \otimes \mathbf{p}_2)^T\boldsymbol{\Gamma}\Big)^{-1}\Big\} \tag{4.23}$$

$$\leq \lambda f(\mathbf{p}_1) + (1-\lambda) f(\mathbf{p}_2) \tag{4.24}$$

where (4.22) follows from (4.8), (4.23) is the result of the properties of Kronecker product, and (4.24) is due to the convexity of $\mathrm{trace}\big\{\mathbf{X}^{-1}\big\}$ for $\mathbf{X} \succ 0$ [139]. Since the constraint sets $\mathcal{P}_1$ in (4.12) and $\mathcal{P}_2$ in (4.13) are linear, and $\mathcal{P}_3$ in (4.17) and $\mathcal{P}_4$ in (4.19) are convex due to the concavity of (4.16) and (4.18) with respect to

[6] With the optimal power allocation strategy in (4.21), the available resources of the LED transmitters can be employed to provide improved localization accuracy and a desired level of illumination simultaneously (i.e., no extra power resources are needed for localization in addition to those utilized for illumination).

$\mathbf{p}$, the combined constraint set $\mathcal{P}$ is convex, thus proving the convexity of (4.21) in $\mathbf{p}$. ■

Based on Lemma 1, it is noted that optimal LED power allocation strategies can be obtained via standard convex optimization tools [139, 140].

4.3 Robust Power Allocation with Overall System Uncertainty

In Section 4.2, the optimal power allocation is performed by assuming perfect knowledge of localization parameters, which however may not be realistic for practical VLP scenarios. In this section, robust optimization schemes will be designed for power allocation among LED transmitters in the presence of *overall uncertainty* in VLP system parameters[7]. In the following, we present the problem formulation for robust power allocation with overall system uncertainty in VLP scenarios and demonstrate that it can be reformulated as a convex optimization problem, which can further be simplified to an SDP via feasible set relaxations.

4.3.1 Problem Statement

Considering the optimization problem in (4.21), the matrix $\mathbf{\Gamma}$ in (4.10) contains all the information required for LED power optimization based on (4.8). Since the knowledge of localization related parameters is imperfect in practice, it is assumed that $\mathbf{\Gamma}$ is measured with some uncertainty; that is,

$$\widehat{\mathbf{\Gamma}} = \mathbf{\Gamma} + \mathbf{\Delta\Gamma} \tag{4.25}$$

where $\widehat{\mathbf{\Gamma}}$ is the estimated/nominal matrix and $\mathbf{\Delta\Gamma}$ represents the error matrix that accumulates all the uncertainties in localization parameters. As in [141–144], a

[7]The meaning of overall uncertainty will be clarified in Section 4.3.1.

deterministically bounded error model is considered for $\mathbf{\Delta\Gamma}$, i.e.,

$$\mathbf{\Delta\Gamma} \in \mathcal{E} \triangleq \{\mathbf{\Delta\Gamma} \in \mathbb{R}^{3N_{\mathrm{L}}\times 3} : \|\mathbf{\Delta\Gamma}\| \leq \delta\} \tag{4.26}$$

for a known size of uncertainty region δ, where $\|\cdot\|$ stands for the matrix spectral norm.

For the robust counterpart of (4.21), the aim is to minimize the worst-case CRLB over all uncertainties in the form of $\|\mathbf{\Delta\Gamma}\| \leq \delta$. Hence, considering the error model in (4.25), the robust min-max design problem corresponding to the CRLB optimization in (4.21) can be stated as follows:

$$\begin{aligned} \underset{\mathbf{p}}{\text{minimize}} \quad & \max_{\mathbf{\Delta\Gamma}\in\mathcal{E}} \ \operatorname{trace}\Big\{\big((\mathbf{I}_3 \otimes \mathbf{p})^T(\widehat{\mathbf{\Gamma}} - \mathbf{\Delta\Gamma})\big)^{-1}\Big\} \\ \text{subject to} \quad & \mathbf{p} \in \mathcal{P} \end{aligned} \tag{4.27}$$

where $\mathcal{E}$ is as defined in (4.26) and $\mathcal{P}$ is the feasible region in (4.21b).

Remark 3. As observed from (4.10), (4.11) and (4.62)–(4.67), the uncertainty in $\mathbf{\Gamma}$ (equivalently, the uncertainty in $\gamma^{(i)}_{k_1,k_2}$ in (4.62)) may result from an imperfect knowledge of the following VLP system parameters: R_p, $\boldsymbol{l}_{\mathrm{r}}$, $\boldsymbol{n}_{\mathrm{r}}$, $\boldsymbol{l}^i_{\mathrm{t}}$, $\boldsymbol{n}^i_{\mathrm{t}}$ and m_i. The maximum possible errors in estimating these parameters can be obtained by utilizing the characteristics of the devices on the LED transmitters and the VLC receiver. For instance, orientation measurement error bounds can be figured out via auxiliary sensor (e.g., gyroscope, accelerometer, magnetometer) properties, while the responsivity of the photodetector and the Lambertian order of the LED transmitters can be determined in a bounded interval from device characteristics. In addition, the uncertainty in $\boldsymbol{l}_{\mathrm{r}}$ can be estimated from the tracking error covariance matrix. Hence, it is reasonable to assume that the uncertainty in $\gamma^{(i)}_{k_1,k_2}$ is bounded and known. Denoting this uncertainty level by $\varepsilon^{(i)}_{k_1,k_2}$ (i.e., $\big|\widehat{\gamma}^{(i)}_{k_1,k_2} - \gamma^{(i)}_{k_1,k_2}\big| \leq \varepsilon^{(i)}_{k_1,k_2}$ where $\widehat{\gamma}^{(i)}_{k_1,k_2}$ represents the estimated value of $\gamma^{(i)}_{k_1,k_2}$), we have

$$\|\mathbf{\Delta\Gamma}\| \leq \|\mathbf{\Delta\Gamma}\|_F = \|\widehat{\mathbf{\Gamma}} - \mathbf{\Gamma}\|_F = \left(\sum_{k_1=1}^{3}\sum_{k_2=1}^{3}\sum_{i=1}^{N_{\mathrm{L}}}\big(\widehat{\gamma}^{(i)}_{k_1,k_2} - \gamma^{(i)}_{k_1,k_2}\big)^2\right)^{1/2} \tag{4.28}$$

$$\leq \left(\sum_{k_1=1}^{3}\sum_{k_2=1}^{3}\sum_{i=1}^{N_{\mathrm{L}}}\big(\varepsilon^{(i)}_{k_1,k_2}\big)^2\right)^{1/2} \triangleq \delta \tag{4.29}$$

where $\|\cdot\|_F$ is the matrix Frobenius norm. Therefore, in practice, the uncertainty level δ in (4.26) can be computed via (4.28) and (4.29).

Remark 4. The motivation for studying the overall system uncertainty comes from its mathematical tractability that allows for the characterization of uncertainties in a large number of individual parameters (e.g, locations, orientations and other device properties) as a single perturbation/error matrix whose spectral norm is upper bounded by a known value. This uncertainty model has also been used in the localization literature (e.g., [144]) and can lead to computationally favorable robust problem formulations, as will be shown in Section 4.3.2. The difference between the overall system uncertainty and individual parameter uncertainties (which will be investigated in Section 4.4) is that the former one reflects the combined effect of all the uncertainties in individual parameters using a conservative error model, i.e., via a matrix perturbation model (as in [144, Sec. III-C]) that involves the aggregate uncertainty, while the latter one exploits the specific characteristics of the individual uncertainty regions (e.g., spherical uncertainty set for the location in (4.42) or bounded angular deviations in orientation measurements in (4.46)) for achieving robustness in localization (i.e., each individual parameter is considered separately). In cases where it is difficult to handle the uncertainty sets collectively for all individual parameters (note that $\gamma_{k_1,k_2}^{(i)}$, defined in (4.62)–(4.67), is a very complicated expression in terms of the uncertainty sources, e.g., R_p, $\boldsymbol{l}_{\mathrm{r}}$, $\boldsymbol{n}_{\mathrm{r}}$, $\boldsymbol{l}_{\mathrm{t}}^i$, $\boldsymbol{n}_{\mathrm{t}}^i$ and m_i [131]), the overall uncertainty model can be especially beneficial in facilitating simultaneous treatment of individual uncertainties. Therefore, it should be emphasized that the individual parameter uncertainties in Section 4.4 are not the special cases of the overall system uncertainty in Section 4.3; rather, they allow us to investigate the effect of each uncertain parameter on the localization performance independently by itself [131].

4.3.2 Equivalent Convex Reformulation of (4.27)

The problem in (4.27) is challenging to solve in its current form and its direct solution is computationally prohibitive. In the following proposition, we demonstrate that (4.27) can be reformulated as a convex program.

Proposition 1. *The robust power allocation problem in* (4.27) *can equivalently be expressed as the following convex optimization problem:*

$$\begin{aligned} \underset{\mathbf{p},t,\mathbf{H},s,\mu}{\text{minimize}} \quad & t && \text{(4.30a)}\\ \text{subject to} \quad & \text{trace}\big\{\mathbf{H}\big\} \leq t - ds && \text{(4.30b)}\\ & \mathbf{\Phi}(\mathbf{p},\mathbf{H},s,\mu) \succeq 0 && \text{(4.30c)}\\ & \mathbf{H} \succeq 0,\ \mu \geq 0 && \text{(4.30d)}\\ & \mathbf{p} \in \mathcal{P} && \text{(4.30e)} \end{aligned}$$

where

$$\mathbf{\Phi}(\mathbf{p},\mathbf{H},s,\mu) \triangleq \begin{bmatrix} \mathbf{H}+s\mathbf{I} & \mathbf{I} & \mathbf{0} \\ \mathbf{I} & (\mathbf{I}_3 \otimes \mathbf{p})^T\widehat{\mathbf{\Gamma}} - \mu\mathbf{I} & -\frac{\delta}{2}(\mathbf{I}_3 \otimes \mathbf{p})^T \\ \mathbf{0} & -\frac{\delta}{2}(\mathbf{I}_3 \otimes \mathbf{p}) & \mu\mathbf{I} \end{bmatrix} \tag{4.31}$$

and d is the dimension of localization.

Proof: We utilize the following lemmas for the proof [142].

Lemma 2 *(18c in [145]). Let $\mathbf{X} \in \mathbb{R}^{d\times d}$ be a symmetric matrix. Then,* $\text{trace}\big\{\mathbf{X}\big\} \leq t$ *if and only if there exists $s \in \mathbb{R}$ and $\mathbf{H} \in \mathbb{R}^{d\times d}$ such that*

$$\text{trace}\big\{\mathbf{H}\big\} \leq t - ds,\ \mathbf{H} \succeq 0,\ \mathbf{H} + s\mathbf{I} \succeq \mathbf{X}\ . \tag{4.32}$$

Lemma 3 *(Lemma 2 in [141]). For matrices $\mathbf{A}$, $\mathbf{B}$ and $\mathbf{C}$ with $\mathbf{A} = \mathbf{A}^T$, the matrix inequality*

$$\mathbf{A} \succeq \mathbf{B}^T\mathbf{X}\mathbf{C} + \mathbf{C}^T\mathbf{X}^T\mathbf{B}\,,\quad \forall \mathbf{X} : \|\mathbf{X}\| \leq \delta \tag{4.33}$$

is satisfied if and only if there exists a $\mu \geq 0$ such that

$$\begin{bmatrix} \mathbf{A} - \mu\mathbf{C}^T\mathbf{C} & -\delta\mathbf{B}^T \\ -\delta\mathbf{B} & \mu\mathbf{I} \end{bmatrix} \succeq 0\ . \tag{4.34}$$

By introducing a slack variable t, (4.27) can equivalently be written in the epigraph form as follows:

$$\underset{\mathbf{p},t}{\text{minimize}} \;\; t \tag{4.35a}$$

$$\text{subject to} \;\; \text{trace}\Big\{\big((\mathbf{I}_3 \otimes \mathbf{p})^T(\widehat{\mathbf{\Gamma}} - \mathbf{\Delta\Gamma})\big)^{-1}\Big\} \leq t\,, \forall \mathbf{\Delta\Gamma} : \mathbf{\Delta\Gamma} \in \mathcal{E} \tag{4.35b}$$

$$\mathbf{p} \in \mathcal{P} \tag{4.35c}$$

First, using Lemma 2 for the constraint in (4.35b) leads to the following inequalities:

$$\text{trace}\big\{\mathbf{H}\big\} \leq t - ds,\; \mathbf{H} \succeq 0 \tag{4.36a}$$

$$\mathbf{H} + s\mathbf{I} \succeq \big((\mathbf{I}_3 \otimes \mathbf{p})^T(\widehat{\mathbf{\Gamma}} - \mathbf{\Delta\Gamma})\big)^{-1},\; \forall \mathbf{\Delta\Gamma} : \mathbf{\Delta\Gamma} \in \mathcal{E} \tag{4.36b}$$

for some $s \in \mathbb{R}$ and $\mathbf{H} \in \mathbb{R}^{d\times d}$. Next, applying the Schur complement lemma to (4.36b), we have

$$\begin{bmatrix} \mathbf{H} + s\mathbf{I} & \mathbf{I} \\ \mathbf{I} & (\mathbf{I}_3 \otimes \mathbf{p})^T(\widehat{\mathbf{\Gamma}} - \mathbf{\Delta\Gamma}) \end{bmatrix} \succeq 0\,,\; \forall \mathbf{\Delta\Gamma} : \mathbf{\Delta\Gamma} \in \mathcal{E}\;. \tag{4.37}$$

Rearranging (4.37), an inequality of the form (4.33) is obtained as

$$\begin{bmatrix} \mathbf{H} + s\mathbf{I} & \mathbf{I} \\ \mathbf{I} & (\mathbf{I}_3 \otimes \mathbf{p})^T\widehat{\mathbf{\Gamma}} \end{bmatrix} \succeq \mathbf{B}^T\mathbf{\Delta\Gamma}\,\mathbf{C} + \mathbf{C}^T\mathbf{\Delta\Gamma}^T\mathbf{B}\,,\; \forall \mathbf{\Delta\Gamma} : \mathbf{\Delta\Gamma} \in \mathcal{E} \tag{4.38}$$

where $\mathbf{B} \triangleq \frac{1}{2}\,[\mathbf{0} \;\; (\mathbf{I}_3 \otimes \mathbf{p})]$ and $\mathbf{C} \triangleq [\mathbf{0} \;\; \mathbf{I}]$. Then, via Lemma 3, (4.38) is transformed into the constraint in (4.30c), which completes the proof. ■

4.3.3 SDP Formulation via Feasible Set Relaxation

Since (4.30c) is a linear matrix inequality (LMI) in the variables $\mathbf{p}$, $\mathbf{H}$, s and μ [146], the problem in (4.30) is convex. In addition, if the general convex constraint (4.30e) can be relaxed to a linear one by replacing $\mathcal{P}$ with an appropriate $\widetilde{\mathcal{P}}$ satisfying $\widetilde{\mathcal{P}} \supseteq \mathcal{P}$, (4.30) simplifies to an SDP with a linear objective and a set of LMI constraints [147]. By squaring both sides of (4.17) and applying the

arithmetic mean-geometric mean inequality, a relaxed version of $\mathcal{P}_3$ is obtained as

$$\widetilde{\mathcal{P}}_3 \triangleq \{\mathbf{p} : \boldsymbol{\phi}(\mathbf{x})^T\mathbf{p} \geq \widetilde{\mathcal{I}}_\ell^2/\mathbf{1}^T\boldsymbol{\phi}(\mathbf{x}),\ \ell = 1, \ldots, L\} \supseteq \mathcal{P}_3 \tag{4.39}$$

where $\boldsymbol{\phi}(\mathbf{x}) = [\phi_1(\mathbf{x}) \ldots \phi_{N_\mathrm{L}}(\mathbf{x})]^T$. Similarly, $\mathcal{P}_4$ in (4.19) can be relaxed to

$$\widetilde{\mathcal{P}}_4 \triangleq \{\mathbf{p} : \boldsymbol{\varphi}^T\mathbf{p} \geq \widetilde{\mathcal{I}}_{\mathrm{avg}}^2/\mathbf{1}^T\boldsymbol{\varphi}\} \supseteq \mathcal{P}_4 \tag{4.40}$$

where $\boldsymbol{\varphi} = [\varphi_1 \ldots \varphi_{N_\mathrm{L}}]^T$ with $\varphi_i \triangleq \frac{\int_{\mathcal{A}} \phi_i(\mathbf{x})d\mathbf{x}}{|\mathcal{A}|}$. Hence, by defining $\widetilde{\mathcal{P}} \triangleq \mathcal{P}_1 \cap \mathcal{P}_2 \cap \widetilde{\mathcal{P}}_3 \cap \widetilde{\mathcal{P}}_4$ and replacing $\mathcal{P}$ with $\widetilde{\mathcal{P}}$ in (4.30e), (4.30) becomes an SDP problem and thus can be solved very efficiently using available convex optimization softwares [140, 148]. The worst-case complexity of an SDP with n variables and m constraints is given by $\mathcal{O}(\max(m,n)^4 n^{1/2}\log(1/\epsilon))$, where ϵ is the tolerance level [149]. Thus, the computational complexity of the SDP version of (4.30), which is obtained from the feasible set relaxations, can be expressed as $\mathcal{O}(N_\mathrm{L}^{4.5}\log(1/\epsilon))$.

4.4 Robust Power Allocation with Individual Parameter Uncertainties

In this section, we consider robust power allocation schemes under individual uncertainties related to localization parameters in VLP systems. In indoor tracking applications, VLC receiver position $\boldsymbol{l}_\mathrm{r}$ can be predicted to lie in a validation region, but its exact position cannot perfectly be known. Similarly, VLC receiver orientation $\boldsymbol{n}_\mathrm{r}$ may be subject to measurement errors since the measurement devices such as gyroscopes tend to generate noisy parameter estimates. Hence, individual parameter uncertainties must be taken into account while deriving optimal strategies for LED power allocation. In the following, we first present the problem formulations in the presence of uncertainties in the location and the orientation of the VLC receiver. Then, we propose an iterative approach to solve the resulting intractable optimization problems.

4.4.1 Uncertainty in VLC Receiver Location

To formulate the robust power allocation problem in the presence of uncertainties about the location of the VLC receiver, we assume that the nominal location $\hat{\boldsymbol{l}}_{\mathrm{r}}$ is a perturbed version of the true location $\boldsymbol{l}_{\mathrm{r}}$, i.e.,

$$\hat{\boldsymbol{l}}_{\mathrm{r}} = \boldsymbol{l}_{\mathrm{r}} + \mathbf{e}_{\boldsymbol{l}_{\mathrm{r}}} . \tag{4.41}$$

As in [131,142,150], we assume a spherical uncertainty set for the location errors, i.e.,

$$\mathbf{e}_{\boldsymbol{l}_{\mathrm{r}}} \in \mathcal{E}_{\boldsymbol{l}_{\mathrm{r}}} \triangleq \{\mathbf{e} \in \mathbb{R}^3 : \|\mathbf{e}\| \leq \delta_{\boldsymbol{l}_{\mathrm{r}}}\} \tag{4.42}$$

where $\delta_{\boldsymbol{l}_{\mathrm{r}}}$ is a known value that represents the size of the uncertainty region. Then, the power allocation problem in (4.21) based on worst-case CRLB minimization can be formulated as

$$\begin{aligned} \underset{\mathbf{p}}{\text{minimize}} \quad & \max_{\mathbf{e}_{\boldsymbol{l}_{\mathrm{r}}} \in \hat{\mathcal{E}}_{\boldsymbol{l}_{\mathrm{r}}}} \ \operatorname{trace}\Big\{ \big((\mathbf{I}_3 \otimes \mathbf{p})^T \boldsymbol{\Gamma}(\hat{\boldsymbol{l}}_{\mathrm{r}} - \mathbf{e}_{\boldsymbol{l}_{\mathrm{r}}}) \big)^{-1} \Big\} \\ \text{subject to} \quad & \mathbf{p} \in \mathcal{P} \end{aligned} \tag{4.43}$$

where $\boldsymbol{\Gamma}(\hat{\boldsymbol{l}}_{\mathrm{r}} - \mathbf{e}_{\boldsymbol{l}_{\mathrm{r}}})$ denotes the matrix $\boldsymbol{\Gamma}$ in (4.10) evaluated at $\boldsymbol{l}_{\mathrm{r}} = \hat{\boldsymbol{l}}_{\mathrm{r}} - \mathbf{e}_{\boldsymbol{l}_{\mathrm{r}}}$.

4.4.2 Uncertainty in VLC Receiver Orientation

The orientation vector of the VLC receiver can be expressed as

$$\boldsymbol{n}_{\mathrm{r}}(\theta, \phi) = [\sin\theta\cos\phi \ \ \sin\theta\sin\phi \ \ \cos\theta]^T \tag{4.44}$$

where θ and ϕ represent the polar and the azimuth angles, respectively [131]. According to (4.44), the uncertainty related to the orientation of the VLC receiver can be modeled as angular uncertainties in θ and ϕ [131]. Hence, the nominal (measured) polar and azimuth angles can be written as

$$\hat{\theta} = \theta + e_\theta, \quad \hat{\phi} = \phi + e_\phi \tag{4.45}$$

where θ and ϕ are the true values of the angles, and e_θ and e_ϕ represent the errors in angular measurements, for which the bounded uncertainty sets can be defined

as

$$e_\theta \in \mathcal{E}_\theta \triangleq \{e \in \mathbb{R} : |e| \leq \delta_\theta\} \tag{4.46a}$$

$$e_\phi \in \mathcal{E}_\phi \triangleq \{e \in \mathbb{R} : |e| \leq \delta_\phi\} \tag{4.46b}$$

with δ_θ and δ_ϕ denoting the maximum possible angular deviations. Then, the robust counterpart of (4.21) in the case of orientation uncertainties can be stated as

$$\begin{aligned} \underset{\mathbf{p}}{\text{minimize}} \; & \max_{\substack{e_\theta \in \mathcal{E}_\theta \\ e_\phi \in \mathcal{E}_\phi}} \operatorname{trace}\Big\{ \Big((\mathbf{I}_3 \otimes \mathbf{p})^T \, \mathbf{\Gamma}\big(\boldsymbol{n}_{\mathrm{r}}(\hat{\theta} - e_\theta, \hat{\phi} - e_\phi)\big) \Big)^{-1} \Big\} \\ & \text{subject to } \mathbf{p} \in \mathcal{P} \end{aligned} \tag{4.47}$$

where $\boldsymbol{n}_{\mathrm{r}}(\cdot\,,\cdot)$ is as defined in (4.44) and $\mathbf{\Gamma}\big(\boldsymbol{n}_{\mathrm{r}}(\theta,\phi)\big)$ is the matrix $\mathbf{\Gamma}$ in (4.10) evaluated at $\boldsymbol{n}_{\mathrm{r}} = \boldsymbol{n}_{\mathrm{r}}(\theta,\phi)$.

4.4.3 Iterative Entropic Regularization Algorithm

In this part, we develop a unified power allocation algorithm design for solving the robust optimization problems in (4.43) and (4.47). To this end, let the error vectors and the corresponding uncertainty sets in (4.42) and (4.46) be defined as follows:

$$\widetilde{\mathbf{e}} \triangleq \begin{cases} \mathbf{e}_{\boldsymbol{l}_{\mathrm{r}}}\,, & \text{uncertainty in VLC receiver location} \\ (e_\theta, e_\phi)\,, & \text{uncertainty in VLC receiver orientation} \end{cases} \tag{4.48}$$

$$\widetilde{\mathcal{E}} \triangleq \begin{cases} \mathcal{E}_{\boldsymbol{l}_{\mathrm{r}}}\,, & \text{uncertainty in VLC receiver location} \\ \mathcal{E}_\theta \times \mathcal{E}_\phi\,, & \text{uncertainty in VLC receiver orientation} \end{cases} \tag{4.49}$$

In addition, the objective functions in (4.43) and (4.47) can be represented by

$$\psi(\mathbf{p}, \widetilde{\mathbf{e}}) \triangleq \begin{cases} \operatorname{trace}\Big\{ \big((\mathbf{I}_3 \otimes \mathbf{p})^T \, \mathbf{\Gamma}(\hat{\boldsymbol{l}}_{\mathrm{r}} - \mathbf{e}_{\boldsymbol{l}_{\mathrm{r}}}) \big)^{-1} \Big\} \\ \operatorname{trace}\Big\{ \Big((\mathbf{I}_3 \otimes \mathbf{p})^T \, \mathbf{\Gamma}\big(\boldsymbol{n}_{\mathrm{r}}(\hat{\theta} - e_\theta, \hat{\phi} - e_\phi)\big) \Big)^{-1} \Big\} \end{cases} \tag{4.50}$$

where the first and second rows denote, respectively, the cases for the uncertainty in the location and the orientation. Then, based on (4.48)–(4.50), the problems in

(4.43) and (4.47) can be unified into a single optimization framework as follows:

$$\underset{\mathbf{p}}{\text{minimize}} \ \max_{\widetilde{\mathbf{e}} \in \widetilde{\mathcal{E}}} \ \psi(\mathbf{p}, \widetilde{\mathbf{e}}) \quad \text{subject to } \mathbf{p} \in \mathcal{P} \tag{4.51}$$

The inner problem in (4.51) is not convex since $\psi(\mathbf{p}, \widetilde{\mathbf{e}})$ is not concave in $\widetilde{\mathbf{e}}$. Moreover, the epigraph form of (4.51) results in a semi-infinite optimization problem whose constraints (in the form of $\psi(\mathbf{p}, \widetilde{\mathbf{e}}) \leq t$, $\forall \widetilde{\mathbf{e}} \in \widetilde{\mathcal{E}}$, for some $t \in \mathbb{R}$) do not admit a tractable convex reformulation, as in (4.35b). Furthermore, the exhaustive search method for solving (4.51) has a computational complexity that is exponential in the number of LED transmitters N_{L}. Therefore, it is challenging to solve (4.51) in a computationally efficient manner via conventional techniques.

To tackle the robust design problem in (4.51), our algorithmic approach is to use an *iterative entropic regularization* procedure that successively decreases the objective value of the outer problem by updating the power vector $\mathbf{p}$ while simultaneously refining the optimal value of the inner maximization problem [151, 152]. Let the objective function of the outer problem in (4.51) be defined as

$$\Psi(\mathbf{p}) \triangleq \max_{\widetilde{\mathbf{e}} \in \widetilde{\mathcal{E}}} \ \psi(\mathbf{p}, \widetilde{\mathbf{e}}) \ . \tag{4.52}$$

The continuous uncertainty set $\widetilde{\mathcal{E}}$ can be discretized using n points in $\widetilde{\mathcal{E}}$ to obtain a subset $\widetilde{\mathcal{E}}_n$ of $\widetilde{\mathcal{E}}$. Then, $\Psi(\mathbf{p})$ in (4.52) can be approximated by $\Psi^n(\mathbf{p}) \triangleq \max_{\widetilde{\mathbf{e}} \in \widetilde{\mathcal{E}}_n} \ \psi(\mathbf{p}, \widetilde{\mathbf{e}})$. To circumvent the non-differentiability of $\Psi^n(\mathbf{p})$, we can employ the following entropic regularized/smoothed approximation of the max function [151], [139, p. 72]:

$$\Psi^n_{\varrho}(\mathbf{p}) \triangleq \frac{1}{\varrho} \log \left\{ \sum_{\widetilde{\mathbf{e}} \in \widetilde{\mathcal{E}}_n} \exp\left(\varrho \, \psi(\mathbf{p}, \widetilde{\mathbf{e}})\right) \right\} \tag{4.53}$$

where ϱ is the regularization constant [152].

Based on the regularized function in (4.53), we propose the iterative entropic regularization algorithm in Algorithm 1, which consists of the following steps [151, 152]:

- *Outer Minimization:* The objective function $\Psi(\mathbf{p})$ in (4.52) is approximated by the smoothed version $\Psi_{\varrho}^{n}(\mathbf{p})$ in (4.53). The resulting convex problem[8] in (4.54) can efficiently be solved via standard tools of convex optimization [139].

- *Inner Maximization:* Using the power vector $\mathbf{p}^{\star}$ obtained from the outer minimization step, the inner maximization problem of (4.51) is solved in (4.55) by performing a three (two)-dimensional grid search over $\widetilde{\mathcal{E}}$ for the case of the uncertainty in the location (orientation) of the VLC receiver.

Algorithm 1 can be shown to converge to a global minimum of (4.51) [151]. It is worth noting that the computational burden of (4.51) is significantly reduced via Algorithm 1 as compared to the exhaustive search approach, as mentioned in the next subsection.

4.4.4 Complexity Analysis

In this part, we discuss the computational complexity of Algorithm 1 and compare it with that of the exhaustive search based solution of (4.51). At each iteration, Algorithm 1 involves solving a convex optimization problem and a grid search over the uncertainty region. Let $\mathcal{O}(C)$ denote the complexity of the convex optimization problem in (4.54) and N_{grid} the number of points employed for the grid search over $\widetilde{\mathcal{E}}$ in (4.55). Then, the per-iteration complexity of Algorithm 1 is given by $\mathcal{O}(C)+\mathcal{O}(N_{\text{grid}})$. Regarding the exhaustive search technique for solving (4.51), let each axis of the feasible region $\mathcal{P} \subset \mathbb{R}^{N_{\text{L}}}$ be discretized using $\mathcal{O}(M)$ different values. Thus, the outer iteration of (4.51) has a computational complexity of $\mathcal{O}(M^{N_{\text{L}}})$. Utilizing N_{grid} points for the inner iteration, the overall complexity becomes $\mathcal{O}(M^{N_{\text{L}}}\, N_{\text{grid}})$. Therefore, the complexity of the exhaustive search method grows exponentially with the number of LED transmitters, whereas that of Algorithm 1 is primarily determined by the convex problem in (4.54), which

[8]Since $\psi(\mathbf{p},\widetilde{\mathbf{e}})$ is a convex function of $\mathbf{p}$ for a given $\widetilde{\mathbf{e}}$ (see (4.50) and Lemma 1) and the log-sum-exp function is convex [139, p. 72], the resulting composition $\Psi_{\varrho}^{n}(\mathbf{p})$ is convex in $\mathbf{p}$.

Algorithm 1 Iterative Entropic Regularization Algorithm to Solve the Robust Power Allocation Problem in (4.51)

Initialization:
Select $\widetilde{\mathbf{e}}_1 \in \widetilde{\mathcal{E}}$, set $\widetilde{\mathcal{E}}_1 = \{\widetilde{\mathbf{e}}_1\}$, $n = 1$ and $k = 1$.
Select $\varrho > 0$, $\epsilon \in (0, 1)$, $\varsigma > 0$ and $N_{\text{grid}} \in \mathbb{Z}^+$.
Iterative Step:
(Outer Problem) Solve the following convex optimization problem with a tolerance level of ϵ^k:

$$\mathbf{p}^\star = \arg \min_{\mathbf{p} \in \mathcal{P}} \ \Psi_\varrho^n(\mathbf{p}) \tag{4.54}$$

where $\Psi_\varrho^n(\mathbf{p})$ is given by (4.53).
(Inner Problem) Obtain a new candidate from the uncertainty region $\widetilde{\mathcal{E}}$ using a grid search over the prespecified N_{grid} points:

$$\widetilde{\mathbf{e}}_{n+1} = \arg \max_{\widetilde{\mathbf{e}} \in \widetilde{\mathcal{E}}} \ \psi(\mathbf{p}^\star, \widetilde{\mathbf{e}}) \tag{4.55}$$

where $\psi(\mathbf{p}, \widetilde{\mathbf{e}})$ is as defined in (4.50).
Update $k = k + 1$.
(Check the Objective Value)
if $\psi(\mathbf{p}^\star, \widetilde{\mathbf{e}}_{n+1}) > \Psi_\varrho^n(\mathbf{p}^\star)$ **then**
    Set $\widetilde{\mathcal{E}}_{n+1} = \widetilde{\mathcal{E}}_n \cup \{\widetilde{\mathbf{e}}_{n+1}\}$.
    Update $n = n + 1$.
    Update $\varrho = \max(\varrho, \log(n)^2)$.
end if
(Check the Tolerance Value)
if $\epsilon^k + \log(n)/\varrho > \varsigma$ **then**
    Update $\varrho = \varrho + \log(n)$.
end if
Stopping Criteria:
$\psi(\mathbf{p}^\star, \widetilde{\mathbf{e}}_{n+1}) \leq \Psi_\varrho^n(\mathbf{p}^\star)$ and $\epsilon^k + \log(n)/\varrho \leq \varsigma$.

can be solved in polynomial time [145]. As a result, Algorithm 1 has significantly lower computational complexity than the exhaustive search based solution.

4.5 Minimum Power Consumption Problem

In practical indoor VLP systems, the power consumption of LEDs and the localization error of VLC receivers must be jointly considered in a power optimization problem. In Section 4.2, Section 4.3 and Section 4.4, the aim is to minimize the localization error while satisfying power and illumination related constraints. However, for improved energy efficiency of VLP systems, the total power consumption of LEDs must also be taken into account in addition to localization performance requirements [153].[9] Therefore, similar to the minimal illumination level problem in VLC systems [56, 135], we consider the *minimum power consumption problem* for VLP systems, where the objective is to minimize the total power consumption of LEDs while keeping the CRLB of the VLC receiver below a predefined level. In the following subsections, we first investigate the problem of total power minimization under perfect knowledge of localization parameters and then study robust power allocation designs in the presence of uncertainties.

4.5.1 Power Minimization with Perfect Knowledge

In the absence of uncertainties in localization parameters, the minimum power consumption problem can be formulated as follows:

$$\underset{\mathbf{p}}{\text{minimize}} \quad \mathbf{1}^T\mathbf{p} \tag{4.56a}$$

$$\text{subject to} \quad \text{trace}\big\{\mathbf{J}^{-1}(\mathbf{p})\big\} \leq \varepsilon \tag{4.56b}$$

$$\mathbf{p} \in \mathcal{P}_s \tag{4.56c}$$

[9] Energy efficient localization algorithms have been considered also for RF sensor networks in the literature (e.g., [154]).

where $\mathbf{1}^T\mathbf{p}$ determines the total electrical power consumption, $\mathcal{P}_s \triangleq \mathcal{P}_1 \cap \mathcal{P}_3 \cap \mathcal{P}_4$ and ε represents the maximum tolerable CRLB level for the localization of the VLC receiver. In (4.56), we seek to find the most energy-efficient LED power assignment scheme satisfying a certain level of localization accuracy. As implied by Lemma 1, the optimization problem in (4.56) is convex.

The significance of the considered problem in (4.56) for VLP systems lies in the fact that it yields the minimum value of P_{T} in (4.13), above which the optimal solution of (4.21) always achieves a lower CRLB than the specified design level, ε. In other words, a certain level of localization performance is guaranteed by setting P_{T} above the obtained minimum value in (4.56), as in the minimal illumination level problem in VLC systems [135].

4.5.2 Robust Power Minimization with Imperfect Knowledge

In this part, we consider the robust counterpart of the power minimization problem in (4.56) under deterministic norm-bounded uncertainty in matrix $\mathbf{\Gamma}$ in (4.10) based on the error model in (4.25). Thus, we assume that the errors in $\mathbf{\Gamma}$ belong to a bounded uncertainty region as in Section 4.3.1 and develop a robust approach that guarantees the localization performance measure for all the uncertainties in the specified region. Accordingly, the robust design problem can be formulated as

$$\underset{\mathbf{p}}{\text{minimize}} \quad \mathbf{1}^T\mathbf{p} \tag{4.57a}$$

$$\text{subject to} \quad \mathrm{trace}\Big\{\big((\mathbf{I}_3 \otimes \mathbf{p})^T(\widehat{\mathbf{\Gamma}} - \mathbf{\Delta\Gamma})\big)^{-1}\Big\} \leq \varepsilon\,,\ \forall \mathbf{\Delta\Gamma} \in \mathcal{E} \tag{4.57b}$$

$$\mathbf{p} \in \mathcal{P}_s \tag{4.57c}$$

where $\mathcal{E}$ is given by (4.26) and ε represents the constraint on the worst-case CRLB. Similar to (4.27), the semi-infinite programming problem in (4.57) can equivalently be reformulated as a convex problem, as shown in the following proposition.

Proposition 2. *The robust power allocation problem in* (4.57) *is equivalent to the following convex optimization problem:*

$$\underset{\mathbf{p},\mathbf{H},s,\mu}{\text{minimize}} \quad \mathbf{1}^T\mathbf{p} \tag{4.58a}$$

$$\text{subject to} \quad \text{trace}\big\{\mathbf{H}\big\} \leq \varepsilon - ds \tag{4.58b}$$

$$\mathbf{\Phi}(\mathbf{p},\mathbf{H},s,\mu) \succeq 0 \tag{4.58c}$$

$$\mathbf{H} \succeq 0,\ \mu \geq 0,\ \mathbf{p} \in \mathcal{P}_s \tag{4.58d}$$

where $\mathbf{\Phi}(\mathbf{p},\mathbf{H},s,\mu)$ *is defined as in* (4.31).

Proof: The proof directly follows from that of Proposition 1. ■

4.6 Numerical Results

In this section, we provide numerical examples to investigate the performance of the proposed optimal and robust power allocation designs for VLP systems.

4.6.1 Simulation Setup

We consider a VLP scenario in a room of size $10\times10\times5$ m^3, where there exist $N_{\rm L} = 4$ LED transmitters and a VLC receiver. The locations and the orientations of the LED transmitters and the VLC receiver are provided in Table 4.1. In addition, $L = 4$ locations are determined for individual illumination constraints, which are also displayed in Table 4.1. The average illuminance in (4.18) is calculated over the horizontal plane of the room at a fixed height of 1 m.

The scaled version of the transmitted signal, $\widetilde{s}_i(t)$, in (4.4) is modeled as $\widetilde{s}_i(t) = \frac{2}{3}(1-\cos(2\pi\, t/T_{s,i}))(1+\cos(2\pi f_{c,i}\, t))$ for $i = 1,\ldots,N_{\rm L}$ and $t \in [0, T_{s,i}]$, where $T_{s,i}$ is the pulse width and $f_{c,i}$ is the center frequency [16,23].[10] From (4.6), the optical

[10]The constant factor 2/3 is included to satisfy $\int_0^{T_{s,i}} (\widetilde{s}_i(t))^2 dt/T_{s,i} = 1$, as indicated in Section 4.2.1.

Table 4.1: Locations and Orientations

Location of LED-1, $\boldsymbol{l}_{\mathrm{t}}^{1}$	$[1\ 1\ 5]^{T}$ m
Location of LED-2, $\boldsymbol{l}_{\mathrm{t}}^{2}$	$[1\ 9\ 5]^{T}$ m
Location of LED-3, $\boldsymbol{l}_{\mathrm{t}}^{3}$	$[9\ 1\ 5]^{T}$ m
Location of LED-4, $\boldsymbol{l}_{\mathrm{t}}^{4}$	$[9\ 9\ 5]^{T}$ m
Orientation of LEDs, $\boldsymbol{n}_{\mathrm{t}}^{i}\,(i=1,2,3,4)$	$[0\ 0\ -1]^{T}$
Location of VLC Receiver, $\boldsymbol{l}_{\mathrm{r}}$	$[3\ 3\ 0.5]^{T}$ m
Orientation of VLC Receiver, $\boldsymbol{n}_{\mathrm{r}}$	$[0.5\ 0\ 0.866]^{T}$
Location of Illumination Constraint-1, $\mathbf{x}_1$	$[1\ 1\ 1]^{T}$ m
Location of Illumination Constraint-2, $\mathbf{x}_2$	$[1\ 9\ 1]^{T}$ m
Location of Illumination Constraint-3, $\mathbf{x}_3$	$[9\ 1\ 1]^{T}$ m
Location of Illumination Constraint-4, $\mathbf{x}_4$	$[9\ 9\ 1]^{T}$ m

Table 4.2: Simulation Parameters

Responsivity of Photo Detector, R_p	$0.4\,\mathrm{mA/mW}$
Area of Photo Detector, S	$1\,\mathrm{cm}^2$
Spectral Density Level of Noise, σ^2	$1.3381\times10^{-22}\,\mathrm{W/Hz}$
LED Lambertian Order, $m_i\,(i=1,2,3,4)$	1
LED Luminous Efficacy, $\kappa_i\,(i=1,2,3,4)$	$284\,\mathrm{lm/W}$
Min. LED Optical Power	$5\,\mathrm{W}$
Max. LED Optical Power	$20\,\mathrm{W}$
Min. Illuminance Level, $\widetilde{\mathcal{I}}_{\mathrm{avg}}, \widetilde{\mathcal{I}}_{\ell}\,(\ell=1,2,3,4)$	$30\,\mathrm{lx}$
Transmitted Pulse Width, $T_{s,i}\,(i=1,2,3,4)$	$1\,\mu\mathrm{s}$
Center Frequency, $f_{c,i}\,(i=1,2,3,4)$	$40+20(i-1)\,\mathrm{MHz}$

power of $\widetilde{s}_i(t)$ is calculated as $\widetilde{E}_i^{\mathrm{opt}}=2/3$. In accordance with [16,23,79,81,131], the VLP system parameters utilized throughout the simulations are given in Table 4.2. In addition, an asynchronous VLP system is considered, i.e., the time offsets $\{\Delta_i\}_{i=1}^{N_{\mathrm{L}}}$ in (4.2) are modeled as unknown parameters.

4.6.2 Power Allocation with Perfect Knowledge

In this part, we investigate the effects of the proposed optimal power allocation approach on the localization performance of the VLC receiver under the assumption of perfect knowledge of localization related parameters. Since this is the first

study to consider power allocation in VLP systems, the uniform power allocation strategy (i.e., $P_i = P_{\mathrm{T}}/N_{\mathrm{L}}$, $i = 1, \ldots, N_{\mathrm{L}}$) is also illustrated for comparison purposes.

Fig. 4.1 plots the CRLB achieved by the optimal solution of (4.21) versus $P_{\mathrm{T}}/N_{\mathrm{L}}$, which determines the average electrical power limit, for various locations of the VLC receiver. It is observed that the optimal power allocation approach can provide significant improvements in localization performance over the conventional uniform power allocation approach. In addition, we note that the performance improvement becomes more pronounced as the VLC receiver moves away from the center of the room. The reason is that the contribution of each LED to the Fisher information in (4.8) becomes almost equal at the room center whereas the LEDs are less symmetric at the corners. Moreover, due to the limited linear operation regime of the LEDs, the optimal strategy exhibits a similar performance to that of the uniform strategy for sufficiently high values of P_{T}. Furthermore, when P_{T} is lower than a certain value, the problem becomes infeasible due to the average illumination constraint, and the uniform and optimal strategies achieve the same CRLB at that value of P_{T}.

In order to evaluate how the optimization based on the CRLB metric reduces the true positioning error, we implement the ML estimator in [18, Eq. (44)] using the LED optical powers obtained from the optimal solution of (4.21). Fig. 4.2 shows the root-MSEs (RMSEs) of the ML estimators corresponding to the optimal and uniform power allocation strategies along with the corresponding CRLBs with respect to $P_{\mathrm{T}}/N_{\mathrm{L}}$. We observe that power optimization based on the CRLB metric can provide a level of performance enhancement in terms of the RMSE of the ML estimator that is congruent with what is predicted by the CRLB.

To investigate the power allocation performance in the presence of multiple VLC receivers, we also consider the problem of average CRLB minimization of N_{V} receivers

$$\underset{\mathbf{p}}{\text{minimize}} \quad \frac{1}{N_{\mathrm{V}}} \sum_{\ell=1}^{N_{\mathrm{V}}} \mathrm{trace}\big\{\mathbf{J}_{\ell}^{-1}(\mathbf{p})\big\} \tag{4.59a}$$

$$\text{subject to} \quad \mathbf{p} \in \mathcal{P} \tag{4.59b}$$

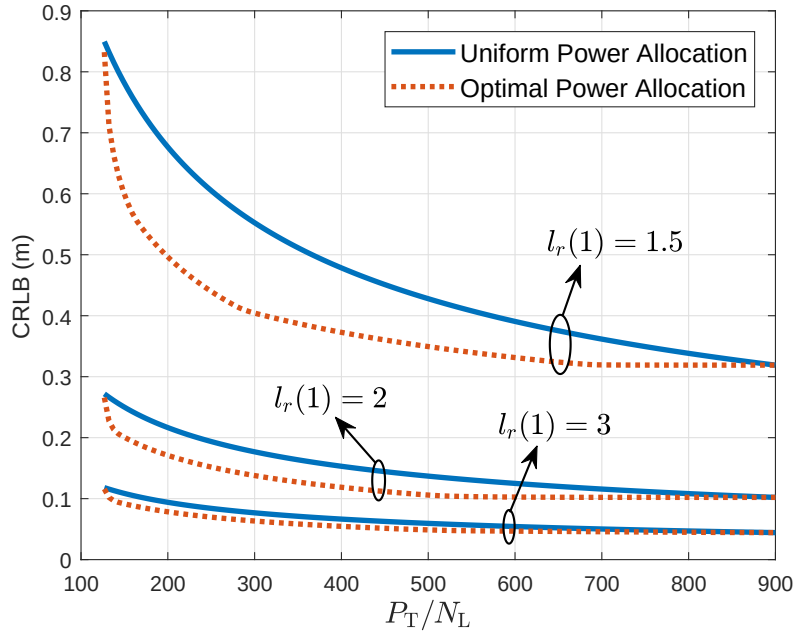

Figure 4.1: CRLB of (4.21) versus $P_{\mathrm{T}}/N_{\mathrm{L}}$ for optimal and uniform power allocation strategies for various locations of the VLC receiver.

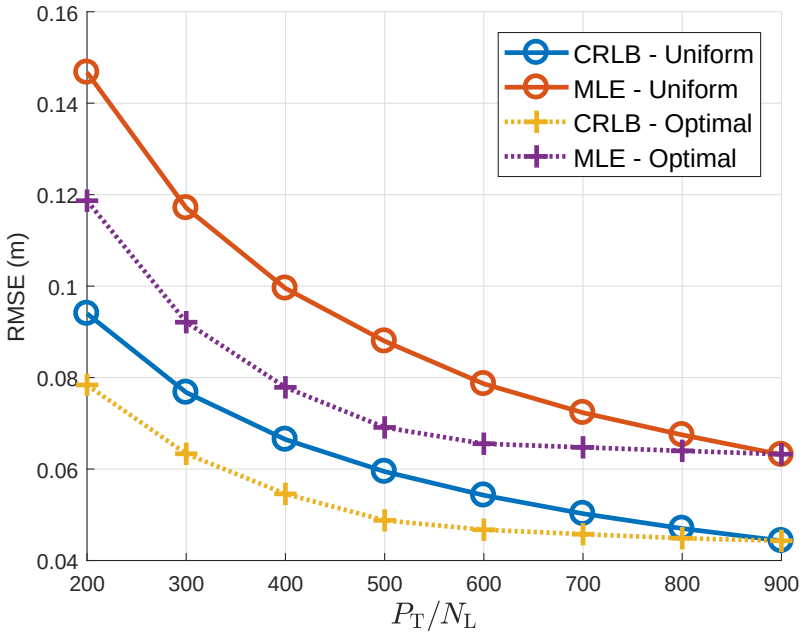

Figure 4.2: RMSEs of the ML estimators and the CRLBs corresponding to optimal and uniform power allocation strategies with respect to $P_{\mathrm{T}}/N_{\mathrm{L}}$.

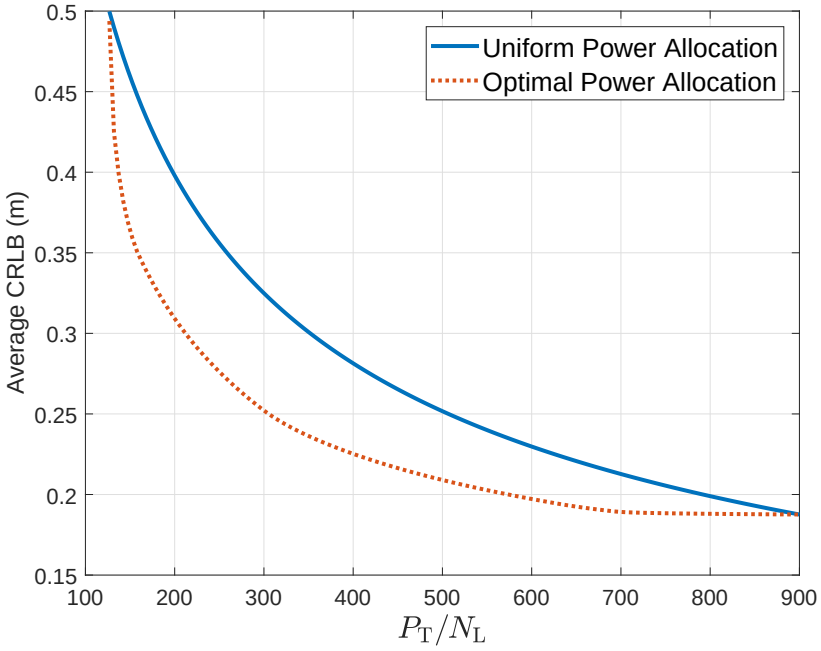

Figure 4.3: Average CRLB of three VLC receivers in (4.59) versus $P_{\mathrm{T}}/N_{\mathrm{L}}$ for optimal and uniform power allocation strategies, where the receiver locations are given by $\boldsymbol{l}_{\mathrm{r}}^{1} = [1.5\ 3\ 0.5]^{T}$ m, $\boldsymbol{l}_{\mathrm{r}}^{2} = [3\ 3\ 0.5]^{T}$ m, $\boldsymbol{l}_{\mathrm{r}}^{3} = [6\ 8\ 0.5]^{T}$ m, and the receiver orientations are given by $\boldsymbol{n}_{\mathrm{r}}^{1} = [0.5\ 0\ 0.866]^{T}$, $\boldsymbol{n}_{\mathrm{r}}^{2} = [0.5\ 0\ 0.866]^{T}$, $\boldsymbol{n}_{\mathrm{r}}^{3} = [-0.2198\ \ -0.6040\ 0.7660]^{T}$.

where $\mathbf{J}_{\ell}(\mathbf{p})$ denotes the FIM for the ℓth receiver. Fig. 4.3 depicts the average CRLB performance of (4.59) with three VLC receivers against $P_{\mathrm{T}}/N_{\mathrm{L}}$ for the cases of optimal and uniform power allocation. Similar to the scenario with a single VLC receiver, substantial localization performance gains within the dynamic range of the LEDs can be achieved via power optimization with multiple receivers. Hence, different receivers can simultaneously utilize the available power resources at the LED transmitters, resulting in improved efficiency of the VLP system.

4.6.3 Robust Power Allocation in the Presence of Overall System Uncertainty

To illustrate the performance of the robust power allocation in the presence of overall system uncertainty, as discussed in Section 4.3, several numerical examples are provided for the problem in (4.30), which is equivalent to the original robust problem in (4.27). Since the goal of robustness is to optimize the worst-case performance, we investigate the worst-case CRLBs achieved by the following strategies:

- *Robust:* The robust strategy takes into account the uncertainty in $\mathbf{\Gamma}$ and solves the problem in (4.30). Then, the resulting optimal value $t^\star$ of the slack variable t yields the worst-case CRLB.

- *Non-robust:* The non-robust strategy ignores the uncertainty in $\mathbf{\Gamma}$ and directly utilizes the nominal matrix $\widehat{\mathbf{\Gamma}}$ in (4.25) to solve the power allocation problem in (4.21). To obtain the worst-case CRLB corresponding to optimal power vector $\mathbf{p}^{\mathrm{n-rob}}$ of (4.21), $\mathbf{p}^{\mathrm{n-rob}}$ is inserted into (4.30) as a fixed quantity. Hence, the worst-case CRLB $t^\star$ is calculated by solving

$$t^\star = \min_{t,\mathbf{H},s,\mu} \quad t \tag{4.60a}$$

$$\text{subject to} \quad \mathrm{trace}\big\{\mathbf{H}\big\} \leq t - ds, \ \mathbf{\Phi}(\mathbf{p}^{\mathrm{n-rob}}, \mathbf{H}, s, \mu) \succeq 0, \ \mathbf{H} \succeq 0, \ \mu \geq 0 \tag{4.60b}$$

  where $\mathbf{\Phi}(\mathbf{p}, \mathbf{H}, s, \mu)$ is given by (4.31).

- *Uniform:* In this strategy, the uniform power allocation vector is used and the corresponding worst-case CRLB is obtained via (4.60) by replacing $\mathbf{p}^{\mathrm{n-rob}}$ with the uniform power vector.

The worst-case CRLBs are averaged over 100 Monte Carlo realizations. For each realization, an error matrix $\mathbf{\Delta\Gamma}$ is randomly chosen from the uncertainty set $\mathcal{E}$ in (4.26) and the nominal matrix $\widehat{\mathbf{\Gamma}}$ is generated according to (4.25). Then, each

strategy is evaluated by using realizations for which that strategy is feasible[11].

Fig. 4.4 shows the worst-case CRLB performance and the feasibility rate of the considered power allocation strategies against the level of uncertainty δ in (4.26). It is observed that the performance of all the strategies deteriorates as the uncertainty increases, as expected. For small uncertainty regions (i.e., small δ), the robust strategy has almost the same performance as its non-robust counterpart. However, the robust strategy outperforms the non-robust strategy for large uncertainty regions, which results from the design philosophy in (4.27). More specifically, since the nominal matrix $\widehat{\mathbf{\Gamma}}$ deviates substantially from the true matrix $\mathbf{\Gamma}$ for large values of δ, the non-robust strategy, which treats $\widehat{\mathbf{\Gamma}}$ as the true matrix in LED power optimization, results in poor worst-case localization performance. On the other hand, the robust approach attempts to minimize the performance degradation by utilizing the properties of the uncertainty region $\mathcal{E}$ in (4.26).

As noted from Fig. 4.4, the robust strategy also provides the highest feasibility rate among all the strategies since the feasible region of (4.60) is smaller than that of (4.30) (the constraint set (4.30e) is replaced by a single point in (4.60)). In addition, the feasibility rate of the uniform strategy undergoes a sharp decline after a certain level of uncertainty, which distorts the monotonic behavior of its worst-case CRLB around the point where this decline occurs. It is worth noting that the non-robust strategy achieves a higher feasibility rate and lower worst-case CRLB than the uniform strategy for small δ, but this trend changes as δ increases. The reason is that for small δ, the non-robust approach can find near-optimal power allocation vectors in the sense of (4.27) (since solving (4.21) is almost equivalent to solving (4.27) for small δ) whereas the uniform power vector does not take into account the localization related parameters (e.g., locations and orientations of the LED transmitters and the VLC receiver) and assigns

[11]More specifically, we fix the number of feasible realizations beforehand and continue to pick new matrices from the uncertainty region until the predefined number of feasible realizations is reached. For the robust strategy, feasibility refers to the problem in (4.30) being feasible for a given realization $\widehat{\mathbf{\Gamma}}$. For the non-robust and uniform strategies, feasibility means that the problem in (4.60) is feasible, which is equivalent to the worst-case CRLB in (4.60a) being finite.

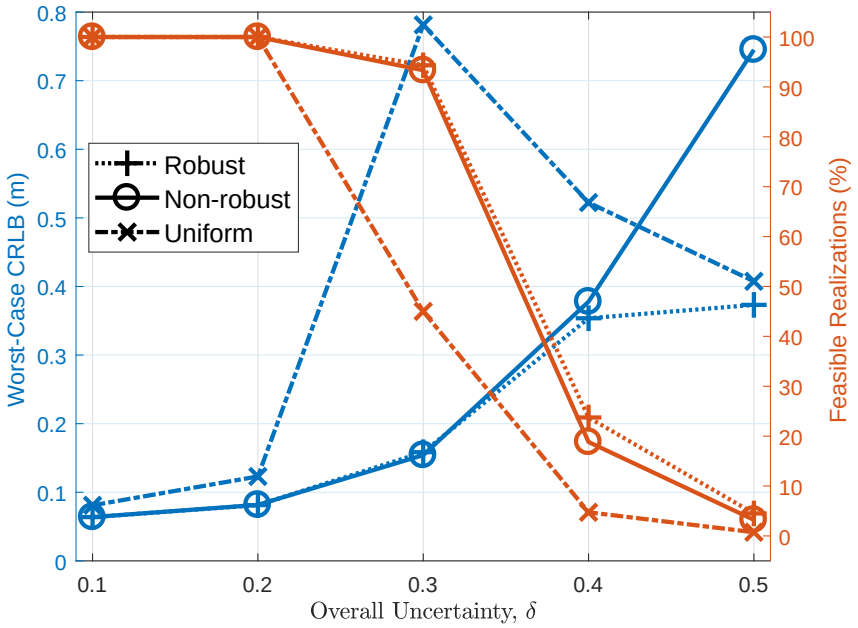

Figure 4.4: Worst-case CRLB and the percentage of feasible realizations in (4.27) versus the level of uncertainty δ, where the average power limit is $P_{\mathrm{T}}/N_{\mathrm{L}} = 400$.

equal power to all the LEDs, which leads to low feasibility rates and large errors in localization. On the other hand, for high δ, the performance of the non-robust strategy becomes worse than that of the uniform strategy with increasing errors in $\widehat{\mathbf{\Gamma}}$.

4.6.4 Robust Power Allocation in the Presence of Individual Parameter Uncertainties

In this part, we consider the robust power allocation schemes designed for the case of individual parameter uncertainties, as discussed in Section 4.4. In the simulations, we explore the performance of the three strategies as mentioned in Section 4.6.3 using 100 Monte Carlo realizations. The robust strategy is obtained by solving (4.51) via Algorithm 1. For the non-robust strategy, the uncertainty set $\widetilde{\mathcal{E}}$ in (4.49) is ignored and the nominal parameters (i.e., $\hat{\boldsymbol{l}}_{\mathrm{r}}$ in (4.41) or $(\hat{\theta}, \hat{\phi})$ in (4.45)) are employed for power allocation via (4.21). To compute the worst-case

CRLB for a given power vector $\mathbf{p}^*$, which corresponds to $\Psi(\mathbf{p}^*)$ in (4.52), we use a multi-start optimization algorithm for globally solving the maximization problem in (4.52).

Fig. 4.5 depicts the worst-case CRLB performance versus the level of uncertainty in the VLC receiver location, $\delta_{\boldsymbol{l}_\mathrm{r}}$, for the considered strategies.[12] As seen from Fig. 4.5, the proposed robust power allocation approach always achieves lower worst-case CRLBs than the other two strategies. In addition, the performance benefit provided by the robust strategy over its non-robust counterpart becomes more evident for larger values of $\delta_{\boldsymbol{l}_\mathrm{r}}$. Hence, the robust scheme in (4.43) can effectively exploit the characteristics of the uncertainty region $\mathcal{E}_{\boldsymbol{l}_\mathrm{r}}$ in (4.42) to optimize the worst-case localization performance. This also indicates that the proposed power allocation algorithm in Algorithm 1 can successfully converge to the optimal solution of (4.43). Moreover, we observe that the uniform strategy performs worse than the non-robust strategy for small $\delta_{\boldsymbol{l}_\mathrm{r}}$. However, as $\delta_{\boldsymbol{l}_\mathrm{r}}$ increases, the non-robust approach is outperformed by the uniform approach since the latter blindly assigns equal powers to the LEDs by disregarding parameter measurements whereas the former employs the highly inaccurate measurement of $\boldsymbol{l}_\mathrm{r}$ for power allocation of the LEDs.

In Fig. 4.6, we plot the worst-case CRLBs against the level of uncertainty in the polar angle of the VLC receiver (δ_θ in (4.46a)) for two different levels of uncertainty in the azimuth angle (δ_ϕ in (4.46b)). As seen from Fig. 4.6, the proposed robust power allocation strategy offers the best worst-case CRLB performance among all strategies. In addition, we note that the performance gain achieved via the robust approach becomes more prominent for larger uncertainty regions

[12] Even though the x-axis (uncertainty in location) and the y-axis (CRLB for location estimation) of Fig. 4.5 may seem to be conflicting with one another, they actually refer to different stages of a positioning/tracking system. In particular, the x-axis corresponds to the uncertainty in the receiver location that derives from the error covariance matrix of the *tracking* filter (e.g., Kalman filter) while the y-axis corresponds to the errors in location *measurements*, which can be quantified by the CRLB expression. In a VLP tracking scenario, the y-axis and the x-axis denote, respectively, the errors in the *measurement* and *tracking* blocks of a positioning system. Therefore, in Fig. 4.5, we aim to optimize the location measurement performance (i.e., CRLB) by utilizing the uncertainty information coming from the tracking block.

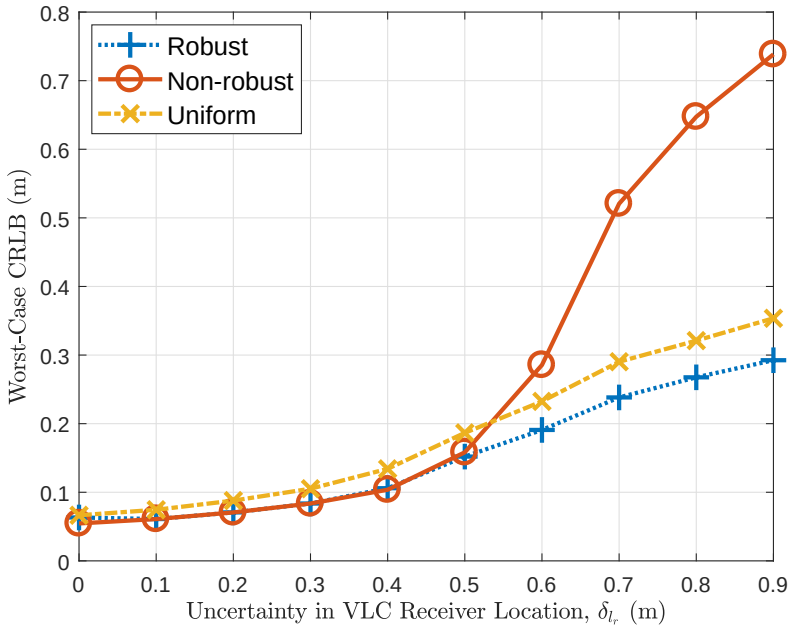

Figure 4.5: Worst-case CRLB of (4.43) versus the level of uncertainty in the location of the VLC receiver $\delta_{\boldsymbol{l}_\mathrm{r}}$, where the average power limit is $P_\mathrm{T}/N_\mathrm{L} = 400$.

$\mathcal{E}_\theta$ and $\mathcal{E}_\phi$ in (4.46). Moreover, additional numerical experiments for computing the worst-case RMSEs achieved by the considered power allocation approaches indicate that the level of improvement in the actual positioning error (i.e., RMSE) is analogous to that achieved by the worst-case CRLB optimization.

4.6.5 Minimum Power Consumption Problem

In this subsection, numerical examples are provided for the power allocation designs in Section 4.5.

4.6.5.1 Power Allocation with Perfect Knowledge

We explore the electrical power consumption corresponding to the optimal solution of (4.56) and provide a comparison with the uniform power allocation

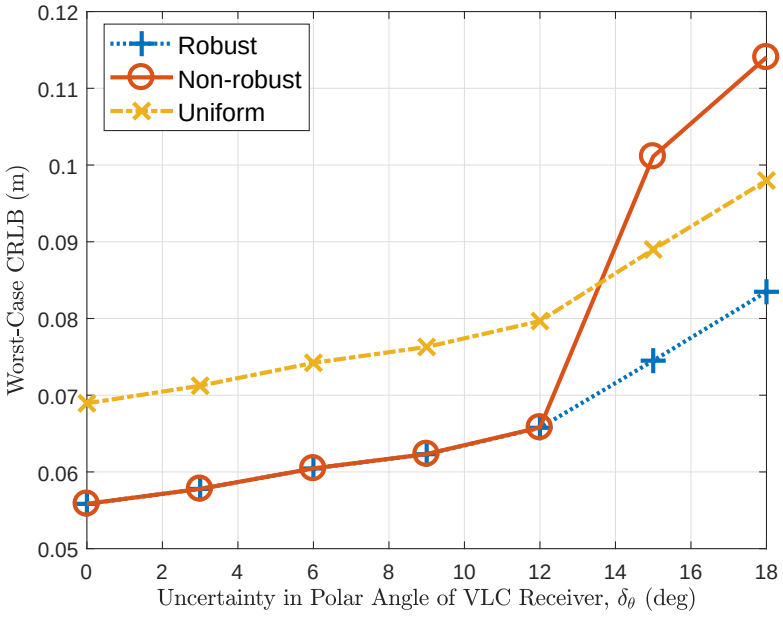

(a) $\delta_\phi = 6°$

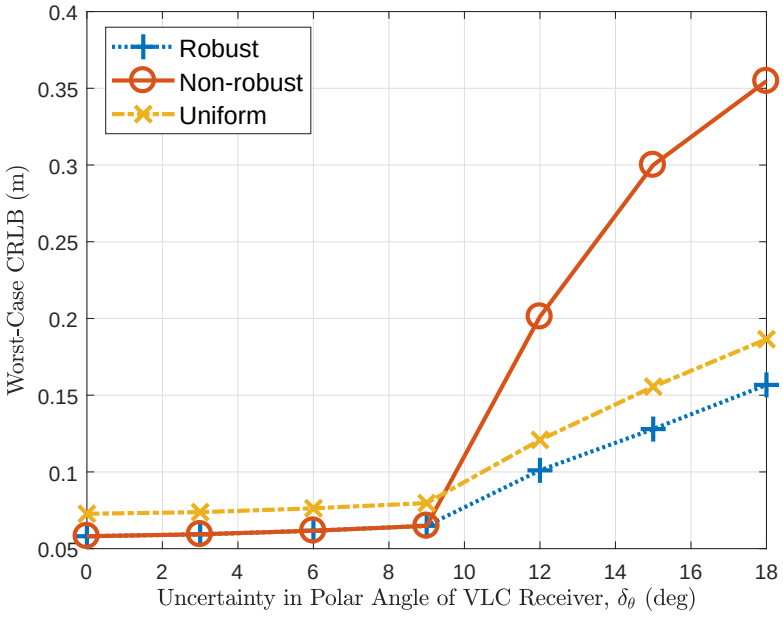

(b) $\delta_\phi = 12°$

Figure 4.6: Worst-case CRLB of (4.47) versus the level of uncertainty in the polar angle of the VLC receiver δ_θ for two different values of uncertainty in the azimuth angle δ_ϕ, where the average power limit is $P_{\mathrm{T}}/N_{\mathrm{L}} = 400$.

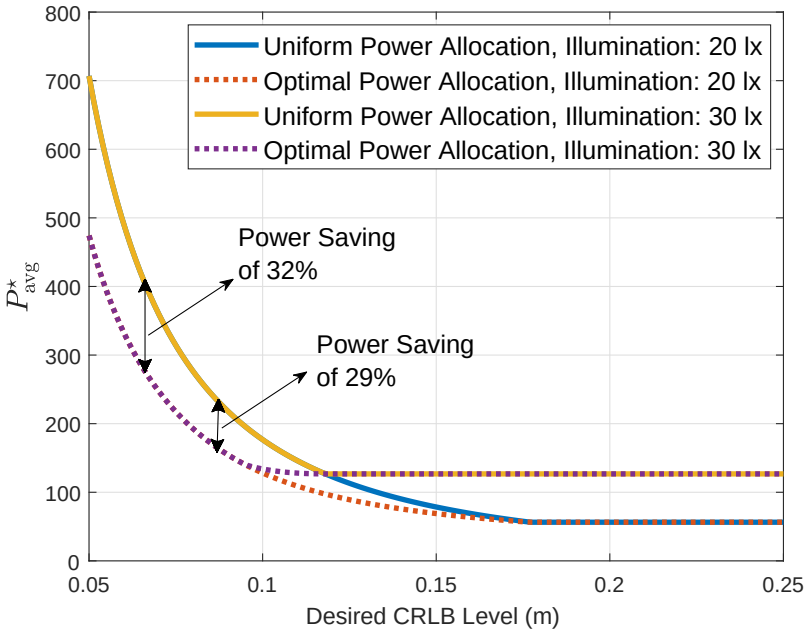

Figure 4.7: Optimal value of (4.56a) divided by N_{L} ($P^{\star}_{\text{avg}}$) versus the desired CRLB level $\sqrt{\varepsilon}$ for optimal and uniform power allocation strategies under various illumination constraints.

scheme, which is obtained from (4.56b) as

$$P_i = \text{trace}\Big\{\big((\mathbf{I}_3 \otimes \mathbf{1})^T \boldsymbol{\Gamma}\big)^{-1}\Big\}/\varepsilon \tag{4.61}$$

for $i = 1, \ldots, N_{\text{L}}$.

Fig. 4.7 plots $P^{\star}_{\text{avg}}$ versus $\sqrt{\varepsilon}$ for the optimal and uniform power allocation strategies, where $P^{\star}_{\text{avg}}$ corresponds to the optimal value of (4.56a) divided by N_{L} (which is proportional to the average electrical power consumption) and ε is the desired CRLB level in (4.56b). From the figure, we observe power saving gains of around 30% via the optimal approach for centimeter-level accuracy requirements. In addition, it is seen that the optimal strategy becomes equivalent to the uniform strategy when the desired level of localization accuracy is sufficiently low, which results from the illumination constraints.

4.6.5.2 Robust Power Allocation with Imperfect Knowledge

We provide examples for the case of uncertainty in VLP system parameters, discussed in Section 4.5.2. For the robust strategy, we solve (4.58), which is equivalent to the original problem in (4.57) by Proposition 2, to get the optimal power vector, while the non-robust strategy is obtained by replacing $\widehat{\mathbf{\Gamma}}$ with $\mathbf{\Gamma}$ in (4.56). In addition, the uniform strategy is given by (4.61) with $\mathbf{\Gamma}$ replaced by $\widehat{\mathbf{\Gamma}}$.

Fig. 4.8 depicts the cumulative distribution function (CDF) of the CRLBs obtained by the considered strategies for two different uncertainty levels, $\delta = 0.1$ and $\delta = 0.2$, by setting the worst-case accuracy level as $\sqrt{\varepsilon} = 0.1\,\mathrm{m}$. It is observed that the robust algorithm, which solves (4.58), satisfies the accuracy constraint in (4.57b) for all the realizations of $\mathbf{\Gamma}$ in accordance with the robust design approach, which also verifies the validity of Proposition 2. On the other hand, the non-robust and uniform strategies are not able to satisfy the accuracy constraint for approximately 50% of the realizations since they do not consider the uncertainty in $\mathbf{\Gamma}$ in allocating powers to the LEDs. Also, the CRLBs are observed to be more spread out for higher δ for all strategies. In Fig. 4.9, we show $P^{\star}_{\mathrm{avg}}$ with respect to δ, where $P^{\star}_{\mathrm{avg}}$ is the optimal value of (4.57a) divided by N_{L}. It is seen that the robust strategy must utilize more transmission power with increasing δ in order to guarantee the specified level of accuracy for larger uncertainty regions, as expected. Hence, the relative performance gain of the robust strategy can be achieved at the cost of higher transmit powers and increased computational complexity, which results from solving (4.58) rather than the original problem (4.56). However, as opposed to the non-robust power allocation, the robust approach provides a solid theoretical guarantee for satisfying the worst-case CRLB constraint in (4.57b).

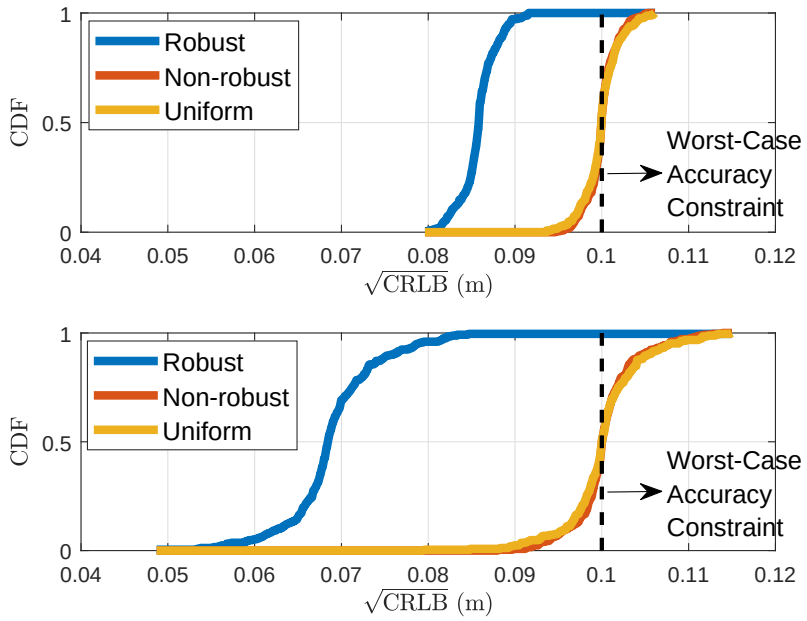

Figure 4.8: CDF of localization CRLBs achieved by robust, non-robust and uniform strategies in the case of deterministic norm-bounded uncertainty for the matrix $\mathbf{\Gamma}$, where the worst-case CRLB constraint in (4.57b) is set to $\sqrt{\varepsilon} = 0.1\,\mathrm{m}$ and two different uncertainty levels are considered, namely, $\delta = 0.1$ (above) and $\delta = 0.2$ (below).

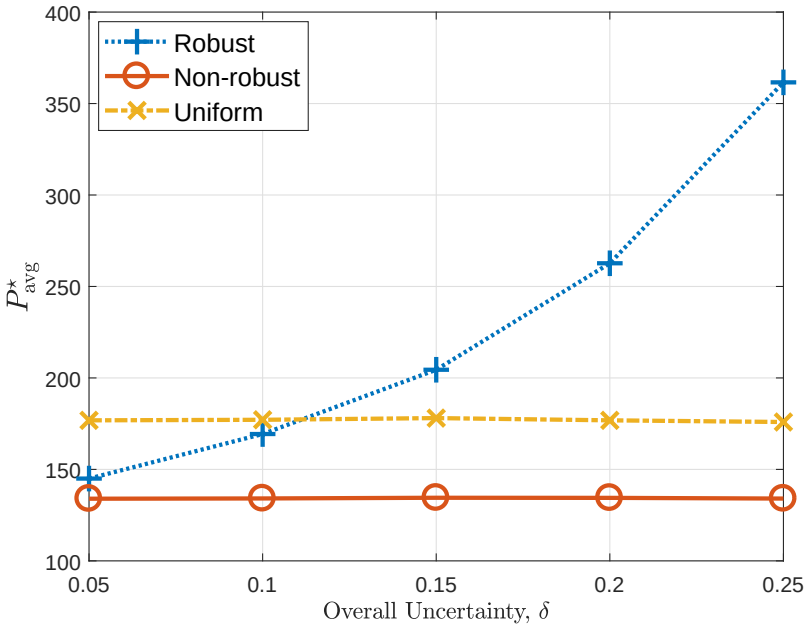

Figure 4.9: Optimal value of (4.57a) divided by N_{L} ($P^{\star}_{\text{avg}}$) versus the level of uncertainty δ for robust, non-robust and uniform power allocation strategies, where the worst-case accuracy constraint is $\sqrt{\varepsilon} = 0.1\,\text{m}$.

4.7 Concluding Remarks

In this chapter, we have considered the problem of optimal power allocation for LED transmitters in a VLP system. The optimization problem has been formulated to minimize the CRLB for the localization of the VLC receiver under practical constraints on transmission powers and illumination levels. Under the assumption of perfect knowledge of localization related parameters, the power allocation problem has been shown to be convex and thus efficiently solvable. In the presence of overall uncertainty, we have investigated the robust design problem that aims to minimize the worst-case CRLB over deterministic norm-bounded uncertainties and proved that it can be reformulated as a convex optimization problem. In addition, we have formulated the robust min-max problems corresponding to the uncertainties in individual parameters, namely, the location and the orientation of the VLC receiver. To solve the min-max problem, we have proposed an iterative entropic regularization algorithm, whereby the original problem

is transformed into a sequence of convex programs and a grid search is performed over the uncertainty region. Moreover, the problem of total power minimization has been explored under preset accuracy requirements. Simulation results have demonstrated the effectiveness of the optimal power allocation approach in enhancing the localization performance compared to the traditional uniform strategy. Furthermore, the proposed robust power allocation designs have been shown to outperform their non-robust counterparts, especially for large uncertainty regions. Regarding the minimum power consumption problem, power saving gains of 30% by the optimal strategy have been observed relative to the uniform power allocation approach.

4.8 Appendices

4.8.1 Definition of $\gamma_{k_1,k_2}^{(i)}$

$\gamma_{k_1,k_2}^{(i)}$ in (4.11) is defined as follows [18]:

$$\gamma_{k_1,k_2}^{(i)} = \begin{cases} \gamma_{k_1,k_2}^{(i),\mathrm{syn}}, & \text{if synchronous VLP system} \\ \gamma_{k_1,k_2}^{(i),\mathrm{asy}}, & \text{if asynchronous VLP system} \end{cases} \tag{4.62}$$

$$\gamma_{k_1,k_2}^{(i),\mathrm{syn}} \triangleq \frac{R_p^2}{\sigma^2}\left(E_2^i \frac{\partial \alpha_i}{\partial l_{\mathrm{r},k_1}} \frac{\partial \alpha_i}{\partial l_{\mathrm{r},k_2}} + E_1^i \alpha_i^2 \frac{\partial \tau_i}{\partial l_{\mathrm{r},k_1}} \frac{\partial \tau_i}{\partial l_{\mathrm{r},k_2}} - E_3^i \alpha_i \left(\frac{\partial \alpha_i}{\partial l_{\mathrm{r},k_1}} \frac{\partial \tau_i}{\partial l_{\mathrm{r},k_2}} + \frac{\partial \tau_i}{\partial l_{\mathrm{r},k_1}} \frac{\partial \alpha_i}{\partial l_{\mathrm{r},k_2}} \right) \right) \tag{4.63}$$

$$\gamma_{k_1,k_2}^{(i),\mathrm{asy}} \triangleq \frac{R_p^2}{\sigma^2}\left(E_2^i - \frac{(E_3^i)^2}{E_1^i} \right) \frac{\partial \alpha_i}{\partial l_{\mathrm{r},k_1}} \frac{\partial \alpha_i}{\partial l_{\mathrm{r},k_2}} \tag{4.64}$$

$$E_1^i \triangleq \int_0^{T_{s,i}} \left(\widetilde{s}_i'(t)\right)^2 dt,\ E_2^i \triangleq \int_0^{T_{s,i}} \left(\widetilde{s}_i(t)\right)^2 dt,\ E_3^i \triangleq \int_0^{T_{s,i}} \widetilde{s}_i(t)\widetilde{s}_i'(t) dt \tag{4.65}$$

$$\frac{\partial \tau_i}{\partial l_{\mathrm{r},k}} = \frac{l_{\mathrm{r},k} - l_{\mathrm{t},k}^i}{c\|\boldsymbol{l}_\mathrm{r} - \boldsymbol{l}_\mathrm{t}^i\|} \tag{4.66}$$

$$\frac{\partial \alpha_i}{\partial l_{\mathrm{r},k}} = -\frac{(m_i+1)S}{2\pi}\left(\frac{\left((\boldsymbol{l}_\mathrm{r} - \boldsymbol{l}_\mathrm{t}^i)^T \boldsymbol{n}_\mathrm{t}^i\right)^{m_i-1}}{\|\boldsymbol{l}_\mathrm{r} - \boldsymbol{l}_\mathrm{t}^i\|^{m_i+3}} \left(m_i\, n_{\mathrm{t},k}^i (\boldsymbol{l}_\mathrm{r} - \boldsymbol{l}_\mathrm{t}^i)^T \boldsymbol{n}_\mathrm{r} + n_{\mathrm{r},k} (\boldsymbol{l}_\mathrm{r} - \boldsymbol{l}_\mathrm{t}^i)^T \boldsymbol{n}_\mathrm{t}^i \right) \right. \tag{4.67}$$

$$- \frac{(m_i+3)(l_{\mathrm{r},k} - l^i_{\mathrm{t},k})}{\|\boldsymbol{l}_{\mathrm{r}} - \boldsymbol{l}^i_{\mathrm{t}}\|^{m_i+5}} \big((\boldsymbol{l}_{\mathrm{r}} - \boldsymbol{l}^i_{\mathrm{t}})^T \boldsymbol{n}^i_{\mathrm{t}}\big)^{m_i} (\boldsymbol{l}_{\mathrm{r}} - \boldsymbol{l}^i_{\mathrm{t}})^T \boldsymbol{n}_{\mathrm{r}} \Big)$$

where $\widetilde{s}'_i(t)$ denotes the derivative of $\widetilde{s}_i(t)$.

Chapter 5

Cooperative Localization in Visible Light Networks

In this chapter, we propose a cooperative localization framework for VLP networks and design distributed algorithms based on iterative gradient projections [20]. The main contributions of this chapter can be summarized as follows:

- For the first time in the literature, we propose to employ cooperative localization for VLP networks via a generic configuration that allows for an arbitrary construction of connectivity sets and transmitter/receiver orientations.
- The CRLB for localization of VLC units is derived in the presence of cooperative measurements (Section 5.1). The effects of cooperation on the performance of localization in VLP systems are illustrated based on the provided CRLB expression (Section 5.5.1).
- The problem of cooperative localization in VLP systems is formulated as a quasiconvex feasibility problem, which circumvents the complexity of the nonconvex ML estimator and facilitates efficient feasibility-seeking algorithms (Section 5.2).

- We design gradient projections based low-complexity iterative algorithms to find solutions to the feasibility problem (Section 5.3). The proposed set-theoretic framework favors the implementation of algorithms in a distributed architecture.
- We provide formal convergence proofs for the proposed algorithms in the consistent case based on the concept of quasi-Fejér convergence (Section 5.4).

5.1 System Model and Theoretical Bounds

5.1.1 System Model

In a cooperative VLP system, there exist N_L LED transmitters with known locations and orientations (i.e., anchor/reference nodes), and N_V VLC units that are to be located (i.e., agent/target nodes), as illustrated in Fig. 1.2. The location of the jth LED transmitter is denoted by $\mathbf{y}_j$ and its orientation vector is given by $\widetilde{\mathbf{n}}_{T,j}$ for $j \in \{1, \ldots, N_L\}$. Each VLC unit not only receives signals from the LED transmitters at known locations but also communicates with other VLC units in the system for cooperation purposes. Therefore, VLC units consist of both LEDs and PDs; namely, there exist L_i LEDs and K_i PDs at the ith VLC unit for $i \in \{1, \ldots, N_V\}$. The unknown location of the ith VLC unit is denoted by $\mathbf{x}_i$, where $i \in \{1, \ldots, N_V\}$. For the jth PD at the ith VLC unit, the location is denoted by $\mathbf{x}_i + \mathbf{a}_{i,j}$ and the orientation vector is given by $\mathbf{n}_{R,j}^{(i)}$, where $j \in \{1, \ldots, K_i\}$. Similarly, for the jth LED at the ith VLC unit, the location is represented by $\mathbf{x}_i + \mathbf{b}_{i,j}$ and the orientation vector is denoted by $\mathbf{n}_{T,j}^{(i)}$, where $j \in \{1, \ldots, L_i\}$. The displacement vectors, $\mathbf{a}_{i,j}$'s and $\mathbf{b}_{i,j}$'s, are known design parameters of the VLC units. In addition, the orientation vectors for the LEDs and PDs at the VLC units are assumed to be known since they can be determined by the VLC unit design and/or via auxiliary sensors (e.g., inertial measurement unit

(IMU) consisting of gyroscope, accelerometer and magnetometer [155–157][1]). To differentiate between the LED transmitters at known locations and the LEDs at the VLC units, the former are called as the *LEDs on the ceiling* in the remainder of this chapter.

In the cooperative VLP system, each PD communicates with a subset of all the LEDs in the network. For this reason, the following connectivity sets are defined to specify the connections between the PDs and the LEDs:

$$\widetilde{S}_k^{(j)} = \big\{\ell \in \{1,\ldots,N_L\} \mid \ell\text{th LED on ceiling is connected to } k\text{th PD of } j\text{th VLC unit}\big\} \tag{5.1}$$

$$S_k^{(i,j)} = \big\{\ell \in \{1,\ldots,L_i\} \mid \ell\text{th LED of } i\text{th VLC unit is connected to } k\text{th PD of } j\text{th VLC unit}\big\}. \tag{5.2}$$

In (5.1), $\widetilde{S}_k^{(j)}$ is the set of LEDs on the ceiling that are connected to the kth PD at the jth VLC unit. Similarly, in (5.2), $S_k^{(i,j)}$ represents the set of LEDs at the ith VLC unit that are connected to the kth PD at the jth VLC unit.

We consider a scenario in which RSS measurements performed by the PDs are employed for estimating the unknown locations of the VLC units, i.e., $\mathbf{x}_1,\ldots,\mathbf{x}_{N_V}$. Let $\widetilde{P}_{\ell,k}^{(j)}$ denote the RSS observation at the kth PD of the jth VLC unit due to the transmission from the ℓth LED on the ceiling. Similarly, let $P_{\ell,k}^{(i,j)}$ represent the RSS observation at the kth PD of the jth VLC unit due to the ℓth LED at the ith VLC unit. From the Lambertian formula [13, 23], $\widetilde{P}_{\ell,k}^{(j)}$ and $P_{\ell,k}^{(i,j)}$ can be stated as follows[2]:

$$\widetilde{P}_{\ell,k}^{(j)} = \widetilde{\alpha}_{\ell,k}^{(j)}(\mathbf{x}_j) + \widetilde{\eta}_{\ell,k}^{(j)} \tag{5.3}$$

$$P_{\ell,k}^{(i,j)} = \alpha_{\ell,k}^{(i,j)}(\mathbf{x}_j,\mathbf{x}_i) + \eta_{\ell,k}^{(i,j)} \tag{5.4}$$

[1]Relative locations and orientations of PDs and LEDs on VLC units can easily be calculated via simple linear operations (i.e., rotations and translations) based on IMU orientation measurements.

[2]Since the wavelength of the visible light carrier (on the order of 10^{-6} m) is much lower than dimensions of typical PDs (i.e., 10^{-2} m), multipath reflections are averaged out by integration of the incident optical power over the area of a PD [4, 11, 104]. Hence, in this study, only LOS links are taken into account in the VLC channel model.

where

$$\widetilde{\alpha}_{\ell,k}^{(j)}(\mathbf{x}_j) \triangleq -\frac{\widetilde{m}_\ell+1}{2\pi}\widetilde{P}_{T,\ell}A_k^{(j)}\frac{\left((\widetilde{\mathbf{d}}_{\ell,k}^{(j)})^T\widetilde{\mathbf{n}}_{T,l}\right)^{\widetilde{m}_\ell}(\widetilde{\mathbf{d}}_{\ell,k}^{(j)})^T\mathbf{n}_{R,k}^{(j)}}{\|\widetilde{\mathbf{d}}_{\ell,k}^{(j)}\|^{\widetilde{m}_\ell+3}} \tag{5.5}$$

$$\alpha_{\ell,k}^{(i,j)}(\mathbf{x}_j,\mathbf{x}_i) \triangleq -\frac{m_\ell^{(i)}+1}{2\pi}P_{T,\ell}^{(i)}A_k^{(j)}\frac{\left((\mathbf{d}_{\ell,k}^{(i,j)})^T\mathbf{n}_{T,\ell}^{(i)}\right)^{m_\ell^{(i)}}(\mathbf{d}_{\ell,k}^{(i,j)})^T\mathbf{n}_{R,k}^{(j)}}{\|\mathbf{d}_{\ell,k}^{(i,j)}\|^{m_\ell^{(i)}+3}} \tag{5.6}$$

for $j \in \{1,\ldots,N_V\}$, $k \in \{1,\ldots,K_j\}$, $i \in \{1,\ldots,N_V\} \setminus j$ and $\ell \in S_k^{(i,j)}$, with $\widetilde{\mathbf{d}}_{\ell,k}^{(j)} \triangleq \mathbf{x}_j + \mathbf{a}_{j,k} - \mathbf{y}_\ell$ and $\mathbf{d}_{\ell,k}^{(i,j)} \triangleq \mathbf{x}_j + \mathbf{a}_{j,k} - \mathbf{x}_i - \mathbf{b}_{i,\ell}$. In (5.5) and (5.6), $\widetilde{m}_\ell$ ($m_\ell^{(i)}$) is the Lambertian order for the ℓth LED on the ceiling (at the ith VLC unit), $\widetilde{P}_{T,\ell}$ ($P_{T,\ell}^{(i)}$) denotes the transmit power of the ℓth LED on the ceiling (at the ith VLC unit), and $A_k^{(j)}$ is the area of the kth PD at the jth VLC unit. In addition, the noise components, $\widetilde{\eta}_{\ell,k}^{(j)}$ and $\eta_{\ell,k}^{(i,j)}$, are modeled by zero-mean Gaussian random variables each with a variance of $\sigma_{j,k}^2$. By utilizing a certain type of multiple access protocol (e.g., time division multiple access among the LEDs at the same VLC unit and on the ceiling, and frequency division multiple access among the LEDs at different VLC units or on the ceiling), $\widetilde{\eta}_{\ell,k}^{(j)}$ and $\eta_{\ell,k}^{(i,j)}$ are assumed to be independent for all different (j,k) pairs and for all ℓ and i.

5.1.2 ML Estimator and CRLB

Let the vector of unknown parameters be represented as $\mathbf{x} \triangleq \left[\mathbf{x}_1^T \ldots \mathbf{x}_{N_V}^T\right]^T$, which has a size of $3N_V \times 1$. The aim is to estimate the elements of $\mathbf{x}$ based on the RSS measurements in (5.3) and (5.4). Let $\mathbf{P}$ denote a vector consisting of all the measurements in (5.3) and (5.4). The elements of $\mathbf{P}$ can be expressed as follows:

$$\left\{\left\{\left\{\widetilde{P}_{\ell,k}^{(j)}\right\}_{\ell\in\widetilde{S}_k^{(j)}}\right\}_{k\in\{1,\ldots,K_j\}}\right\}_{j\in\{1,\ldots,N_V\}}$$
$$\left\{\left\{\left\{\left\{P_{\ell,k}^{(i,j)}\right\}_{\ell\in S_k^{(i,j)}}\right\}_{i\in\{1,\ldots,N_V\}\setminus\{j\}}\right\}_{k\in\{1,\ldots,K_j\}}\right\}_{j\in\{1,\ldots,N_V\}}$$

Then, the conditional PDF of $\mathbf{P}$ given $\mathbf{x}$ can be expressed as

$$f(\mathbf{P}\,|\,\mathbf{x}) = \left(\prod_{j=1}^{N_V}\prod_{k=1}^{K_j}\frac{1}{\left(\sqrt{2\pi}\,\sigma_{j,k}\right)^{N_{tot}^{(j,k)}}}\right)e^{-\sum_{j=1}^{N_V}\sum_{k=1}^{K_j}\frac{h_{j,k}(\mathbf{x})}{2\sigma_{j,k}^2}} \tag{5.7}$$

where $N_{tot}^{(j,k)}$ denotes the total number of LEDs that can communicate with the kth PD at the jth VLC unit; that is, $N_{tot}^{(j,k)} \triangleq |\widetilde{S}_k^{(j)}| + \sum_{i=1,i\neq j}^{N_V} |S_k^{(i,j)}|$, and $h_{j,k}(\mathbf{x})$ is defined as

$$h_{j,k}(\mathbf{x}) \triangleq \sum_{\ell \in \widetilde{S}_k^{(j)}} \left(\widetilde{P}_{\ell,k}^{(j)} - \widetilde{\alpha}_{\ell,k}^{(j)}(\mathbf{x}_j)\right)^2 + \sum_{i=1,i\neq j}^{N_V} \sum_{\ell \in S_k^{(i,j)}} \left(P_{\ell,k}^{(i,j)} - \alpha_{\ell,k}^{(i,j)}(\mathbf{x}_j, \mathbf{x}_i)\right)^2. \quad (5.8)$$

Based on (5.7), the MLE is obtained as

$$\hat{\mathbf{x}}_{\mathrm{ML}} = \arg\min_{\mathbf{x}} \sum_{j=1}^{N_V} \sum_{k=1}^{K_j} \frac{h_{j,k}(\mathbf{x})}{\sigma_{j,k}^2} \quad (5.9)$$

and the Fisher information matrix (FIM) [122] is given by

$$[\mathbf{J}]_{t_1,t_2} = \mathbb{E}\left\{ \frac{\partial \log f(\mathbf{P} \,|\, \mathbf{x})}{\partial x_{t_1}} \frac{\partial \log f(\mathbf{P} \,|\, \mathbf{x})}{\partial x_{t_2}} \right\} \quad (5.10)$$

where x_{t_1} (x_{t_2}) represents element t_1 (t_2) of vector $\mathbf{x}$ with $t_1, t_2 \in \{1, 2, \ldots, 3N_V\}$. Then, the CRLB is expressed as

$$\mathrm{CRLB} = \mathrm{trace}(\mathbf{J}^{-1}) \leq \mathbb{E}\{\|\hat{\mathbf{x}} - \mathbf{x}\|^2\} \quad (5.11)$$

where $\hat{\mathbf{x}}$ represents an unbiased estimator of $\mathbf{x}$. From (5.7) and (5.8), the elements of the FIM in (5.10) can be calculated after some manipulation as

$$[\mathbf{J}]_{t_1,t_2} = \sum_{j=1}^{N_V} \sum_{k=1}^{K_j} \frac{1}{\sigma_{j,k}^2} \Bigg(\underbrace{\sum_{\ell \in \widetilde{S}_k^{(j)}} \frac{\partial \widetilde{\alpha}_{\ell,k}^{(j)}(\mathbf{x}_j)}{\partial x_{t_1}} \frac{\partial \widetilde{\alpha}_{\ell,k}^{(j)}(\mathbf{x}_j)}{\partial x_{t_2}}}_{\text{noncooperative}} + \underbrace{\sum_{i=1,i\neq j}^{N_V} \sum_{\ell \in S_k^{(i,j)}} \frac{\partial \alpha_{\ell,k}^{(i,j)}(\mathbf{x}_j, \mathbf{x}_i)}{\partial x_{t_1}} \frac{\partial \alpha_{\ell,k}^{(i,j)}(\mathbf{x}_j, \mathbf{x}_i)}{\partial x_{t_2}}}_{\text{cooperative}} \Bigg). \quad (5.12)$$

where we can observe the contributions of noncooperative (i.e., measurements due to LEDs on ceiling) and cooperative (i.e., measurements due to LEDs at the VLC units) terms to the Fisher information.

5.1.3 Discussions on Practical Aspects

In this part, we remark on possible challenges that may arise in practical cooperative VLP scenarios and demonstrate how these can be overcome by employing

simple yet effective techniques. In particular, we focus on two possible real-life applications of the proposed cooperative VLP framework; namely, indoor scenarios with infrared uplink transmission and vehicular VLC networks.

5.1.3.1 Optical Power of LEDs on VLC units

In certain indoor scenarios, increasing the optical power of LEDs installed in VLC units to enable signal detection may lead to a concern for the human eye safety. However, this can easily be handled by performing localization at low powers via pulse combining. In localization applications, significantly higher SNR values than those in communication systems can be achieved by transmitting signals over much longer durations or by combining measurements from a large number of pulses (transmitted signals). Unlike communication systems in which signal durations cannot be increased arbitrarily due to high data rate requirements, we can improve the SNR of measurements (and, thus, the localization accuracy) in localization systems by repeating measurements to accumulate signal energy over longer observation times [158]. Therefore, regarding the proposed cooperative VLP framework, the LEDs installed in the VLC units can operate at low optical powers to eliminate eye safety risks and still achieve high accuracy localization by measurement integration.

As an alternative to the visible light spectrum (400 to 700 nm), we can utilize the infrared band (> 700 nm) for communications among VLC units to comply with eye safety requirements [104]. Although spectral transmittance through the eye is relatively high in the visible light region (400 to 700 nm), it decreases significantly in the infrared wavelengths, especially above 1200 nm [159], which motivates the use of the infrared band for device-to-device VLC links. Recently, low-cost and high-performance PD designs providing high responsivity in the eye-safe infrared region (1550 nm) have been reported in the literature [160–162]. Regarding practical scenarios, a large number of potential VLC applications utilizing infrared wavelengths for uplink and device-to-device transmissions (i.e., among VLC units) have been proposed [2, 4, 101–103, 163].

Even though eye safety might be a concern for manned environments (which can be eliminated by using the aforementioned approaches), VLC units operating in unmanned environments do not pose any risks to human health. With the advent of industrial autonomous robots, industrial production takes place mainly in unmanned settings, leading to the concept of unmanned factories. Therefore, VLC units mounted on robotic devices can cooperate with one another in such environments for improved localization performance without jeopardizing human health.

5.1.3.2 LOS Blockage Scenarios

LOS paths between the VLC units can be blocked by obstacles in some indoor environments involving densely placed objects, which may reduce cooperation gains in localization. Vehicular networks involving V2V and V2I links represent a prominent example of the proposed cooperative VLC localization framework that overcomes the limitations caused by LOS blockage [99, 164]. Since most modern vehicles are equipped with LEDs in their headlights, taillights and turn signals, V2V communications can easily be realized via VLC [97–99, 165]. For the receiver part of V2V links, PDs can be placed in various sides of vehicles (e.g., backsides of sideview mirrors, near headlights and taillights [99, Fig. 1]) to obtain measurements from LEDs of neighboring vehicles [97, 98]. Regarding V2I communications, the infrastructure consists of fixed known-position nodes (i.e., anchor nodes), such as traffic lights, street lights and digital signage [97–99,166]. Integrating V2I and V2V communications in cooperative vehicular VLC scenarios, we can establish a low-cost and highly reliable cooperative VLP system that facilitates efficient traffic management applications (e.g., collision avoidance, cooperative adaptive cruise control, lane assistance) [97, 99, 100, 164, 167]. As VLP systems can produce much more precise location estimates than GPS, they can be employed to provide the desired level of accuracy (e.g., on the order of centimeters) for vehicle safety applications with strict accuracy requirements [97, 99, 164, 167, 168].

It is worth noting that besides its usage in cooperative vehicular settings, the proposed system model in Section 5.1.1 is generic in the sense that it comprises any cooperation scenario using the connectivity sets between LEDs and PDs, as defined in (5.1) and (5.2). Therefore, the theoretical analysis is valid also for the case of LOS blockage between some VLC units.

5.2 Cooperative Localization as a Quasiconvex Feasibility Problem

In this section, the problem of cooperative localization in VLP networks is investigated in the framework of convex/quasiconvex feasibility. First, the feasibility approach to the localization problem is motivated, and the problem formulation is presented. Then, the convexity analysis is carried out for the resulting constraint sets.

5.2.1 Motivation

For the localization of the VLC units, the MLE in (5.9) has very high computational complexity as it requires a search over a $3N_V$ dimensional space. In addition, the formulation in (5.9) presents a nonconvex optimization problem; hence, convex optimization tools cannot be employed to obtain the (global) optimal solution of (5.9). As the number of VLC units increases, centralized approaches obtained as solutions to a given optimization problem (such as (5.9)) may become computationally prohibitive. Besides scalability issues, centralized methods also require all measurements gathered at the VLC units to be relayed to a central unit for joint processing, which may lead to communication bottlenecks. Therefore, low-complexity algorithms amenable to distributed implementation are needed to efficiently solve the cooperative localization problem in VLP networks. To that aim, the localization problem is cast as a feasibility problem with the purpose of

finding a point in a finite dimensional Euclidean space that lies within the intersection of some constraint sets. Feasibility-seeking methods enjoy the advantage of not requiring an objective function, thereby eliminating the concerns for nonconvexity or nondifferentiability of the objective function [169]. Hence, modeling the localization problem as a feasibility problem *(i)* alleviates the computational burden of minimizing a (possibly nonconvex) cost function in the highly unfavorable centralized setting and *(ii)* facilitates the use of efficient distributed algorithms involving parallel or sequential processing at individual VLC units.

5.2.2 Problem Formulation

Considering the Lambertian formula in (5.3)–(5.6), an RSS measurement at a PD can be expressed as

$$\hat{P}_r = P_r + \eta \tag{5.13}$$

where P_r is the true observation (as in (5.5) or (5.6)) and η is the measurement noise. Suppose that the RSS measurement errors are negative, which yields $\hat{P}_r \leq P_r$.[3] Then, based on (5.5) and (5.6), the following inequality is obtained:

$$g(\mathbf{x}; \mathbf{y}, \mathbf{n}_T, \mathbf{n}_R, m, \gamma) \leq 0 \tag{5.14}$$

where $g : \mathbb{R}^d \to \mathbb{R}$ is the Lambertian function with respect to the unknown PD location $\mathbf{x}$, defined as

$$g(\mathbf{x}; \mathbf{y}, \mathbf{n}_T, \mathbf{n}_R, m, \gamma) \triangleq \gamma - \frac{\left[(\mathbf{x}-\mathbf{y})^T \mathbf{n}_T\right]^m (\mathbf{y}-\mathbf{x})^T \mathbf{n}_R}{\|\mathbf{x}-\mathbf{y}\|^{m+3}}, \tag{5.15}$$

$\mathbf{y}$, $\mathbf{n}_T$, $\mathbf{n}_R$, and m are known, d is the dimension of the visible light localization network, and γ is given by $\gamma = \frac{\hat{P}_r}{P_t} \frac{2\pi}{(m+1)A}$. The field-of-views (FOVs) of the LED

[3] In order to satisfy the negative error assumption, a constant value can always be subtracted from the actual RSS measurement [170]. Decreasing the value of an RSS measurement is equivalent to enlarging the corresponding feasible set. Although this assumption does not have a physical justification, it facilitates theoretical derivations and feasibility modeling of the localization problem. It will be justified via simulations in Section 5.5.2 that the proposed feasibility-seeking algorithms will converge for realistic noise models (e.g., Gaussian), as well.

transmitters and the PDs are taken as 90°, which implies that $(\mathbf{x}-\mathbf{y})^T\mathbf{n}_T \geq 0$ and $(\mathbf{y}-\mathbf{x})^T\mathbf{n}_R \geq 0$. Under the assumption of negative measurement errors, the feasible set in which the true PD location resides is given by the following lower level set of $g(\mathbf{x})$:

$$\mathcal{L} = \Big\{ \mathbf{x} \in \mathbb{R}^d \;\Big|\; g(\mathbf{x}; \mathbf{y}, \mathbf{n}_T, \mathbf{n}_R, m, \gamma) \leq 0 \Big\} \tag{5.16}$$

which will hereafter be referred to as the *Lambertian set*. In RF wireless localization networks, such feasible sets are generally obtained as balls [92, 94], hyperplanes [171], or ellipsoids [172], all of which lead to closed-form expressions for orthogonal projection. For $k \in \{1, \ldots, K_j\}$ and $j \in \{1, \ldots, N_V\}$, the Lambertian set corresponding to the kth PD of the jth VLC unit based on the signal received from the ℓth LED on the ceiling for $\ell \in \widetilde{S}_k^{(j)}$ is defined as follows:

$$\mathcal{N}_{\ell,k}^{(j)} = \Big\{ \mathbf{z} \in \mathbb{R}^d \;\Big|\; \tilde{g}_{\ell,k}^{(j)}(\mathbf{z}) \leq 0 \Big\} \tag{5.17}$$

where $\tilde{g}_{\ell,k}^{(j)}(\mathbf{z})$ is given by

$$\tilde{g}_{\ell,k}^{(j)}(\mathbf{z}) \triangleq g\big(\mathbf{z}; \mathbf{y}_\ell - \mathbf{a}_{j,k}, \widetilde{\mathbf{n}}_{T,\ell}, \mathbf{n}_{R,k}^{(j)}, \widetilde{m}_\ell, \tilde{\gamma}_{\ell,k}^{(j)}\big) \tag{5.18}$$

and $\tilde{\gamma}_{\ell,k}^{(j)}$ is calculated from (5.3). Similarly, the Lambertian set corresponding to the kth PD of the jth VLC unit based on the signal received from the ℓth LED of the ith VLC unit for $\ell \in S_k^{(i,j)}$ is defined as

$$\mathcal{C}_{\ell,k}^{(i,j)} = \Big\{ \mathbf{z} \in \mathbb{R}^d \;\Big|\; g_{\ell,k}^{(i,j)}(\mathbf{z}, \mathbf{x}_i) \leq 0 \Big\} \tag{5.19}$$

where $g_{\ell,k}^{(i,j)}(\mathbf{z}, \mathbf{x}_i)$ is given by

$$g_{\ell,k}^{(i,j)}(\mathbf{z}, \mathbf{x}_i) \triangleq g\big(\mathbf{z}; \mathbf{x}_i + \mathbf{b}_{i,\ell} - \mathbf{a}_{j,k}, \mathbf{n}_{T,\ell}^{(i)}, \mathbf{n}_{R,k}^{(j)}, m_\ell^{(i)}, \gamma_{\ell,k}^{(i,j)}\big) \tag{5.20}$$

and $\gamma_{\ell,k}^{(i,j)}$ is calculated from (5.4). The sets defined as in (5.17) represent noncooperative localization as they are constructed from the RSS measurements corresponding to the LEDs on the ceiling, whereas the sets in (5.19) are based on the signals from the LEDs of the other VLC units and represent the cooperation among the VLC units. Assuming negatively biased RSS measurements, the problem of cooperative localization in a visible light network reduces to that of finding a point in the intersection of sets as defined in (5.17) and (5.19) for each VLC

unit. If the Lambertian function in (5.15) is assumed to be quasiconvex[4], then the *quasiconvex feasibility problem* (QFP) can be formulated as follows [105,173]:

Problem 1. *Let* $\mathbf{x} \triangleq (\mathbf{x}_1, \ldots, \mathbf{x}_{N_V})$. *The feasibility problem for cooperative localization of VLC units is given by*[5]

$$\begin{aligned} &\text{find} \quad \mathbf{x} \in \mathbb{R}^{dN_V} \\ &\text{subject to} \quad \mathbf{x}_j \in \Lambda_j \cap \Upsilon_j,\ j = 1, \ldots, N_V \end{aligned} \tag{5.21}$$

where

$$\Lambda_j = \bigcap_{k=1}^{K_j} \bigcap_{\ell \in \widetilde{S}_k^{(j)}} \mathcal{N}_{\ell,k}^{(j)} \tag{5.22}$$

$$\Upsilon_j = \bigcap_{k=1}^{K_j} \bigcap_{i=1}^{N_V} \bigcap_{\ell \in S_k^{(i,j)}} \mathcal{C}_{\ell,k}^{(i,j)} \ . \tag{5.23}$$

5.2.3 Convexity Analysis of Lambertian Sets

The Lambertian sets as defined in (5.16) are not convex in general. The following lemma presents the conditions under which the Lambertian sets become convex.

Lemma 1. *Consider the* α*-sublevel set*

$$\mathcal{B} = \Big\{ \mathbf{x} \in \Omega \ \Big| \ g_\epsilon(\mathbf{x}) \leq \alpha \Big\} \tag{5.24}$$

of $g_\epsilon(\mathbf{x})$*, which is given by*

$$g_\epsilon(\mathbf{x}) = \gamma - \frac{(\mathbf{y} - \mathbf{x})^T \mathbf{n}_R}{\|\mathbf{x} - \mathbf{y}\|^k + \epsilon} \tag{5.25}$$

[4]The conditions under which the Lambertian function is quasiconvex are investigated in Section 5.2.3.

[5]It may be more convenient to regard the problem in (5.21) as an *implicit* quasiconvex feasibility problem (IQFP) since the Lambertian sets $\mathcal{C}_{\ell,k}^{(i,j)}$ depend on the locations of the VLC units, which are not known *a priori* [94]. It should be emphasized that the feasibility problem posed in Problem 1 is different from those in RF-based localization systems (e.g., [93,94]) since the constraint sets and the associated quasiconvex functions have distinct characteristics as compared to convex functions (e.g., distance to a ball) encountered in RF-based systems.

where ϵ is a small positive constant to avoid non-differentiability and non-continuity of $g_\epsilon(\cdot)$ at $\mathbf{y}$, as in [174, Eq. 7], $k \geq 1$ and $\gamma > 0$ are real numbers, and $\Omega \subset \mathbb{R}^d$ is defined as

$$\Omega = \left\{ \mathbf{x} \in \mathbb{R}^d \;\middle|\; (\mathbf{y} - \mathbf{x})^T \mathbf{n}_R \geq 0 \right\}. \tag{5.26}$$

Then, $\mathcal{B}$ is convex for each $\alpha \in \mathbb{R}$.

Proof: Suppose that $\mathbf{x}_1 \in \mathcal{B}$, $\mathbf{x}_2 \in \mathcal{B}$, and $\alpha < \gamma$. It is clear that for any $\lambda \in (0,1)$, $\lambda\mathbf{x}_1 + (1-\lambda)\mathbf{x}_2 \in \Omega$. Also, for any $\lambda \in (0,1)$,

$$g_\epsilon(\lambda\mathbf{x}_1 + (1-\lambda)\mathbf{x}_2) \tag{5.27}$$

$$= \gamma - \frac{\lambda(\mathbf{y} - \mathbf{x}_1)^T \mathbf{n}_R + (1-\lambda)(\mathbf{y} - \mathbf{x}_2)^T \mathbf{n}_R}{\|\lambda(\mathbf{x}_1 - \mathbf{y}) + (1-\lambda)(\mathbf{x}_2 - \mathbf{y})\|^k + \epsilon} \tag{5.28}$$

$$\leq \gamma - \frac{\lambda(\mathbf{y} - \mathbf{x}_1)^T \mathbf{n}_R + (1-\lambda)(\mathbf{y} - \mathbf{x}_2)^T \mathbf{n}_R}{\lambda\|\mathbf{x}_1 - \mathbf{y}\|^k + (1-\lambda)\|\mathbf{x}_2 - \mathbf{y}\|^k + \epsilon} \tag{5.29}$$

$$\leq \gamma - \frac{\lambda(\gamma-\alpha)(\|\mathbf{x}_1 - \mathbf{y}\|^k + \epsilon) + (1-\lambda)(\gamma-\alpha)(\|\mathbf{x}_2 - \mathbf{y}\|^k + \epsilon)}{\lambda(\|\mathbf{x}_1 - \mathbf{y}\|^k + \epsilon) + (1-\lambda)(\|\mathbf{x}_2 - \mathbf{y}\|^k + \epsilon)} \tag{5.30}$$

$$= \alpha \tag{5.31}$$

is obtained, where (5.29) is due to the convexity of $\|.\|^k$, $\mathbf{x}_1 \in \Omega$, and $\mathbf{x}_2 \in \Omega$, and (5.30) follows from $\mathbf{x}_1 \in \mathcal{B}$ and $\mathbf{x}_2 \in \mathcal{B}$. Hence, (5.27)–(5.31) implies the convexity of $\mathcal{B}$ for $\alpha < \gamma$. For $\alpha \geq \gamma$, $g_\epsilon(\mathbf{x}) \leq \alpha$ is satisfied $\forall \mathbf{x} \in \Omega$, which implies $\mathcal{B} = \Omega$. Therefore, $\mathcal{B}$ is convex $\forall \alpha \in \mathbb{R}$. ■

Remark 1. Lemma 1 characterizes the type of Lambertian functions whose sublevel sets are convex. Since a function whose all sublevel sets are convex is quasiconvex [175], Lambertian functions of the form (5.25) are quasiconvex over the halfspace Ω in (5.26). It can be noted that Ω consists of those VLC unit locations which are able to obtain measurements from an LED located at $\mathbf{y}$ due to the receiver FOV limit of 90°.

5.2.4 Convexification of Lambertian Sets

In this part, we utilize Lemma 1 to investigate the following two cases in which the Lambertian functions can be transformed into the form of (5.25) and Problem 1 becomes a QFP.

5.2.4.1 Case 1: Convexification via Majorization

We propose to approximate the Lambertian function $g(\mathbf{x})$ in (5.15) by a *quasiconvex minorant* $\tilde{g}(\mathbf{x})$ such that $\tilde{g}(\mathbf{x}) \leq g(\mathbf{x})$ for $\mathbf{x} \in \Omega$ and $\mathcal{L} \subseteq \tilde{\mathcal{L}}$, where $\tilde{\mathcal{L}} \triangleq \left\{\mathbf{x} \in \Omega \;\middle|\; \tilde{g}(\mathbf{x}) \leq 0\right\}$ represents a majorization of the original set $\mathcal{L} \triangleq \left\{\mathbf{x} \in \Omega \;\middle|\; g(\mathbf{x}) \leq 0\right\}$. Assuming $\mathbf{x} \in \Omega$, we have

$$g(\mathbf{x}) = \gamma - \frac{\left[(\mathbf{x}-\mathbf{y})^T\mathbf{n}_T\right]^m (\mathbf{y}-\mathbf{x})^T\mathbf{n}_R}{\|\mathbf{x}-\mathbf{y}\|^{m+3}} \tag{5.32}$$

$$\geq \gamma - \frac{\|\mathbf{x}-\mathbf{y}\|^m \|\mathbf{n}_T\|^m (\mathbf{y}-\mathbf{x})^T\mathbf{n}_R}{\|\mathbf{x}-\mathbf{y}\|^{m+3}} \tag{5.33}$$

$$= \gamma - \frac{(\mathbf{y}-\mathbf{x})^T\mathbf{n}_R}{\|\mathbf{x}-\mathbf{y}\|^3} \triangleq \tilde{g}(\mathbf{x}) \tag{5.34}$$

where (5.33) is due to the Cauchy-Schwarz inequality and $\mathbf{x} \in \Omega$, and (5.34) follows from the unit norm property of the orientation vector. Then, including ϵ in the denominator, we construct the Lambertian sets as (hereafter called *expanded Lambertian sets*)

$$\mathcal{L} = \left\{\mathbf{x} \in \Omega \;\middle|\; \tilde{g}_\epsilon(\mathbf{x}) \leq 0\right\} \tag{5.35}$$

with

$$\tilde{g}_\epsilon(\mathbf{x}) = \gamma - \frac{(\mathbf{y}-\mathbf{x})^T\mathbf{n}_R}{\|\mathbf{x}-\mathbf{y}\|^3 + \epsilon} \tag{5.36}$$

and Ω being as in (5.26). According to Lemma 1, $\mathcal{L}$ in (5.35) is convex, $\tilde{g}_\epsilon(\mathbf{x})$ in (5.36) is quasiconvex over Ω and the resulting problem of determining a point inside the intersection of such sets turns into a QFP, which can be studied through iterative projection algorithms [105, 173].

5.2.4.2 Case 2: Known VLC Height, Perpendicular LED

In this case, as in [15, 16, 23, 28], it is assumed that the LED transmitters on the ceiling have perpendicular orientations, i.e., $\widetilde{\mathbf{n}}_{T,j} = [0 \;\; 0 \;\; -1]^T$ for each $j \in \{1, \ldots, N_L\}$, and the height of each VLC unit is known. This assumption is valid for some practical scenarios, an example of which is a VLP network where the LEDs on the ceiling are pointing downwards and the VLC units are attached to robots that move over a two-dimensional plane [5, Fig. 3]. Assuming that the height of the LED transmitters relative to the VLC units is h and $\mathbf{n}_T = [0 \;\; 0 \;\; -1]^T$, the Lambertian function in (5.15) can be rewritten as follows:

$$g(\mathbf{x}; \mathbf{y}, \mathbf{n}_T, \mathbf{n}_R, m, \gamma) = \gamma - \frac{h^m (\mathbf{y} - \mathbf{x})^T \mathbf{n}_R}{\|\mathbf{x} - \mathbf{y}\|^{m+3}} \,. \tag{5.37}$$

Then, the Lambertian set corresponding to the function in (5.37) by introducing ϵ in the denominator is obtained as

$$\mathcal{L} = \left\{ \mathbf{x} \in \Omega \;\middle|\; \tilde{g}_\epsilon(\mathbf{x}) \leq 0 \right\} \tag{5.38}$$

with

$$\tilde{g}_\epsilon(\mathbf{x}) = \tilde{\gamma} - \frac{(\mathbf{y} - \mathbf{x})^T \mathbf{n}_R}{\|\mathbf{x} - \mathbf{y}\|^{m+3} + \epsilon} \tag{5.39}$$

where Ω is given by (5.26) and $\tilde{\gamma} = \gamma / h^m$. Note that the Lambertian set in (5.38) is effectively defined on $\mathbb{R}^2$ since the height of the VLC unit is already known. According to Lemma 1, the set defined in (5.38) is convex. Therefore, in this case, the noncooperative sets as defined in (5.17) are originally convex.

Based on the discussion above, it is concluded that in the case of a known VLC height and perpendicular LED transmitter orientations, the expanded Lambertian sets in (5.35) defined on $\mathbb{R}^2$ must be used for the measurements among the VLC units (i.e., cooperative measurements) in order to ensure that Problem 1 is a QFP. For the general case in which the LED orientations are arbitrary and/or the heights of the VLC units are unknown, all the noncooperative and cooperative Lambertian sets must be replaced by the corresponding expanded versions in (5.35).

A noncooperative VLP network is illustrated in Fig. 5.1(a), where there exist four LED transmitters on the ceiling and two VLC units. In the network, it is assumed that the heights of the VLC units are known and the LEDs on the ceiling have perpendicular orientations so that Case 2 type convex Lambertian sets can be utilized for the measurements between the LEDs on the ceiling and the VLC units. Fig. 5.1(b) shows the cooperative version of the VLP network with cooperative Lambertian sets including both the nonexpanded (original) sets as in (5.19) and Case 1 type expanded sets as in (5.35). It is noted from Fig. 5.1(b) that incorporating cooperative Lambertian sets into the localization geometry can significantly reduce the region of intersection of the Lambertian sets.

5.3 Gradient Projections Algorithms

In this section, we design iterative subgradient projections based algorithms to solve Problem 1. The idea of using subgradient projections is to approach a convex set defined as a lower contour set of a convex/quasiconvex function by moving in the direction that decreases the value of that function at each iteration, i.e., in the opposite direction of the subgradient of the function at the current iterate [112, 176]. First, the definition of the gradient projector is presented as follows:

Definition 1. The gradient projection operator $G_f^\lambda : \mathbb{R}^d \to \mathbb{R}^d$ onto the zero-sublevel set of a continuously differentiable function $f : \mathbb{R}^d \to \mathbb{R}$ is given by [177]

$$G_f^\lambda : \mathbf{x} \mapsto \begin{cases} \mathbf{x} - \lambda \frac{f(\mathbf{x})}{\|\nabla f(\mathbf{x})\|^2} \nabla f(\mathbf{x}), & \text{if } f(\mathbf{x}) > 0 \\ \mathbf{x}, & \text{if } f(\mathbf{x}) \leq 0 \end{cases} \tag{5.40}$$

where λ is the relaxation parameter and ∇ is the gradient operator. The gradient projector can also be expressed as

$$G_f^\lambda(\mathbf{x}) = \mathbf{x} - \lambda \frac{f^+(\mathbf{x})}{\|\nabla f(\mathbf{x})\|^2} \nabla f(\mathbf{x}) \tag{5.41}$$

with $f^+(\mathbf{x})$ denoting the positive part, i.e., $f^+(\mathbf{x}) = \max\{0, f(\mathbf{x})\}$. In the sequel, it is assumed that $G_f^\lambda(\mathbf{x}) = \mathbf{x}$ when $\mathbf{x}$ is outside the region where f is quasiconvex.

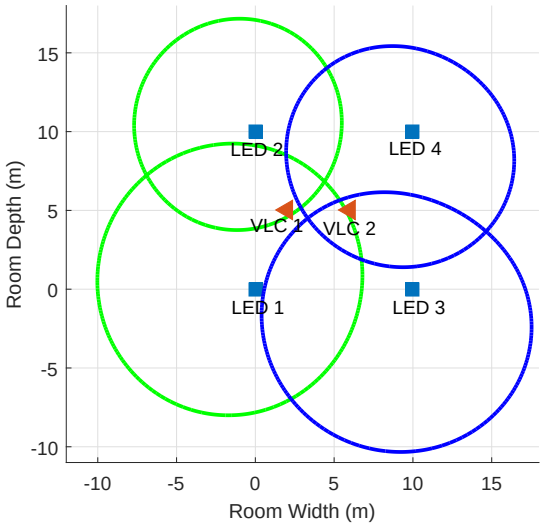

(a)

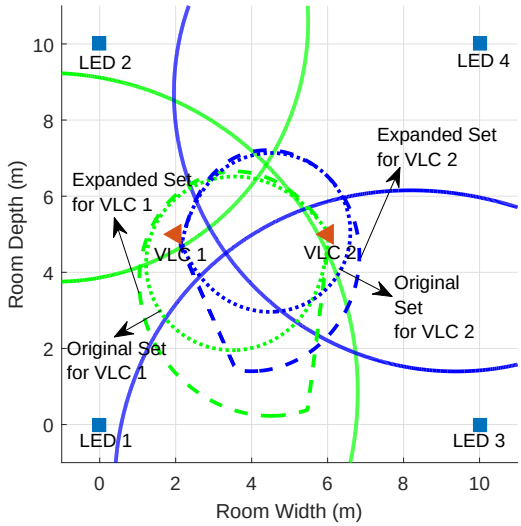

(b)

Figure 5.1: (a) A noncooperative VLP network consisting of four LED transmitters on ceiling and two VLC units. VLC-1 is connected to LED-1 and LED-2, and VLC-2 is connected to LED-3 and LED-4. Green and blue regions represent the noncooperative Lambertian sets for VLC-1 and VLC-2, respectively. (b) Cooperative version of the VLP system in Fig. 5.1(a), shown by zooming onto VLC units. Case 1 type expanded cooperative Lambertian sets and their nonexpanded (original) counterparts are illustrated along with noncooperative Lambertian sets. Cooperation helps shrink the intersection region of Lambertian sets for VLC units.

5.3.1 Projection Onto Intersection of Halfspaces

Since the functions of the form (5.25) are continuously differentiable and quasiconvex on the halfspace Ω in (5.26), a special case of subgradient projections, namely, gradient projections, can be utilized to solve Problem 1, under the constraint that iterates must be inside Ω to guarantee quasiconvexity. Hence, at the start of each iteration of gradient projections, projections onto the intersection of halfspaces of the form Ω in (5.26) can be performed to keep the iterates inside the quasiconvex region. The procedure for projection onto the intersection of halfspaces

$$\Gamma_j = \bigcap_{k=1}^{K_j} \bigcap_{\ell \in \widetilde{S}_k^{(j)}} \tilde{\Omega}_{\ell,k}^{(j)} \tag{5.42}$$

corresponding to the jth VLC unit for $j \in \{1, \ldots, N_V\}$, with the halfspaces given by

$$\tilde{\Omega}_{\ell,k}^{(j)} \triangleq \left\{ \mathbf{x} \in \mathbb{R}^d \;\middle|\; (\mathbf{y}_\ell - \mathbf{a}_{j,k} - \mathbf{x})^T \mathbf{n}_{R,k}^{(j)} \geq 0 \right\}, \tag{5.43}$$

is provided in Algorithm 2[6]. In order to find a point inside the intersection of halfspaces, the method of alternating (cyclic) projections is employed in Algorithm 2, where the current iterate is projected onto each halfspace in a cyclic manner. Convergence properties of this method are well studied in the literature [178, 179]. Γ_j is guaranteed to be nonempty since it represents the set of possible locations for the jth VLC unit at which the RSS measurements from the connected LEDs on the ceiling can be acquired. However, the intersection of the halfspaces corresponding to the LEDs of the other VLC units that are connected to the jth VLC unit may be empty due to the VLC unit locations being unknown and variable during iterations.

5.3.2 Step Size Selection

An important phase of the proposed projection algorithms is determining the relaxation parameters (i.e., step sizes) associated with the gradient projector.

[6] $P_{\mathcal{C}}(\mathbf{x})$ denotes the orthogonal projection operator, i.e., $P_{\mathcal{C}}(\mathbf{x}) = \arg\min_{\mathbf{w} \in \mathcal{C}} \|\mathbf{w} - \mathbf{x}\|$.

Algorithm 2 Projection Onto Intersection of Halfspaces Γ_j

function $P_{\Gamma_j}(\mathbf{x}_j)$

Initialization: $\mathbf{x}_j^{(0)} = \mathbf{x}_j$

Iterative Step: Given the nth iterate $\mathbf{x}_j^{(n)} \in \mathbb{R}^d$

for $k = 1, \ldots, K_j$ **do**

for $\ell \in \widetilde{S}_k^{(j)}$ **do**

$$\mathbf{x}_j^{(n)} = P_{\tilde{\Omega}_{\ell,k}^{(j)}}(\mathbf{x}_j^{(n)}) \tag{5.44}$$

end for

end for

Set $\mathbf{x}_j^{(n+1)} = \mathbf{x}_j^{(n)}$

Stopping Criterion: $\|\mathbf{x}_j^{(n+1)} - \mathbf{x}_j^{(n)}\| < \delta$ for some $\delta > 0$.

end function

The step size selection procedure exploits the well-known Armijo rule, which is an inexact line search method used extensively for gradient descent methods in the literature [180, 181], [182, Section 1.2]. Algorithm 3 provides an Armijo-like procedure for step size selection given a set of Lambertian functions, the initial step size value λ, a fixed constant $\beta \in (0, 1)$ specifying the degree of decline in the value of the function, step size shrinkage factor $\xi \in (0, 1)$, and the current point $\mathbf{x}$. The guarantee of existence of a step size as described in Algorithm 3 can be shown similarly to [183, Lemma 4].

Algorithm 3 Armijo Rule for Step Size Selection

function $\mathcal{J}(\{f_i\}_{i=1}^M, \lambda, \beta, \xi, \mathbf{x})$

Output: New step size $\tilde{\lambda}$

Set the step size as

$$\tilde{\lambda} = \lambda \xi^{\tilde{m}} \tag{5.45}$$

where

$$\tilde{m} = \min \left\{ m \in \mathbb{Z}_{\geq 0} \mid f_i(G_{f_i}^{\lambda \xi^m}(\mathbf{x})) \leq f_i(\mathbf{x})(1 - \beta \lambda \xi^m),\ \forall i \in \{1, \ldots, M\} \right\} \tag{5.46}$$

end function

5.3.3 Iterative Projection Based Algorithms

In this work, two classes of gradient projections algorithms, namely, sequential (i.e., cyclic) [176] and simultaneous (i.e., parallel) [184] projections, are considered for the QFP described in Problem 1. The proposed algorithm for cyclic projections, namely, the cooperative cyclic gradient projections (CCGP) algorithm, for cooperative localization of VLC units is provided in Algorithm 4. In the proposed cyclic projections, the current iterate, which signifies the location of the given VLC unit, is first projected onto the intersection of halfspaces corresponding to the LEDs on the ceiling via Algorithm 2. Then, the resulting point is projected onto the noncooperative Lambertian set that leads to the highest function value, i.e., the most violated constraint set [105]. Similarly, projection onto the most violated constraint set among the cooperative Lambertian sets is performed and the projections obtained by noncooperative and cooperative sets are weighted to obtain the next iterate.

The cooperative simultaneous gradient projections (CSGP) algorithm is proposed as detailed in Algorithm 5. Simultaneous projections are based on projecting the current point onto each noncooperative and cooperative Lambertian set separately and then averaging all the resulting points to obtain the next iterate. At each iteration, the parallel projection stage is preceded by projection onto the intersection of halfspaces, which aims to ensure that the current iterate resides in the region where all the Lambertian functions corresponding to the fixed anchors (i.e., the LEDs on the ceiling) are quasiconvex. It should be noted that for both cyclic and simultaneous projections, the cooperative Lambertian sets are determined by the latest estimates of the VLC unit locations [94], which are updated in the ascending order of their indices. In addition, the step sizes are updated using the Armijo rule in Algorithm 3.

Remark 2. Both Algorithm 4 and Algorithm 5 can be implemented in a distributed manner by employing a gossip-like procedure among the VLC units [185]. After refining its location estimate via projection methods, each VLC unit broadcasts the resulting updated location to other VLC units to which it is connected.

In order to save computation time, a synchronous counterpart of this asynchronous/sequential algorithm can be devised, where VLC units work in parallel to update their locations based on the most recent broadcast information. Hence, the synchronous/parallel implementation trades off the localization accuracy for faster convergence to the desired solution.

5.3.4 Complexity Analysis

In this part, we provide the complexity analysis of Algorithm 4, Algorithm 5, and the MLE in (5.9).

5.3.4.1 Complexity Analysis for Algorithm 4

We first analyze the complexity of Algorithm 4 for the jth VLC unit at each iteration. Each sub-step in the iterative step of Algorithm 4 is investigated as follows:

Assume that Algorithm 2 requires $\mathcal{O}(N_1)$ iterations for convergence. Then, the computational complexity of (5.47) is given by $\mathcal{O}\left(N_1 \sum_{k=1}^{K_j} |\widetilde{S}_k^{(j)}|\right)$. Since the number of functions $\tilde{g}_{\ell,k}^{(j)}(\,\cdot\,)$ in (5.48) is equal to $\sum_{k=1}^{K_j} |\widetilde{S}_k^{(j)}|$, evaluating (5.48) has the complexity $\mathcal{O}\left(\sum_{k=1}^{K_j} |\widetilde{S}_k^{(j)}|\right)$. Similar to the case of noncooperative projections in (5.48), evaluating (5.49) requires a computational complexity of $\mathcal{O}\left(\sum_{k=1}^{K_j} \sum_{i=1, i\neq j}^{N_V} |S_k^{(i,j)}|\right)$. To analyze (5.53) and (5.54), assume that Algorithm 3 requires $\mathcal{O}(N_2)$ trials for determining a non-negative integer m. At each trial, (5.46) requires $\mathcal{O}(M)$ operations, where M is the number of functions at the input of Algorithm 3. Then, the computational complexity of step size selection in (5.53) and (5.54) is computed as $\mathcal{O}\left(N_2 \sum_{k=1}^{K_j} \left[|\widetilde{S}_k^{(j)}| + \sum_{i=1, i\neq j}^{N_V} |S_k^{(i,j)}|\right]\right)$. Since the evaluation of the gradient projection operator in (5.41) requires $\mathcal{O}(1)$ operations, the averaging step in (5.52) has the complexity of $\mathcal{O}(1)$. Therefore, the

Algorithm 4 Cooperative Cyclic Gradient Projections (CCGP)

Initialization: Choose an arbitrary initial point $\left(\mathbf{x}_1^{(0)}, \ldots, \mathbf{x}_{N_V}^{(0)}\right) \in \mathbb{R}^{dN_V}$.

Iterative Step: Given the nth iterate $\left(\mathbf{x}_1^{(n)}, \ldots, \mathbf{x}_{N_V}^{(n)}\right) \in \mathbb{R}^{dN_V}$

for $j = 1, \ldots, N_V$ **do**

Projection Onto Intersection of Halfspaces Γ_j by Algorithm 2:

$$\tilde{\mathbf{x}}_j^{(n)} = P_{\Gamma_j}(\mathbf{x}_j^{(n)}) \tag{5.47}$$

Most Violated Constraint Control for Noncooperative Projections:

$$(\hat{k}_{\rm nc}, \hat{\ell}_{\rm nc}) = \arg\max_{k,\ell} \tilde{g}_{\ell,k}^{(j)}\big(\tilde{\mathbf{x}}_j^{(n)}\big) \tag{5.48}$$

Most Violated Constraint Control for Cooperative Projections:

$$(\hat{k}_{\rm c}, \hat{i}_{\rm c}, \hat{\ell}_{\rm c}) = \arg\max_{k,i,\ell} \mathcal{G}_j^{(n)} \tag{5.49}$$

where

$$\mathcal{G}_j^{(n)} \triangleq \left\{ g_{\ell,k}^{(i,j)}(\tilde{\mathbf{x}}_j^{(n)}, \mathbf{x}_i^{(\hat{n})}) \;\middle|\; \tilde{\mathbf{x}}_j^{(n)} \in \Omega_{\ell,k}^{(i,j)} \right\} \tag{5.50}$$

$$\Omega_{\ell,k}^{(i,j)} \triangleq \left\{ \mathbf{x} \in \mathbb{R}^d \;\middle|\; (\mathbf{x}_i^{(\hat{n})} + \mathbf{b}_{i,\ell} - \mathbf{a}_{j,k} - \mathbf{x})^T \mathbf{n}_{R,k}^{(j)} \geq 0 \right\} \tag{5.51}$$

with $\hat{n} = n$ for $i > j$, $\hat{n} = n+1$ for $i < j$.

Averaging:

$$\mathbf{x}_j^{(n+1)} = \vartheta_{\rm nc} G^{\lambda_{j,\rm nc}^{(n)}}_{\tilde{g}^{(j)}_{\hat{\ell}_{\rm nc},\hat{k}_{\rm nc}}}(\tilde{\mathbf{x}}_j^{(n)}) + \vartheta_{\rm c} G^{\lambda_{j,\rm c}^{(n)}}_{g^{(\hat{i}_{\rm c},j)}_{\hat{\ell}_{\rm c},\hat{k}_{\rm c}}(\cdot,\mathbf{x}_i^{(\hat{n})})}(\tilde{\mathbf{x}}_j^{(n)}) \tag{5.52}$$

where $\vartheta_{\rm nc} + \vartheta_{\rm c} = 1$ and $\vartheta_{\rm nc} \geq 0$, $\vartheta_{\rm c} \geq 0$.

end for

Stopping Criterion: $\sum_{j=1}^{N_V} \|\mathbf{x}_j^{(n+1)} - \mathbf{x}_j^{(n)}\|^2 < \delta$ for some $\delta > 0$.

Relaxation Parameters: Initialize $\lambda_{j,\rm nc}^{(0)} = \lambda_{j,\rm c}^{(0)} = \lambda_0$ and update using Algorithm 3 as

$$\lambda_{j,\rm nc}^{(n)} = \mathcal{J}(\tilde{g}^{(j)}_{\hat{\ell}_{\rm nc},\hat{k}_{\rm nc}}, \lambda_{j,\rm nc}^{(n-1)}, \beta, \xi, \tilde{\mathbf{x}}_j^{(n)}) \tag{5.53}$$

$$\lambda_{j,\rm c}^{(n)} = \begin{cases} \mathcal{J}(g^{(\hat{i}_{\rm c},j)}_{\hat{\ell}_{\rm c},\hat{k}_{\rm c}}(\cdot,\mathbf{x}_i^{(\hat{n})}), \lambda_{j,\rm c}^{(n-1)}, \beta, \xi, \tilde{\mathbf{x}}_j^{(n)}), & \text{if } \mathcal{G}_j^{(n)} \neq \emptyset \\ \lambda_{j,\rm c}^{(n-1)} & \text{otherwise} \end{cases} \tag{5.54}$$

for $j \in \{1, \ldots, N_V\}$.

Algorithm 5 Cooperative Simultaneous Gradient Projections (CSGP)

Initialization: Choose an arbitrary initial point $\left(\mathbf{x}_1^{(0)}, \ldots, \mathbf{x}_{N_V}^{(0)}\right) \in \mathbb{R}^{dN_V}$.

Iterative Step: Given the nth iterate $\left(\mathbf{x}_1^{(n)}, \ldots, \mathbf{x}_{N_V}^{(n)}\right) \in \mathbb{R}^{dN_V}$

for $j = 1, \ldots, N_V$ **do**

Projection Onto Intersection of Halfspaces Γ_j *by Algorithm 2:*

$$\tilde{\mathbf{x}}_j^{(n)} = P_{\Gamma_j}\left(\mathbf{x}_j^{(n)}\right) \tag{5.55}$$

Parallel Projection Onto Lambertian Sets:

$$\mathbf{x}_j^{(n+1)} = \sum_{k=1}^{K_j} \left[\sum_{\ell \in \widetilde{S}_k^{(j)}} \tilde{\kappa}_{\ell,k}^{(j)} G_{\tilde{g}_{\ell,k}^{(j)}}^{\lambda_j^{(n)}}(\tilde{\mathbf{x}}_j^{(n)}) + \sum_{i=1, i\neq j}^{N_V} \sum_{\ell \in S_k^{(i,j)}} \kappa_{\ell,k}^{(i,j)} G_{g_{\ell,k}^{(i,j)}(\cdot, \mathbf{x}_i^{(\hat{n})})}^{\lambda_j^{(n)}}(\tilde{\mathbf{x}}_j^{(n)}) \right] \tag{5.56}$$

where $\hat{n} = n$ for $i > j$, $\hat{n} = n + 1$ for $i < j$ and the weights satisfy

$$\sum_{k=1}^{K_j} \left(\sum_{\ell \in \widetilde{S}_k^{(j)}} \tilde{\kappa}_{\ell,k}^{(j)} + \sum_{i=1, i\neq j}^{N_V} \sum_{\ell \in S_k^{(i,j)}} \kappa_{\ell,k}^{(i,j)} \right) = 1 \tag{5.57}$$

and $\tilde{\kappa}_{\ell,k}^{(j)} \geq 0$, $\kappa_{\ell,k}^{(i,j)} \geq 0$, $\forall i, \ell, k$.

end for

Stopping Criterion: $\sum_{j=1}^{N_V} \|\mathbf{x}_j^{(n+1)} - \mathbf{x}_j^{(n)}\|^2 < \delta$ for some $\delta > 0$.

Relaxation Parameters: Initialize $\lambda_j^{(0)} = \lambda_0$ and update using Algorithm 3 as

$$\lambda_j^{(n)} = \mathcal{J}(\widetilde{\mathcal{F}}_j \cup \mathcal{S}_j^{(n)}, \lambda_j^{(n-1)}, \beta, \xi, \tilde{\mathbf{x}}_j^{(n)}) \tag{5.58}$$

for $j \in \{1, \ldots, N_V\}$, where $\widetilde{\mathcal{F}}_j$ and $\mathcal{F}_j$ are given by (5.69) and (5.70) in the supplementary material, respectively, and

$$\mathcal{S}_j^{(n)} \triangleq \left\{ f \in \mathcal{F}_j \mid f(\tilde{\mathbf{x}}_j^{(n)}) \leq \gamma_{\ell,k}^{(i,j)} \right\}. \tag{5.59}$$

overall complexity for the jth VLC unit is given by $\mathcal{O}\Bigg(\sum_{k=1}^{K_j} \Big[(N_1+N_2)|\widetilde{S}_k^{(j)}| + N_2 \sum_{i=1,i\neq j}^{N_V} |S_k^{(i,j)}| \Big] \Bigg)$. Assuming that the number of iterations for the convergence of Algorithm 4 is on the order of $\mathcal{O}(N_3)$, the overall complexity of Algorithm 4 can be expressed as

$$\mathcal{O}\left(N_3 \sum_{j=1}^{N_V} \sum_{k=1}^{K_j} \Big[\underbrace{(N_1+N_2)|\widetilde{S}_k^{(j)}|}_{\text{noncooperative}} + \underbrace{N_2 \sum_{i=1,i\neq j}^{N_V} |S_k^{(i,j)}|}_{\text{cooperative}} \Big] \right) . \tag{5.60}$$

where we can observe the contribution of the terms corresponding to noncooperative and cooperative projections separately.

5.3.4.2 Complexity Analysis for Algorithm 5

Following a similar approach to that in Algorithm 4, the complexity of Algorithm 5 can be obtained as

$$\mathcal{O}\left(N_3 \sum_{j=1}^{N_V} \sum_{k=1}^{K_j} \Big[\underbrace{(N_1+N_2)|\widetilde{S}_k^{(j)}|}_{\text{noncooperative}} + \underbrace{N_2 \sum_{i=1,i\neq j}^{N_V} |S_k^{(i,j)}|}_{\text{cooperative}} \Big] \right) . \tag{5.61}$$

5.3.4.3 Complexity Analysis for MLE in (5.9)

Due to the nonconvexity of the MLE, we evaluate the complexity by assuming the use of the exhaustive search method over a bounded region. Suppose that each VLC unit can take N_{smp} different values in each of the three axes. Then, the number of possible locations for N_V VLC units is on the order of $\mathcal{O}({N_{\text{smp}}}^{3N_V})$. At each search location, we need $\mathcal{O}\Bigg(\sum_{j=1}^{N_V} \sum_{k=1}^{K_j} \Big[|\widetilde{S}_k^{(j)}| + \sum_{i=1,i\neq j}^{N_V} |S_k^{(i,j)}| \Big] \Bigg)$ operations for evaluating the cost function in (5.9). Hence, the overall complexity

of the MLE can be computed as

$$\mathcal{O}\left({N_{\text{smp}}}^{3N_V} \sum_{j=1}^{N_V} \sum_{k=1}^{K_j} \Big[\underbrace{|\widetilde{S}_k^{(j)}|}_{\text{noncooperative}} + \underbrace{\sum_{i=1, i\neq j}^{N_V} |S_k^{(i,j)}|}_{\text{cooperative}} \Big] \right) . \tag{5.62}$$

As observed from (5.60) and (5.61), the complexity of the proposed algorithms depends on the number of iterations and the size of the connectivity sets. On the other hand, the complexity of the MLE, expressed in (5.62), is exponential in the number of VLC units, which limits its scalability, as discussed in Section 5.2.1. Hence, the proposed projection based algorithms provide low-complexity alternatives to the MLE in cooperative VLP scenarios.

5.4 Convergence Analysis

In this section, the convergence analysis of the proposed algorithms in Algorithm 4 and Algorithm 5 is performed in the consistent case. To that aim, it is assumed that for each $j \in \{1, \ldots, N_V\}$, the intersection of the noncooperative and cooperative Lambertian sets in (5.21) is nonempty; that is, $\Lambda_j \cap \Upsilon_j \neq \emptyset$, where Λ_j and Υ_j are given by (5.22) and (5.23), respectively. In the following, we present the definitions of quasiconvexity and quasi-Fejér convergence, which will be used for the convergence proofs.

Definition 2 *(Quasiconvexity [186]).* A differentiable function $f : \mathbb{R}^n \to \mathbb{R}$ is quasiconvex if and only if $f(\mathbf{x}) \leq f(\mathbf{y})$ implies $\nabla f(\mathbf{y})^T(\mathbf{x} - \mathbf{y}) \leq 0 \ \forall \mathbf{x}, \mathbf{y} \in \mathbb{R}^n$.

Definition 3 *(Quasi-Fejér Convergence [106]).* A sequence $\{\mathbf{y}^k\} \subset \mathbb{R}^n$ is quasi-Fejér convergent to a nonempty set $\mathcal{V}$ if for each $\mathbf{y} \in \mathcal{V}$, there exists a non-negative integer M and a sequence $\{\epsilon^k\} \subset \mathbb{R}_{\geq 0}$ such that $\sum_{k=0}^{\infty} \epsilon_k < \infty$ and

$$\|\mathbf{y}^{k+1} - \mathbf{y}\|^2 \leq \|\mathbf{y}^k - \mathbf{y}\|^2 + \epsilon_k, \ \forall k \geq M. \tag{5.63}$$

For the convergence analysis, we make the following assumptions:

- *A1.* Considering any $\mathbf{x}_j \in \Lambda_j \cap \Upsilon_j$ and $\widehat{\mathbf{x}}_j \notin \Lambda_j \cap \Upsilon_j$, the inequality $g_{\ell,k}^{(i,j)}(\mathbf{x}_j, \mathbf{x}_i^{(n)}) \leq g_{\ell,k}^{(i,j)}(\widehat{\mathbf{x}}_j, \mathbf{x}_i^{(n)})$ holds for every iteration index n and $\forall \ell, k, i, j$.

- *A2.* The sequence of path lengths taken by the iterations of the proposed algorithms are square summable, i.e.,

$$\sum_{n=0}^{\infty} \left(\|\tilde{\mathbf{x}}_j^{(n)} - \mathbf{x}_j^{(n)}\|^2 + \|\mathbf{x}_j^{(n+1)} - \tilde{\mathbf{x}}_j^{(n)}\|^2 \right) < \infty \tag{5.64}$$

  for $j \in \{1, \ldots, N_V\}$.

Assumption A1 is valid especially when the cooperative algorithms can be initialized at some $\mathbf{x} = (\mathbf{x}_1, \ldots, \mathbf{x}_{N_V})$ with $\mathbf{x}_j \in \Lambda_j$, $\forall j \in \{1, \ldots, N_V\}$. Assumption A1 implies that any point inside the intersection of the noncooperative and cooperative constraint sets is closer, in terms of the function value (whose zero-sublevel sets are the constraint sets), to the cooperative constraint sets than any point outside the intersection. When the iterations in the cooperative case start from coarse location estimates obtained in the absence of cooperation, the corresponding cooperative sets, which are dynamically changing at each iteration, may involve the set $\Lambda_j \cap \Upsilon_j$, but exclude the points outside $\Lambda_j \cap \Upsilon_j$, which yields $g_{\ell,k}^{(i,j)}(\mathbf{x}_j, \mathbf{x}_i^{(n)}) \leq 0 < g_{\ell,k}^{(i,j)}(\widehat{\mathbf{x}}_j, \mathbf{x}_i^{(n)})$. On the other hand, Assumption A2 represents a realistic scenario through the Armijo rule in (5.45) and (5.46), which ensures a certain level of decline in the Lambertian functions at each iteration and generates a nonincreasing sequence of step sizes.

5.4.1 Quasi-Fejér Convergence

In the convergence analysis, the proof of convergence is based on the concept of quasi-Fejér convergent sequences, which possess nice properties that facilitate further investigation, as will be presented in Lemma 2. The following proposition establishes the quasi-Fejér convergence of the sequences generated by Algorithm 5 to the set $\Lambda_j \cap \Upsilon_j$.

Proposition 1. *Assume A1 and A2 hold. Let* $\{\mathbf{x}^{(n)}\}_{n=0}^{\infty}$ *be any sequence generated by Algorithm 5, where* $\mathbf{x}^{(n)} \triangleq \left(\mathbf{x}_1^{(n)}, \ldots, \mathbf{x}_{N_V}^{(n)}\right)$. *Then, for each* $j \in \{1, \ldots, N_V\}$, *the sequence* $\{\mathbf{x}_j^{(n)}\}_{n=0}^{\infty}$ *is quasi-Fejér convergent to the set* $\Lambda_j \cap \Upsilon_j$.

Proof: Since $\Lambda_j \cap \Upsilon_j \neq \emptyset$, consider any point $\mathbf{x}_j \in \Lambda_j \cap \Upsilon_j$. At the nth iteration, it can be assumed that $\mathbf{x}_j^{(n)} \notin \Lambda_j \cap \Upsilon_j$ because otherwise iterations will stop via (5.56) and (5.40), which implies quasi-Fejér convergence of $\{\mathbf{x}_j^{(n)}\}_{n=0}^{\infty}$ to $\Lambda_j \cap \Upsilon_j$ based on Definition 3. Then, based on the iterative step in (5.56), the following is obtained:

$$\|\mathbf{x}_j^{(n+1)} - \mathbf{x}_j\|^2 = \|\tilde{\mathbf{x}}_j^{(n)} - \mathbf{x}_j - \lambda_j^{(n)} \boldsymbol{\theta}_j^{(n)}\|^2 \tag{5.65}$$

where

$$\boldsymbol{\theta}_j^{(n)} \triangleq \sum_{k=1}^{K_j} \left(\sum_{\ell \in \widetilde{S}_k^{(j)}} \tilde{\kappa}_{\ell,k}^{(j)} H_{\tilde{g}_{\ell,k}^{(j)}}(\tilde{\mathbf{x}}_j^{(n)}) + \sum_{i=1, i \neq j}^{N_V} \sum_{\ell \in S_k^{(i,j)}} \kappa_{\ell,k}^{(i,j)} H_{g_{\ell,k}^{(i,j)}(\cdot, \mathbf{x}_i^{(\hat{n})})}(\tilde{\mathbf{x}}_j^{(n)}) \right) \tag{5.66}$$

with the scaled gradient operator being defined as

$$H_f(\mathbf{x}) = \frac{f^+(\mathbf{x})}{\|\nabla f(\mathbf{x})\|^2} \nabla f(\mathbf{x}). \tag{5.67}$$

From (5.65), it follows that

$$\|\mathbf{x}_j^{(n+1)} - \mathbf{x}_j\|^2 = \|\tilde{\mathbf{x}}_j^{(n)} - \mathbf{x}_j\|^2 + \left(\lambda_j^{(n)}\right)^2 \|\boldsymbol{\theta}_j^{(n)}\|^2 - 2\lambda_j^{(n)} \left(\boldsymbol{\theta}_j^{(n)}\right)^T \left(\tilde{\mathbf{x}}_j^{(n)} - \mathbf{x}_j\right). \tag{5.68}$$

Let $\widetilde{\mathcal{F}}_j$ and $\mathcal{F}_j$ be the sets of Lambertian functions for the jth VLC unit corresponding to the noncooperative and cooperative cases, respectively, which are given by

$$\widetilde{\mathcal{F}}_j = \left\{ \{\tilde{g}_{\ell,k}^{(j)}\}_{\ell \in \widetilde{S}_k^{(j)}} \right\}_{k \in \{1, \ldots, K_j\}} \tag{5.69}$$

$$\mathcal{F}_j = \left\{ \{\{g_{\ell,k}^{(i,j)}(\cdot, \mathbf{x}_i^{(\hat{n})})\}_{\ell \in \widetilde{S}_k^{(j)}}\}_{i \in \{1, \ldots, N_V\} \setminus j} \right\}_{k \in \{1, \ldots, K_j\}} \tag{5.70}$$

For any function $f \in \widetilde{\mathcal{F}}_j \cup \mathcal{F}_j$, $f(\mathbf{x}_j) \leq 0$ holds since $\mathbf{x}_j \in \Lambda_j \cap \Upsilon_j$ (see (5.17), (5.19), (5.22), and (5.23)). Consider the following mutually exclusive and exhaustive subsets of $\widetilde{\mathcal{F}}_j \cup \mathcal{F}_j$:

$$\mathcal{F}_{j,n}^{\star} = \{f \in \widetilde{\mathcal{F}}_j \cup \mathcal{F}_j \mid f(\tilde{\mathbf{x}}_j^{(n)}) \leq 0\} \tag{5.71}$$

$$\mathcal{F}_{j,n}^{\diamond} = \{f \in \widetilde{\mathcal{F}}_j \cup \mathcal{F}_j \mid f(\tilde{\mathbf{x}}_j^{(n)}) > 0\} \ . \tag{5.72}$$

It is clear from (5.67) that for any $f^\star \in \mathcal{F}_{j,n}^\star$

$$H_{f^\star}(\tilde{\mathbf{x}}_j^{(n)}) = 0 \tag{5.73}$$

is satisfied. On the other hand, for any $f^\diamond \in \mathcal{F}_{j,n}^\diamond \cap \widetilde{\mathcal{F}}_j$, $f^\diamond(\mathbf{x}_j) = 0 < f^\diamond(\tilde{\mathbf{x}}_j^{(n)})$, and, for any $f^\diamond \in \mathcal{F}_{j,n}^\diamond \cap \mathcal{F}_j$, $f^\diamond(\mathbf{x}_j) < f^\diamond(\tilde{\mathbf{x}}_j^{(n)})$ via Assumption A1. Then, the following inequality holds for any $f^\diamond \in \mathcal{F}_{j,n}^\diamond$:

$$f^\diamond(\mathbf{x}_j) < f^\diamond\big(\tilde{\mathbf{x}}_j^{(n)}\big) \ . \tag{5.74}$$

Since $\mathbf{x}_j$ and $\tilde{\mathbf{x}}_j^{(n)}$ both lie inside the halfspaces of the form (5.43) and (5.51) corresponding to the set of functions $\mathcal{F}_{j,n}^\diamond$ ($\mathbf{x}_j \in \Lambda_j \subset \Gamma_j$ and $\tilde{\mathbf{x}}_j^{(n)} \in \Gamma_j$, see (5.42), (5.43), (5.55) and (5.22)), they are in the region where any $f^\diamond \in \mathcal{F}_{j,n}^\diamond$ is quasiconvex. Hence, from (5.74) and Definition 2,

$$\big(\nabla f^\diamond(\tilde{\mathbf{x}}_j^{(n)})\big)^T\big(\mathbf{x}_j - \tilde{\mathbf{x}}_j^{(n)}\big) \leq 0 \tag{5.75}$$

follows, which, based on (5.67), implies that

$$\Big(H_{f^\diamond}(\tilde{\mathbf{x}}_j^{(n)})\Big)^T\Big(\tilde{\mathbf{x}}_j^{(n)} - \mathbf{x}_j\Big) \geq 0 \ . \tag{5.76}$$

The inner product term (the rightmost term) in (5.68) can be decomposed into two parts corresponding to the sets $\mathcal{F}_{j,n}^\star$ and $\mathcal{F}_{j,n}^\diamond$. The part that corresponds to $\mathcal{F}_{j,n}^\star$ is 0 via (5.73) and the remaining part is greater than or equal to 0 via (5.76). Hence, the following inequality is obtained:

$$\big(\boldsymbol{\theta}_j^{(n)}\big)^T\big(\tilde{\mathbf{x}}_j^{(n)} - \mathbf{x}_j\big) \geq 0 \ , \tag{5.77}$$

which, based on (5.68), yields

$$\|\mathbf{x}_j^{(n+1)} - \mathbf{x}_j\|^2 \leq \|\tilde{\mathbf{x}}_j^{(n)} - \mathbf{x}_j\|^2 + \epsilon_j^{(n)} \tag{5.78}$$

where

$$\epsilon_j^{(n)} \triangleq \Big(\lambda_j^{(n)}\Big)^2 \|\boldsymbol{\theta}_j^{(n)}\|^2. \tag{5.79}$$

From the fact that $\mathbf{x}_j \in \Gamma_j$, the following can be written:

$$\|\tilde{\mathbf{x}}_j^{(n)} - \mathbf{x}_j\| \overset{\text{(a)}}{=} \|P_{\Gamma_j}(\mathbf{x}_j^{(n)}) - P_{\Gamma_j}(\mathbf{x}_j)\| \overset{\text{(b)}}{\leq} \|\mathbf{x}_j^{(n)} - \mathbf{x}_j\| \tag{5.80}$$

where (a) follows from (5.55), and (b) is due to the non-expansivity of the orthogonal projection operator. Combining (5.80) with (5.78) yields the following inequality:

$$\|\mathbf{x}_j^{(n+1)} - \mathbf{x}_j\|^2 \leq \|\mathbf{x}_j^{(n)} - \mathbf{x}_j\|^2 + \epsilon_j^{(n)}. \tag{5.81}$$

Based on the parallel projection step in (5.56), it can easily be shown that

$$\|\mathbf{x}_j^{(n+1)} - \tilde{\mathbf{x}}_j^{(n)}\| = \lambda_j^{(n)} \|\boldsymbol{\theta}_j^{(n)}\| \tag{5.82}$$

where $\boldsymbol{\theta}_j^{(n)}$ is given by (5.66). Then, from Assumption A2, it follows that $\sum_{n=0}^{\infty} \|\mathbf{x}_j^{(n+1)} - \tilde{\mathbf{x}}_j^{(n)}\|^2 < \infty$, which leads to $\sum_{n=0}^{\infty} \epsilon_j^{(n)} < \infty$ via (5.82) and (5.79). Finally, using (5.81) and Definition 3 yields the desired result. ■

The following proposition states the quasi-Fejér convergence of the sequences generated by Algorithm 4.

Proposition 2. *Assume A1 and A2 hold. Let* $\{\mathbf{x}^{(n)}\}_{n=0}^{\infty}$ *be any sequence generated by Algorithm 4, where* $\mathbf{x}^{(n)} \triangleq \left(\mathbf{x}_1^{(n)}, \ldots, \mathbf{x}_{N_V}^{(n)}\right)$. *Then, for each* $j \in \{1, \ldots, N_V\}$, *the sequence* $\{\mathbf{x}_j^{(n)}\}_{n=0}^{\infty}$ *is quasi-Fejér convergent to the set* $\Lambda_j \cap \Upsilon_j$.

Proof: Following the same steps as stated in the proof of Proposition 1, the following inequality is obtained based on (5.52):

$$\|\mathbf{x}_j^{(n+1)} - \mathbf{x}_j\|^2 \leq \|\mathbf{x}_j^{(n)} - \mathbf{x}_j\|^2 + \epsilon_j^{(n)} \tag{5.83}$$

where

$$\epsilon_j^{(n)} \triangleq \|\vartheta_{\text{nc}} \lambda_{j,\text{nc}}^{(n)} H_{\tilde{g}_{\hat{\ell}_{\text{nc}},\hat{k}_{\text{nc}}}^{(j)}}(\tilde{\mathbf{x}}_j^{(n)}) + \vartheta_{\text{c}} \lambda_{j,\text{c}}^{(n)} H_{g_{\hat{\ell}_{\text{c}},\hat{k}_{\text{c}}(\cdot,\mathbf{x}_i^{(\hat{n})})}^{(\hat{\imath}_{\text{c}},j)}}(\tilde{\mathbf{x}}_j^{(n)})\|^2 \tag{5.84}$$

with H_f being defined as in (5.67). The averaging step in (5.52) leads to $\|\mathbf{x}_j^{(n+1)} - \tilde{\mathbf{x}}_j^{(n)}\| = \sqrt{\epsilon_j^{(n)}}$, where $\epsilon_j^{(n)}$ is given by (5.84). Assuming that A2 holds and following an approach similar to that in the proof of Proposition 1, the inequality $\sum_{n=0}^{\infty} \epsilon_j^{(n)} < \infty$ is obtained, thus establishing the quasi-Fejér convergence of the sequence $\{\mathbf{x}_j^{(n)}\}_{n=0}^{\infty}$ to $\Lambda_j \cap \Upsilon_j$. ■

As the quasi-Fejér convergence of the sequences generated by the proposed algorithms is stated, the following lemma presents the properties of quasi-Fejér convergent sequences.

Lemma 2 *(Theorem 4.1 in [106]). If a sequence* $\{\mathbf{y}^k\}$ *is quasi-Fejér convergent to a nonempty set* $\mathcal{V}$*, the following conditions hold:*

1. $\{\mathbf{y}^k\}$ *is bounded.*
2. *If* $\mathcal{V}$ *contains an accumulation point of* $\{\mathbf{y}^k\}$*, then* $\{\mathbf{y}^k\}$ *converges to a point* $\mathbf{y} \in \mathcal{V}$*.*

5.4.2 Limiting Behavior of Step Size Sequences

In this part, we investigate the limiting behavior of the step size sequences, which are updated according to the procedure in Algorithm 3. The following two lemmas prove that the step size sequences generated by Algorithm 5 and Algorithm 4 have positive limits.

Lemma 3. *Any step size sequence* $\lambda_j^{(n)}$ *generated by Algorithm 5 has a positive limit, i.e.,*

$$\lim_{n\to\infty} \lambda_j^{(n)} > 0. \tag{5.85}$$

Proof: The proof is based on contradiction. Suppose that $\lim_{n\to\infty} \lambda_j^{(n)} = 0$. Then, for each $\zeta > 0$, there exists an iteration index $n(\zeta)$ such that $\lambda_j^{(n(\zeta))} < \zeta$. Based on the Armijo step size selection rule (5.46) in Algorithm 3 and the step size update equation (5.58) in Algorithm 5, there exists a function $f^\circ \in \widetilde{\mathcal{F}}_j \cup \mathcal{F}_j$ such that the inequality in (5.46) is not satisfied for the step size

$$\tilde{\zeta} = \lambda_j^{(n(\zeta)-1)} \xi^{\bar{m}} \tag{5.86}$$

where

$$\bar{m} = \max\{m \in \mathbb{Z}_{\geq 0} \mid \lambda_j^{(n(\zeta)-1)} \xi^m > \zeta\} \ . \tag{5.87}$$

Hence, the following inequality is obtained:

$$f^{\circ}(G_{f^{\circ}}^{\tilde{\zeta}}(\tilde{\mathbf{x}}_j^{(n(\zeta))})) > f^{\circ}(\tilde{\mathbf{x}}_j^{(n(\zeta))})(1-\beta\tilde{\zeta}) \ . \tag{5.88}$$

It is clear that $f^{\circ}(\tilde{\mathbf{x}}_j^{(n(\zeta))}) > 0$ since otherwise the step size selection procedure would not need to be applied, meaning that $\tilde{\mathbf{x}}_j^{(n(\zeta))}$ is inside the zero-sublevel set of every function in $\widetilde{\mathcal{F}}_j \cup \mathcal{F}_j$, i.e., $\tilde{\mathbf{x}}_j^{(n(\zeta))} \in \Lambda_j \cap \Upsilon_j$, which completes the proof of convergence of the iterates $\{\mathbf{x}_j^{(n)}\}_{n=0}^{\infty}$ to the set Λ_j via Lemma 2. Then, the left hand side of (5.88) can be rewritten using the Taylor series expansion and (5.41) as follows:

$$f^{\circ}(G_{f^{\circ}}^{\tilde{\zeta}}(\tilde{\mathbf{x}}_j^{(n(\zeta))})) = f^{\circ}(\tilde{\mathbf{x}}_j^{(n(\zeta))}) - \tilde{\zeta} f^{\circ}(\tilde{\mathbf{x}}_j^{(n(\zeta))}) + O(\tilde{\zeta}^2) \tag{5.89}$$

where $O(\tilde{\zeta}^2)$ represents the terms with $\tilde{\zeta}^s$ for $s \geq 2$. Since $\lim_{\tilde{\zeta}\to 0} O(\tilde{\zeta}^2)/\tilde{\zeta} = 0$, there exists $\upsilon > 0$ such that

$$O(\tilde{\zeta}^2)/\tilde{\zeta} < f^{\circ}(\tilde{\mathbf{x}}_j^{(n(\zeta))})(1-\beta) \tag{5.90}$$

is satisfied for $0 < \tilde{\zeta} \leq \upsilon$. The existence of υ satisfying (5.90) is guaranteed by $f^{\circ}(\tilde{\mathbf{x}}_j^{(n(\zeta))}) > 0$ and $\beta \in (0,1)$. Inserting (5.90) into (5.89) yields the inequality

$$f^{\circ}(G_{f^{\circ}}^{\tilde{\zeta}}(\tilde{\mathbf{x}}_j^{(n(\zeta))})) < f^{\circ}(\tilde{\mathbf{x}}_j^{(n(\zeta))})(1-\beta\tilde{\zeta}) \ , \tag{5.91}$$

which contradicts with (5.88). Therefore, the initial assumption is not valid, which implies $\lim_{n\to\infty} \lambda_j^{(n)} > 0$. ■

Lemma 4. *Any step size sequences $\lambda_{j,\mathrm{nc}}^{(n)}$ and $\lambda_{j,\mathrm{c}}^{(n)}$ generated by Algorithm 4 have positive limits, i.e.,*

$$\lim_{n\to\infty} \lambda_{j,\mathrm{nc}}^{(n)} > 0 \ \text{ and } \ \lim_{n\to\infty} \lambda_{j,\mathrm{c}}^{(n)} > 0. \tag{5.92}$$

Proof: The proof can be obtained by invoking similar arguments to those in the proof of Lemma 3 and using the step size update rule in (5.53) and (5.54).■

Lemma 3 and Lemma 4 will prove to be useful for deriving the fundamental convergence properties of the proposed algorithms, as investigated next.

5.4.3 Main Convergence Results

In this part, we present the main convergence results for the proposed algorithms, i.e., convergence to a solution of Problem 1.

Proposition 3. *Let* $\{\mathbf{x}^{(n)}\}_{n=0}^{\infty}$ *be any sequence generated by Algorithm 5, where* $\mathbf{x}^{(n)} \triangleq \left(\mathbf{x}_1^{(n)}, \ldots, \mathbf{x}_{N_V}^{(n)}\right)$. *Then, for each* $j \in \{1, \ldots, N_V\}$, *the sequence* $\{\mathbf{x}_j^{(n)}\}_{n=0}^{\infty}$ *converges to a point* $\mathbf{x}_j \in \Lambda_j \cap \Upsilon_j$, *i.e., a solution of Problem 1.*

Proof: From Proposition 1, $\sum_{n=0}^{\infty} \epsilon_j^{(n)} < \infty$, where $\epsilon_j^{(n)}$ is given by (5.79) in the supplementary material. Hence, $\lim_{n\to\infty} \epsilon_j^{(n)} = 0$ is obtained. Based on Lemma 3, (5.66), and (5.79), it follows that

$$\lim_{n\to\infty} \left\| \sum_{k=1}^{K_j} \left(\sum_{\ell \in \widetilde{S}_k^{(j)}} \tilde{\kappa}_{\ell,k}^{(j)} H_{\tilde{g}_{\ell,k}^{(j)}}(\tilde{\mathbf{x}}_j^{(n)}) + \sum_{i=1, i\neq j}^{N_V} \sum_{\ell \in S_k^{(i,j)}} \kappa_{\ell,k}^{(i,j)} H_{g_{\ell,k}^{(i,j)}(\cdot, \mathbf{x}_i^{(\hat{n})})}(\tilde{\mathbf{x}}_j^{(n)}) \right) \right\| = 0 \ , \tag{5.93}$$

which implies that

$$\lim_{n\to\infty} J_f(\tilde{\mathbf{x}}_j^{(n)}) = 0 \tag{5.94}$$

is satisfied $\forall f \in \widetilde{\mathcal{F}}_j \cup \mathcal{F}_j$, where the operator J_f defined on $\mathbb{R}^d$ for the set of continuously differentiable functions $f : \mathbb{R}^d \to \mathbb{R}$ is given by

$$J_f(\mathbf{x}) = \left(\frac{f^+(\mathbf{x})}{\|\nabla f(\mathbf{x})\|} \right)^2 . \tag{5.95}$$

For a generic Lambertian function in (5.25), the norm square of the gradient can be expressed as

$$\begin{aligned} \|\nabla g_\epsilon(\mathbf{x})\|^2 &= \frac{1}{\left(\|\mathbf{x}-\mathbf{y}\|^k + \epsilon\right)^2} \\ &+ \left(\frac{(\mathbf{y}-\mathbf{x})^T \mathbf{n}_R}{\|\mathbf{x}-\mathbf{y}\|^k + \epsilon} \right)^2 \frac{k\|\mathbf{x}-\mathbf{y}\|^{k-2} \left((k-2)\|\mathbf{x}-\mathbf{y}\|^k - 2\epsilon\right)}{\left(\|\mathbf{x}-\mathbf{y}\|^k + \epsilon\right)^2}. \end{aligned} \tag{5.96}$$

Since the sequence of iterates $\{\tilde{\mathbf{x}}_j^{(n)}\}_{n=0}^{\infty}$ is bounded by Lemma 2, $\left\{\|\tilde{\mathbf{x}}_j^{(n)} - \mathbf{y}\|\right\}_{n=0}^{\infty}$ is also bounded, which implies the boundedness of $\|\nabla g_\epsilon(\mathbf{x})\|$ via (5.96). Therefore, based on (5.94) and (5.95), it follows that

$$\lim_{n\to\infty} f^+(\tilde{\mathbf{x}}_j^{(n)}) = 0, \quad \forall f \in \widetilde{\mathcal{F}}_j \cup \mathcal{F}_j \, . \tag{5.97}$$

From the Bolzano-Weierstrass Theorem [187, Section 3.4], the boundedness of $\{\tilde{\mathbf{x}}_j^{(n)}\}_{n=0}^{\infty}$ requires that $\{\tilde{\mathbf{x}}_j^{(n)}\}_{n=0}^{\infty}$ has a convergent subsequence. Denote the limit of this subsequence by $\mathbf{x}_j^{\star}$. From (5.97), it turns out that $\mathbf{x}_j^{\star} \in \Lambda_j \cap \Upsilon_j$. Therefore, $\Lambda_j \cap \Upsilon_j$ contains a limit point of $\{\tilde{\mathbf{x}}_j^{(n)}\}_{n=0}^{\infty}$, which, based on Lemma 2, yields the result that $\{\tilde{\mathbf{x}}_j^{(n)}\}_{n=0}^{\infty}$ converges to a point inside $\Lambda_j \cap \Upsilon_j$. Based on (5.55) and the fact that $\Lambda_j \subset \Gamma_j$ (see (5.22) and (5.42)), it follows that the sequence $\{\mathbf{x}_j^{(n)}\}_{n=0}^{\infty}$ converges to a point $\mathbf{x}_j \in \Lambda_j \cap \Upsilon_j$. ■

Proposition 4. *Let $\{\mathbf{x}^{(n)}\}_{n=0}^{\infty}$ be any sequence generated by Algorithm 4, where $\mathbf{x}^{(n)} \triangleq \left(\mathbf{x}_1^{(n)}, \ldots, \mathbf{x}_{N_V}^{(n)}\right)$. Then, for each $j \in \{1, \ldots, N_V\}$, the sequence $\{\mathbf{x}_j^{(n)}\}_{n=0}^{\infty}$ converges to a point $\mathbf{x}_j \in \Lambda_j \cap \Upsilon_j$, i.e., a solution of Problem 1.*

Proof: Applying similar steps to those in the proof of Proposition 3 and exploiting Proposition 2 and Lemma 4, the following results are obtained:

$$\lim_{n\to\infty} \left[\tilde{g}^{(j)}_{\hat{\ell}_{\rm nc},\hat{k}_{\rm nc}}(\tilde{\mathbf{x}}_j^{(n)})\right]^+ = 0 \tag{5.98}$$

$$\lim_{n\to\infty} \left[g^{(\hat{i}_{\rm c},j)}_{\hat{\ell}_{\rm c},\hat{k}_{\rm c}}(\tilde{\mathbf{x}}_j^{(n)}, \mathbf{x}_i^{(\hat{n})})\right]^+ = 0 \tag{5.99}$$

Based on the most violated constraint control in (5.48) and (5.49), it is obvious that

$$\tilde{f}(\tilde{\mathbf{x}}_j^{(n)}) \leq \tilde{g}^{(j)}_{\hat{\ell}_{\rm nc},\hat{k}_{\rm nc}}(\tilde{\mathbf{x}}_j^{(n)}),\ \forall \tilde{f} \in \widetilde{\mathcal{F}}_j \tag{5.100}$$

$$f(\tilde{\mathbf{x}}_j^{(n)}) \leq g^{(\hat{i}_{\rm c},j)}_{\hat{\ell}_{\rm c},\hat{k}_{\rm c}}(\tilde{\mathbf{x}}_j^{(n)}, \mathbf{x}_i^{(\hat{n})}),\ \forall f \in \mathcal{F}_j \tag{5.101}$$

which implies via (5.98) and (5.99) that

$$\lim_{n\to\infty} f^+(\tilde{\mathbf{x}}_j^{(n)}) = 0, \quad \forall f \in \widetilde{\mathcal{F}}_j \cup \mathcal{F}_j\ . \tag{5.102}$$

The rest of the proof is the same as that in Proposition 3. ■

5.5 Numerical Results

In this section, numerical examples are provided to investigate the theoretical bounds on cooperative localization in VLP networks and to evaluate the performance of the proposed projection-based algorithms. The VLP network parameters are determined in a similar manner to the work in [23] and [16]. The area

of each PD is selected as $1\,\mathrm{cm}^2$ and the Lambertian order of all the LEDs is set to $m = 1$. In addition, the noise variances are computed using [135, Eq. 6]. The parameters for noise variance calculation are the same as those used in Table I in [135].

The VLP network considered in the simulations is illustrated in Fig. 5.2. A room of size 10m×10m×5m is considered, where there exist $N_L = 4$ LED transmitters on the ceiling which are located at $\mathbf{y}_1 = [1\ 1\ 5]^T\mathrm{m}$, $\mathbf{y}_2 = [1\ 9\ 5]^T\mathrm{m}$, $\mathbf{y}_3 = [9\ 1\ 5]^T\mathrm{m}$, and $\mathbf{y}_4 = [9\ 9\ 5]^T\mathrm{m}$. The LEDs on the ceiling have perpendicular orientations, i.e., $\widetilde{\mathbf{n}}_{T,j} = [0\ \ 0\ -1]^T$ for $j \in \{1, 2, 3, 4\}$. In addition, there exist $N_V = 2$ VLC units whose locations are given by $\mathbf{x}_1 = [2\ 5\ 1]^T\mathrm{m}$ and $\mathbf{x}_2 = [6\ 6\ 1.5]^T\mathrm{m}$. Each VLC unit consists of two PDs and one LED, whose offsets with respect to the center of the VLC unit are given by $\mathbf{a}_{j,1} = [0\ -0.1\ 0]^T\mathrm{m}$, $\mathbf{a}_{j,2} = [0\ 0.1\ 0]^T\mathrm{m}$, and $\mathbf{b}_{j,1} = [0.1\ 0\ 0]^T\mathrm{m}$ for $j = 1, 2$. The orientation vectors of the PDs and the LEDs on the VLC units are set to be the normalized versions (the orientation vectors are unit-norm) of the following vectors: $\mathbf{n}_{R,1}^{(1)} = [0.3\ -0.1\ 1]^T$, $\mathbf{n}_{R,1}^{(2)} = [0.2\ 0.4\ 1]^T$, $\mathbf{n}_{R,2}^{(1)} = [0.8\ 0.6\ 0.1]^T$, $\mathbf{n}_{R,2}^{(2)} = [-0.7\ 0.2\ 0.1]^T$, $\mathbf{n}_{T,1}^{(1)} = [0.9\ 0.4\ 0.1]^T$, and $\mathbf{n}_{T,1}^{(2)} = [-0.8\ 0.1\ 0.1]^T$. Furthermore, the connectivity sets are defined as $S_1^{(i,j)} = \emptyset$, $S_2^{(i,j)} = \{1\}$ for $i, j \in \{1, 2\}, i \neq j$ for the cooperative measurements and $\widetilde{S}_1^{(1)} = \{1, 2, 3\}$, $\widetilde{S}_1^{(2)} = \{2, 3, 4\}$ and $\widetilde{S}_2^{(j)} = \emptyset$ for $j \in \{1, 2\}$ for the noncooperative measurements.

5.5.1 Theoretical Bounds

In this part, the CRLB expression derived in Section 5.1 is investigated to illustrate the effects of cooperation on the localization performance of VLP networks.

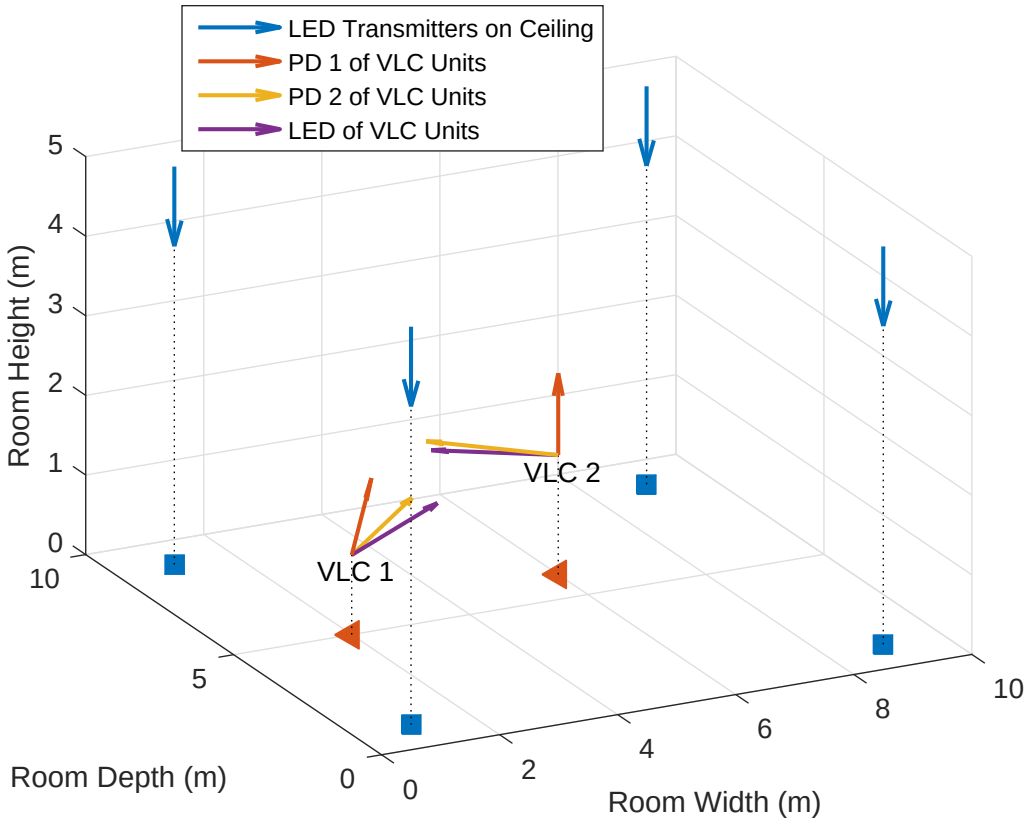

Figure 5.2: VLP network used in the simulations. Each VLC unit is equipped with two PDs and one LED. PD 1 of the VLC units gathers measurements from the LEDs on the ceiling while PD 2 of the VLC units is used to communicate with the LED of the other VLC unit for cooperative localization. The squares and the triangles denote the projections of the LEDs and the VLC units on the floor, respectively.

5.5.1.1 Performance with Respect to Transmit Power of LEDs on Ceiling

In order to evaluate the localization performance of the VLC units with respect to the transmit powers of the LEDs on the ceiling (equivalently, anchors), individual CRLBs for localization of the VLC units in noncooperative and cooperative scenarios are plotted with respect to the transmit powers of LEDs on the ceiling in Fig. 5.3 by fixing the transmit powers of the VLC units to 1 W. As seen from Fig. 5.3, cooperation among VLC units can provide substantial improvements in localization accuracy (about 43 cm and 14 cm improvement, respectively, for VLC 1 and VLC 2 for the LED transmit power of 300 mW). We note that the improvement gained by employing cooperation is higher for VLC 1 as compared to that for VLC 2. This is an expected result since VLC 1 acquires its location information mainly through LED 1 and LED 2 (due to much longer distances to other LEDs), and cooperative measurements enhance the localization accuracy for VLC 1 more significantly than they do for VLC 2. Note that VLC 2 can obtain informative measurements from the LEDs on the ceiling even in the absence of cooperation, as seen from the network geometry in Fig. 5.2. In addition, the CRLBs in the cooperative scenario converge to those in the noncooperative scenario as the transmit powers of the LEDs increase, which is in compliance with the FIM expression in (5.12). Hence, the effect of cooperation on localization performance becomes more evident as the transmit power decreases, which agrees with the results obtained for RF based cooperative localization networks [85].

5.5.1.2 Performance with Respect to Transmit Power of VLC Units

Secondly, we explore the localization performance of the VLC units with respect to the transmit powers of the VLC units by fixing the transmit powers of the LEDs on the ceiling to 1 W. In Fig. 5.4, the CRLBs for localization of the VLC units are shown with respect to the transmit powers of the VLC units in the noncooperative and cooperative cases. Similar to Fig. 5.3, cooperation results in a higher improvement in the performance of VLC 1. In addition, we note that

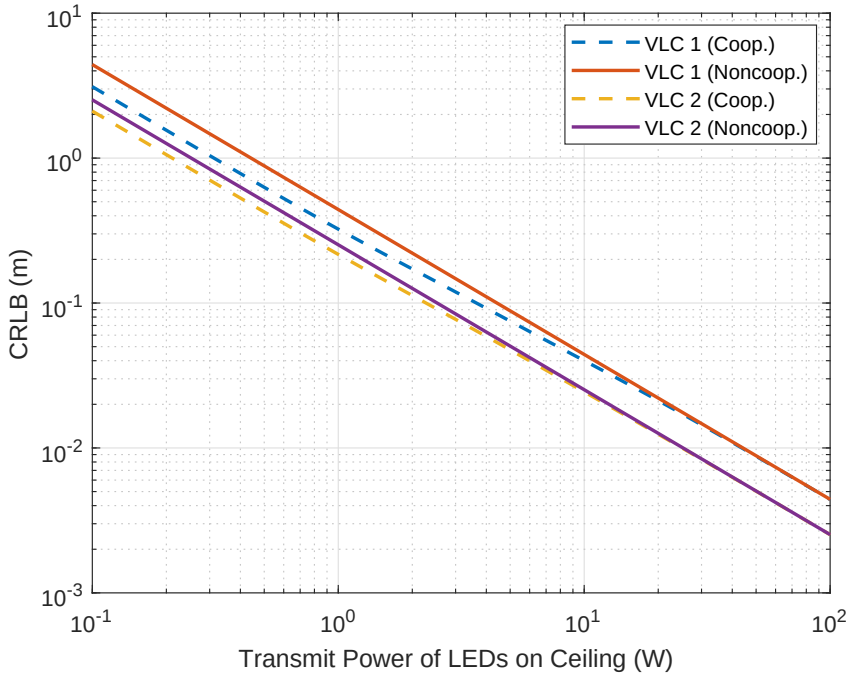

Figure 5.3: Individual CRLBs for localization of VLC units in the absence and presence of cooperation with respect to the transmit power of LEDs on ceiling, where the transmit power of VLC units is set to 1W.

the contribution of cooperation to localization performance gets higher as the transmit powers of the VLC units increase, which complies with (5.12). Unlike Fig. 5.3, the CRLB begins to saturate above a certain power level. The main reason for this difference between the CRLB trends in Fig. 5.3 and Fig. 5.4 can be explained as follows: For a fixed transmit power of the VLC units, the localization error by using three anchors (i.e., three LEDs on the ceiling that are connected to the corresponding VLC unit) converges to zero as the transmit powers of the anchors increase regardless of whether VLC units cooperate or not. On the other hand, for a fixed transmit power of the LEDs on the ceiling, increasing the transmit power of the VLC unit (i.e., one of the anchors) cannot improve the accuracy after a certain level.

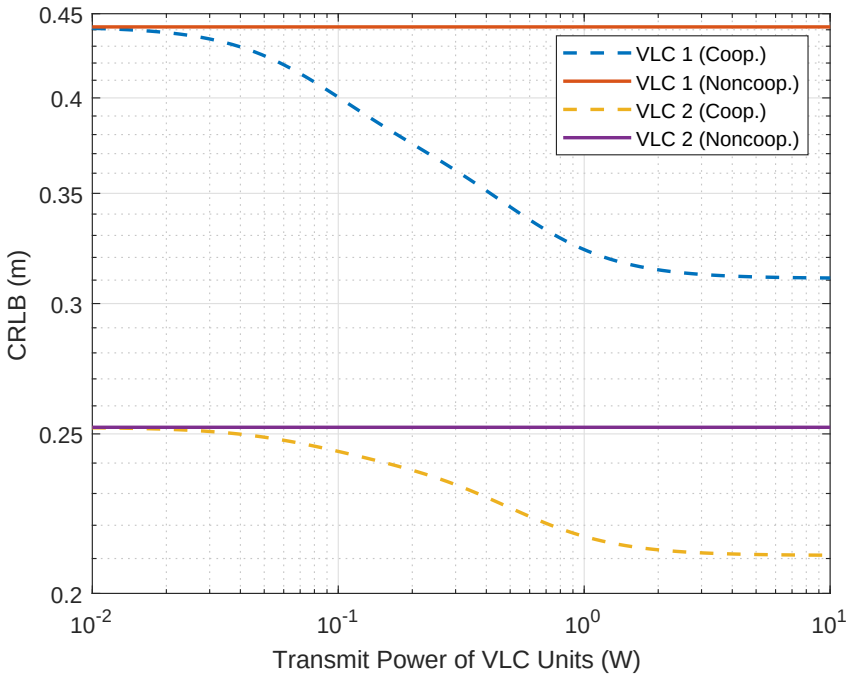

Figure 5.4: Individual CRLBs for localization of VLC units in the absence and presence of cooperation with respect to the transmit power of VLC units, where the transmit power of LEDs on ceiling is set to 1W.

5.5.2 Performance of the Proposed Algorithms

In this part, the proposed algorithms in Algorithm 4 (CCGP) and Algorithm 5 (CSGP) are evaluated in terms of localization performance and convergence speed. For both algorithms, the initial step size is selected as $\lambda_0 = 1$, the step size shrinkage factor and the degree of decline in the Armijo rule in Algorithm 3 are set to $\xi = 0.5$ and $\beta = 0.001$, respectively. The VLC units are initialized at the positions of the closest LEDs on the ceiling which are connected to the corresponding VLC units.

Localization performances of the algorithms are presented in both the absence and the presence of cooperation and compared against those of the ML estimator in (5.9) and the CRLBs derived in Section 5.1. In order to ensure convergence

to the global minimum, the ML estimator is implemented using a multi-start optimization algorithm with 100 initial points randomly selected from the interval $[0\ 10]$ m at each axis.[7] In addition, two different measurement noise distributions, namely, Gaussian and exponential, are considered while evaluating the proposed algorithms as in [93]. The Gaussian noise is used to model the case in which the RSS measurement noise can be both positive and negative, whereas the exponentially distributed noise (subtracted from the true value) represents the scenario in which the RSS measurements are negatively biased, which leads to the feasibility modeling of the localization problem in Section 5.2.2. Furthermore, the average residuals at each iteration are calculated to assess the convergence speed of the proposed algorithms [94]:

$$\varrho_n = \frac{1}{MN_V} \sum_{m=1}^{M} \|\mathbf{x}^{(n,m)} - \mathbf{x}^{(n-1,m)}\| \tag{5.103}$$

where $\mathbf{x}^{(n,m)} = \left(\mathbf{x}_1^{(n,m)}, \ldots, \mathbf{x}_{N_V}^{(n,m)}\right)$ denotes the position vector of all the VLC units at the nth iteration for the mth Monte Carlo realization of measurement noises and M is the number of Monte Carlo realizations.

In the simulations, two-dimensional localization is performed by assuming that the VLC units have known heights. Therefore, with the knowledge of perpendicular LED orientations, Case 2 type Lambertian sets in Section 5.2.4.2 are utilized for localization based on the measurements from the LEDs on the ceiling. The cooperation among the VLC units is modeled by Case 1 type Lambertian sets in Section 5.2.4.1.

[7] The implemented estimator is effectively a MAP estimator with a uniform prior distribution over the interval $[0\ 10]$ m, based on the prior information that VLC units are inside the room. Hence, the implemented ML estimator may achieve smaller RMSEs than the CRLB in the low SNR regime, where the prior information becomes more significant as the measurements are very noisy.

5.5.2.1 Gaussian Noise

In Fig. 5.5, the average localization errors of the VLC units for the different algorithms are plotted against the transmit power of the LEDs on the ceiling for the case of the Gaussian measurement noise by fixing the transmit powers of the LEDs at the VLC units to 1 W. From Fig. 5.5, it is observed that the cooperative approach can significantly reduce the localization errors, especially in the low SNR regime (about 60 cm and 70 cm reduction for CSGP and CCGP algorithms, respectively, for 100 mW LED transmit power). In addition, both Algorithm 4 (CCGP) and Algorithm 5 (CSGP) can attain the localization error levels that asymptotically converge to zero at the same rate as that of the CRLB. Moreover, it can be inferred from Fig. 5.5 that the proposed iterative methods achieve higher localization performance than the ML estimator in the low SNR regime for both the noncooperative and the cooperative scenarios. Although the ML estimator is forced to converge to the global minimum via the multi-start optimization procedure involving 100 different executions of a local solver, whose complexity may be prohibitive for practical implementations, it has lower performance than the proposed approaches, which depend on low-complexity iterative gradient projections. Hence, at low SNRs, the proposed algorithms are superior to the MLE in terms of both the localization performance and the computational complexity. Furthermore, the simultaneous projections outperforms the cyclic projections at low SNRs at the cost of a higher number of set projections, but the two approaches converge asymptotically as the SNR increases.

Fig. 5.6(a) and Fig. 5.6(b) report the average residuals calculated by (5.103) corresponding to the proposed algorithms versus the number of iterations for 100 mW and 1 W of transmit powers of the LEDs on the ceiling, respectively. CSGP in the absence of cooperation has the fastest convergence rate and exhibits an almost monotonic convergence behavior. However, CSGP in the cooperative scenario shows relatively slow convergence in general and a locally nonmonotonic behavior when several consecutive iterations are taken into account. This is due to the cooperative Lambertian sets being involved in the simultaneous projection operations. In addition, cyclic projections tend to settle into limit cycle

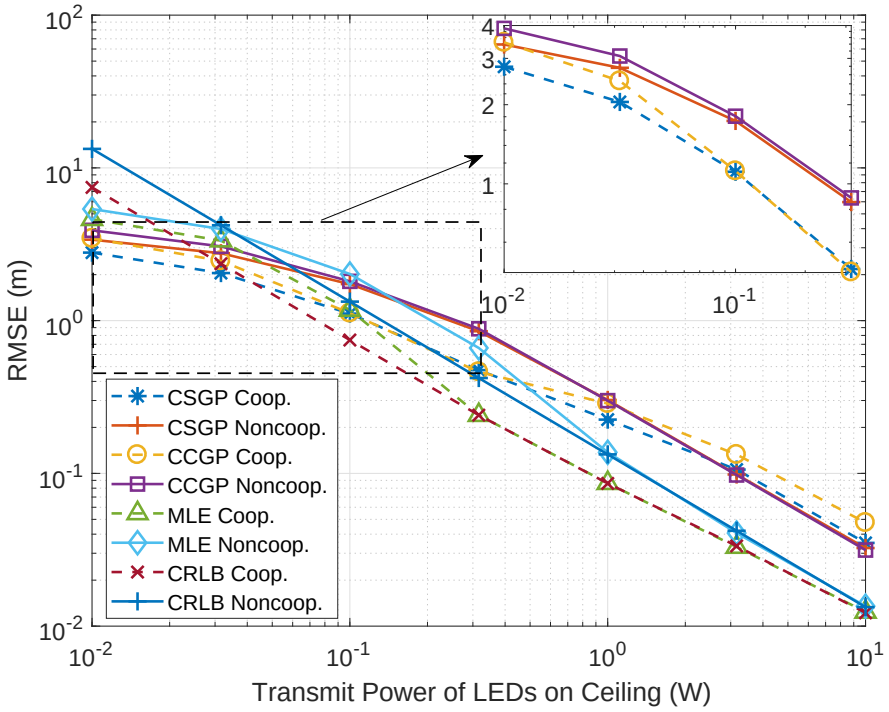

Figure 5.5: Average localization error of VLC units with respect to the transmit power of LEDs on ceiling for the proposed algorithms in Algorithm 4 (CCGP) and Algorithm 5 (CSGP) along with the MLE and CRLB for the case of Gaussian measurement noise.

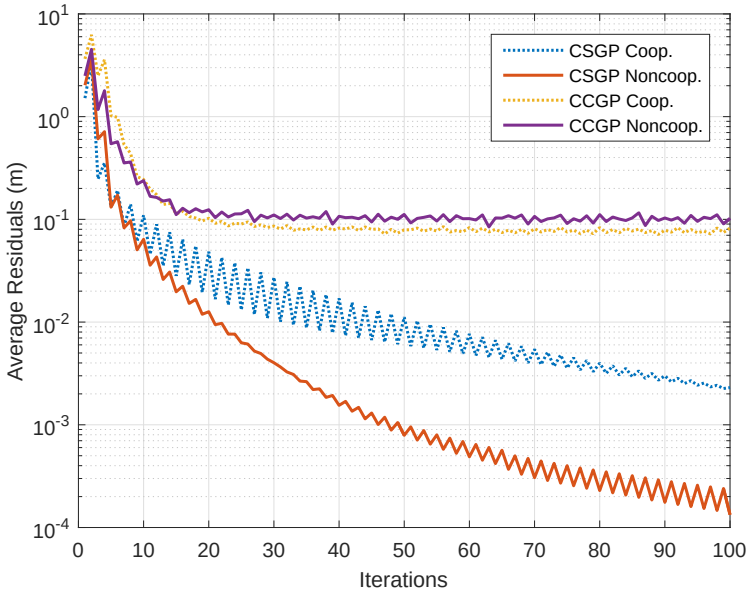

(a)

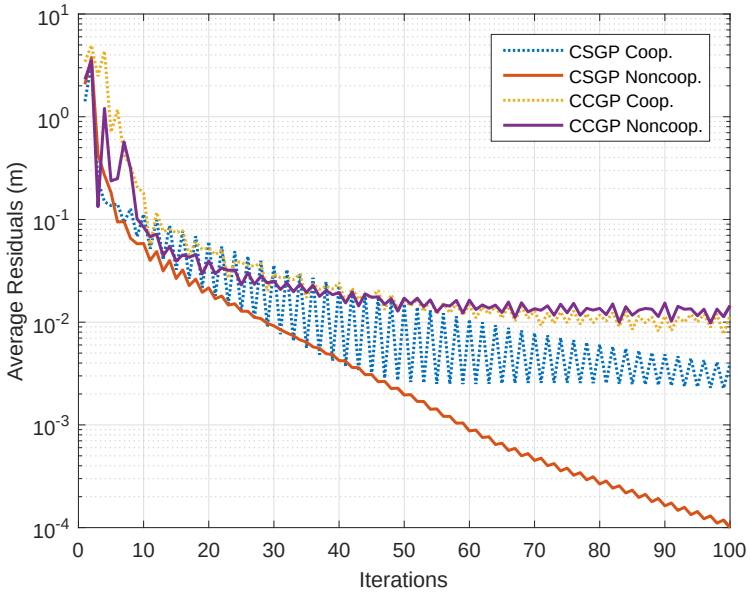

(b)

Figure 5.6: Convergence rate of the average residuals in (5.103) for the proposed algorithms in Algorithm 4 and Algorithm 5 for the case of Gaussian measurement noise, where the transmit power of LEDs on ceiling is (a) 100 mW and (b) 1 W.

oscillations[8] after few iterations, thus implying that the sequence itself does not converge to a point, but it has several subsequences that converge [112]. This behavior, called *cyclic convergence*, is encountered in cyclic (sequential) projections if the feasibility problem is inconsistent [112, 188]. Furthermore, by comparing Fig. 5.6(a) and Fig. 5.6(b), it is observed that the magnitude of limit cycle oscillations in the CCGP algorithm gets smaller as the SNR increases since the region of uncertainty becomes narrower at higher SNR values, thereby making the convergent subsequences close to each other.

5.5.2.2 Exponential Noise

To investigate the performance of the algorithms under exponentially distributed measurement noise, the average localization errors are plotted against the transmit power of the LEDs on the ceiling for the case of the subtractive exponential noise in Fig. 5.7. Similar to the case of the Gaussian noise, the proposed algorithms succeed in converging to the true VLC unit positions as the SNR increases. Since the projection based methods rely on the assumption of negatively biased measurements, they perform slightly better at low SNRs as compared to the case of the Gaussian noise. On the other hand, the MLE produces larger errors at low SNRs for the exponentially distributed noise since its derivation is based on the assumption of Gaussian noise.

The average residuals in the case of the exponentially distributed noise are illustrated in Fig. 5.8(a) and Fig. 5.8(b) for two different LED power levels. In contrary to the case of Gaussian noise, cyclic projections do not fall into limit cycles and provide globally monotonic convergence results as the feasibility problem is consistent, which complies with the results presented in the literature

[8] In inconsistent feasibility problems (i.e., those with empty region of intersection), the sequence of points obtained by cyclic projections does not converge [112]. However, it has convergent subsequences each of which converges to a different point [112]. In the limit, the cyclic projections based algorithm (i.e., CCGP) visits each of these limiting points in a sequential fashion, leading to a cyclic behavior called *limit cycle*. In this case, average residuals in (5.103) (i.e., distances between consecutive iteration points) can be regarded as *limit cycle oscillations*.

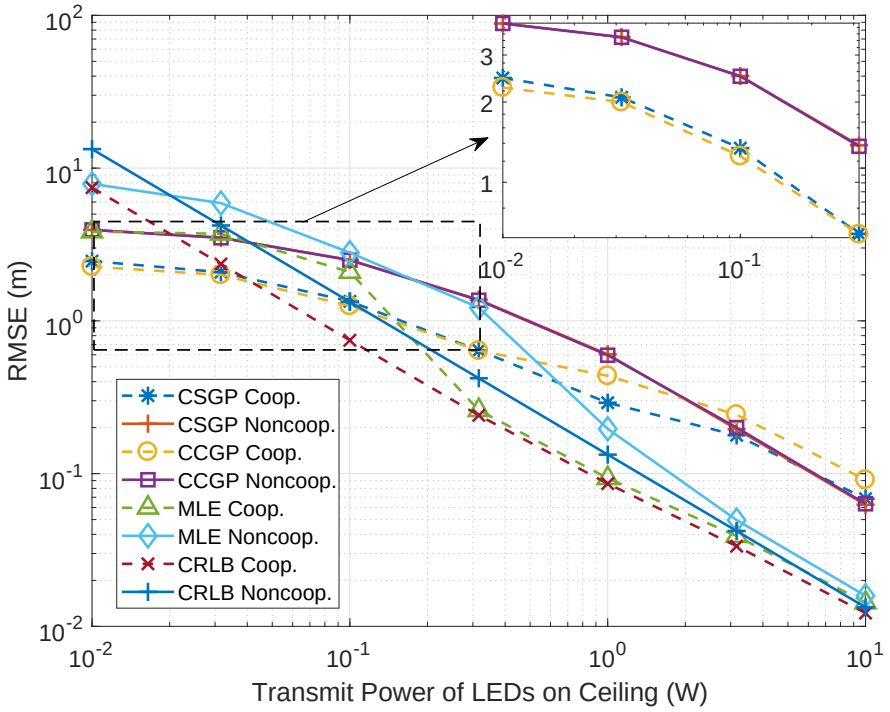

Figure 5.7: Average localization error of VLC units with respect to the transmit power of LEDs on ceiling for the proposed algorithms in Algorithm 4 (CCGP) and Algorithm 5 (CSGP) along with the MLE and CRLB for the case of exponentially distributed measurement noise.

pertaining to the study of CFPs [112]. In addition, it is observed that both the cyclic and the sequential projection methods have faster convergence for lower SNR values since it takes fewer iterations to get inside the intersection of the constraint sets, which becomes larger as the SNR decreases.[9]

[9] Since the measured RSS is always smaller than the true RSS value in the case of negative exponential noise (see (5.13)), the Lambertian sets become larger at lower SNR values (as the size of a Lambertian set $\mathcal{L}$ in (5.16) is inversely proportional to the corresponding RSS measurement $\hat{P}_r$, or, equivalently γ in (5.15)).

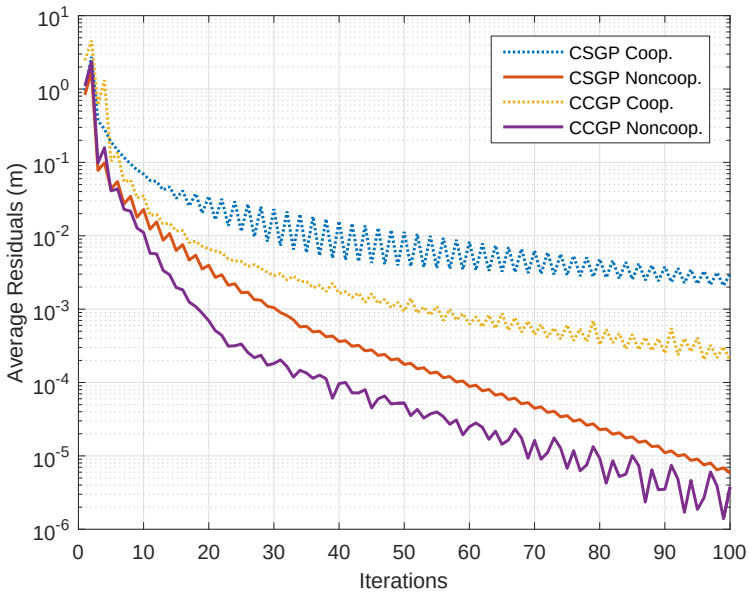

(a)

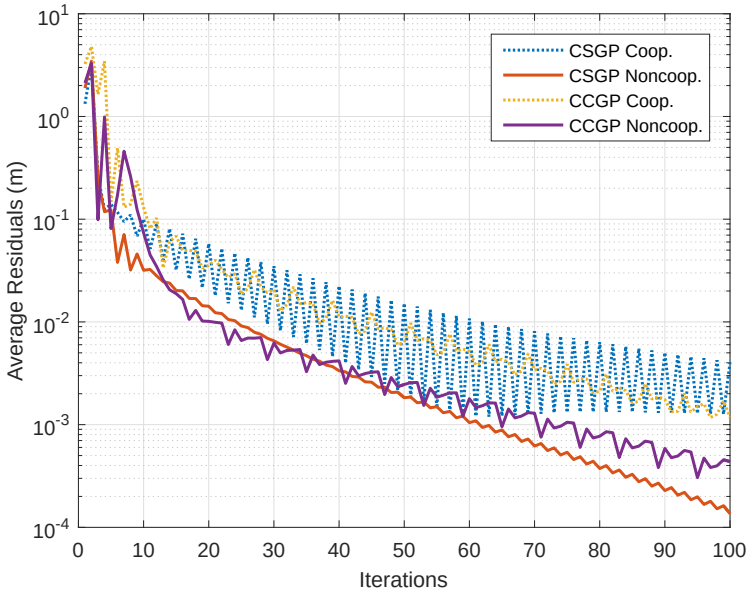

(b)

Figure 5.8: Convergence rate of the average residuals in (5.103) for the proposed algorithms in Algorithm 4 and Algorithm 5 for the case of exponentially distributed measurement noise, where the transmit power of LEDs on ceiling is (a) 100 mW and (b) 1 W.

5.6 Concluding Remarks

In this chapter, a cooperative VLP network has been proposed based on a generic system model consisting of LED transmitters at known locations and VLC units with multiple LEDs and PDs. First, the CRLB on the overall localization error of the VLC units has been derived to quantify the effects of cooperation on the localization accuracy of VLP networks. Then, due to the nonconvex nature of the corresponding ML expression, the problem of cooperative localization has been formulated as a QFP, which facilitates the development of low-complexity decentralized feasibility-seeking methods. In order to solve the feasibility problem, iterative gradient projections based algorithms have been proposed. Furthermore, based on the notion of quasi-Fejér convergent sequences, formal convergence proofs have been provided for the proposed algorithms in the consistent case. Finally, numerical examples have been presented to illustrate the significance of cooperation in VLP networks and to investigate the performance of the proposed algorithms in terms of localization accuracy and convergence speed. It has been verified that the proposed iterative methods asymptotically converge to the true positions of VLC units at high SNR and exhibit superior performance over the ML estimator at low SNRs in terms of both implementation complexity and localization accuracy.

An important research direction for future studies is to explore the convergence properties of Algorithm 4 and Algorithm 5 when the proposed QFP is inconsistent. In the inconsistent case, simultaneous projection algorithms tend to converge to a minimizer of a *proximity function* that specifies the distance to constraint sets [112, 189]. For the implicit CFP (ICFP) considered in TOA-based wireless network localization, the POCS based simultaneous algorithm is shown to converge to the minimizer of a convex function, which is the sum of squares of the distances to the constraint sets [94]. Therefore, finding proximity functions characterizing the behavior of simultaneous projections (e.g., Algorithm 5) for the inconsistent QFPs [105] would be a significant extension for the set-theoretic estimation literature.

5.7 Appendices

5.7.1 Partial Derivatives in (5.12)

From (5.5) and (5.6), the partial derivatives in (5.12) can be computed as follows:

$$\frac{\partial\widetilde{\alpha}_{l,k}^{(j)}(\mathbf{x}_j)}{\partial x_t} = -\frac{(\widetilde{m}_\ell+1)\widetilde{P}_{T,\ell}A_k^{(j)}\big((\widetilde{\mathbf{d}}_{\ell,k}^{(j)})^T\widetilde{\mathbf{n}}_{T,l}\big)^{\widetilde{m}_\ell}}{2\pi\|\widetilde{\mathbf{d}}_{\ell,k}^{(j)}\|^{\widetilde{m}_\ell+3}}$$
$$\times\Big(\widetilde{m}_\ell\widetilde{n}_{T,l}(t-3j+3)(\widetilde{\mathbf{d}}_{\ell,k}^{(j)})^T\mathbf{n}_{R,k}^{(j)}\big((\widetilde{\mathbf{d}}_{\ell,k}^{(j)})^T\widetilde{\mathbf{n}}_{T,l}\big)^{-1}+n_{R,k}^{(j)}(t-3j+3)$$
$$-(\widetilde{m}_\ell+3)\widetilde{d}_{l,k}^{(j)}(t-3j+3)(\widetilde{\mathbf{d}}_{\ell,k}^{(j)})^T\mathbf{n}_{R,k}^{(j)}\|\widetilde{\mathbf{d}}_{\ell,k}^{(j)}\|^{-2}\Big) \tag{5.104}$$

for $t\in\{3j-2,3j-1,3j\}$ and $\partial\widetilde{\alpha}_{l,k}^{(j)}(\mathbf{x}_j)/\partial x_t=0$ otherwise, where $\widetilde{n}_{T,l}(t-3j+3)$, $n_{R,k}^{(j)}(t-3j+3)$, and $\widetilde{d}_{l,k}^{(j)}(t-3j+3)$ denote the $(t-3j+3)$th elements of $\widetilde{\mathbf{n}}_{T,l}$, $\mathbf{n}_{R,k}^{(j)}$, and $\widetilde{\mathbf{d}}_{\ell,k}^{(j)}$, respectively. Similarly,

$$\frac{\partial\alpha_{l,k}^{(i,j)}(\mathbf{x}_j,\mathbf{x}_i)}{\partial x_t} = -\frac{(m_\ell^{(i)}+1)P_{T,\ell}^{(i)}A_k^{(j)}\big((\mathbf{d}_{\ell,k}^{(i,j)})^T\mathbf{n}_{T,\ell}^{(i)}\big)^{m_\ell^{(i)}}}{2\pi\|\mathbf{d}_{\ell,k}^{(i,j)}\|^{m_\ell^{(i)}+3}}$$
$$\times\Big(m_\ell^{(i)}n_{T,l}^{(i)}(t-3j+3)(\mathbf{d}_{\ell,k}^{(i,j)})^T\mathbf{n}_{R,k}^{(j)}\big((\mathbf{d}_{\ell,k}^{(i,j)})^T\mathbf{n}_{T,\ell}^{(i)}\big)^{-1}+n_{R,k}^{(j)}(t-3j+3)$$
$$-(m_\ell^{(i)}+3)d_{l,k}^{(i,j)}(t-3j+3)(\mathbf{d}_{\ell,k}^{(i,j)})^T\mathbf{n}_{R,k}^{(j)}\|\mathbf{d}_{\ell,k}^{(i,j)}\|^{-2}\Big) \tag{5.105}$$

for $t\in\{3j-2,3j-1,3j\}$, $\partial\alpha_{l,k}^{(i,j)}(\mathbf{x}_i,\mathbf{x}_j)/\partial x_t$ is equal to the negative of (5.105) with $(t-3j+3)$'s being replaced by $(t-3i+3)$'s for $t\in\{3i-2,3i-1,3i\}$, and $\partial\alpha_{l,k}^{(i,j)}(\mathbf{x}_i,\mathbf{x}_j)/\partial x_t=0$ otherwise. In (5.105), $n_{T,l}^{(i)}(t-3j+3)$ and $d_{l,k}^{(i,j)}(t-3j+3)$ denote the $(t-3j+3)$th elements of $\mathbf{n}_{T,\ell}^{(i)}$ and $\mathbf{d}_{\ell,k}^{(i,j)}$, respectively.

Chapter 6

Conclusions and Future Work

As a key enabler for low-cost and high-accuracy indoor wireless localization services, the VLP technology constitutes a vital ingredient of next-generation location-aware applications. Therefore, it is imperative, for both researchers in the academia and practical system designers in the industry, to acquire a meticulous understanding of the fundamental trends in position estimation via visible light signals and their impacts on the performance of VLP systems under various operation environments. In this dissertation, we have considered the problem of localization in visible light systems by providing fundamental performance limits and statistical estimators, devising localization algorithms and investigating optimal resource allocation approaches.

In Chapter 2, we have derived the CRLBs and MLEs for distance estimation in VLP systems based on TOA and/or RSS information. We have proposed hybrid TOA/RSS distance estimation for VLP systems and determined the conditions under which the hybrid approach outperforms TOA based and RSS based estimators. To mitigate the effects of finite sampling rate in practical systems, a modified hybrid TOA/RSS based distance estimator has been developed. In addition to the CRLB, we have also derived the ZZB for ranging in synchronous VLP systems by taking into account the time delay and the optical channel attenuation parameters along with the prior information. Moreover, we have obtained

the BCRB, the WCRB and the ECRB expressions for range estimation in synchronous scenarios.

In Chapter 3, the direct position estimation approach has been considered for both synchronous and asynchronous VLP systems. The CRLBs and direct positioning based ML estimators have been derived for a generic three-dimensional VLP scenario. In addition, we have also designed two-step position estimators and characterized their asymptotic performance, i.e., whether they can attain the CRLB in the high SNR regime. It has been shown that the two-step estimation based on TOA and RSS parameters in the first-step is asymptotically optimal for synchronous VLP systems, whereas for asynchronous systems, the two-step approach is optimal in all SNR regimes for practical ranging signals. Another related conclusion is that the benefits of direct positioning are especially significant in the low SNR regime for synchronous VLP systems.

In Chapter 4, we have considered optimal LED power allocation strategies to maximize the localization accuracy of VLC receivers subject to power and illumination constraints. The performance limits derived in Chapter 3 have been employed as optimization metrics for quantification of localization accuracy. The problem of optimal power allocation has been shown to be formulated as a convex program, on the basis of which the optimal power vectors have been derived efficiently to showcase the performance benefits over the conventional uniform power allocation approach. In addition, robust power allocation algorithms have been developed to provide accurate location estimates under imperfect knowledge of localization related parameters.

Finally, in Chapter 5, we have devised a cooperative VLP system architecture that utilizes communications among VLC receiver units to improve the accuracy of localization via cooperation. Our main motivation comes from vehicular VLC networks where V2V and V2I links are available to provide the necessary foundation for cooperative ITS applications. A cooperative localization algorithm that is amenable to distributed implementation has been proposed to illustrate the improvements in localization performance via the use of cooperation among

the VLC units. Moreover, we have provided a convergence analysis of the proposed algorithm under certain conditions on the mathematical structure of the localization problem.

Although significant improvements are being made for VLP systems in the literature, there are still some issues which have not adequately been addressed and should be investigated in future work. A recent study in the literature has shown that omitting multipath reflections in VLP systems may considerably reduce the accuracy of localization in certain indoor environments [190]. For that reason, VLP systems should be designed in consideration of multipath propagation. In a similar context, the common algorithms and methods in the literature do not consider the situation when the LOS between the LED transmitter and the VLC receiver is lost; that is, when an LOS blockage occurs. Regarding this issue, the approaches for VLP systems should be adapted for the case of LOS blockage. In addition, the VLP systems should be invulnerable to various interference sources such as sunlight and other lighting systems. Moreover, most VLP systems cannot be treated separately from illumination systems, and consequently the design of such systems requires the consideration of not only localization performance but also illumination constraints. Furthermore, in scenarios with mobile entities, temporal cooperation can be utilized by taking into account the previous state information of a VLC receiver in the design of VLP algorithms in order to achieve robust localization results. Overall, in view of these challenges and remarks, fully integrated superior designs can be developed for VLP systems in the future.

Bibliography

[1] H. Burchardt, N. Serafimovski, D. Tsonev, S. Videv, and H. Haas, "VLC: Beyond point-to-point communication," *IEEE Communications Magazine*, vol. 52, pp. 98–105, July 2014.

[2] P. Pathak, X. Feng, P. Hu, and P. Mohapatra, "Visible light communication, networking, and sensing: A survey, potential and challenges," *IEEE Communications Surveys Tutorials*, vol. 17, pp. 2047–2077, Fourthquarter 2015.

[3] A. Jovicic, J. Li, and T. Richardson, "Visible light communication: Opportunities, challenges and the path to market," *IEEE Communications Magazine*, vol. 51, pp. 26–32, Dec. 2013.

[4] D. Karunatilaka, F. Zafar, V. Kalavally, and R. Parthiban, "LED based indoor visible light communications: State of the art," *IEEE Communications Surveys Tutorials*, vol. 17, pp. 1649–1678, thirdquarter 2015.

[5] J. Armstrong, Y. Sekercioglu, and A. Neild, "Visible light positioning: A roadmap for international standardization," *IEEE Communications Magazine*, vol. 51, pp. 68–73, Dec. 2013.

[6] C. G. Gavrincea, J. Baranda, and P. Henarejos, "Rapid prototyping of standard-compliant visible light communications system," *IEEE Communications Magazine*, vol. 52, pp. 80–87, July 2014.

[7] L. Grobe, A. Paraskevopoulos, J. Hilt, D. Schulz, F. Lassak, F. Hartlieb, C. Kottke, V. Jungnickel, and K. D. Langer, "High-speed visible light communication systems," *IEEE Communications Magazine*, vol. 51, pp. 60–66, Dec. 2013.

[8] K. Panta and J. Armstrong, "Indoor localisation using white LEDs," *Electronics Letters*, vol. 48, no. 4, pp. 228–230, 2012.

[9] H.-S. Kim, D.-R. Kim, S.-H. Yang, Y.-H. Son, and S.-K. Han, "An indoor visible light communication positioning system using a RF carrier allocation technique," *Journal of Lightwave Technology*, vol. 31, pp. 134–144, Jan. 2013.

[10] M. F. Keskin, A. D. Sezer, and S. Gezici, "Localization via visible light systems," *Proceedings of the IEEE*, vol. 106, pp. 1063–1088, June 2018.

[11] Z. Ghassemlooy, L. N. Alves, S. Zvanovec, and M.-A. Khalighi, *Visible Light Communications: Theory and Applications*. CRC Press, 2017.

[12] T. Komine and M. Nakagawa, "Fundamental analysis for visible-light communication system using LED lights," *IEEE Transactions on Consumer Electronics*, vol. 50, pp. 100–107, Feb. 2004.

[13] L. Li, P. Hu, C. Peng, G. Shen, and F. Zhao, "Epsilon: A visible light based positioning system," in *11th USENIX Symposium on Networked Systems Design and Implementation (NSDI)*, (Seattle, WA), pp. 331–343, Apr. 2014.

[14] W. Zhang, M. I. S. Chowdhury, and M. Kavehrad, "Asynchronous indoor positioning system based on visible light communications," *Optical Engineering*, vol. 53, no. 4, pp. 045105–1–045105–9, 2014.

[15] S.-H. Yang, E.-M. Jung, and S.-K. Han, "Indoor location estimation based on LED visible light communication using multiple optical receivers," *IEEE Communications Letters*, vol. 17, pp. 1834–1837, Sep. 2013.

[16] M. F. Keskin and S. Gezici, "Comparative theoretical analysis of distance estimation in visible light positioning systems," *Journal of Lightwave Technology*, vol. 34, pp. 854–865, Feb. 2016.

[17] M. F. Keskin, E. Gonendik, and S. Gezici, "Improved lower bounds for ranging in synchronous visible light positioning systems," *Journal of Lightwave Technology*, vol. 34, pp. 5496–5504, Dec. 2016.

[18] M. F. Keskin, S. Gezici, and O. Arikan, "Direct and two-step positioning in visible light systems," *IEEE Transactions on Communications*, vol. 66, pp. 239–254, Jan. 2018.

[19] M. F. Keskin, A. D. Sezer, and S. Gezici, "Optimal and robust power allocation for visible light positioning systems under illumination constraints," *IEEE Transactions on Communications*, under review, 2018.

[20] M. F. Keskin, O. Erdem, and S. Gezici, "Cooperative localization in hybrid infrared/visible light networks: Theoretical limits and distributed algorithms," *IEEE Transactions on Signal and Information Processing over Networks*, accepted for publication, 2018.

[21] D. Ganti, W. Zhang, and M. Kavehrad, "VLC-based indoor positioning system with tracking capability using Kalman and particle filters," in *IEEE International Conference on Consumer Electronics (ICCE)*, pp. 476–477, Jan. 2014.

[22] Z. Zhou, M. Kavehrad, and P. Deng, "Indoor positioning algorithm using light-emitting diode visible light communications," *Optical Engineering*, vol. 51, no. 8, p. 085009, 2012.

[23] T. Wang, Y. Sekercioglu, A. Neild, and J. Armstrong, "Position accuracy of time-of-arrival based ranging using visible light with application in indoor localization systems," *Journal of Lightwave Technology*, vol. 31, pp. 3302–3308, Oct. 2013.

[24] S.-Y. Jung, S. Hann, and C.-S. Park, "TDOA-based optical wireless indoor localization using LED ceiling lamps," *IEEE Transactions on Consumer Electronics*, vol. 57, pp. 1592–1597, Nov. 2011.

[25] M. Bilgi, A. Sevincer, M. Yuksel, and N. Pala, "Optical wireless localization," *Wireless Networks*, vol. 18, pp. 215–226, Feb. 2012.

[26] S.-H. Yang, H.-S. Kim, Y.-H. Son, and S.-K. Han, "Three-dimensional visible light indoor localization using AOA and RSS with multiple optical receivers," *Journal of Lightwave Technology*, vol. 32, pp. 2480–2485, July 2014.

[27] Y. Eroglu, I. Guvenc, N. Pala, and M. Yuksel, "AOA-based localization and tracking in multi-element VLC systems," in *IEEE 16th Annual Wireless and Microwave Technology Conference (WAMICON)*, Apr. 2015.

[28] X. Zhang, J. Duan, Y. Fu, and A. Shi, "Theoretical accuracy analysis of indoor visible light communication positioning system based on received signal strength indicator," *Journal of Lightwave Technology*, vol. 32, pp. 4180–4186, Nov. 2014.

[29] A. Sahin, Y. S. Eroglu, I. Guvenc, N. Pala, and M. Yuksel, "Hybrid 3-D localization for visible light communication systems," *Journal of Lightwave Technology*, vol. 33, pp. 4589–4599, Nov. 2015.

[30] D. Dardari, C.-C. Chong, and M. Win, "Improved lower bounds on time-of-arrival estimation error in realistic UWB channels," in *IEEE International Conference on Ultra-Wideband (ICUWB)*, pp. 531–537, Sep. 2006.

[31] H. L. Van Trees and K. L. Bell (editors), *Bayesian bounds for parameter estimation and nonlinear filtering/tracking*. New Jersey: Wiley-Interscience, 2007.

[32] E. Gonendik and S. Gezici, "Fundamental limits on RSS based range estimation in visible light positioning systems," *IEEE Communications Letters*, vol. 19, pp. 2138–2141, Dec. 2015.

[33] Z. Sahinoglu, S. Gezici, and I. Guvenc, *Ultra-Wideband Positioning Systems: Theoretical Limits, Ranging Algorithms, and Protocols*. New York, Cambridge University Press, 2008.

[34] M. Aminikashani, W. Gu, and M. Kavehrad, "Indoor positioning with OFDM visible light communications," in *2016 13th IEEE Annual Consumer Communications Networking Conference (CCNC)*, pp. 505–510, Jan. 2016.

[35] C. Wang, L. Wang, X. Chi, S. Liu, W. Shi, and J. Deng, "The research of indoor positioning based on visible light communication," *China Communications*, vol. 12, pp. 85–92, Aug. 2015.

[36] W. Xu, J. Wang, H. Shen, H. Zhang, and X. You, "Indoor positioning for multiphotodiode device using visible-light communications," *IEEE Photonics Journal*, vol. 8, pp. 1–11, Feb. 2016.

[37] G. B. Prince and T. D. C. Little, "Latency constrained device positioning using a visible light communication two-phase received signal strength - angle of arrival algorithm," in *2015 International Conference on Indoor Positioning and Indoor Navigation (IPIN)*, pp. 1–7, Oct. 2015.

[38] A. J. Weiss and A. Amar, "Direct position determination of multiple radio signals," *EURASIP Journal on Advances in Signal Processing*, vol. 2005, no. 1, pp. 37–49, 2005.

[39] O. Bialer, D. Raphaeli, and A. J. Weiss, "Maximum-likelihood direct position estimation in dense multipath," *IEEE Transactions on Vehicular Technology*, vol. 62, pp. 2069–2079, June 2013.

[40] A. J. Weiss, "Direct position determination of narrowband radio frequency transmitters," *IEEE Signal Processing Letters*, vol. 11, pp. 513–516, May 2004.

[41] A. Amar and A. J. Weiss, "New asymptotic results on two fundamental approaches to mobile terminal location," in *3rd International Symposium on Communications, Control and Signal Processing*, pp. 1320–1323, Mar. 2008.

[42] P. Closasy, C. Fernández-Pradesz, and J. A. Fernández-Rubioy, "Direct position estimation approach outperforms conventional two-steps positioning," in *2009 17th European Signal Processing Conference*, pp. 1958–1962, Aug. 2009.

[43] A. Amar and A. J. Weiss, "Localization of narrowband radio emitters based on doppler frequency shifts," *IEEE Transactions on Signal Processing*, vol. 56, pp. 5500–5508, Nov. 2008.

[44] N. Garcia, A. M. Haimovich, M. Coulon, and J. A. Dabin, "High precision TOA-based direct localization of multiple sources in multipath," *CoRR*, vol. abs/1505.03193, 2015.

[45] N. Vankayalapati, S. Kay, and Q. Ding, "TDOA based direct positioning maximum likelihood estimator and the Cramer-Rao bound," *IEEE Transactions on Aerospace and Electronic Systems*, vol. 50, pp. 1616–1635, July 2014.

[46] N. Garcia, H. Wymeersch, E. G. Larsson, A. M. Haimovich, and M. Coulon, "Direct localization for massive MIMO," *IEEE Transactions on Signal Processing*, vol. 65, pp. 2475–2487, May 2017.

[47] O. Bar-Shalom and A. J. Weiss, "Direct positioning of stationary targets using MIMO radar," *Signal Processing*, vol. 91, no. 10, pp. 2345–2358, 2011.

[48] L. Tzafri and A. J. Weiss, "High-resolution direct position determination using MVDR," *IEEE Transactions on Wireless Communications*, vol. 15, pp. 6449–6461, Sep. 2016.

[49] H. Steendam, T. Q. Wang, and J. Armstrong, "Cramer-Rao bound for indoor visible light positioning using an aperture-based angular-diversity receiver," in *2016 IEEE International Conference on Communications (ICC)*, pp. 1–6, May 2016.

[50] H. Steendam, T. Q. Wang, and J. Armstrong, "Theoretical lower bound for indoor visible light positioning using received signal strength measurements and an aperture-based receiver," *Journal of Lightwave Technology*, vol. 35, pp. 309–319, Jan. 2017.

[51] G. Kail, P. Maechler, N. Preyss, and A. Burg, "Robust asynchronous indoor localization using LED lighting," in *2014 IEEE International Conference on Acoustics, Speech and Signal Processing (ICASSP)*, pp. 1866–1870, May 2014.

[52] Z. Zheng, L. Liu, and W. Hu, "Accuracy of ranging based on DMT visible light communication for indoor positioning," *IEEE Photonics Technology Letters*, vol. 29, pp. 679–682, Apr. 2017.

[53] K. Ying, H. Qian, R. J. Baxley, and S. Yao, "Joint optimization of precoder and equalizer in MIMO VLC systems," *IEEE Journal on Selected Areas in Communications*, vol. 33, pp. 1949–1958, Sep. 2015.

[54] R. Wang, Q. Gao, J. You, E. Liu, P. Wang, Z. Xu, and Y. Hua, "Linear transceiver designs for MIMO indoor visible light communications under lighting constraints," *IEEE Transactions on Communications*, vol. 65, pp. 2494–2508, June 2017.

[55] B. Li, R. Zhang, W. Xu, C. Zhao, and L. Hanzo, "Joint dimming control and transceiver design for MIMO-aided visible light communication," *IEEE Communications Letters*, vol. 20, pp. 2193–2196, Nov. 2016.

[56] Q. Gao, C. Gong, and Z. Xu, "Joint transceiver and offset design for visible light communications with input-dependent shot noise," *IEEE Transactions on Wireless Communications*, vol. 16, pp. 2736–2747, May 2017.

[57] K. H. Park, Y. C. Ko, and M. S. Alouini, "On the power and offset allocation for rate adaptation of spatial multiplexing in optical wireless MIMO channels," *IEEE Transactions on Communications*, vol. 61, pp. 1535–1543, Apr. 2013.

[58] D. Bykhovsky and S. Arnon, "Multiple access resource allocation in visible light communication systems," *Journal of Lightwave Technology*, vol. 32, pp. 1594–1600, Apr. 2014.

[59] C. Gong, S. Li, Q. Gao, and Z. Xu, "Power and rate optimization for visible light communication system with lighting constraints," *IEEE Transactions on Signal Processing*, vol. 63, pp. 4245–4256, Aug. 2015.

[60] X. Ling, J. Wang, X. Liang, Z. Ding, and C. Zhao, "Offset and power optimization for DCO-OFDM in visible light communication systems," *IEEE Transactions on Signal Processing*, vol. 64, pp. 349–363, Jan. 2016.

[61] Y. S. Eroğlu, I. Güvenç, A. Şahin, Y. Yapıcı, N. Pala, and M. Yüksel, "Multi-element VLC networks: LED assignment, power control, and optimum combining," *IEEE Journal on Selected Areas in Communications*, vol. 36, pp. 121–135, Jan. 2018.

[62] R. Jiang, Z. Wang, Q. Wang, and L. Dai, "Multi-user sum-rate optimization for visible light communications with lighting constraints," *Journal of Lightwave Technology*, vol. 34, pp. 3943–3952, Aug. 2016.

[63] X. Zhang, Q. Gao, C. Gong, and Z. Xu, "User grouping and power allocation for NOMA visible light communication multi-cell networks," *IEEE Communications Letters*, vol. 21, pp. 777–780, Apr. 2017.

[64] R. Jiang, Q. Wang, H. Haas, and Z. Wang, "Joint user association and power allocation for cell-free visible light communication networks," *IEEE Journal on Selected Areas in Communications*, vol. 36, pp. 136–148, Jan. 2018.

[65] T. V. Pham, H. Le-Minh, and A. T. Pham, "Multi-user visible light communication broadcast channels with zero-forcing precoding," *IEEE Transactions on Communications*, vol. 65, pp. 2509–2521, June 2017.

[66] X. Zhang, S. Dimitrov, S. Sinanovic, and H. Haas, "Optimal power allocation in spatial modulation OFDM for visible light communications," in *2012 IEEE 75th Vehicular Technology Conference (VTC Spring)*, pp. 1–5, May 2012.

[67] J. Lian and M. Brandt-Pearce, "Multiuser MIMO indoor visible light communication system using spatial multiplexing," *Journal of Lightwave Technology*, vol. 35, pp. 5024–5033, Dec. 2017.

[68] W. W. L. Li, Y. Shen, Y. J. Zhang, and M. Z. Win, "Robust power allocation for energy-efficient location-aware networks," *IEEE/ACM Transactions on Networking*, vol. 21, pp. 1918–1930, Dec. 2013.

[69] Y. Shen, W. Dai, and M. Z. Win, "Power optimization for network localization," *IEEE/ACM Transactions on Networking*, vol. 22, pp. 1337–1350, Aug. 2014.

[70] W. Dai, Y. Shen, and M. Z. Win, "Distributed power allocation for cooperative wireless network localization," *IEEE Journal on Selected Areas in Communications*, vol. 33, pp. 28–40, Jan. 2015.

[71] T. Zhang, C. Qin, A. F. Molisch, and Q. Zhang, "Joint allocation of spectral and power resources for non-cooperative wireless localization networks," *IEEE Transactions on Communications*, vol. 64, pp. 3733–3745, Sep. 2016.

[72] J. Chen, W. Dai, Y. Shen, V. K. Lau, and M. Z. Win, "Power management for cooperative localization: A game theoretical approach," *IEEE Transactions on Signal Processing*, vol. 64, pp. 6517–6532, Dec. 2016.

[73] A. Shahmansoori, G. Seco-Granados, and H. Wymeersch, "Power allocation for OFDM wireless network localization under expectation and robustness constraints," *IEEE Transactions on Wireless Communications*, vol. 16, pp. 2027–2038, Mar. 2017.

[74] W. Dai, Y. Shen, and M. Z. Win, "A computational geometry framework for efficient network localization," *IEEE Transactions on Information Theory*, vol. 64, pp. 1317–1339, Feb. 2018.

[75] W. Dai, Y. Shen, and M. Z. Win, "Energy-efficient network navigation algorithms," *IEEE Journal on Selected Areas in Communications*, vol. 33, pp. 1418–1430, July 2015.

[76] T. Wang, G. Leus, and L. Huang, "Ranging energy optimization for robust sensor positioning based on semidefinite programming," *IEEE Transactions on Signal Processing*, vol. 57, pp. 4777–4787, Dec. 2009.

[77] J. Chen, W. Dai, Y. Shen, V. K. N. Lau, and M. Z. Win, "Resource management games for distributed network localization," *IEEE Journal on Selected Areas in Communications*, vol. 35, pp. 317–329, Feb. 2017.

[78] H. Elgala, R. Mesleh, and H. Haas, "An LED model for intensity-modulated optical communication systems," *IEEE Photonics Technology Letters*, vol. 22, pp. 835–837, June 2010.

[79] J. Gancarz, H. Elgala, and T. D. C. Little, "Impact of lighting requirements on VLC systems," *IEEE Communications Magazine*, vol. 51, pp. 34–41, Dec. 2013.

[80] A. Tsiatmas, C. P. M. J. Baggen, F. M. J. Willems, J. P. M. G. Linnartz, and J. W. M. Bergmans, "An illumination perspective on visible light communications," *IEEE Communications Magazine*, vol. 52, pp. 64–71, July 2014.

[81] Y. S. Eroglu, A. Sahin, I. Guvenc, N. Pala, and M. Yuksel, "Multi-element transmitter design and performance evaluation for visible light communication," in *2015 IEEE Globecom Workshops*, pp. 1–6, Dec. 2015.

[82] J. Grubor, S. Randel, K. D. Langer, and J. W. Walewski, "Broadband information broadcasting using LED-based interior lighting," *Journal of Lightwave Technology*, vol. 26, pp. 3883–3892, Dec. 2008.

[83] N. Patwari, J. N. Ash, S. Kyperountas, A. O. Hero, R. L. Moses, and N. S. Correal, "Locating the nodes: cooperative localization in wireless sensor networks," *IEEE Signal Processing Magazine*, vol. 22, pp. 54–69, July 2005.

[84] H. Wymeersch, J. Lien, and M. Z. Win, "Cooperative localization in wireless networks," *Proceedings of the IEEE*, vol. 97, pp. 427–450, Feb. 2009.

[85] M. R. Gholami, M. F. Keskin, S. Gezici, and M. Jansson, *Cooperative Positioning in Wireless Networks*, pp. 1–19. Wiley Encyclopedia of Electrical and Electronics Engineering, 2016.

[86] P. Biswas, T.-C. Lian, T.-C. Wang, and Y. Ye, "Semidefinite programming based algorithms for sensor network localization," *ACM Transactions on Sensor Networks*, vol. 2, no. 2, pp. 188–220, 2006.

[87] K. W. K. Lui, W. K. Ma, H. C. So, and F. K. W. Chan, "Semi-definite programming algorithms for sensor network node localization with uncertainties in anchor positions and/or propagation speed," *IEEE Transactions on Signal Processing*, vol. 57, pp. 752–763, Feb. 2009.

[88] R. W. Ouyang, A. K. S. Wong, and C. T. Lea, "Received signal strength-based wireless localization via semidefinite programming: Noncooperative and cooperative schemes," *IEEE Transactions on Vehicular Technology*, vol. 59, pp. 1307–1318, Mar. 2010.

[89] P. Tseng, "Second-order cone programming relaxation of sensor network localization," *SIAM Journal on Optimization*, vol. 18, pp. 156–185, Feb. 2007.

[90] G. Naddafzadeh-Shirazi, M. B. Shenouda, and L. Lampe, "Second order cone programming for sensor network localization with anchor position uncertainty," *IEEE Transactions on Wireless Communications*, vol. 13, pp. 749–763, Feb. 2014.

[91] C. Soares, J. Xavier, and J. Gomes, "Simple and fast convex relaxation method for cooperative localization in sensor networks using range measurements," *IEEE Transactions on Signal Processing*, vol. 63, pp. 4532–4543, Sep. 2015.

[92] D. Blatt and A. O. Hero, "Energy-based sensor network source localization via projection onto convex sets," *IEEE Transactions on Signal Processing*, vol. 54, pp. 3614–3619, Sep. 2006.

[93] M. R. Gholami, H. Wymeersch, E. G. Ström, and M. Rydström, "Wireless network positioning as a convex feasibility problem," *EURASIP Journal on Wireless Communications and Networking*, vol. 2011, no. 1, p. 161, 2011.

[94] M. R. Gholami, L. Tetruashvili, E. G. Ström, and Y. Censor, "Cooperative wireless sensor network positioning via implicit convex feasibility," *IEEE Transactions on Signal Processing*, vol. 61, pp. 5830–5840, Dec. 2013.

[95] Y. Zhang, Y. Lou, Y. Hong, and L. Xie, "Distributed projection-based algorithms for source localization in wireless sensor networks," *IEEE Transactions on Wireless Communications*, vol. 14, pp. 3131–3142, June 2015.

[96] J. A. Costa, N. Patwari, and A. O. Hero, III, "Distributed weighted-multidimensional scaling for node localization in sensor networks," *ACM Transactions on Sensor Networks*, vol. 2, pp. 39–64, Feb. 2006.

[97] M. Uysal, Z. Ghassemlooy, A. Bekkali, A. Kadri, and H. Menouar, "Visible light communication for vehicular networking: Performance study of a V2V system using a measured headlamp beam pattern model," *IEEE Vehicular Technology Magazine*, vol. 10, no. 4, pp. 45–53, 2015.

[98] A.-M. Căilean and M. Dimian, "Toward environmental-adaptive visible light communications receivers for automotive applications: A review," *IEEE Sensors Journal*, vol. 16, no. 9, pp. 2803–2811, 2016.

[99] S.-H. Yu, O. Shih, H.-M. Tsai, N. Wisitpongphan, and R. D. Roberts, "Smart automotive lighting for vehicle safety," *IEEE Communications Magazine*, vol. 51, no. 12, pp. 50–59, 2013.

[100] A. Căilean and M. Dimian, "Current challenges for visible light communications usage in vehicle applications: A survey," *IEEE Communications Surveys Tutorials*, vol. 19, pp. 2681–2703, Fourthquarter 2017.

[101] M. Kavehrad, "Sustainable energy-efficient wireless applications using light," *IEEE Communications Magazine*, vol. 48, no. 12, pp. 66–73, 2010.

[102] D. Tagliaferri and C. Capsoni, "High-speed wireless infrared uplink scheme for airplane passengers' communications," *Electronics Letters*, vol. 53, no. 13, pp. 887–888, 2017.

[103] C. Quintana, V. Guerra, J. Rufo, J. Rabadan, and R. Perez-Jimenez, "Reading lamp-based visible light communication system for in-flight entertainment," *IEEE Transactions on Consumer Electronics*, vol. 59, no. 1, pp. 31–37, 2013.

[104] J. M. Kahn and J. R. Barry, "Wireless infrared communications," *Proceedings of the IEEE*, vol. 85, no. 2, pp. 265–298, 1997.

[105] Y. Censor and A. Segal, "Algorithms for the quasiconvex feasibility problem," *Journal of Computational and Applied Mathematics*, vol. 185, no. 1, pp. 34 – 50, 2006.

[106] A. N. Iusem, B. F. Svaiter, and M. Teboulle, "Entropy-like proximal methods in convex programming," *Mathematics of Operations Research*, vol. 19, no. 4, pp. 790–814, 1994.

[107] T. Jia and R. M. Buehrer, "A set-theoretic approach to collaborative position location for wireless networks," *IEEE Transactions on Mobile Computing*, vol. 10, no. 9, pp. 1264–1275, 2011.

[108] A. Carmi, Y. Censor, and P. Gurfil, "Convex feasibility modeling and projection methods for sparse signal recovery," *Journal of Computational and Applied Mathematics*, vol. 236, no. 17, pp. 4318–4335, 2012.

[109] P. L. Combettes, "Convex set theoretic image recovery by extrapolated iterations of parallel subgradient projections," *IEEE Transactions on Image Processing*, vol. 6, pp. 493–506, Apr. 1997.

[110] Y. Censor, A. Gibali, F. Lenzen, and C. Schnorr, "The implicit convex feasibility problem and its application to adaptive image denoising," *arXiv:1606.05848*, 2016.

[111] Y. Censor and A. Segal, "Iterative projection methods in biomedical inverse problems," in *Procceding of the interdisciplinary workshop on Mathematical Methods in Biomedical Imaging and Intensity-Modulated Radiation Therapy (IMRT)*, pp. 65–96, Pisa, Italy, Oct. 2008.

[112] D. Butnariu, Y. Censor, P. Gurfil, and E. Hadar, "On the behavior of subgradient projections methods for convex feasibility problems in Euclidean spaces," *SIAM Journal on Optimization*, vol. 19, no. 2, pp. 786–807, 2008.

[113] M. Yasir, S. W. Ho, and B. N. Vellambi, "Indoor positioning system using visible light and accelerometer," *Journal of Lightwave Technology*, vol. 32, pp. 3306–3316, Oct. 2014.

[114] A. Hatami and K. Pahlavan, "Hybrid TOA-RSS based localization using neural networks," in *IEEE Global Telecommunications Conference (GLOBECOM)*, Nov. 2006.

[115] C. Fritsche and A. Klein, "Cramer-Rao lower bounds for hybrid localization of mobile terminals," in *Workshop on Positioning, Navigation and Communication (WPNC)*, pp. 157–164, Mar. 2008.

[116] B. Sieskul, T. Kaiser, and F. Zheng, "A hybrid SS-ToA wireless NLoS geolocation based on path attenuation: Cramer-Rao bound," in *IEEE 69th Vehicular Technology Conference (VTC Spring)*, Apr. 2009.

[117] S. Gezici, Z. Tian, G. B. Giannakis, H. Kobayashi, A. F. Molisch, H. V. Poor, and Z. Sahinoglu, "Localization via ultra-wideband radios: A look at positioning aspects for future sensor networks," *IEEE Signal Processing Magazine*, vol. 22, pp. 70–84, July 2005.

[118] Z. Liu, J. Shen, Z. Yao, M. Lu, and Y. Zhao, "The Ziv-Zakai bound for time-of-arrival estimation of new generation GNSS signals," in *International Technical Meeting of The Institute of Navigation*, (Monterey, CA), pp. 639–646, Jan. 2016.

[119] D. Dardari and M. Win, "Ziv-Zakai bound on time-of-arrival estimation with statistical channel knowledge at the receiver," in *IEEE International Conference on Ultra-Wideband (ICUWB)*, pp. 624–629, Sep. 2009.

[120] Y. Qi and H. Kobayashi, "Cramér-Rao lower bound for geolocation in non-line-of-sight environment," in *IEEE International Conference on Acoustics, Speech, and Signal Processing (ICASSP)*, vol. 3, pp. III–2473–III–2476, May 2002.

[121] N. Decarli and D. Dardari, "Ziv-Zakai bound for time delay estimation of unknown deterministic signals," in *IEEE International Conference on Acoustics Speech and Signal Processing (ICASSP)*, pp. 4673–4677, May 2014.

[122] H. V. Poor, *An Introduction to Signal Detection and Estimation*. New York: Springer-Verlag, 1994.

[123] S. Gezici, H. Celebi, H. Poor, and H. Arslan, "Fundamental limits on time delay estimation in dispersed spectrum cognitive radio systems," *IEEE Transactions on Wireless Communications*, vol. 8, pp. 78–83, Jan. 2009.

[124] S. Gezici and Z. Sahinoglu, "Ranging in a Single-Input Multiple-Output (SIMO) system," *IEEE Communications Letters*, vol. 12, pp. 197–199, Mar. 2008.

[125] D. H. Kwon, S. H. Yang, and S. K. Han, "Modulation bandwidth enhancement of white-LED-based visible light communications using electrical equalizations," *Proceedings of SPIE*, vol. 9387, pp. 93870T–1–93870T–6, 2015.

[126] Y. Qi, H. Kobayashi, and H. Suda, "On time-of-arrival positioning in a multipath environment," *IEEE Transactions on Vehicular Technology,*, vol. 55, pp. 1516–1526, Sep. 2006.

[127] Y. Hou, S. Xiao, H. Zheng, and W. Hu, "Multiple access scheme based on block encoding time division multiplexing in an indoor positioning system using visible light," *IEEE/OSA Journal of Optical Communications and Networking*, vol. 7, pp. 489–495, May 2015.

[128] K. L. Bell, Y. Steinberg, Y. Ephraim, and H. L. V. Trees, "Extended Ziv-Zakai lower bound for vector parameter estimation," *IEEE Transactions on Information Theory*, vol. 43, pp. 624–637, Mar. 1997.

[129] C. Amini, A. Taherpour, T. Khattab, and S. Gazor, "On the more accurate channel model and positioning based on time-of-arrival for visible light localization," *Optical Engineering*, vol. 56, no. 1, p. 016110, 2017.

[130] A. Goldsmith, *Wireless Communications*. Cambridge University Press, 2004.

[131] A. Mostafa and L. Lampe, "Optimal and robust beamforming for secure transmission in MISO visible-light communication links," *IEEE Transactions on Signal Processing*, vol. 64, pp. 6501–6516, Dec. 2016.

[132] S. D. Lausnay, L. D. Strycker, J. P. Goemaere, B. Nauwelaers, and N. Stevens, "A survey on multiple access visible light positioning," in *IEEE International Conference on Emerging Technologies and Innovative Business Practices for the Transformation of Societies (EmergiTech)*, pp. 38–42, Aug. 2016.

[133] H. L. V. Trees, *Detection, Estimation, and Modulation Theory*. John Wiley & Sons, New York, 2004.

[134] T. D. C. Little and H. Elgala, "Adaptation of OFDM under visible light communications and illumination constraints," in *2014 48th Asilomar Conference on Signals, Systems and Computers*, pp. 1739–1744, Nov. 2014.

[135] H. Ma, L. Lampe, and S. Hranilovic, "Coordinated broadcasting for multiuser indoor visible light communication systems," *IEEE Transactions on Communications*, vol. 63, pp. 3313–3324, Sep. 2015.

[136] L. Chen, B. Krongold, and J. Evans, "Theoretical characterization of nonlinear clipping effects in IM/DD optical OFDM systems," *IEEE Transactions on Communications*, vol. 60, pp. 2304–2312, Aug. 2012.

[137] E. F. Schubert, *Light-Emitting Diodes*. Cambridge University Press, 2003.

[138] A. Pandharipande and D. Caicedo, "Adaptive illumination rendering in LED lighting systems," *IEEE Transactions on Systems, Man, and Cybernetics: Systems*, vol. 43, pp. 1052–1062, Sep. 2013.

[139] S. Boyd and L. Vandenberghe, *Convex Optimization*. Cambridge University Press, 2004.

[140] M. Grant and S. Boyd, "CVX: Matlab software for disciplined convex programming, version 2.1." `http://cvxr.com/cvx`, Mar. 2014.

[141] Y. C. Eldar, A. Ben-Tal, and A. Nemirovski, "Robust mean-squared error estimation in the presence of model uncertainties," *IEEE Transactions on Signal Processing*, vol. 53, pp. 168–181, Jan. 2005.

[142] M. B. Shenouda and T. N. Davidson, "On the design of linear transceivers for multiuser systems with channel uncertainty," *IEEE Journal on Selected Areas in Communications*, vol. 26, pp. 1015–1024, Aug. 2008.

[143] J. Wang and D. P. Palomar, "Worst-case robust MIMO transmission with imperfect channel knowledge," *IEEE Transactions on Signal Processing*, vol. 57, pp. 3086–3100, Aug. 2009.

[144] Y. Hu and G. Leus, "Robust differential received signal strength-based localization," *IEEE Transactions on Signal Processing*, vol. 65, pp. 3261–3276, June 2017.

[145] A. Ben-Tal and A. Nemirovski, *Lectures on Modern Convex Optimization*. Society for Industrial and Applied Mathematics, 2001.

[146] S. Boyd, L. El Ghaoui, E. Feron, and V. Balakrishnan, *Linear matrix inequalities in system and control theory*. SIAM, 1994.

[147] L. Vandenberghe and S. Boyd, "Semidefinite programming," *SIAM Review*, vol. 38, no. 1, pp. 49–95, 1996.

[148] J. Löfberg, "YALMIP : A toolbox for modeling and optimization in Matlab," in *In Proceedings of the CACSD Conference*, (Taipei, Taiwan), 2004.

[149] Z. Q. Luo, W. K. Ma, A. M. C. So, Y. Ye, and S. Zhang, "Semidefinite relaxation of quadratic optimization problems," *IEEE Signal Processing Magazine*, vol. 27, pp. 20–34, May 2010.

[150] E. Xu, Z. Ding, and S. Dasgupta, "Source localization in wireless sensor networks from signal time-of-arrival measurements," *IEEE Transactions on Signal Processing*, vol. 59, pp. 2887–2897, June 2011.

[151] R.-L. Sheu and J. Lin, "Solving continuous min-max problems by an iterative entropic regularization method," *Journal of Optimization Theory and Applications*, vol. 121, no. 3, pp. 597–612, 2004.

[152] H. M. Soliman and A. Leon-Garcia, "Game-theoretic demand-side management with storage devices for the future smart grid," *IEEE Transactions on Smart Grid*, vol. 5, pp. 1475–1485, May 2014.

[153] I. Din and H. Kim, "Energy-efficient brightness control and data transmission for visible light communication," *IEEE Photonics Technology Letters*, vol. 26, pp. 781–784, Apr. 2014.

[154] E. Masazade, R. Niu, P. K. Varshney, and M. Keskinoz, "Energy aware iterative source localization for wireless sensor networks," *IEEE Transactions on Signal Processing*, vol. 58, pp. 4824–4835, Sep. 2010.

[155] Y. E. Ustev, O. Durmaz Incel, and C. Ersoy, "User, device and orientation independent human activity recognition on mobile phones: Challenges and

a proposal," in *Proceedings of the 2013 ACM conference on Pervasive and ubiquitous computing adjunct publication*, pp. 1427–1436, ACM, 2013.

[156] F. Li, C. Zhao, G. Ding, J. Gong, C. Liu, and F. Zhao, "A reliable and accurate indoor localization method using phone inertial sensors," in *Proceedings of the 2012 ACM Conference on Ubiquitous Computing*, pp. 421–430, ACM, 2012.

[157] V. Renaudin and C. Combettes, "Magnetic, acceleration fields and gyroscope quaternion (MAGYQ)-based attitude estimation with smartphone sensors for indoor pedestrian navigation," *Sensors*, vol. 14, no. 12, pp. 22864–22890, 2014.

[158] S. Gezici, "Theoretical limits for estimation of periodic movements in pulse-based UWB systems," *IEEE Journal of Selected Topics in Signal Processing*, vol. 1, pp. 405–417, Oct. 2007.

[159] E. A. Boettner and J. R. Wolter, "Transmission of the ocular media," *Investigative Ophthalmology & Visual Science*, vol. 1, no. 6, pp. 776–783, 1962.

[160] J. Michel, J. Liu, and L. C. Kimerling, "High-performance Ge-on-Si photodetectors," *Nature Photonics*, vol. 4, no. 8, p. 527, 2010.

[161] A. Pospischil, M. Humer, M. M. Furchi, D. Bachmann, R. Guider, T. Fromherz, and T. Mueller, "CMOS-compatible graphene photodetector covering all optical communication bands," *Nature Photonics*, vol. 7, no. 11, p. 892, 2013.

[162] T. Mueller, F. Xia, and P. Avouris, "Graphene photodetectors for high-speed optical communications," *Nature Photonics*, vol. 4, no. 5, p. 297, 2010.

[163] R. Perez-Jimenez, J. Rufo, C. Quintana, J. Rabadan, and F. Lopez-Hernandez, "Visible light communication systems for passenger in-flight data networking," in *Consumer Electronics (ICCE), 2011 IEEE International Conference on*, pp. 445–446, IEEE, 2011.

[164] M. Falcitelli and P. Pagano, "Visible light communication for cooperative ITS," in *Intelligent Transportation Systems*, pp. 19–47, Springer, 2016.

[165] A. Cailean, B. Cagneau, L. Chassagne, S. Topsu, Y. Alayli, and J.-M. Blosseville, "Visible light communications: Application to cooperation between vehicles and road infrastructures," in *Intelligent Vehicles Symposium (IV), 2012 IEEE*, pp. 1055–1059, IEEE, 2012.

[166] N. Kumar, N. Lourenço, D. Terra, L. N. Alves, and R. L. Aguiar, "Visible light communications in intelligent transportation systems," in *Intelligent Vehicles Symposium (IV), 2012 IEEE*, pp. 748–753, IEEE, 2012.

[167] X. Li, R. Zhang, and L. Hanzo, "Optimization of visible-light optical wireless systems: Network-centric versus user-centric designs," *IEEE Communications Surveys Tutorials*, 2018.

[168] R. Roberts, P. Gopalakrishnan, and S. Rathi, "Visible light positioning: Automotive use case," in *Vehicular Networking Conference (VNC), 2010 IEEE*, pp. 309–314, IEEE, 2010.

[169] S. Penfold, R. Zalas, M. Casiraghi, M. Brooke, Y. Censor, and R. Schulte, "Sparsity constrained split feasibility for dose-volume constraints in inverse planning of intensity-modulated photon or proton therapy," *Physics in Medicine and Biology*, vol. 62, p. 3599, May 2017.

[170] S. Yousefi, H. Wymeersch, X. W. Chang, and B. Champagne, "Tight two-dimensional outer-approximations of feasible sets in wireless sensor networks," *IEEE Communications Letters*, vol. 20, pp. 570–573, Mar. 2016.

[171] M. R. Gholami, M. Rydstrom, and E. G. Strom, "Positioning of node using plane projection onto convex sets," in *2010 IEEE Wireless Communication and Networking Conference*, pp. 1–5, Apr. 2010.

[172] M. R. Gholami, S. Gezici, E. G. Ström, and M. Rydström, "A distributed positioning algorithm for cooperative active and passive sensors," in *Proc. IEEE International Symposium on Personal, Indoor and Mobile Radio Communications (PIMRC)*, Sep. 2010.

[173] H. H. Bauschke and J. M. Borwein, "On projection algorithms for solving convex feasibility problems," *SIAM Review*, vol. 38, no. 3, pp. 367–426, 1996.

[174] Y. Mathlouthi, A. Mitiche, and I. B. Ayed, *Boundary Preserving Variational Image Differentiation*, pp. 355–364. Cham: Springer International Publishing, 2016.

[175] M. Bazarra, H. Sherali, and C. Shetty, *Nonlinear Programming: Theory and Algorithms*. Wiley-Interscience, 2006.

[176] Y. Censor and A. Lent, "Cyclic subgradient projections," *Mathematical Programming*, vol. 24, no. 1, pp. 233–235, 1982.

[177] P. L. Combettes, "Quasi-Fejérian analysis of some optimization algorithms," in *Inherently Parallel Algorithms in Feasibility and Optimization and their Applications* (Y. C. Dan Butnariu and S. Reich, eds.), vol. 8 of *Studies in Computational Mathematics*, pp. 115–152, Elsevier, 2001.

[178] J. Von Neumann, *Functional Operators (AM-22), Volume 2: The Geometry of Orthogonal Spaces.(AM-22)*, vol. 2. Princeton University Press, 2016.

[179] I. Halperin, "The product of projection operators," *Acta Sci. Math.(Szeged)*, vol. 23, no. 1, pp. 96–99, 1962.

[180] L. Armijo, "Minimization of functions having Lipschitz continuous first partial derivatives," *Pacific Journal of Mathematics*, vol. 16, no. 1, pp. 1–3, 1966.

[181] P. Wolfe, "Convergence conditions for ascent methods," *SIAM Review*, vol. 11, no. 2, pp. 226–235, 1969.

[182] D. P. Bertsekas, *Nonlinear Programming*. Athena Scientific, 2nd ed., 1999.

[183] J. Fliege and B. F. Svaiter, "Steepest descent methods for multicriteria optimization," *Mathematical Methods of Operations Research*, vol. 51, no. 3, pp. 479–494, 2000.

[184] L. T. D. Santos, "A parallel subgradient projections method for the convex feasibility problem," *Journal of Computational and Applied Mathematics*, vol. 18, no. 3, pp. 307–320, 1987.

[185] S. Boyd, A. Ghosh, B. Prabhakar, and D. Shah, "Randomized gossip algorithms," *IEEE Transactions on Information Theory*, vol. 52, pp. 2508–2530, June 2006.

[186] O. L. Mangasarian, *Nonlinear programming*. SIAM, 1994.

[187] R. G. Bartle and D. R. Sherbert, *Introduction to Real Analysis*. John Wiley & Sons, 2000.

[188] L. Gubin, B. Polyak, and E. Raik, "The method of projections for finding the common point of convex sets," *USSR Computational Mathematics and Mathematical Physics*, vol. 7, no. 6, pp. 1–24, 1967.

[189] Y. Censor, A. R. D. Pierro, and M. Zaknoon, "Steered sequential projections for the inconsistent convex feasibility problem," *Nonlinear analysis: theory, method, and application, series A*, vol. 59, pp. 385–405, 2004.

[190] W. Gu, M. Aminikashani, P. Deng, and M. Kavehrad, "Impact of multipath reflections on the performance of indoor visible light positioning systems," *Journal of Lightwave Technology*, vol. 34, pp. 2578–2587, May 2016.